University of Alberta

Nuclear Magnetic Resonance metabolomic fingerprint of the Interleukin 10 gene deficient mouse model of Inflammatory Bowel Disease

by

Victor Key Tso

A thesis submitted to the Faculty of Graduate Studies and Research
in partial fulfillment of the requirements for the degree of

Master of Science

in

Experimental Medicine

Medicine

Fall 2010

Edmonton, Alberta

Examining Committee

Dr. Richard Fedorak MD, Medicine

Dr. Karen Madsen PhD, Medicine

Dr. Carolyn Slupsky PhD, UC Davis, Food Science and Technology

LIST OF TABLES

LIST OF FIGURES

LIST OF ABBREVIATIONS

ATG16L1	Autophagy-related protein 16-1
CD	Crohn's Disease
CE	Capillary electrophoresis
DLG5	Drosophila-discs large-homolog 5
DMBT1	Deleted-in–malignant-brain-tumors 1
FT-IR	Fourier Transform Infrared spectrometry
GC	Gas chromatography
HPLC	high-performance liquid chromatography
IBD	Inflammatory Bowel Disease
ICOS	Inducible co-stimulatory molecule
IFNγ	Interferon gamma
IL 2	Interleukin 2
IL 4	Interleukin 4
IL 5	Interleukin 5
IL 6	Interleukin 6
IL-10 KO	Interleukin-10 knockout or gene-deficient mouse
IL 10	Interleukin 10
IL 12	Interleukin 12
IL 13	Interleukin 13
IL 17	Interleukin 17
IL 27	Interleukin 27
IRGM	Immunity-related GTPase family, M

ITLN1	Intelectin 1
LDL	Low-density lipoprotein
LPS	Lipopolysaccharide
MAGUK	Membrane-associated guanylate kinase
MAS	Magic-angle spinning
MS	Mass Spectrometry
NSAID	Nonsteroidal anti-inflammatory drugs
NMR	Nuclear Magnetic Resonance
NOD2	Nucleotide-binding oligomerization domain-containing 2
OCTN	Organic cation-transporter gene
PCA	Principal Components Analysis
PLS-DA	Partial Least-Squares Discriminant Analysis
PRR	Pattern Recognition Receptor
RF	Radio frequency
SCFA	Short-chain fatty acid
TGF β	Transforming growth-factor beta
TH 2	T-helper cell 2
TH 17	T-helper cell 17
TLR 4	Toll-Like Receptor 4
TOFMS	Time-of-flight mass spectrometry
UC	Ulcerative Colitis
VLDL	Very-low-density lipoprotein
WT	Wild-type

Chapter 1 - Introduction

1.1 Inflammatory Bowel Disease – Background

Inflammatory bowel disease (IBD) is a common disease that leads to inflammation of the colon and small intestine. IBD can be characterized into two main groups; Ulcerative Colitis (UC) and Crohn's Disease (CD). UC can be distinguished from Crohn's because the inflammation in UC always includes the rectum, extends proximally and is continuous, not displaying any skip lesions. The inflammation also only occurs in the mucosal layer of the affected tissue (Xavier and Podolsky 2007). The mucosa in UC patients is dominated by CD4+ lymphocytes with an atypical type 2 helper T-cell phenotype that leads to production of transforming growth-factor beta (TGF-β) and IL-5 (Fuss, Neurath et al. 1996). While UC is limited to the colon, CD can occur anywhere from the mouth to the anus. CD is characterized by a transmural inflammation that affects the entire tissue, as opposed to UC which is only in the mucosa. The inflammation in CD is also discontinuous, and there are skipped sections, but CD usually involves the terminal ileum and most often is found to occur above Peyer's patches (Xavier and Podolsky 2007). The mucosa of CD patients appears to be dominated by CD4+ lymphocytes with a type 1 helper phenotype that leads to the production of interferon gamma (IFN – γ) and IL 2 (Fuss, Neurath et al. 1996). Although the direct cause of IBD is unknown, several main factors are known to contribute to IBD.

One factor is a genetic predisposition to developing IBD. Scanning of the genome has been successful in indentifying genes that appear to contribute to the susceptibility of the disease. These genes can be subdivided into a number of categories according to innate pattern recognition, differentiation of lymphocytes, autophagy, and maintenance of epithelial barrier integrity (Van Limbergen, Wilson et al. 2009). Another factor is the interaction of the host immune system with the microflora present in the gut (discussed later).

The NOD 2 (aka CARD 15 or IBD 1) gene has been identified as one susceptibility gene in Crohn's disease (Hugot, Chamaillard et al. 2001; Ogura, Bonen et al. 2001). The NOD 2 gene belongs to the family of pattern-recognition receptors (PRR), PRRs are used to recognize microbial components. More specifically, the NOD 2 gene is responsible for the recognition of Muramyl dipeptide which is produced by the degradation of peptidoglycan, which is found in the cell wall of both gram-positive and gram-negative bacteria via its leucine-rich repeats (Van Limbergen, Wilson et al. 2009). The NOD2 gene has been one of the strongest genetic determinants of genetic Crohn's-disease susceptibility (Barrett, Hansoul et al. 2008).

Along with NOD 2, several other PRR genes have been implicated in IBD causation. Toll-Like Receptor 4 (TLR4) is another PRR that has drawn a

lot of interest as to what role it might play in IBD. TLR4 is found on cell membranes and binds to a number of bacterial products such as LPS (Van Limbergen, Russell et al. 2007). Others have also proposed that the TLR4 receptor has evolved to bind specific molecules such as defensins, uric acid, LPS, peptidoglycan, and other immunostimulatory microbial products such as flagella (Seong and Matzinger 2004). The CARD9 gene also has possible links to IBD. CARD 9 possesses functional properties linking TLR and NOD2, as well as C-type lectins, with the adaptive immune response, most notably T-cell differentiation and development of Th17 cells (Bertin, Guo et al. 2000; Gross, Gewies et al. 2006; Hsu, Zhang et al. 2007).

Responding to the signaling of the innate immune response (such as PPRs) is the next step in the defense mechanism against specific pathogens after recognition. The differentiation of lymphocytes to respond to different types of tissue-specific inflammation is at the level of T-helper cells (Bettelli, Korn et al. 2008). The differentiation of naïve T cells can take several different paths, and the path that the T-cell differentiation takes determines whether a pro-inflammatory or an anti-inflammatory response is mounted. This differentiation is determined by clusters of differentiation markers, effector-cytokine profiles, and transcription factors. Differentiation into anti-inflammatory T cells is due to TGF β activity via the SMAD molecules, IL27, and ICOS signaling (Awasthi, Carrier et al. 2007;

Liu, Zhang et al. 2008; O'Garra, Stockinger et al. 2008). In the gut, ICOSLG (inducible T-cell costimulator ligand) is a costimulatory molecule expressed on intestinal epithelial cells; certain germline mutations have been recently identified as contributing to the genetic susceptibility for Crohn's Disease (Barrett, Hansoul et al. 2008).

Differentiation into pro-inflammatory T cells such as Th1 cells is influenced by IL-12 and interferon-γ, while Th2 cells are influenced by IL-4 and IL13, and Th17 cells differentiate when influenced by TGFβ and IL6 (Bettelli, Korn et al. 2008; Galli, Tsai et al. 2008). Germline mutations in the pro-inflammatory or anti-inflammatory signaling pathways have led to genetic susceptibility to IBD.

Several autophagy genes have also been identified as contributing to a genetic susceptibility to IBD. Autophagy involves the delivery of portions of the cytoplasm to the lysosome for degradation (Barrett, Hansoul et al. 2008; Mizushima, Levine et al. 2008). ATG16L1 is an autophagy gene crucial for Paneth cell biology in the ileum (Cadwell, Liu et al. 2008; Kuballa, Huett et al. 2008). It has been shown that ATG16L1-deficient Paneth cells have abnormalities in the pathway that regulates granule exocytosis (Cadwell, Liu et al. 2008). Other studies have also shown that ATG16L1-deficient mice display an increased severity of disease with the dextran sodium sulfate-induced colitis model (Saitoh, Fujita et al. 2008).

Such autophagy defects found in gut cells have been shown to be contributing factors for Crohn's disease (Van Limbergen, Wilson et al. 2009). IRGM is another autophagy gene that has been linked to genetic susceptibility to IBD. IRGM is responsible for controlling intracellular pathogens through autophagy (Collazo, Yap et al. 2001). IRGM plays a role in protecting mature effector CD4+ T lymphocytes against IFN-γ-induced autophagic cell death; IRGM acts via a feedback mechanism in the Th1 response that limits the detrimental effects of IFN-γ on effector T-lymphocyte survival (Feng, Zheng et al. 2008). A common deletion polymorphism in the promoter region of IRGM can affect the efficacy of autophagy (McCarroll, Huett et al. 2008).

There are also several genes that aid in the maintenance of the epithelial barrier. For instance, Peltekova et al. identified mutations in the organic cation-transporter genes (OCTN 1&2) that are located on the IBD5 locus. They found that these mutations had an association with the TC-haplotype and increased susceptibility to CD in their Canadian population (Peltekova, Wintle et al. 2004). Further analysis of the IBD5 locus has shown that disruptions of several other genes within this cytokine gene cluster are also possible causative agents for IBD (Reinhard and Rioux 2006; Silverberg, Duerr et al. 2007). Another gene that plays a role in maintenance of the epithelial barrier is DLG5 (Drosophila-discs large-homolog 5). This gene is a member of the MAGUK (membrane-associated

guanylate kinase) family found on chromosome 10 (Stoll, Corneliussen et al. 2004). MAGUK proteins are used to form scaffolds for other proteins that are needed for intracellular signal transduction. A mutation in this gene can lead to a disruption in the intregity of the epithelial barrier (Van Limbergen, Russell et al. 2007). ITLN1 is a mammalian calcium-dependent lectin that is expressed in Paneth and goblet cells and plays a protective role in the innate immune response (Tsuji, Uehori et al. 2001; Wrackmeyer, Hansen et al. 2006). This ITLN1 intelectin serves as an organizer and stabilizer of the brush-border membrane. A mutation in this gene can lead to the breakdown of the brush border (Wrackmeyer, Hansen et al. 2006). Heavily sulfated membrane glycoproteins, such as Muclin, are products of DMBT1 (deleted-in–malignant-brain-tumors 1) and are strongly expressed in organs of the GI tract. Dysregulated intestinal DMBT1 expression due to mutations in NOD2/CARD15 may contribute to the pathophysiology of barrier dysfunction (Rosenstiel, Sina et al. 2007; De Lisle, Xu et al. 2008).

1.2 Gut Microbes

Most of the microbes found in the gut fall into the category of commensal bacteria. Commensal bacteria can be found on body surfaces covered by epithelial cells that are exposed to the external environment, e.g. the skin, the respiratory tract, and the gastrointestinal tract (Tlaskalova-Hogenova, Stepankova et al. 2004). The gut itself is home to about 10^14 bacteria which can be classified into hundreds of different species (Zoetendal,

Vaughan et al. 2006). The microbes found in the gut play an essential role in gut development, gut immunity, digestion of food, and energy uptake.

Bacterial interaction helps in the development and maintenance of gut sensory and motor functions, such as the promotion of intestinal propulsive activity (Barbara, Stanghellini et al. 2005). Germ-free animals have restricted and slower-migrating motor complexes than do their conventional counterparts (Strandberg, Sedvall et al. 1966). Microbes also influence epithelial villus lengths, increase the turnover time of epithelial cells (Savage, Siegel et al. 1981), promote the development of villus capillary networks (Stappenbeck, Hooper et al. 2002), increase the population of mucin-producing Goblet cells (Kandori, Hirayama et al. 1996), and change the configuration of the mucins that are being secreted (Bry, Falk et al. 1996). Gut microbes aid in the establishment of the host's mucosal immune defenses. Germ-free mice have very immature spleens and lymph nodes (Bauer, Horowitz et al. 1963), as well as poorly developed Payer's patches (Yamanaka, Helgeland et al. 2003). Interestingly, the decreased motor complexes and the immature immune systems found in germ-free mice seem to be reversed when these animals become colonized by the gut microflora of conventional animals (Husebye, Hellstrom et al. 1994).

The presence of microbes in the gut also provides the host with protection against potentially pathogenic microbes. The presence of commensal microflora has been shown to negate the colonization efficiency of other bacteria (Lievin-Le Moal and Servin 2006). However, although gut microflora play an essential role in gut immunity, it is also important for the host's mucosal immune system to develop a tolerance to these commensal population, so that the continuous exposure to the antigens produced by these microbes does not stimulate an immune response (Neish 2009). Dysregulation of the intestinal immune response to normal gut microflora is thought to play an essential role in inflammatory diseases such as IBD (Elson and Cong 2002).

Along with a genetic predisposition, another contributing factor for IBD is the interaction between the host and the gut microbes. Currently, there are several theories about how these microbes interact with the host. One theory is that IBD is caused by a specific pathogenic infection in the intestine. Another theory is that subtle changes in bacterial function and/or overall composition are causative factors. Other researchers believe that IBD is due to an over-reaction to normal gut microbes as a result of a defective mucosal barrier, and, lastly, it may be due to a loss of tolerance to normal luminal antigens (Farrell and LaMont 2002).

Because of the high occurrence of Crohn's disease in areas of highest luminal bacterial concentrations, many microbial pathogens have been suggested to be the triggering factor (Sartor 1997). Pathogens such as *Mycobacterium paratuberculosis* and *Listeria monocytogenes* have been explored as possible triggers of IBD. Interest in *Mycobacterium paratuberculosis* arose from the discovery of the presence of M. *paratuberculosis* in some CD tissues that were not present in tissues of patients with other diseases (Chiodini, Van Kruiningen et al. 1984; Abubakar, Myhill et al. 2007). Currently, 12 cultures from five different centers in three different continents have yielded identical strains of M. *paratuberculosis* from CD patients. Other studies have shown non specific humoral and cellular immune responses to mycobacterial species suggesting continuous exposure or defective immunosuppression to luminal bacteria (Ibbotson, Lowes et al. 1992; Walmsley, Ibbotson et al. 1996). However epidemiological data does not support the mycobacterial theory since there is no evidence that there is an increased occurrence of CD in spouses of patients or physicians treating CD patients (Afdhal, Long et al. 1991; Gui, Thomas et al. 1997; Thomas, Swift et al. 1998). *Listeria monocytogenes* is another possible pathogen that has been explored, it is a human pathogen that is found in cheese and other foods. L. *monocytogenes* invades M cells in the intestine producing experimental ileocolitis (Farrell and LaMont 2002). One study was able to show by immunohistochemistry in macrophages and giant cells in the involved

mucosa of 75% of CD patients compared with 13% of UC patients and 0% of control patients. Positive serology of L. *monocytogenes* was also found in 30% of CD while only found in 8% of controls. However these results were limited to 2 families found in rural France and previous investigators have not been able to show similar results in either positive cultures of serological tests (Liu, van Kruiningen et al. 1995). Other microbes that have been investigated include Paramyxovirus (Bernstein and Blanchard 2000; Bernstein, Rawsthorne et al. 2007), *Chlamydia* (Schuller, Piket-van Ulsen et al. 1979; Chen, Li et al. 2002), *Shigella, Salmonella, Yersinia, Campylobacter* (Sibartie, Scully et al.; Linskens, Huijsdens et al. 2001), *Saccharomyces cerevisiae* (Koutroubakis, Drygiannakis et al.; Paganelli, Pallone et al. 1985), Coccoid rod bacteria such as *Eubacteria, Peptostreptococcus,* and *Coprococcus* (Van de Merwe, Schmitz et al. 1981), and *Escherichia coli* (Tabaqchali, O'Donoghue et al. 1978). Some of these investigations have lead to some positive results but none of them have provided convincing evidence that they do play an important role in the onset of IBD. *E. coli* has recently been further investigated since it has been discovered that the *E. coli* of IBD patients is more adherent to epithelial cells then those of normal controls(Wine, Ossa et al. 2009). This adhesive ability allows for *E. coli* to colonize the mucosa and prevents it from being mechanically removed in the intestine. Studies on these properties have lead to the general conclusion that IBD associated *E. coli* are able to adhere to many human cells along with various cell lines

(Rolhion and Darfeuille-Michaud 2007). A comparison of adhesive properties of *E. coli* strains isolated from CD patiens showed 80% of *E. coli* strains with adhesive properties present in the CD patients and only 30% of these *E. coli* present in the controls (Darfeuille-Michaud, Neut et al. 1998). The invasive properties of *E. coli* have also been studied. Invasive bacteria have the ability to invade a wide range of epithelial cell lines and cause lesions. Three independent studies have reported the presence of intramucosal *E. coli* in IBD patients or mucosa-associated *E. coli* with invasive properties. These bacterial were found in 29%-36% in CD patients, 12%-19% of UC patients and only 3%-9% of controls (Darfeuille-Michaud, Boudeau et al. 2004; Rolhion and Darfeuille-Michaud 2007)

Evidence to support the theory that subtle changes in bacterial function or overall composition in the pathogenesis of IBD comes to us via animal models and human studies. There are several types of experimental animal models all of which are considerably variable from each other. However, one constant throughout all these models is their dependence on the presence of microflora in order to facilitate the onset of full disease. In many of these gene knockout or transgenic animal models, colitis is observed to occur spontaneously. But in germ-free or gnotobiotic animals or even animals treated with broad spectrum antibiotics, inflammation in the mucosa does not occur or is significantly attenuated (Farrell and

LaMont 2002). Work in this area has been slow since at least half of the microflora present in the gut cannot be cultured. The microfloral population is regulated by several factors including diet, pH, redox potential, motility, non-absorbed dietary and host derived carbohydrates, antibiotics, and host genetic characteristics (Van de Merwe, Stegeman et al. 1983; Simon and Gorbach 1984). Since redox potential, pH and short chain fatty acid concentrations stay relatively stable when diet and antibiotic use is unaltered, any subtle change in bacterial function can have implications for mucosal barrier function and immunity (Farrell and LaMont 2002). Human studies have also shown that the composition of luminal bacteria in patients with IBD have a reduced number of beneficial bacteria such as *Bifidobacterium* and *Lactobacillus* while also having an increase in pathogenic bacteria like *E. coli* or *Bacteroids (Darfeuille-Michaud, Neut et al. 1998; Swidsinski, Ladhoff et al. 2002).* Other studies have also shown that the concentrations of mucosal becteria are lower in controls and higher in patients with IBD and more specifically in CD (Swidsinski, Ladhoff et al. 2002). Swidsinski et al found that the concentration of mucosal bacteria was greater than 10^9/ml in 90% - 95% of IBD patients while these concentrations were only found in 35% of controls (Swidsinski, Weber et al. 2005).

A defect in the mucosal barrier of the intestine is another theory that has been investigated as a contributing factor towards IBD. A defective

mucosal barrier would allow for increased absorption of bacterial antigens and pro-inflammatory molecules such as the endotoxin lipopolysaccharide (Farrell and LaMont 2002). It has also been observed that mucosal permeability is increased in diseases such as IBD. But it is unknown whether the increase in permeability is a primary event in the onset of IBD or if it is the result of another trigger such as smoking or the use of nonsteroidal anti-inflammatory drugs (NSAIDs). Nevertheless an increase in antigens can lead intestinal immune cells to secrete cytokines and reactive oxygen metabolites that lead to local damage(Sartor 2000). Furthermore, the observations that relatives of CD patients also had enhanced mucosal permeability (Hollander, Vadheim et al. 1986; May, Sutherland et al. 1993), and evidence of an excessive response to NSAIDs , and that the symptomatic IBD patients had a permeability defect all lead to an underlying defect in intestinal permeability (Hilsden, Meddings et al. 1996; Sartor 1997). Whether the increase in mucosal permeability is considered a primary or secondary event, it is established that injury in experimental IBD requires the presence of microflora, and studies have shown that the presence of flora in the intestine influences the function and structure of the mucosa. The presence of bacteria can further enhance mucosal permeability and establish a self sustaining cycle of inflammation and uptake of bacterial antigens (Gordon, Hooper et al. 1997; Shanahan 2000).

A loss of tolerance to normal bacterial antigens is another possible factor contributing to the onset of IBD. It is possible that normal bacteria may induce IBD in patients if there is an abnormal response from the host immune system. The progression or regression of this inflammatory response then responds to the balance between pro-inflammatory and anti-inflammatory cytokines being produced. Indeed, recently, in an animal model, commensal bacteria were used to induce pro-inflammatory mediator, such as transforming-growth factor-beta (TGF-β), activity, which led to intestinal fibrosis (Mourelle, Salas et al. 1998). This is exactly what was done with an animal model of colitis. Researchers took T cells from colitic mice and “transferred” those T cells and their IBD to other mice (Brandwein, McCabe et al. 1997). Another study took an animal model of colitis and proliferated mucosal T cells in vitro by exposing them to cecal bacteria; however, these same T cells did not proliferate when exposed to food or intestinal epithelial-cell antigens (Cong, Brandwein et al. 1998). It is thus the combination of immune stimulation and the targeted disruption of immunosuppressive cytokines, like IL 10, that results in the unopposed activation of macrophages and other immune cells and leads to the development of colitis when the gut is stimulated by luminal microflora (Berg, Davidson et al. 1996).

1.3 Gut Metabolism

Bacteria found in the gut are also essential to a number of metabolic processes that occur in the intestines; these processes include

fermentation of dietary residues, generation of short chain fatty acids, and vitamin synthesis (Saemann, Bohmig et al. 2002). The bacterially-related salvaging of energy can be deduced from the fact that germ-free rodents require 30% more energy from their diets and require supplementation with vitamins K and B for growth (Savage 1986). The human digestive system is poor at digesting complex carbohydrates such as starch and relies on the microbe population found within the gut to digest these carbohydrates through fermentation. Fermentation leads to the creation of a slurry of organic acids including short-chain fatty acids like butyrate and succinate (Topping and Clifton 2001; Hooper, Midtvedt et al. 2002). Butyrate, for example, can have affects on cell proliferation, membrane synthesis, and sodium absorption; it has even been shown to be protective against colorectal cancer (Zampa, Silvi et al. 2004). Short-chain fatty acids are also an important source of energy for colonic epithelium and for the host; it has been estimated that they account for anywhere from 5% to 15% of human energy requirements (Bergman 1990).

Several studies on metabolomics (see section 1.5) and IBD have been conducted. Although the methods used, and the samples studied, vary, the studies are all similar in that they measure small molecular metabolites in hopes that they can identify biomarkers that are significant for either finding the cause of the disease or aiding in the diagnosis. Studies of both humans and mice have made use of Nuclear Magnetic Resonance (NMR)

spectroscopy or Mass Spectrometry (MS) and have been done on urine, stool, and blood (Marchesi, Holmes et al. 2007; Murdoch, Fu et al. 2008; Lin, Edmunds et al. 2009; Martin, Rezzi et al. 2009; Williams, Cox et al. 2009). Marchesi et al. took fecal extracts from patients with either CD or UC and obtained 1H NMR spectra results from the fecal extracts. They found that patients with IBD had reduced levels of butyrate, acetate, methylamine, and trimethylamine compared to normal controls. They suggest that this is due to changes in the gut flora community. They also observed that there were increased levels of amino acids in the IBD groups, findings which they attributed to malabsorption (Marchesi, Holmes et al. 2007). Lin et al. collected spot urine samples from wild-type and IL-10 KO mice at ages 5.5, 7, 8.5, and 10.5 weeks of age. They used gas chromatography-mass spectrometry (GCMS) to analyze their urine samples. They found elevated levels of xanthurenic acid and fucose in the IL-10 KO mice, relative to the wild-type results, and attributed these elevations to tryptophan catabolism and perturbed fucosylation in the IL-10 KO mice. They also suggested a down-regulation of fatty-acid oxidation in the IL-10 KO mice due to decreased levels of three short-chain dicarboxylic-acid metabolites (Lin, Edmunds et al. 2009). Martin et al. also used IL-10 KO mice, but they took blood plasma samples from the mice at ages 1, 8, 16, and 24 weeks of age. They also obtained ^{1}H NMR spectra result. They observed that the IL-10 KO mice had decreased levels of VLDL and increased LDL and polyunsaturated fatty acid concentrations. In

addition, they found elevated levels of lactate, pyruvate, and citrate, as well as lower glucose concentrations, were attributable to an increase in glycolysis and fatty-acid oxidation, while higher levels of free amino acids suggested muscle atrophy and protein breakdown (Martin, Rezzi et al. 2009). The Williams et al. study was conducted on humans. They collected urine samples from a group of 206 subjects. The number breaks down into 86 CD patients, 60 UC patients, and 60 controls. Once again, they obtained 1H NMR spectra results and found that levels of hippurate, formate, and 4-cresol-sulfate levels were significantly different between CD, UC, and control groups. Using multivariate statistical methods, the researchers were also able to distinguish the different groups on their multivariate statistical plots (Williams, Cox et al. 2009).

1.4 IL-10 KO mouse model

The cytokine IL 10 is an essential immunoregulator in the GI tract (Kuhn, Lohler et al. 1993). Its purpose is to physiologically limit and down-regulate inflammation by affecting the activation, growth, and differentiation of many pro-inflammatory cytokines and cells (de Waal Malefyt, Abrams et al. 1991). At a young age, the IL-10 gene-knockout mouse is observed to have a normal lymphocytic development and antibody response, but, as the mice begin to age, they develop anemia, growth retardation, and a chronic inflammatory bowel disease (IBD) (Elson, Sartor et al. 1995). These developments are thought to be due to the absence of the general suppressive effect of IL 10 on the production of

pro-inflammatory mediators by macrophages and Th1-like T cells, leading to an unregulated Th1 response (Kuhn, Lohler et al. 1993). This model develops a chronic colitis with macroscopic and histological similarities to the human form of colitis. The spontaneous development of intestinal inflammation is distinguished by transmural and discontinuous lesions that can be found in the small and large intestines and also by a dysregulated production of proinflammatory cytokines (Rennick and Fort 2000). In a manner similar to other models of IBD, bacteria here appear to be the driving force that stimulates the development of colitis in this model, since if the mice are kept in germ-free conditions, they do not develop inflammation (Kuhn, Lohler et al. 1993). However, with these mice, the onset of disease occurs just after they have been removed from their germ-free environments and been colonized by bacteria. This onset timing suggests that the disease localizes in the intestine because of the strong antigenic presence of the newly-established bacterial flora (Elson, Sartor et al. 1995). Inflammatory processes are marked with the associated diarrhea, increase in protein catabolism, and loss of lean-tissue mass, as well as loss of appetite (Caligiuri, Rudling et al. 2003). Recent work involving both IL-10 KO mice and IBD patients has shown that the initiation of endoplasmic reticulum-mediated stress responses in intestinal epithelial cells might also be a factor contributing towards a chronic inflammatory state in the intestine (Shkoda, Ruiz et al. 2007).

1.5 Metabolomics

Metabolomics is the newest addition to the scientific family of “omics.” Other family members include genomics, proteomics, and transcriptomics. The scientific “family” approach of the “omics” is used to try and gain a greater understanding of global-systems biology (S. Rochfort 2005).

Terms

Metabolomics is such a new science that often the terms metabolomics and metabonomics are used incorrectly or they are interchanged. Metabolomics has been defined as a non-biased identification and quantification of all metabolites in a biological system under defined conditions, and it usually combines many analytical technologies (W. B. Dunn et al 2005; Q. Z. Wang 2005), while metabonomics is the quantitative measurement of the dynamic multiparametric metabolic responses of living systems to pathophysiological stimuli or genetic modification (W. B. Dunn et al 2005). For our purposes, metabolomics will be defined as a science that entails the study of entire metabolite profiles in systems like cells, tissues, or other organisms that are subjected to a given condition (S. Rochfort 2005). Metabolite profiling is a technique that quantifies a series of metabolites in one or several metabolic pathways (Q. Z. Wang et al 2005). A metabolite profile is constructed by collecting the metabolites that are produced when a system is placed into a given environment. These metabolites result from the interaction of the

system's genome with its environment and are not simply the end-products of gene expression; in fact, they form part of the regulatory system in an integrated manner (S. Rochfort 2005). The metabolome is the final downstream product of the genome and is classified as the total quantitative collection of small molecular-weight compounds (metabolites) that are produced by gene expression (W. B. Dunn et al 2005). The metabolome represents a comprehensive data set that defines the small molecules present in a system. The information that is contained in this data set should theoretically make it possible to understand the relationships and trends between different metabolite levels and of cell responses to nutritional and chemical stimuli, as well as with responses to disease and stress (M. G. Miller 2006).

Characteristics / Potential

Compared to the proteome or transcriptome, the metabolome is the most diverse in terms of chemical and physical properties because of the variations in the atomic arrangements of metabolites (W. B. Dunn et al 2005). The scientific power of metabolomics comes from its ability to produce a complete compositional representation of individual biological samples that can be used for comparison (J. B. German et al. 2005). It is this sensitivity that gives metabolomics the potential to revolutionize an entire field of scientific discovery and possibly some day allow for an all-encompassing approach to understanding total, yet fundamental, changes

that occur during normal and abnormal cell function, disease activities, and drug interactions (S. Rochfort 2005). The study of the metabolome involves the analysis of a very wide range of chemical species. These range from low molecular-weight polar molecules like ethanol to high molecular-weight polar glucosides, non-polar lipids, and inorganic species (W. B. Dunn et al 2005). The concentration of metabolites also spans a large range. Metabolite concentrations can vary over nine orders of magnitude (pM-mM) (W. B. Dunn et al 2005).

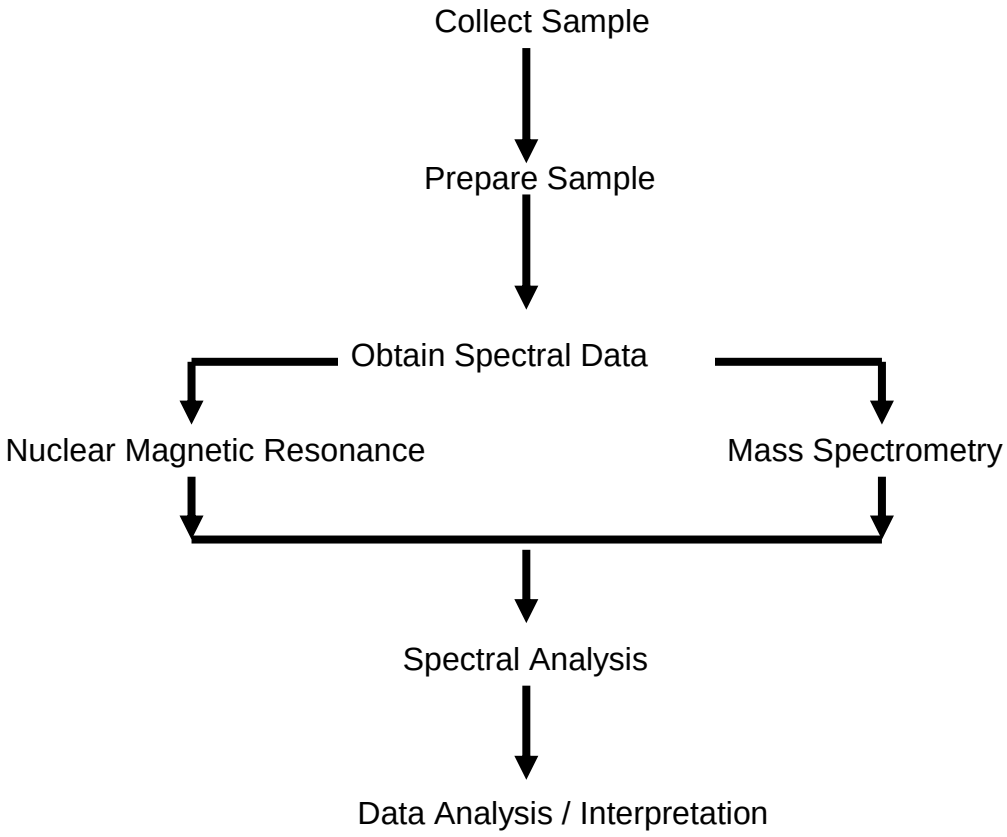

Figure 1.5.1 – Typical metabolomics workflow

Brief History

The first publication relating to the concept of metabolic profiles appeared in 1971 and was authored by Horning and Horning (Horning 1971).This paper appeared many years before Stephen Oliver would first suggest the name of “metabolomics” in 1998 (Oliver, Winson et al. 1998) In 2002, Fiehn published a fairly comprehensive review of metabolomics studies but focused mainly on plants (Fiehn 2002). Also in 2002, Kell (Kell 2002) published a paper addressing the comprehensive metabolic footprint, and in 2003, Allen et al. (Allen, Davey et al. 2003) published a paper that also addressed metabolic footprinting. The history of these papers was obtained from a review by Wang et al. (Wang, Wu et al. 2006). Figure 1.5.2 shows the results of a recent PubMed search of metabolomics-related papers on a per-year basis.

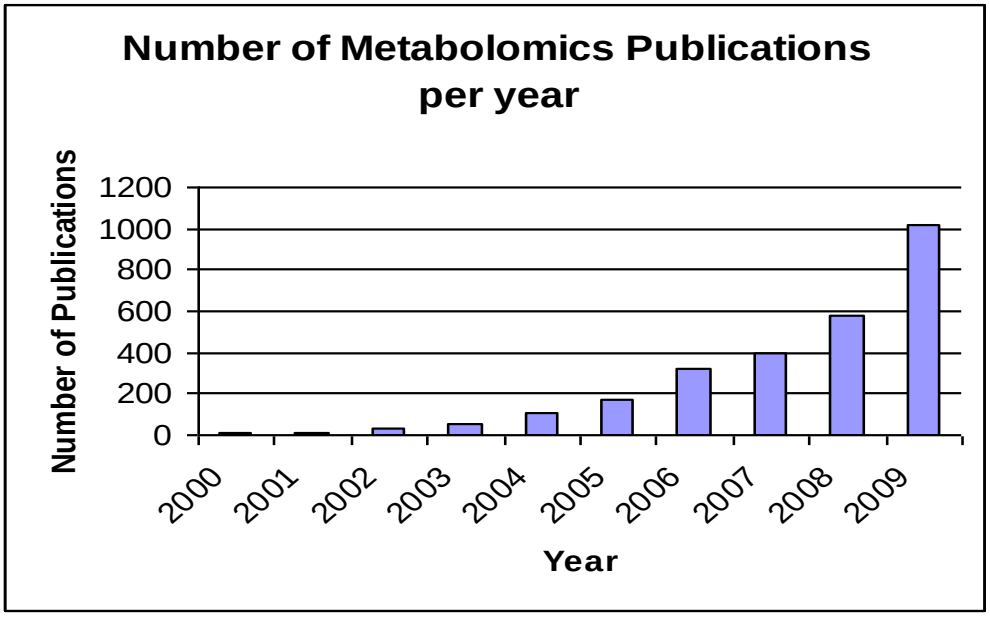

Figure 1.5.2 – Number of metabolomics based publications in a given year, generated from a PubMed search

Techniques

Since metabolomics is such a new science, there is no single method that can be used to analyze data. In a perfect world, a universal metabolomics platform would contain certain features. The first feature would be that it would be able to measure as many metabolites as possible from a single sample. The second feature would be that it would yield rigorously quantitative data. This is important for mapping the results of the analysis to biochemical pathways, for comparison of individual results to population averages, and for ease of storage in a permanently-integrated database. The last feature would be that the platform has a high throughput, is capable of producing data from small biological samples, and is inexpensive to operate. Given that no analytical technique is able to meet all of these criteria, we must rely on a combination of techniques (S. M. Watkins et al. 2002). Two of the most common techniques currently being used to study metabolites are Nuclear Magnetic Resonance (NMR) and Mass Spectrometry (MS). Other techniques used include combining techniques such as Gas Chromatography (GC), High Performance Liquid Chromatography (HPLC), and Capillary Electrophoresis (CE) with the popular MS technique. Vibrational spectroscopy techniques, such as Fourier Transform-Infrared spectrometry (FT-IR) and Raman spectroscopy, can also be effective methods of data analysis (S. Rochfort 2005; W. B. Dunn et al. 2005)

Nuclear Magnetic Resonance

NMR has been widely used in metabolomics studies for the last 20 years (W. B. Dunn et al. 2005). NMR works by taking advantage of the spin properties of the nucleus of atoms (S. Moco et al. 2007). The spin-spin coupling of the atoms indicates the number and nature of nearby nuclei, along with their electromagnetic connectivity. Along with the spin properties of the atom, chemical shifts in the NMR spectrum give information on the nature of the chemical environment in which the nucleus is located (W. B. Dunn et al. 2005). An NMR spectrometer is comprised of 4 major parts. The first part is a stable magnet. The second part is a radio-frequency transmitter used to emit a precise radio frequency (RF). The third part is a detector, which measures the amount of RF that is absorbed by the sample. The final piece is a computer, used to record the amount of energy absorbed (RF) as a function of the magnetic field strength (L. G. Wade 2003). While the ^{1}H nucleus is the nucleus most commonly used in NMR spectroscopy metabolomics, the carbon 13 nucleus (^{13}C) has also be used. In ^{13}C NMR spectroscopy, the chemical shift can be up to 20 times greater and the spin interactions may be removed because of decoupling. These results give the user the opportunity to significantly reduce the complexity (simplify) of the spectrum acquired in terms of the resonance overlap from common nuclei (W. B. Dunn et al. 2005). ^{13}C NMR spectroscopy also does not require solvent suppression for aqueous samples, while ^{1}H NMR spectroscopy requires

solvent suppression for aqueous samples, possibly leading to the loss of some spectral information (W. B Dunn et al. 2005).

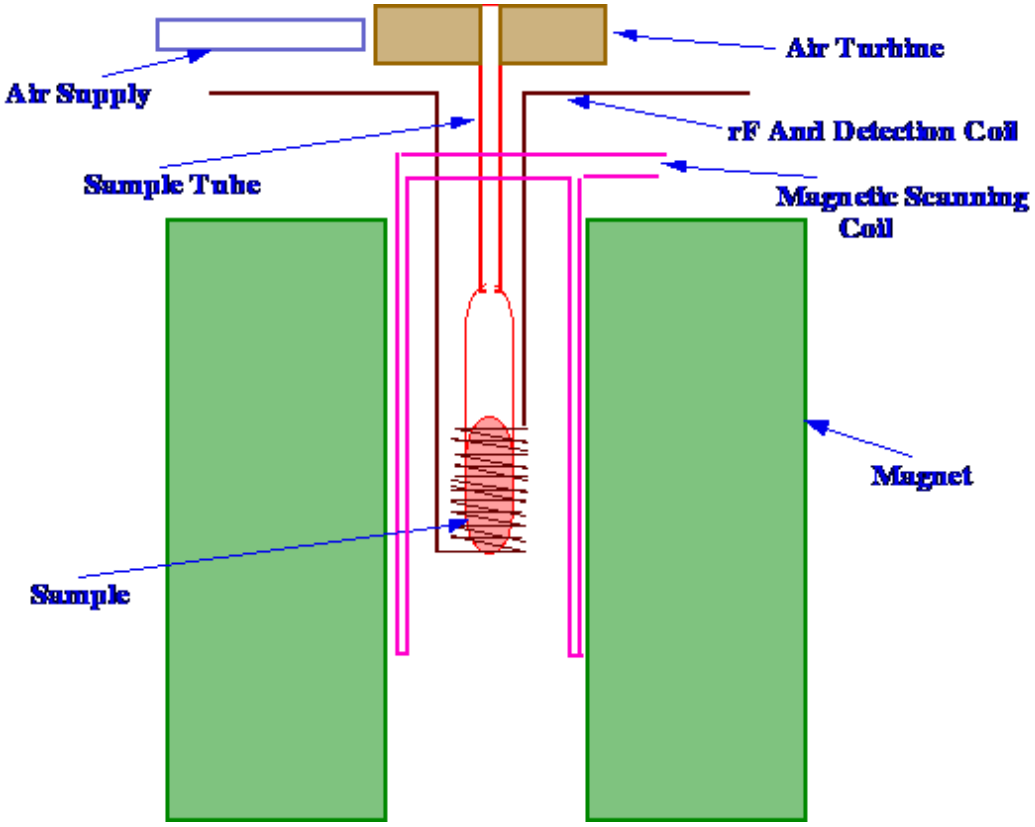

Figure 1.5.3 – Schematic of an NMR

(http://www.analyticalspectroscopy.net/ap7_html_m4ebd312e.gif)

NMR has many advantages. One advantage to NMR is that it is specific but it is not selective. This means that every resonance that is recorded in an NMR spectrum is unique to a particular compound, and each resonance peak also helps to provide information about the structural components of the sample (W. B. Dunn et al. 2005). Rather than measure individual metabolites, an NMR is able to profile all of the proton magnetic resonances that can be induced within a sample; this broad ability means

NMR is a quantitative, non-destructive technique that can obtain high-resolution spectra results for a variety of biological fluids (J. B. German et al. 2005). Another advantage to using NMR for metabolomics studies is that, since it is a non-destructive technology (W. B. Dunn et al. 2005), the sample can be recovered after analysis and saved in case the sample has to be run again or for future reference. NMR spectroscopy can also be used to analyze intact tissues (brain or kidney) through a technique known as magic-angle spinning (MAS). The analysis of a solid or a semi-solid sample on a conventional NMR would result in very broad lines and a loss of spectral information. This is due to the fact that the solid or semi-solid sample is not homogeneous; thus, it would not provide a constant sample for the NMR. However, in the MAS-NMR technique, the tissue sample is spun very fast (usually at a few kHz) at the “magic angle” of 54.7° and in the direction of the magnetic field. This process eliminates the broad lines that are caused by the inhomogeneity and restores ability to record the information present in the sample. The MAS technique is one of the most powerful tools used in metabolomics analysis (W. B. Dunn et al. 2005). NMR is an effective analytical technique because it is able to provide unambiguous information about a molecule. The NMR can elucidate chemical structures, and provide highly specific characteristics for the identification of a molecule. Also, since the number of nuclear spins is directly related to the intensity of the signal, NMR is a quantitative technique (S. Moco et al. 2007).

NMR techniques have been utilized in many studies. One such study used NMR to identify the metabolic phenotype of silent mutations in yeast by a method termed functional analysis by co-responses in yeast (FANCY). The researchers analyzed two strains of yeast which had mutations in either the PFK 26 or PFK 27 gene (each gene encodes one copy of 6-phosphofructo-2-kinase). The researchers were able to confirm the effect of each deletion on the metabolic profile. They were also able to identify the difference between the single mutations and a phosphofructokinase-deficient mutation (S. M. Watkins et al. 2002). Another group was able to identify the metabolic differences between strains of inbred mice. The researchers profiled the urine of C57BL10J and Alpk:ApfCD mice, and they used principal-components analysis to demonstrate that the profiles of excreted metabolites were well-clustered according to mouse strain (S. M. Watkins et al. 2002).

Mass Spectrometry

Mass Spectrometry (MS) is another technique that has been utilized in the study of metabolomics. MS can either be used by itself or in combination with another type of chromatography to identify metabolites. A mass spectrometer works by taking the sample, bombarding it with electrons, and breaking the molecule apart. Then the spectrometer registers the molecular weight of each fragment produced. Sometimes it is also possible to determine the molecular formula, but this is not always the

case. The data collected using a mass spectrometer can also provide clues to a molecule's structure and to the presence of functional groups (L. G Wade 2003).

Using MS for metabolomics analysis also has many advantages. One advantage of MS is that its sensitivity allows for the detection of metabolites at concentrations which are orders of magnitude lower than those detectable by NMR (J. B. German et al. 2005). Usually when MS techniques are used in metabolomics analysis, MS is combined with a prior separation method (S. Moco et al 2007). The techniques used to separate the sample before MS are gas chromatography (GC), high-performance liquid chromatography (HPLC), and capillary electrophoresis (CE). The principal advantage to using these classic detection techniques is that they can be focused to provide quantitative data suitable for creating an integrated and seamless database of metabolite concentrations (S. M. Watkins et al. 2002), thus allowing for the accurate identification of specific metabolites .

Gas Chromatography – Mass Spectrometry

GC-MS-based metabolomics applications for the analysis of volatile and thermally stable polar and non-polar metabolites have been developed very quickly (W. B. Dunn et al. 2005). GC can provide rigorous quantitative analyses, but it has often been criticized as slow and ill-suited for high-throughput platforms (S. M. Watkins et al. 2002). Although this

was initially a problem, new technologies such as fast GC and robotics have helped increase the throughput of these techniques (S. M. Watkins et al. 2002). in one study, biomarkers of adrenarche were examined for a large study group of 400 subjects using GC-MS techniques, while a variation of GC-MS technology known as GC-TOFMS (Time-Of-Flight Mass Spectrometry) has been employed in the analysis of the metabolites produced in rye grass (S. Rochfort 2005).

High Performance Liquid Chromatography – Mass Spectrometry

Early on in metabolomics studies, technological limitations of the HPLC-MS interfered with its initial development and wide-spread application. This was due to the difficulties of introducing liquids at high pressure into low-pressure vacuum regions and analyzing thermally labile analytes at high temperatures (W. B Dunn et al. 2005). However, technological advances in HPLC-MS have allowed it to become a standard analytical tool for qualitative and quantitative analysis of potential pharmaceuticals and their related metabolites; it is used in many study steps, from initial discovery to very large-scale production (W. B Dunn et al. 2005). One problem that still seems to plague the HPLC is that, even with technological advances like fast liquid chromatography, the technology is still considered very slow, not a high-throughput platform of analysis (S. M. Watkins et al. 2002).

Capillary Electrophoresis – Mass Spectrometry

CE-MS operates on a similar matter to the HPLC-MS technique. Metabolites are first separated by chromatographic separation of ion species and size. This is followed by the application of a high voltage and then the ions are selectively detected using MS (W. B. Dunn et al. 2005, J. C. Lindon et al. 2007). One advantage to using CE is its high chromatographic resolution, sensitivity, and fast separation of charged metabolites, but the technique is not, as of yet, well-used in metabolomics (W. B. Dunn et al. 2005).

Other techniques

Although mass spectrometry and NMR are the most common techniques used, other techniques have been employed for metabolomics work with some success. Techniques such as Fourier Transform Infrared (FTIR) spectroscopy and High-Performance Liquid Chromatography coupled with Ultraviolet-Visible spectroscopy (HPLC-UV) can also be used. FTIR approaches have shown a potential for profiling salt-stressed tomatoes and for analysis of urine for pharmaceutical product absorption, distribution, metabolism, and excretion studies (S. Rochfort 2005). Using methods like HPLC-UV in combination with statistical grouping can also be effective. This approach has been used to profile phenolic compounds in lignin biosynthesis, to determine the metabolic differences between patients with hepatitis and liver cancer, and to separate transgenic from

wild-type plants (S Rochfort 2005). Although these techniques can be used, they are not considered high-throughput techniques and could not be effectively used to handle a large load of samples (S. M. Watkins et al. 2002).

Applications

The science of metabolomics has the potential to be applied to various fields of research. Indeed, metabolomics has already been applied to the study of plants, toxicology, nutrition, medical diagnosis, and pharmaceutical drugs (S. Moco et al 2007).

Plant Metabolomics

The interest in plant metabolomics comes primarily from the potential of the technology to provide knowledge of plant metabolism and biochemical composition for practical application in various fields. In fact, plant-based products make up a large portion of the food intake for humans regardless of financial status or location (R. D. Hall et al 2008). Plant metabolomics has played an important role in the study of plant breeding, along with measurement of the quality of crop that is being produced. It has also been used to help plants produce a higher yield (S. Moco et al 2007). Quantity of yield and quality of crop have affected the farming industry for a long time. On the one hand, farmers make their money from of the amount of their yields; the larger the yield, presumably the larger the pay

cheque. On the other hand, sometimes greater yields can lead to a lower-quality crop because the crops have been packed tighter in fields in order to produce a higher yield, and thus that crop is not provided adequate space to grow. This is why it is essential for plant metabolomics to be able to identify molecular markers and key loci that play significant roles in plant growth: to help design better crops that produce a high-quality product along with a high yield (R. D. Hall et al. 2008). Along with investigating ways to produce quality crops at a high yield, metabolomics is also helping us to better assess the components that are present in foods and the ways they are synthesized. It can also be used to help determine how genetic and environmental factors influence the composition of the food along with its stability (R. D. Hall et al. 2008). Such investigations could help keep plants fresher during storage and transport and lead to less waste of product.

Toxicology

One field where metabolomics has made a great impact on research is that of toxicology and pharmaceuticals. Metabolomics can be applied to both preclinical and clinical toxicology. There are three broad areas in which metabolomics is having and will continue to have significant impact: screening, biomarkers of safety, and mechanisms of action (D. G. Robertson 2005). Having the perfect safety screen has long been the desired gold standard for clinical toxicology. In a perfect world, this screen

would be fast, only require a very small sample, and be very accurate (D. G. Robertson 2005). Unfortunately, in order to be able to model the effects of a substance on humans, a toxicologist would need to obtain the primary human cells that he or she would like to study. But this is difficult, because such cells are hard to obtain, culture, and maintain for a reasonable amount of study time. This difficulty means that, for now, *in vivo* assessment in animal models will remain the primary method for identifying safety issues (D. G. Robertson 2005). Although there are genetic differences between species (e.g. humans, mice, rats), many of their metabolites are very similar; for example, the fat, cholesterol, and glucose metabolism in rats and humans are the same (L. Bren 2005). Metabolomics could also have a significant impact on the study of the previously-mentioned animal models. Metabolomics could be used to identify toxicity at an early stage in a drug's development; this means that fewer animals would have to be sacrificed at certain stages of a study to study tissues. This, in turn, would allow the user to reduce the amount of time and money and number of animals needed to complete a study (L. Bren 2005). An example of such a toxicological investigation is the extensive study of the effects of the hepatotoxin hydrazine in the rat model by analysis of urine and blood, pre-dose to 7 days post-dose. In these studies, dose-dependent trajectory plots showed increasing metabolic insult and recovery, with Krebs-cycle intermediates being shown to be decreased in dosed animals (W. B. Dunn et al. 2005).

Pharmaceuticals

Metabolomics could also be used prominantly in the pharmaceutical industry. A good understanding of normal biochemical profiles is necessary in order to evaluate the metabolic changes caused by xenobiotics or disease. This is why metabolomics has been used in animal model investigations to identify changes that can be attributed to factors such as aging, sex and genetic modification, as distinct from changes related to the administration of a drug (J. C. Lindon et al. 2007). Potential pharmaceutical study benefits of metabolomics include the speeding up of the discovery and development of new drugs, the making of safer drugs because of earlier predictions or identification of possible adverse effects, and the screening of particular groups of patients to determine which groups are most likely to benefit while excluding those who could be harmed by the drug (L. Bren 2005). Since metabolomics studies related to the area of pharmaceuticals are generally done with biofluids or cell/tissue extracts, these samples are relatively easy to obtain and the procedures are usually non-invasive. This set of possibilities allows for speedy “diagnosis” of a drug that is currently undergoing clinical trials (J. C. Lindon et al. 2007). Metabolomic use could allow clinical trials to identify groups of people who might have a bad reaction to a drug, which could help researchers design more effective clinical trials, only including those people for whom the drug has the most likely chance of providing a benefit while excluding those individuals for whom the drug would be toxic

or ineffective (L. Bren 2005). In addition to developing safer drugs and more effective clinical trials, metabolomics can also be used to save time and money. Metabolomics can help weed out drugs that are entirely ineffective or unsafe earlier on in development, saving the pharmaceutical companies both time and money (L. Bren 2005). Recently, pharmacology and metabolomics have been teamed up to start a new branch of study called pharmacometabonomics. Pharmacometabonomics has been used to try and predict the metabolism and toxicity of a dosing substance, based solely on the analysis and modeling of a pre-dose metabolic profile. Pharmacometabonomics is sensitive to both the genetic and the environmental influences that shape the metabolic profile of each individual (J. C. Lindon et al. 2007).

Nutrition

Metabolomics is emerging as a tool which may help provide us with the knowledge needed to aid individuals to live a healthy life and achievetheir health goals (J. B. German et al. 2005). Nevertheless, the application of metabolomics in the field of nutritional research has met with unique challenges. First off, very little is known about how changes in the nutrient content of a diet change the metabolic profile of an individual. Also, the metabolic signal produced by nutrient absorption must compete with non-nutrient signals, as well as the signals that are produced by the gut microflora present in the large bowel (M. J. Gibney et al. 2005). Although

this competition seems like a grave problem, it can be solved through the use of pattern-recognition statistics for assigned and unassigned metabolite signals and by collecting comprehensive data sets that will allow for distinguishing between different dietary treatments and baseline readings (M. J. Gibney et al. 2005).

One essential factor in living a healthy lifestyle is food. We eat food not only because it tastes good but because it provides our bodies with nourishment. However, for many people, improper food choices have lead to metabolic imbalances. Chronic imbalances in normal metabolic pathways can lead to increased risk of diseases such as atherosclerosis, obesity, type 2 diabetes, hypertension, osteoporosis, food allergies and intolerances, gastrointestinal disorders, and inflammatory diseases (J. B. German et al. 2003, J. B. German et al. 2004). Unfortunately, simply identifying that an individual has nutrient deficiencies does not provide an easy solution to the problem. In theory, the goal of many drug and food interventions is to influence single biochemical targets. But, in reality, no single drug or food influences only one biochemical target (J. B. German et al. 2003, J. B. German et al. 2004). A specific diet that is used by one individual to maintain health and quality of life might lead to obesity and metabolic imbalance in another individual (J. B. German et al 2003). Metabolomics testing could allow nutritionists the ability to personalize diets for each individual. Nutritionists would be able to assess the

nutritional statuses of their clients, then provide their clients with individualized assessments of their nutritional health and with specific diets. It will also allow the nutritionist with ways to ensure that the clients are complying with their new programs and to track their progress (J. B. German et al 2005). For instance, if an obese person wanted to lose weight, the first step would be to determine the metabolic condition of that individual, then, based on that condition, the nutritionist could recommend the specific weight-loss strategy most likely to work for that individual (L. Bren 2005).

Medical Diagnosis

Medical diagnosis is perhaps the field where metabolomics has the potential to have the greatest impact. Metabolomics is, in fact, a molecular way of doing what physicians have been doing for many years, which is to diagnose disease based on a set of symptoms (L. Bren 2005). The metabolomics approach has the potential to diagnose and predict disease earlier, determine the effectiveness of a treatment, and follow an individual's progress over time. Diseases that result from chronic metabolic imbalances do not usually produce biomarkers of damage until the disease in question has been established, but metabolomic testing may have the potential to detect subtle changes before diseases are well-established (J. B. German et al. 2003). Following an individual over time would allow for researchers to track the changes of a disease as it

progresses. Metabolomics could also be used to monitor healthy people, to ensure that they are maintaining their health (L. Bren 2005). This approach could be used to identify metabolic shifts due to external influences such as environmental and lifestyle changes, along with aging and maturation (J. B. German et al. 2005).

Currently, in medicinal testing, single biomarkers have been used as indicators of disease. For example, high levels of the metabolite cholesterol in the blood indicate that that there is an increased risk of heart disease, while an elevated level of glucose (another metabolite) is an indicator of diabetes (L. Bren 2005). But in the case of diagnosis of metabolic diseases, rarely does a single biomarker indicate that there is a metabolic imbalance causing disease. Usually, it is not the appearance or disappearance of a single biomarker, but instead it is differences in metabolite concentrations that may lead to difference between health and disease (J. B. German et al. 2003). But the aim of metabolomics will be to replace the single biomarker approach with a comprehensive profile of an individual's entire metabolic profile and to link it to assessments of health and disease (J. B German et al. 2005). With metabolomics, one could look at a broad range of potential problems by examining the entire metabolome, instead of only looking at a limited number of factors, as we currently do (L. Bren 2005). Looking at the entire metabolome will also speed up the discovery of other essential biomarkers and aid in the

transition from study of single biomarkers to a more holistic approach (R. D. Hall et al. 2008).

Of course, in order to effectively use metabolomic diagnostic tools, we need to know what is normal and what is abnormal. Thus, the first goal of metabolomics is to measure and quantify all metabolites that would be present in the biological sample being tested (J. B. German et al 2005). After this has been done, a database can be established to provide the resources to explore statistical correlations between the different concentrations and the ways they relate to phenotypic outcomes. Then, researchers will be able to apply this knowledge to molecular, cellular, and animal models, to establish which mechanisms are responsible for causing these relationships (J. B. German et al 2003). This will provide us with a greater understanding of how the metabolism works and what we can do to promote better metabolic health.

1.6 Aims and objectives

The primary objective of this project was to determine the metabolic differences between wild-type and IL-10 KO mice in both conventional and axenic environments. In the conventional environment, the metabolic profile was constructed from metabolites produced by both the host and the microbial population present in the gut. In the axenic environment, the metabolic profile was constructed only from the host. Another purpose of

this project was to determine the differences to be seen in metabolic profiles of axenic mice removed from their axenic environments and colonized with fecal bacteria.

Chapter 2 - Methods

2.1 Metabolic cage preparation

Metabolic cages were purchased from Nalgene. After construction of the metabolic cages, 100 µL of paraffin oil was added to the urine cup, to prevent the urine from evaporating during the collection timeframe.

2.2 Urine collection in metabolic cages

Having been weaned at 3 weeks of age, the mice were placed in the metabolic cages at weeks 4, 6, 8, 12, 16, and 20 weeks of age for a period of 22 hours. They were only allowed access to drinking water; they were given no food for this period of time. The urine collection cups for the metabolic cages were prepped with 100 µL of paraffin oil to prevent evaporation. After 22 hours, the mice were placed back in their normal cages and, maintained on a normal rodent diet. Urine collection was done using 1500 µL of sterile water (750 µL x 2) (set 100-1000 µL pipette to 75) in a pipette; the pipette was used to gently wash and scrape dry urine from the wire rack, funnel, and urine/stool separator. 500 µL of 0.02% sodium azide solution (set 100-1000 µL pipette to 50) was added to the urine to prevent any bacterial growth. The urine was then transferred to a labeled Corning Cryogenic Vial (4.0mL) and stored in a -80°C freezer. Urine collection from the axenic bubbles was performed by the staff of the animal facility (HSLAS). The procedure for urine collection from the axenic

bubble is the exact same procedure, without the addition of sodium azide to the sample. Sodium azide was not added to the sample because it is unnecessary in the axenic environment.

2.3 Fecal Colonization

10 pieces of stool from wild-type mice and 10 pieces of stool from IL-10 KO mice (approx. 20 weeks in age in both cases) were collected. The stool was placed in a 50 mL conical vial, and 2mL of water was added. Forceps were used to crush and mix the stool in the water to create the fecal slurry. A 100-1000 µL pipette was used to deliver 100 µL of slurry onto the belly and into the mouth of the mice. The mice were then place in metabolic cages, and the urine collection protocol for metabolic cages was used to collect the urine.

2.4 Sample Preparation (non-automation) – day before NMR acquisition

Desired samples were removed from the -80°C freezer and allowed to thaw in the biohood. While the samples were thawing, Nanosep filters were cleaned 7 times with double-distilled H_2O by spinning water through the filters in a microcentrifuge at 13x1000 rpm for 3 minutes. 65µL of DSS-d6 Chenomx internal standard (5.1436 mM DSS-d6, 0.196 %NaN3 w/v, 98% D20 v/v) were added to labeled eppendorf tubes. The unfiltered urine was then filtered through the cleaned filters until a volume of 585 µL was reached; a new filter was used for each sample. The 585 µL of filtered

urine was added to the labeled eppendorf tube already containing the Chenomx DSS-D6 internal standard. Samples were then stored overnight in a 4°C fridge.

2.5 Sample Preparation (for automation) – day before NMR acquisition

Desired samples were removed from the -80°C freezer and allowed to thaw in the biohood. While samples were thawing, Nanosep filters were cleaned 7 times with double distilled H_2O by spinning water through the filters in a microcentrifuge at 13x1000 rpm for 3 minutes. 75µL of DSS-D6 Chenomx internal standard were added to labeled eppendorf tubes. The unfiltered urine was then filtered through the cleaned filters until a volume of 675 µL was reached; a new filter was used for each sample. The 675 µL of urine was added to the labeled eppendorf tube already containing the Chenomx DSS-D6 internal standard. Samples were then stored overnight in a 4°C fridge. The increase in volume from the non-automation amount was due to robot specifications.

2.6 Sample Preparation (for non-automation) – day of NMR acquisition

Samples were removed from the 4°C fridge. Next, the Accumet XL15 pH meter was calibrated with pH buffers. After calibration, samples were pH-corrected to a pH of between 6.7 and 6.8. Solutions of 1.0 m, 0.1 m, and 0.01 m NaOH and HCl were used to achieve the proper pH for each

sample. After pH correction, 600 µL of the sample were loaded into a labeled NMR tube using Rainin 100-1000 µL pipettes (300 µL x 2), and the tube was then capped.

2.7 Sample Preparation (for automation) – day of NMR acquisition

Samples were removed from the 4°C fridge. Next, the Accumet XL15 pH meter was calibrated with pH buffers. After calibration, samples were pH-corrected to a pH of between 6.7 and 6.8. Solutions of 1.0 m, 0.1 m, and 0.01 m NaOH and HCl were used to achieve the proper pH for each sample. After pH correction, 700 µL of sample were loaded into a labeled NMR tube using Rainin 100-1000 µL pipettes (350 µL x 2), and the tube was then capped.

2.8 NMR acquisition (manual mode)

NMR acquisition was performed on an Oxford 600Hz NMR spectrometer with a Varian VNMRS two-channel console running VNMRJ software version 2.2C on a RHEL 4 host computer. The spectrometer was equipped with an HX probe with Z-axis gradients. Before samples were inserted into the spectrometer, the outside of the tubes was first cleaned with ethanol and kimwipes® to remove any debris or oils from handling. Samples (600 uL) were set to a depth of 66 mm in the depth gage and then inserted into the spectrometer. All samples were run at a sweep width (sw) of 7225.43 Hz. The saturation frequency (sfrq), transmitter

offset (tof), and pulse width (pw) were all individually calibrated at the start of each day. The tof typically ranged from (-213 to -215 Hz), and the pw ranged from 6 to 8 microseconds. Shims were optimized until an acceptable line-width value was obtained at relative peak heights of: 50% (< 1.0 Hz), 0.55% (< 12.0 Hz), and 0.11% (< 20.0 Hz). Finally, during post-processing, zero filling was used to resolve the actual acquired data points to the next higher factor of 2, and no weighting functions were applied.

We utilized the first increment of a 2D-^{1}H,^{1}H-NOESY pulse sequence for the acquisition of ^{1}H-NMR data and for suppressing the solvent signal. Experiments used a 100 ms mixing time along with a 990 ms pre-saturation (~80 Hz gammaB_1). Spectra were collected at 25°C through a total of 32 scans over a period of 3.5 minutes; a total recycle delay of 5 seconds was also used (*i.e.* a 1-second recovery delay/saturation and a 4-second acquisition).

2.9 NMR acquisition (automation mode)

Automated runs followed exactly the same experimental procedures used in the manual runs, with the exception of an additional 30 seconds of equilibration time used in the NMR in order to allow the sample to equilibrate to 25°C. All sample handling was done with a Varian 768 AS sample-handling robot. Any spectra that did not meet acceptable line-

height values were discarded and the sample was re-run. 4-inch robot tubes were used instead of the 6-inch tubes.

2.10 Post-acquisition

After spectra had been obtained, each sample was removed from its NMR tube using a glass Pasteur pipette and transferred into its appropriate eppendorf tube. The pH meter was recalibrated and then used to do a pH recheck to ensure that the pH had not shifted a significant amount. Samples were then stored in the -80°C freezer.

2.11 Cleaning of NMR tubes

NMR tubes were cleaned by filling them with bleach followed by soapy water, alcoholic KOH, and concentrated HCl. Between each wash solution, the tubes were rinsed five times with double-distilled H_2O. After the tubes were cleaned, they were inverted on an NMR rack and allowed to air dry for a minimum of 48 hours.

2.12 Spectral analysis

Spectral analysis was done using Chenomx Inc. NMR-suite software version 4.6. Before samples were analyzed, they were subjected to processing in which phasing of the spectra was fine-tuned, the water peak was eliminated from the spectra, and the baseline was corrected. The line shape of the spectra was then set to a width of 1.3 Hz. Finally, the

analysis was done using the Chenomx chemical compound library constructed for a pH range of between 6 and 8. 2,2-Dimethyl-2-silapentane-5-sulfonate-d6 sodium salt (DSS-d6) was used as the internal standard. A total of 56 metabolites were identified and quantified, not including the DSS-d6 standard. After all spectra were analyzed, their metabolite concentrations were exported from the program into an Excel file.

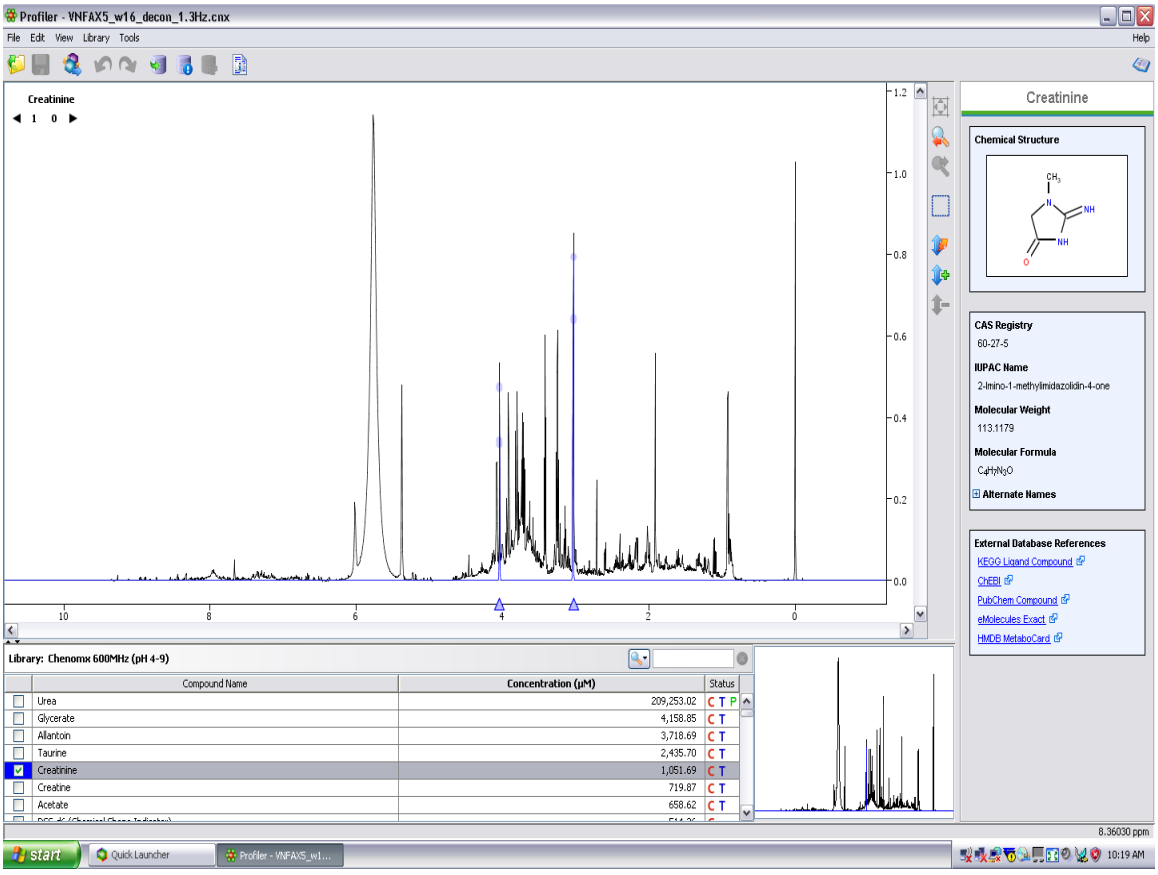

Figure 2.12.1 – Screen-shot of Chenomx NMR suite version 4.6, along with an example of an NMR spectrum

2.13 Statistical analysis

Multivariate statistical analysis was done using Simca P+ version 12.0.1 created by Umetrics. Simca P+ was used to perform Principal Component Analysis (PCA) and Partial Least Squares – Discriminante Analysis (PLS-DA). The Excel files generated after spectral analysis were then grouped according to environment in which the mice grew up, sex, strain, and age.

PCA is an unsupervised technique of statistical analysis; it is a variable-reduction procedure that works by taking multi-dimensional data with a number of correlated variables and transforming it into a smaller number of uncorrelated variables called principal components. It is especially useful when one has obtained a large number of variables and believes that there is the possibility of some redundancy amongst those variables (Weljie, Newton et al. 2006).

PLS-DA is a regression extension of PCA. PLS-DA is a supervised technique of statistical analysis that takes advantage of class information provided by the user in an attempt to maximize the separation of the groups being observed using the variables with which it has been provided (Weljie, Newton et al. 2006). PLS-DA plots were evaluated using a permutation test, though which we were looking to observe two positively sloped lines, along with the R2Y value and the Q2 value. With regards to the R2Y and Q2 values, there is no set cutoff for the measurement of

quality of separation, only the guideline that the closer the values are to 1, the better. Each PLS-DA model was also validated using a validation plot, and a total of 20 permutations were used to construct a plot. Plots with a positive slope indicate that the model constructed is better than any random model. PLS-DA charts also allowed us to create important metabolite graphs. During PLS-DA analysis, each metabolite is assigned a score, and this score corresponds to the impact the metabolite has on the creation of the model. Metabolites with a score of greater than 1 are considered to be important metabolites and to have had a significant impact on the model and on shaping the separation that can be observed in the models.

Chapter 3 - Axenic Mice

3.1 Wild-type population

3.1.1 Wild-type population: comparison of male and female at various ages

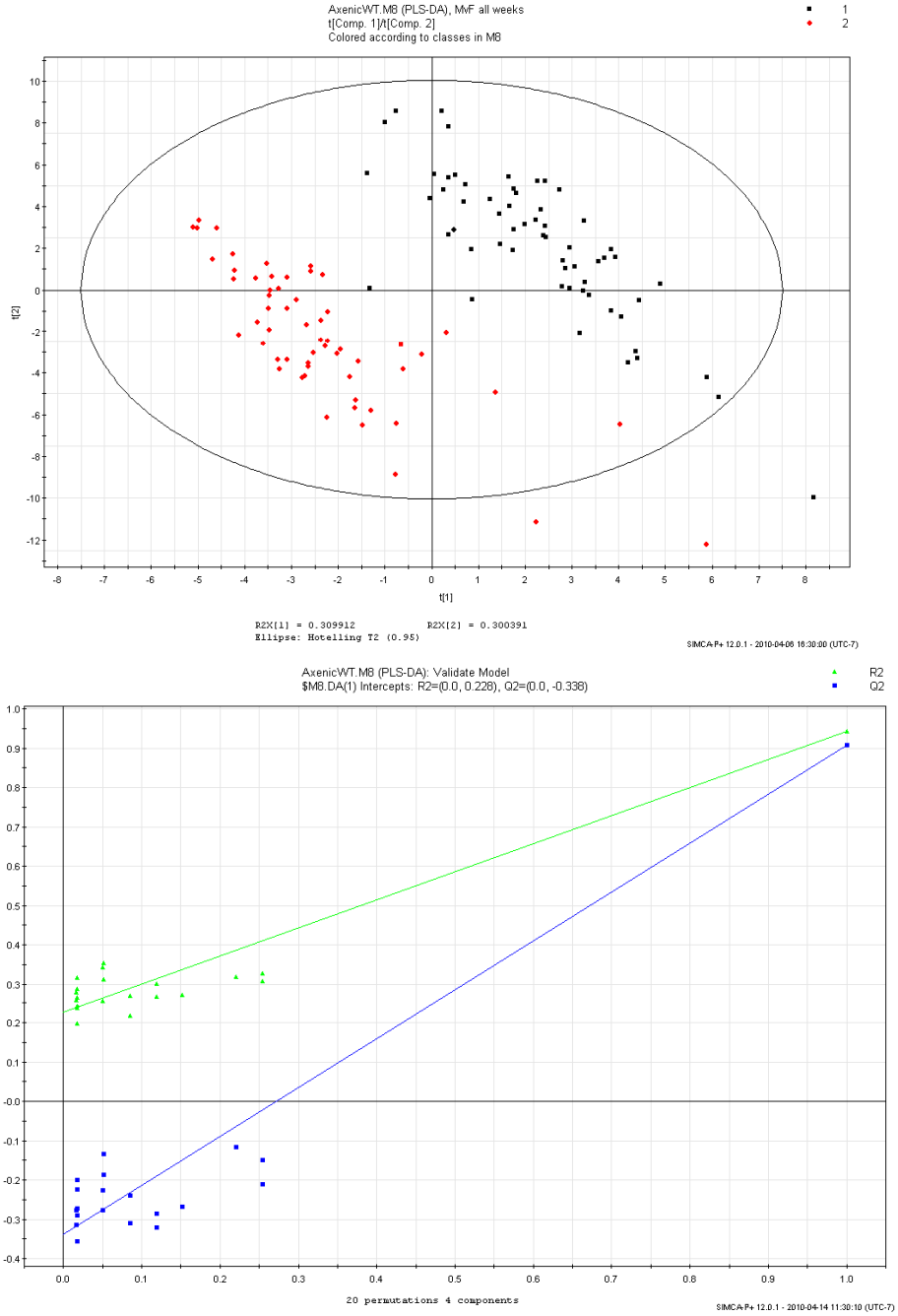

Figure 3.1.1.1 – PLS-DA plot of the urine metabolomic profiles of all male and female axenic wild-type mice; urine collected from mice in their axenic environments at 4, 6, 8,

12, 16 and 20 weeks of age. The male group comprises 58 points and the female group comprises 60 data points. Male mice are shown in red and female mice are shown in black. Despite a slight overlap and a few outliers, there is a clear separation between the two groups. Below the PLS-DA plot is the validation plot; positive slopes on the plots indicate that the original model generated is the best model that can be constructed.

Figure 3.1.1.1 is a PLS-DA plot that was constructed using the urine metabolomic profiles collected from all the axenic mice over all weeks of collection while they were in the axenic bubble. While there appears to be some overlap between a few points, and a couple of outliers are present, the male results and the female results do form two separate and distinct clusters. Analysis of the two outliers on the extreme right side of the graph reveals that, in fact, these two samples had been diluted out, and the concentrations of the majority of the metabolites measured were half those that were being observed for the rest of their groups. These diluted urine samples are the result of low volumes of urine being collected from the mice during the 22-hour collection period. The validation plot (included below) was constructed using 20 different permutations in the data; the positive slopes of both the R^2 and Q^2 lines indicate that the original plot constructed is the best possible model for the data.

In order to further investigate the findings related to the male and female groups, we divided these groups into their respective weeks and analyzed them on a week-by-week comparison basis.

Week 4

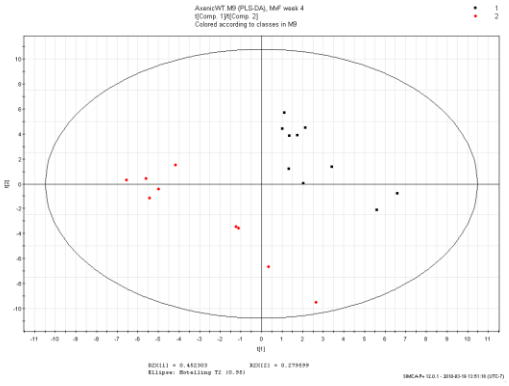

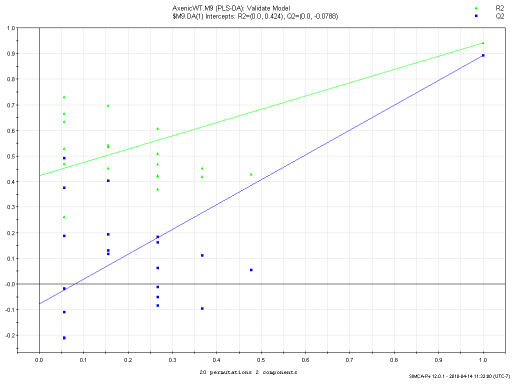

Week 6

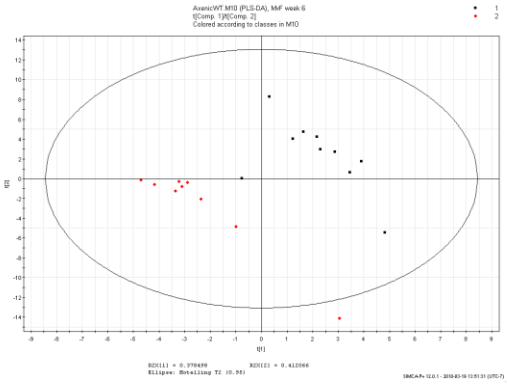

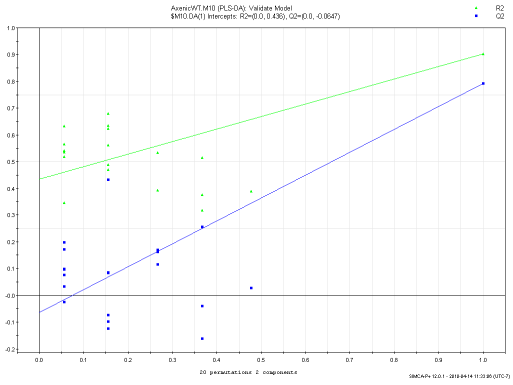

Week 8

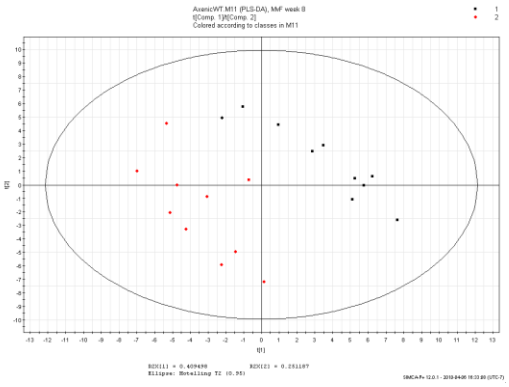

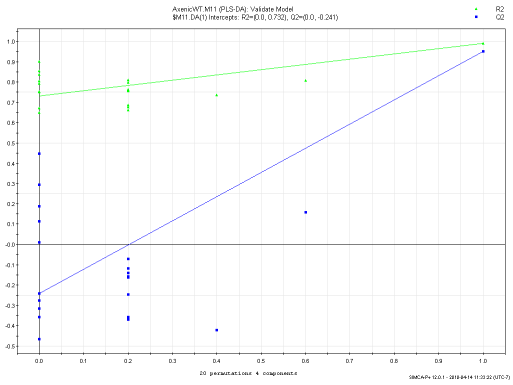

Week 12

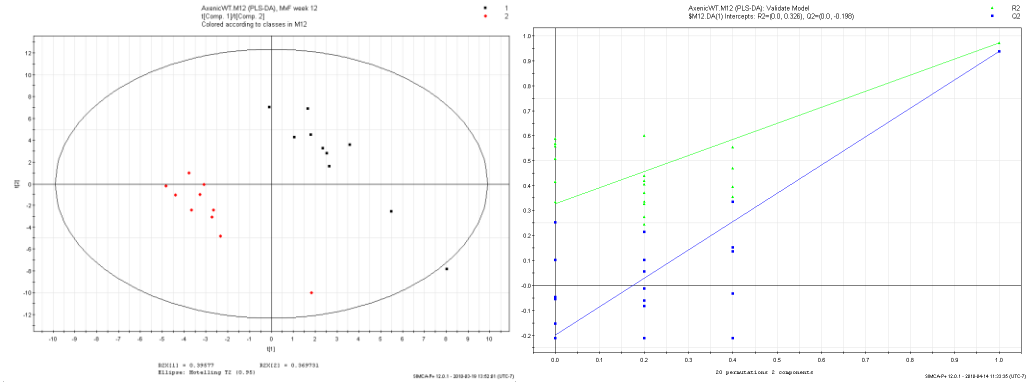

Week 16

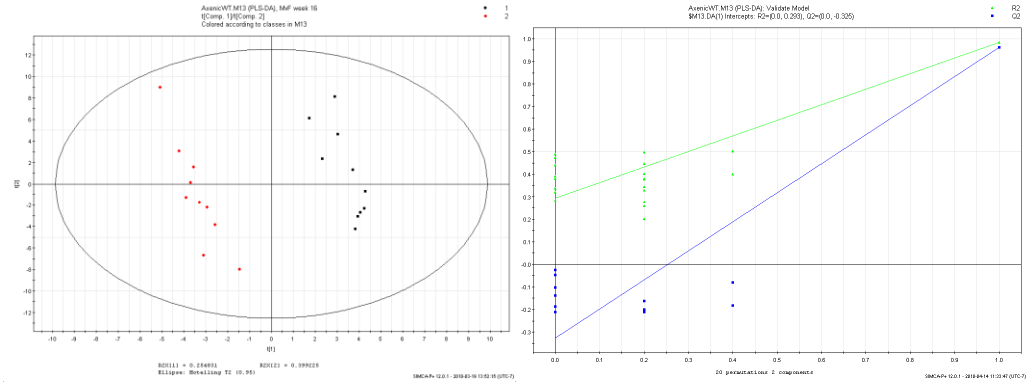

Week 20

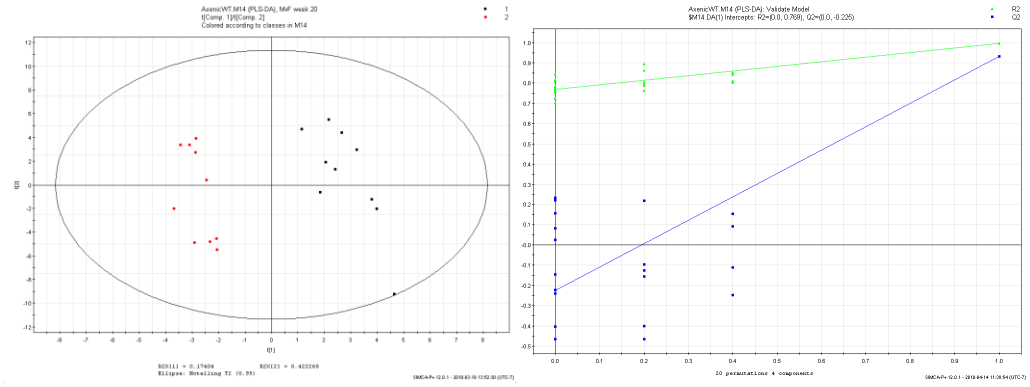

Figure 3.1.1.2 – PLS-DA plots of the urine metabolomic profiles of the axenic wild-type mice broken up by week of urine collection; males are displayed in red and females are displayed in black. Each week comprises 10 males and 10 females, except for weeks 4

and 6, in which there are only 9 male points. Beside each PLS-DA plot is the corresponding validation plot.

Week-by-week analysis of the axenic male vs. axenic female data for wild-type mice show us a very clear picture of the distinction between sexes. Each plot is composed of two distinct clusters, one cluster for the male group and one cluster for the female group, and there is no overlap between the two. The validation plots also allow indicate that each model created is the best model that could have been created for the data, as each model's validation contains positive slopes for both the R^2 and Q^2 values.

plot	R2Y	Q2
All weeks	0.888	0.858
week 4	0.941	0.893
week 6	0.903	0.791
week 8	0.819	0.709
week 12	0.973	0.938
week 16	0.983	0.962
week 20	0.995	0.933

Table 3.1.1.1 - R2Y and Q2 values for the PLS-DA plots constructed for axenic wild-type male vs. axenic wild-type female.

3.1.2 Wild-type males: comparison of urine metabolomics over all collection weeks

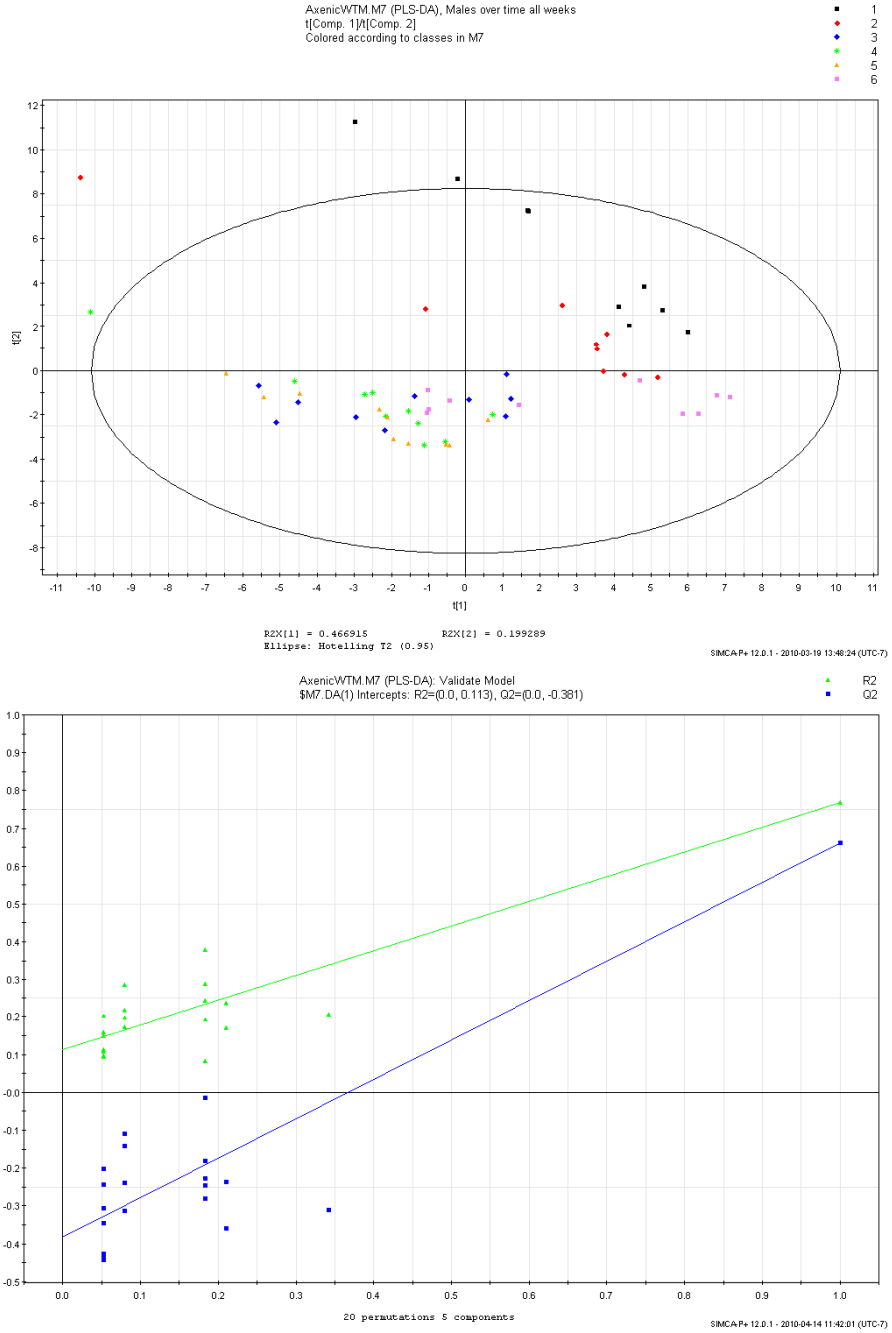

Figure 3.1.2.1– PLS-DA plot of urine metabolomic profiles of all male wild-type axenic mice over all collection time points. There are a total of 58 points, and each week is constructed from 10 points, with the exceptions of weeks 4 and 6, in which only 9 points were used. Each week is are displayed in a different color: week 4 (black), week 6 (red), week 8 (blue), week 12 (green), week 16 (yellow), week 20 (purple). This plot shows the

progression of the urine metabolomic profile of male wild-type mice as they grow in an axenic environment. Below the PLS-DA plot is the validation plot.

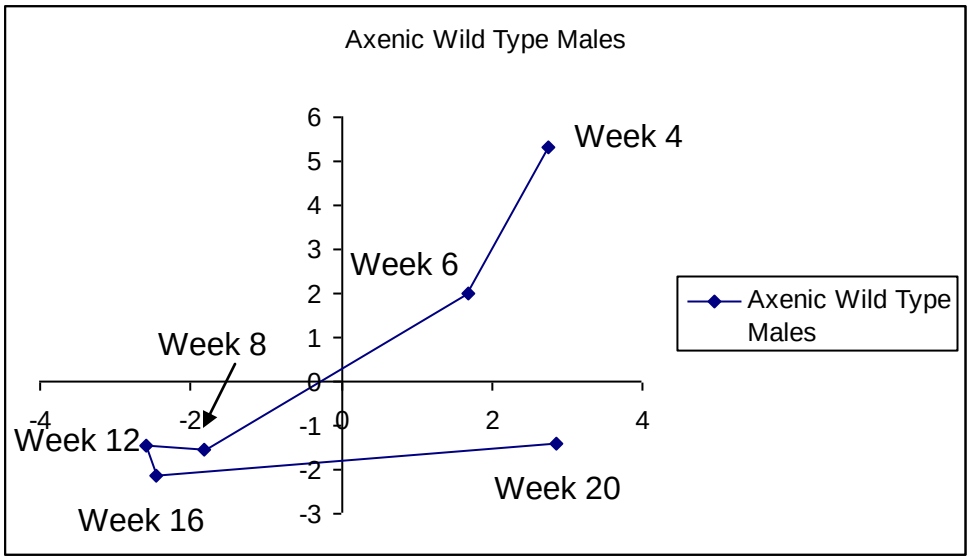

Figure 3.1.2.2– Metabolic trajectory of the axenic wild-type males; the plot was constructed by taking the coordinates of all the points for each week and calculating a single mean coordinate for each week.

Figure 3.1.2.1 is a PLS-DA of all axenic wild-type males over all the weeks of collection. The male outlier that was discovered during the gender analysis is once again present. The smaller sample group has yielded 3 new possible outliers for this the male group, two of which occurred during week 4 and the other occurred during week 12. Once again, however, it appears that these outliers are due to dilution of the samples of urine collected. Dilute samples at week 4 occur for several reasons; at week 4 the mouse is still very small and will not produce very much urine to start off with, so anything other than maximal urine production will result in a

diluted sample. Another reason for limited urine production at week 4 is that this is the first time the mouse finds itself in the metabolic cage; both the stress of being in the cage and the unfamiliarity of the cage and location of the water bottle can contribute to lower urine production. However, the dilution of the sample found at week 12 seems to be a significant anomaly. In this case, this outlier is most likely the result of the sample being spilt or not fully collected because of an error in the construction of the cage which resulted in less than optimum conditions for urine collection.

Analysis of the metabolic trajectories plot (Figure 3.1.2.2) shows that the most noticeable changes occur during weeks 4 to 8. During these weeks, the groups move along the plot and also separate from each other. During weeks 8-16 the groups seem to cluster together for the most part. The shifting of the points during weeks 4-8 can be attributed to growth and development, which assessment also explains why there is little movement of points in weeks 8-20, since the mice have basically already matured. The week 20 group appears to be broken into two groups, and the one group on the far right of the plot pulls the mean towards it. The split in the group was a result of the urine samples being collected under different living conditions as one group was collected after the axenic colony had to be restarted due to a breach of the axenic environment. Some initial samples were collected before the axenic environment had to

be restarted, and the others were collected after the axenic environment was restarted. Although there is a split present, it does show that this technique is quite robust, since the groups of mice still separate according to their age.

Week 4 vs. Week 6

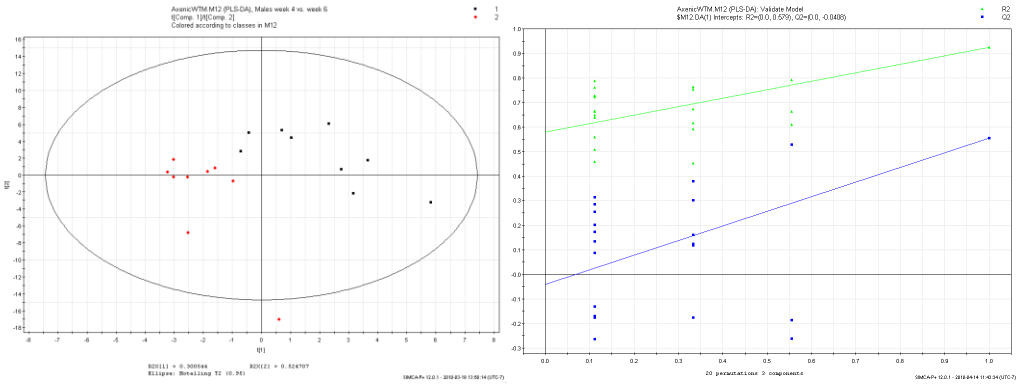

Week 4 vs. Week 8

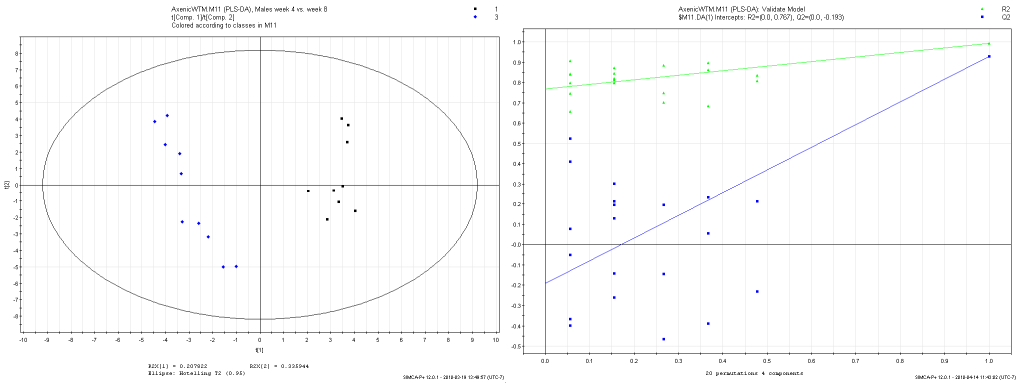

Week 4 vs. Week 12

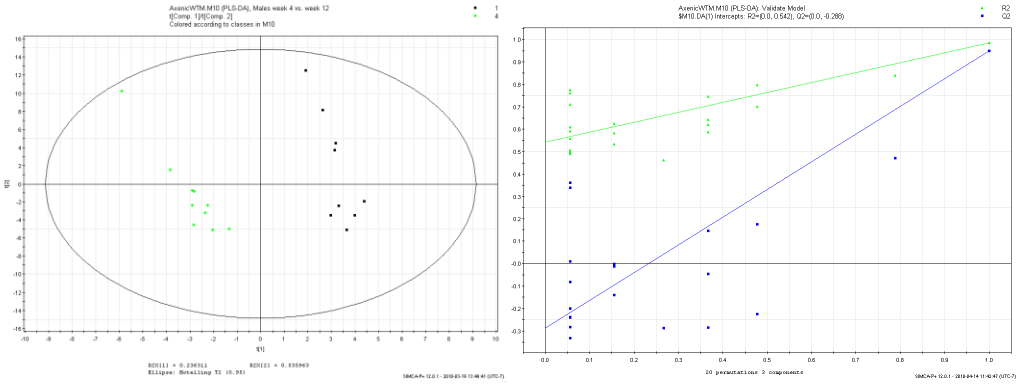

Week 4 vs. Week 16

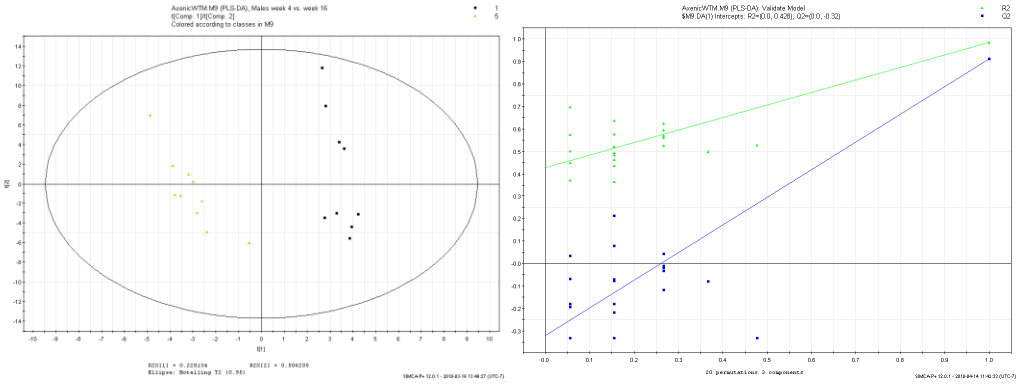

Week 4 vs. Week 20

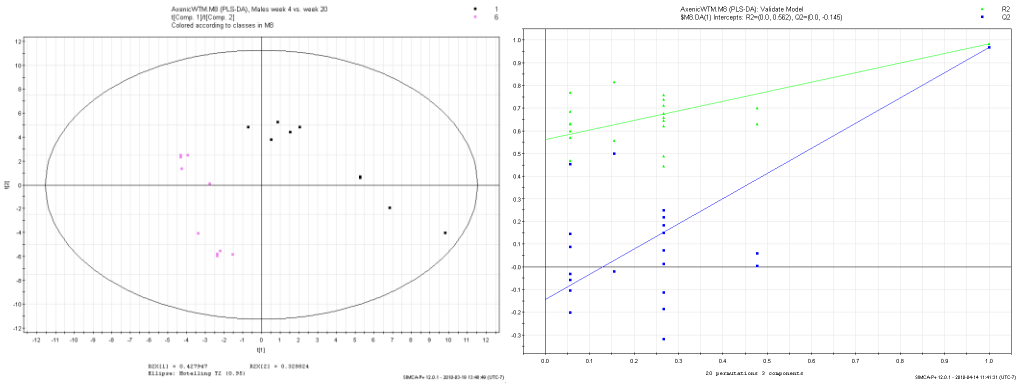

Figure 3.1.2.3 – PLS-DA plots of urine metabolomics profiles of wild-type male axenic mice in reference to week 4; each group is made up of the same 10 mice from week 4 and is referenced against the other groups of 10 mice in the other weeks collected. Beside each PLS-DA plot is the corresponding validation plot.

Figure 3.1.2.3 is a PLS-DA plot comparing each week in which urine was collected in reference to week 4. By using week 4 as the baseline, we can observe how each subsequent week changes in reference to this one static point (week 4). When we compared the other weeks to week 4, we immediately found that not one week was similar to week 4. Even at week 6, when there is almost a slight overlap between the two groups, two very distinct clusters appear. Weeks 8, 12, and 16 all completely separate out to clusters which have no overlap when referenced to week 4. Week 20 also completely separates out from week 4, but the separation between the two groups is not as dramatic as the ones observed for weeks 8,12, and 16.

plot	R2Y	Q2
all weeks	0.582	0.369
4 v 6	0.924	0.556
4 v 8	0.992	0.928
4 v 12	0.986	0.949
4 v 16	0.984	0.912
4 v 20	0.984	0.968

Table 3.1.2.1 - R2Y and Q2 values for the PLS-DA plots constructed for the axenic wild-type males over time.

3.1.3 Wild-type females: comparison of urine metabolomics over all collection weeks

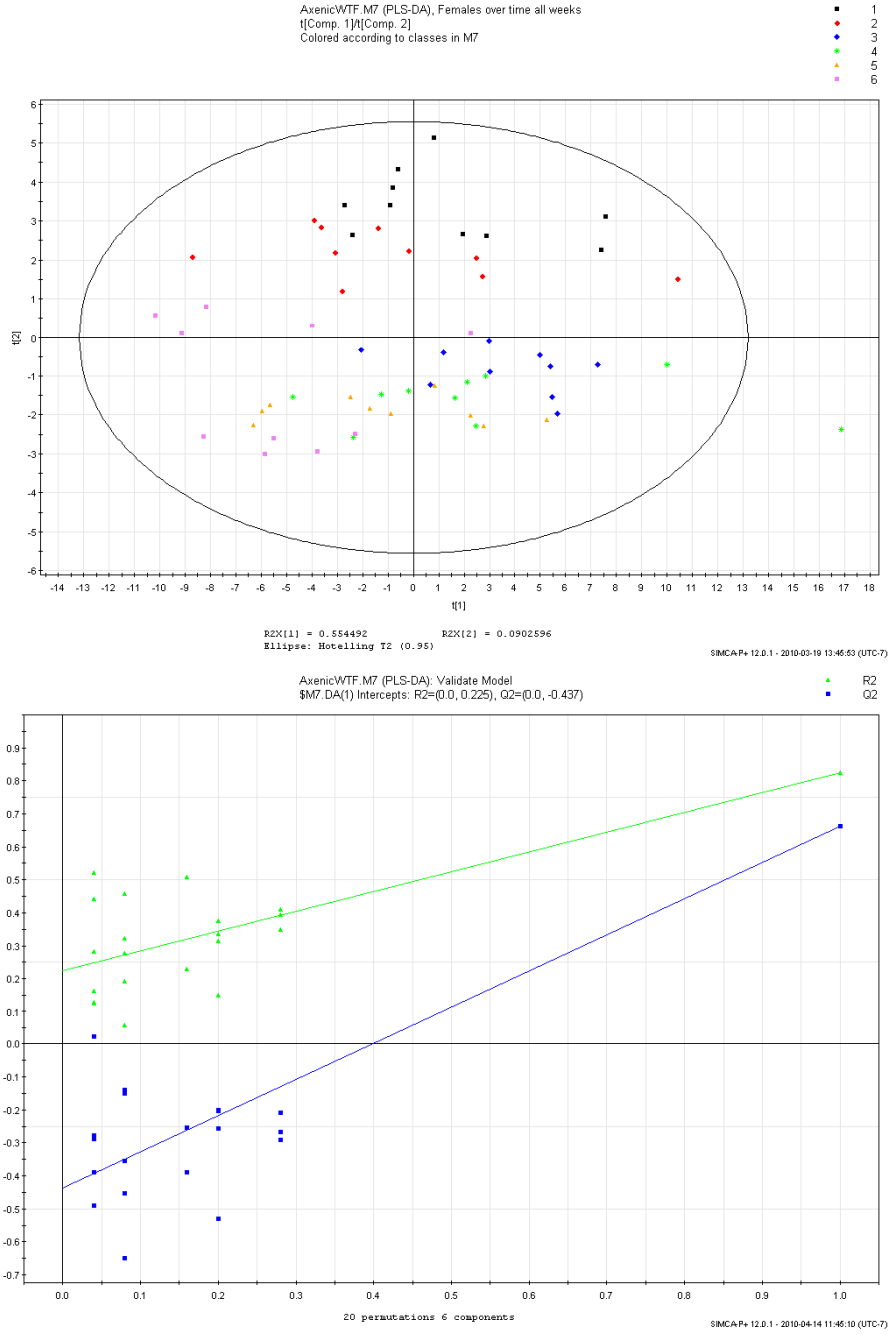

Figure 3.1.3.1– PLS-DA plot of urine metabolomic profiles of all female wild-type axenic mice over all collection time points. Each week is constructed from 10 points and is displayed in a different color: week 4 (black), week 6 (red), week 8 (blue), week 12 (green), week 16 (yellow), week 20 (purple). This plot shows the progression of the urine

metabolomic profile of female wild-type mice as they grow in an axenic environment. Below the PLS-DA plot is the validation plot.

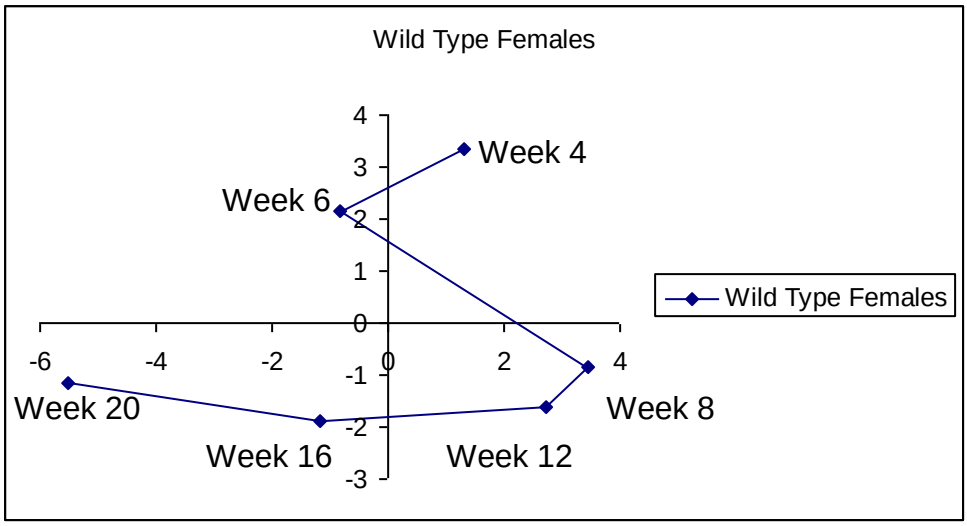

Figure 3.1.3.2– Metabolic trajectory of the axenic wild-type females; the plot was constructed by taking the coordinates of all the points for each week and calculating a single mean coordinate for each week.

Figure 3.1.3.1 is a PLS-DA of all axenic wild-type females over all the weeks of collection. The female outlier that was discovered during the male/female comparison analysis is once again present. Once again, it appears that the outlier results from a diluted sample of urine. Similar to the findings observed for the males, it appears that the most noticeable changes in this plot occur between weeks 4 and 8, where the groups move along the plot and also separate from each other. During weeks 8, 12, and 16 the groups seem to cluster together for the most part. The Shifting of the points during weeks 4-8 is once again most likely due to growth and development. However there appears to be additional

movement for the female mice between week 16 and week 20. Although similar trends occur on both the male and female plots, the female plot does not cluster together as nicely as the male plot does.

Analysis of the metabolic trajectory plot (Figure 3.1.3.2) shows similar trends to the male plot; much of the movement can be seen between weeks 4-8, and the least amount of movement is observed between weeks 8-12. However, discretion should be used when interpreting this plot, since the points used to construct the mean values are not bunched together very tightly, and there is therefore a greater range in the coordinates used, possibly skewing the mean.

Week 4 vs. Week 6

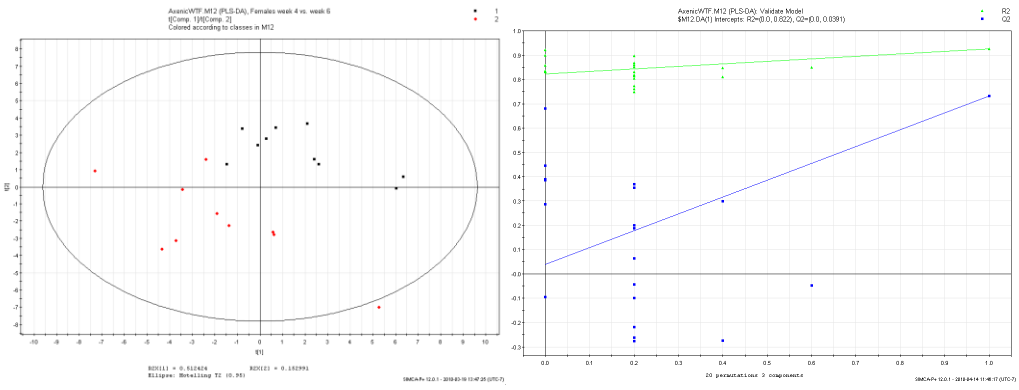

Week 4 vs. Week 8

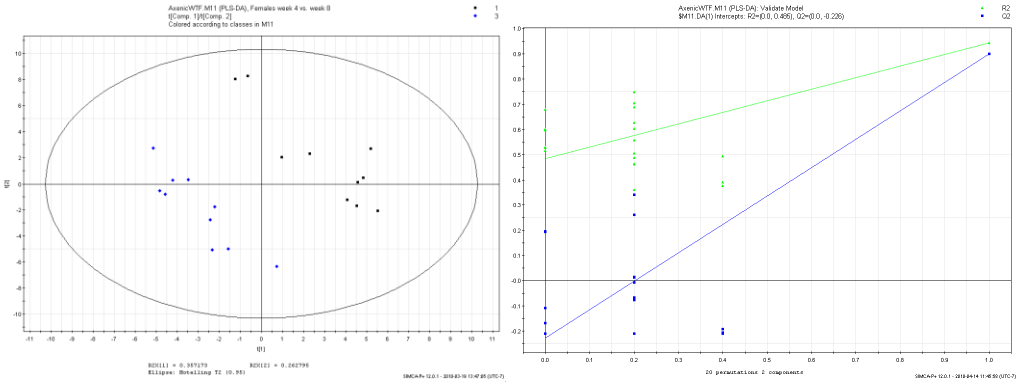

Week 4 vs. Week 12

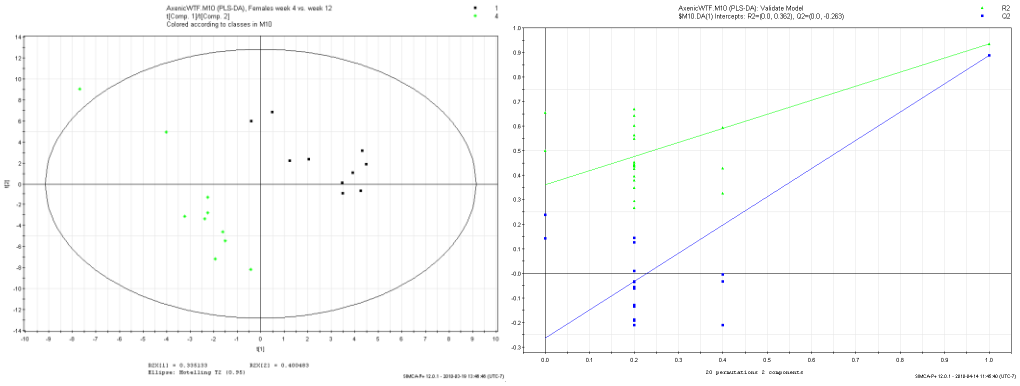

Week 4 vs. Week 16

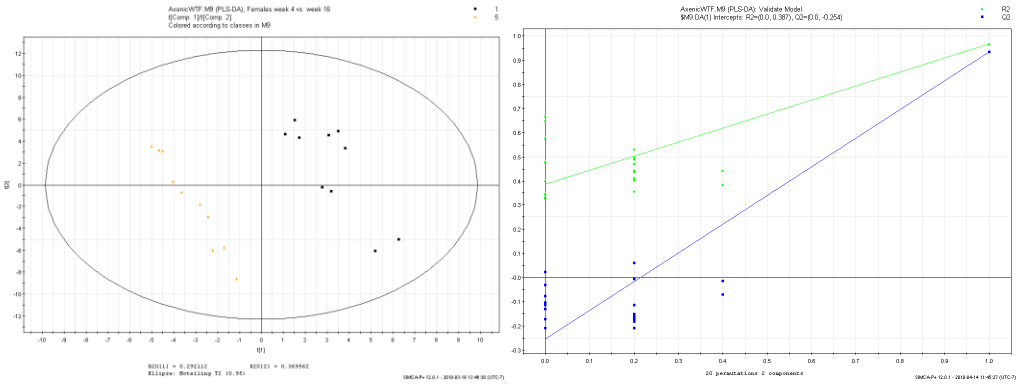

Week 4 vs. Week 20

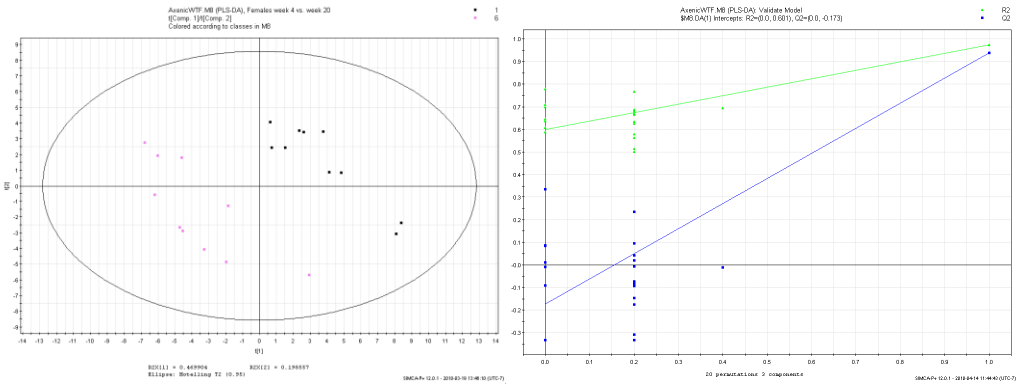

Figure 3.1.3.3 – PLS-DA plot of urine metabolomic profiles of female wild-type axenic mice in reference to week 4; each group is comprised of the same 10 mice from week 4 and is referenced against the other groups of 10 mice for the other weeks collected. Beside each PLS-DA plot is the corresponding validation plot.

Figure 3.1.3.3 is a PLS-DA plot comparing each week in which urine was collected to week 4. The week 4 vs. week 6 PLS-DA plot is the only comparison where the two clusters come close to overlapping, but even on this plot the two clusters form two distinct groups without actually overlapping. The comparisons at weeks 8, 12 and 16 are similar to those of the males, in that they all show clear and distinct separation and clustering when referenced to week 4. The week 4 vs. week 20 comparison is also similar to what was observed in the males; the gap between the two clusters seems to be slightly reduced.

plot	R2Y	Q2
all weeks	0.62	0.409
4 v 6	0.926	0.732
4 v 8	0.944	0.9
4 v 12	0.934	0.888

4 v 16	0.969	0.934
4 v 20	0.975	0.939

Table 3.1.3.1 - R2Y and Q2 values for the PLS-DA plots constructed for the axenic wild-type females over time.

3.2 IL-10 KO population

3.2.1 IL-10 KO population: comparison of male and female at various ages

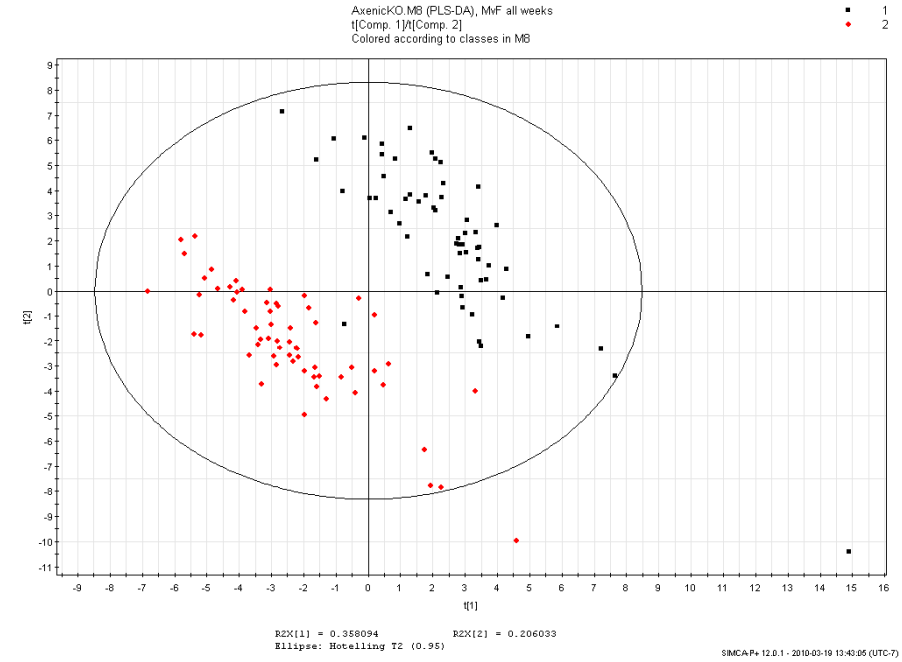

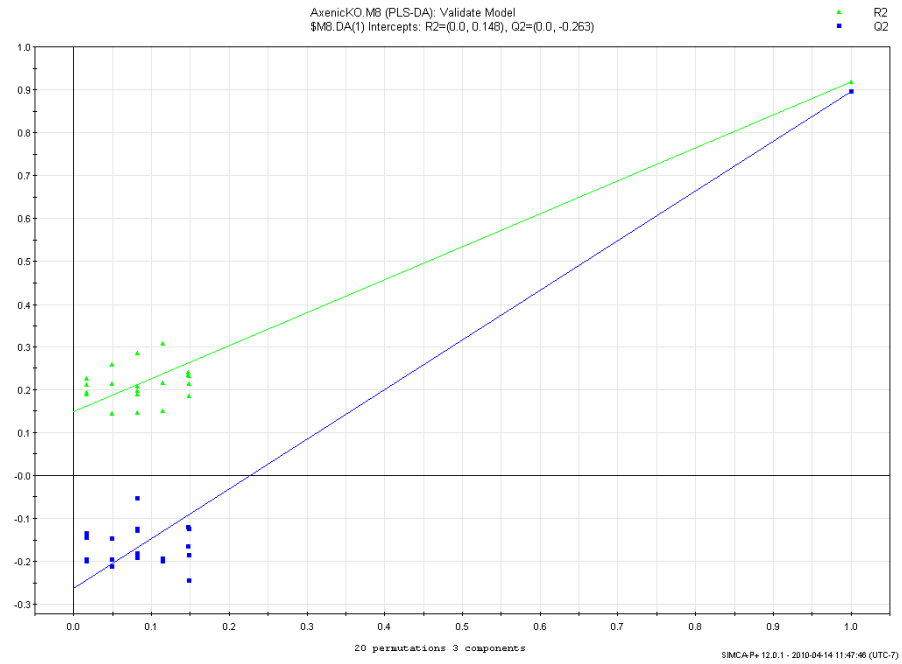

Figure 3.2.1.1 – PLS-DA plot of the urine metabolomic profiles of all male and female IL-10 KO axenic mice, samples collected from the axenic environments on weeks 4, 6, 8, 12, 16, and 20. The male and female groups each have 60 data points (10 points per

week). Male mice are shown in red and female mice are shown in black. Below the PLS-DA plot is the validation plot.

Figure 3.2.1.1 is a PLS-DA plot of all axenic IL-10 knockout mice. Examination of the plot shows that two groups have formed, one group consisting of the male mice and the other group consisting of the female mice. The male and the female groups show very little overlap between the two groups, with only one female point found in the male cluster. There are also a couple of outliers present, once again resulting from low volumes of urine in samples taken during the initial collection period.

Week 4

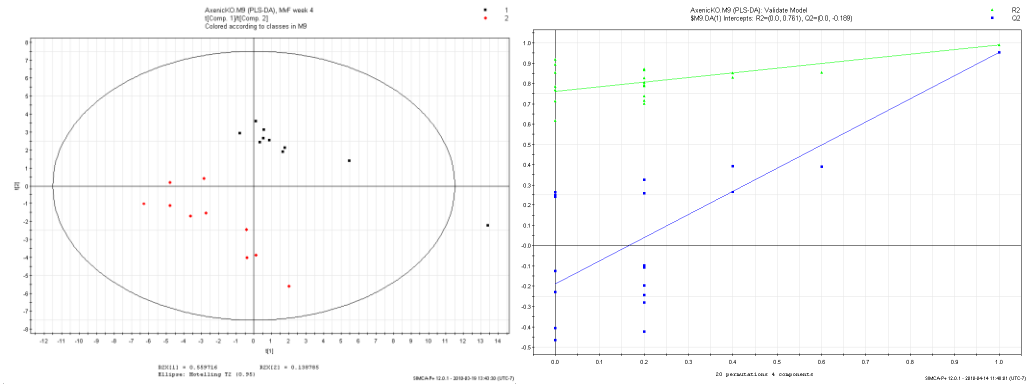

Week 6

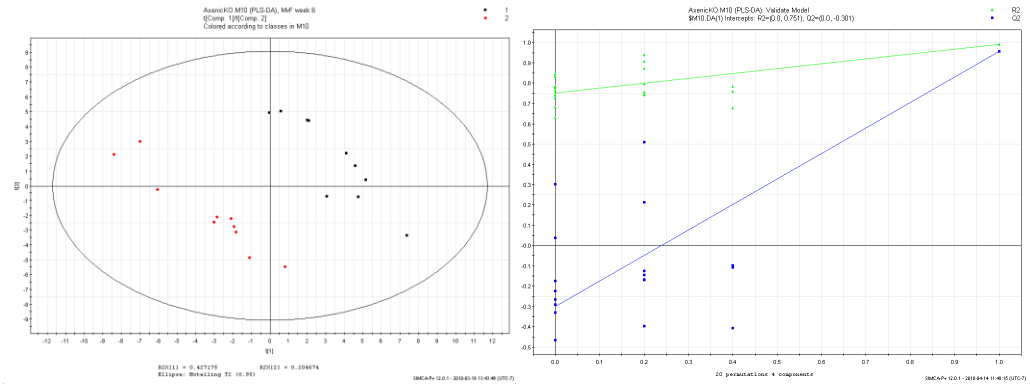

Week 8

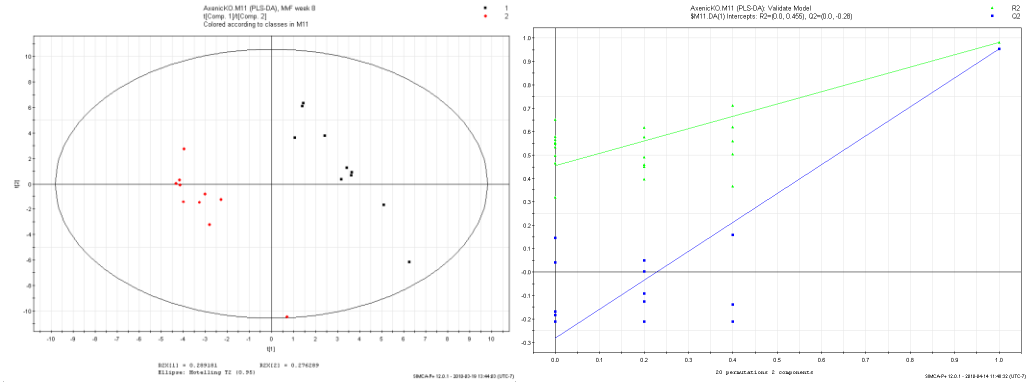

Week 12

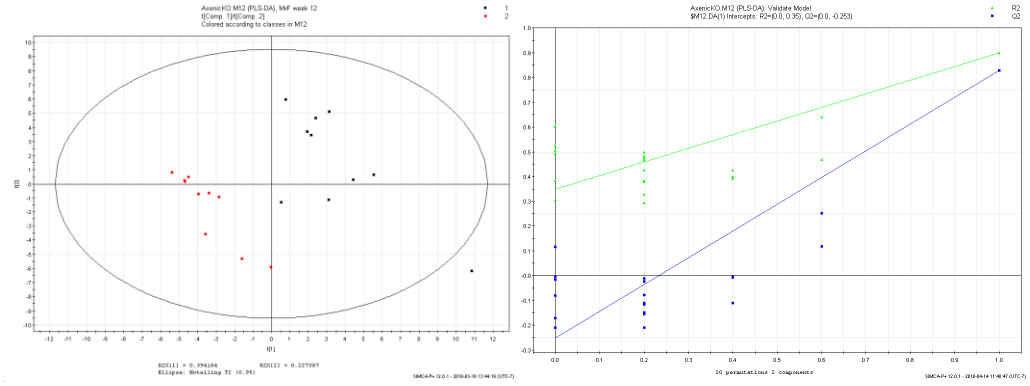

Week16

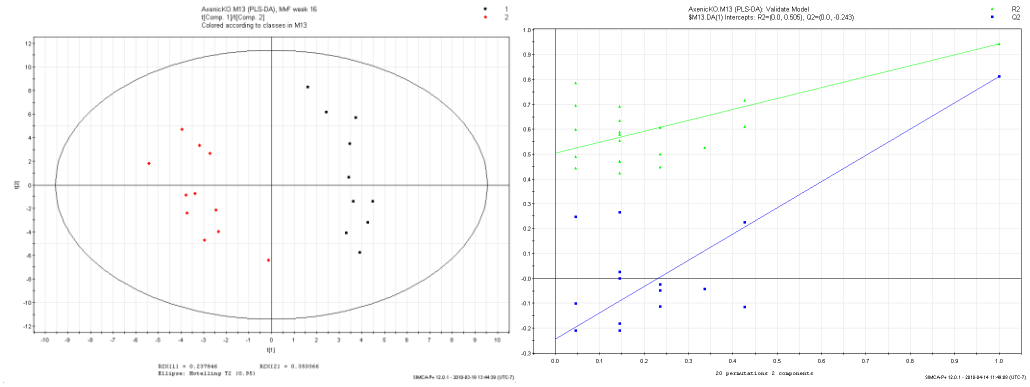

Week 20

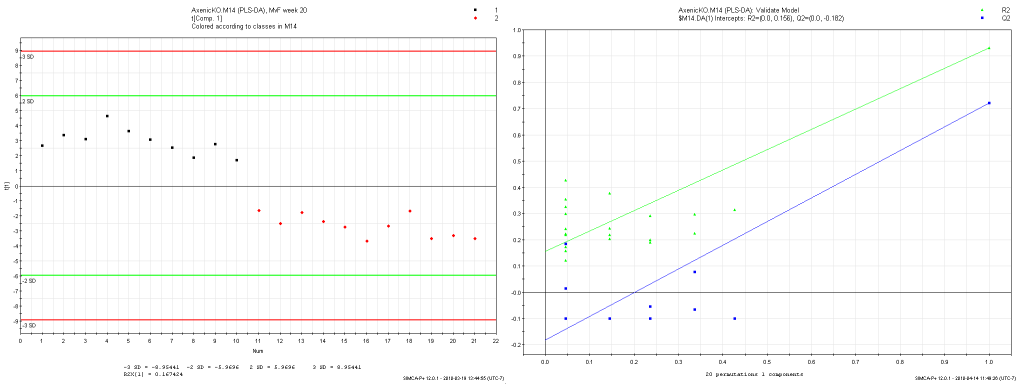

Figure 3.2.1.2 – PLS-DA plots of the urine metabolomic profiles of the axenic IL-10 KO mice broken up by week of urine collection; males are displayed in red and females are displayed in black. Each week has 10 males and 10 females. Beside each PLS-DA plot is the corresponding validation plot.

A week-by-week comparison of the axenic IL-10 KO mice reveals a similar trend to what was observed for the wild-type mice. In the wild-type data, we saw separation between the males and females at week 4 continuing throughout the other weeks until week 20. In the IL-10 KO mice data, we see the same thing. Beginning at week 4, two distinct and separate clusters have formed, one male cluster and one female cluster; the male and female clusters alsoseparate out from each other with no overlapping. Weeks 6 through 16 show similar results to those observed in week 4. However, week 20 shows some interesting results. The PLS-DA plot for week 20 only required one component to separate the data; a second component could have been generated but to do so would have weakened the quality of our model by reducing the R2Y and Q2 scores.

plot	R2Y	Q2
All weeks	0.918	0.896
week 4	0.991	0.952
week 6	0.99	0.956
week 8	0.98	0.953
week 12	0.899	0.828
week 16	0.944	0.812
week 20	0.931	0.722

Table 3.2.1.1 - R2Y and Q2 values for the PLS-DA plots constructed for the axenic IL-10 KO male vs. axenic IL-10 KO female.

3.2.2 IL-10 KO males: comparison of urine metabolomics over all collection weeks

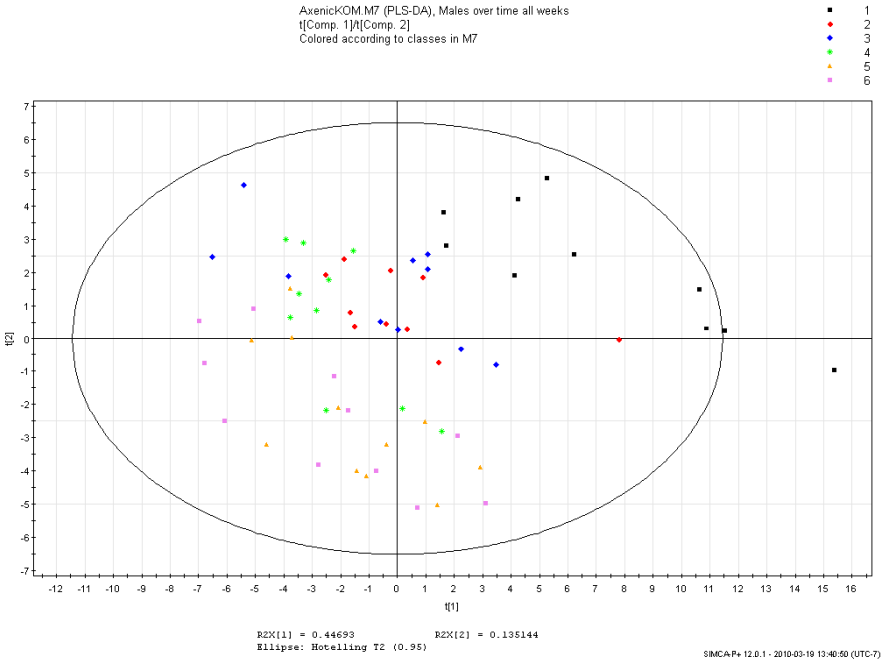

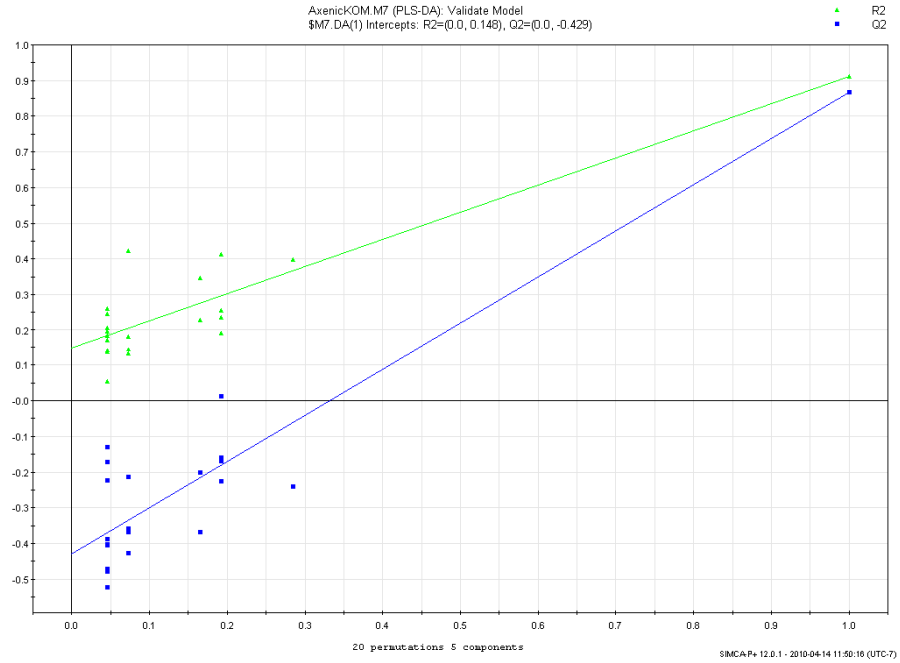

Figure 3.2.2.1– PLS-DA plot of urine metabolomic profiles of all male IL-10 KO axenic mice over all collection time-points. Each week is constructed from 10 points and is displayed in a different color: week 4 (black), week 6 (red), week 8 (blue), week 12 (green), week 16 (yellow), week 20 (purple). This plot shows the progression of the urine metabolomic profiles of male wild-type mice as they grow in an axenic environment. Below the PLS-DA plot is the validation plot.

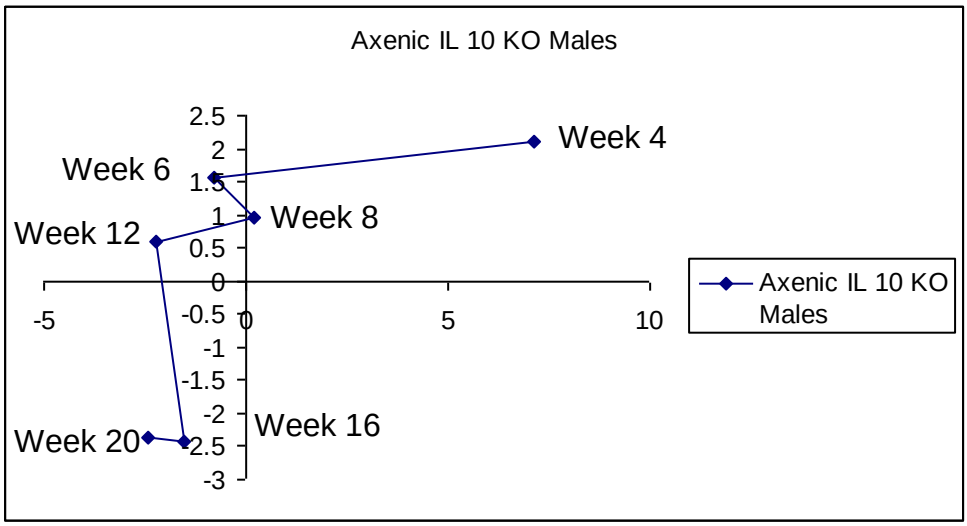

Figure 3.2.2.2– Metabolic trajectory of the axenic IL-10 KO males; the plot was constructed by taking the coordinates of all the points for each week and calculating a single mean coordinate for each week.

Figure 3.2.2.1 is a PCA plot for all axenic knockout males. Clearly, the IL-10 KO mice data do not seem to cluster together as nicely as that from the wild-type mice. Due to the scattering of the points, it is difficult to decipher what is actually going on in the plot. Once again, there appears to be one outlier (one of the week 4 points), most likely due to a low volume of urine being collected during the initial collection period. Analysis of the metabolic trajectories plot (Figure 3.2.2.2) shows that the greatest amount of movement occurs between weeks 4-6 and in weeks 12-16. The movement from weeks 4-6 is most likely due to growth and the change in food. To further investigate the interaction of the different clusters, we referenced the other weeks against week 4.

Week 4 vs. Week 6

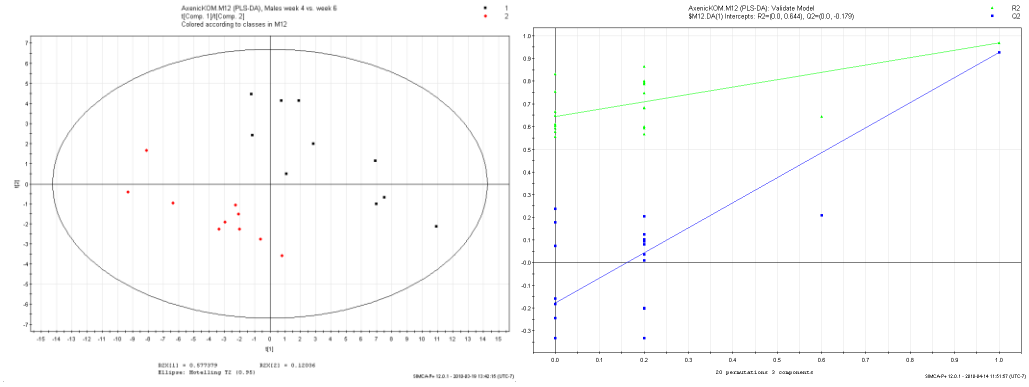

Week 4 vs. Week 8

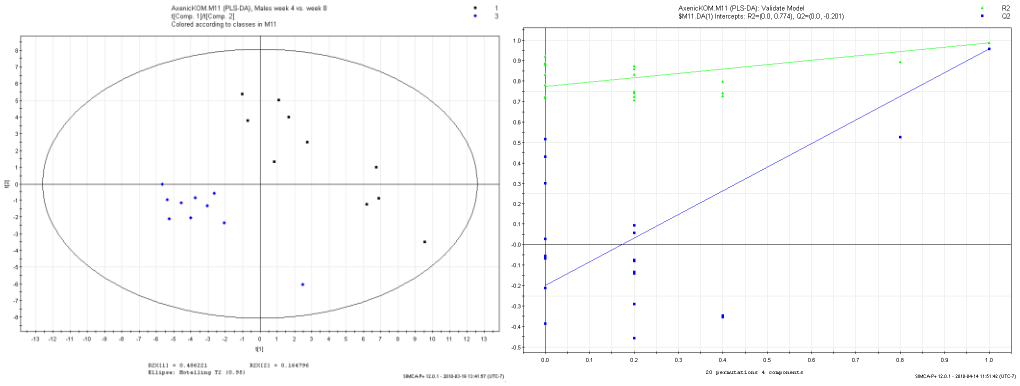

Week 4 vs. Week 12

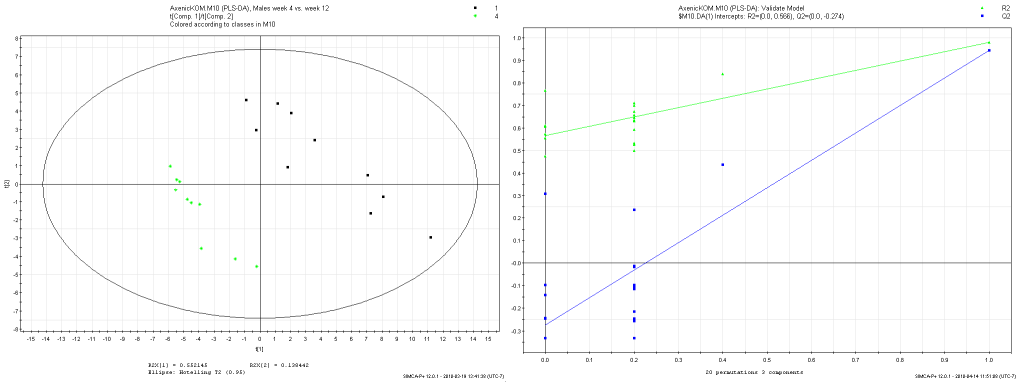

Week 4 vs. Week 16

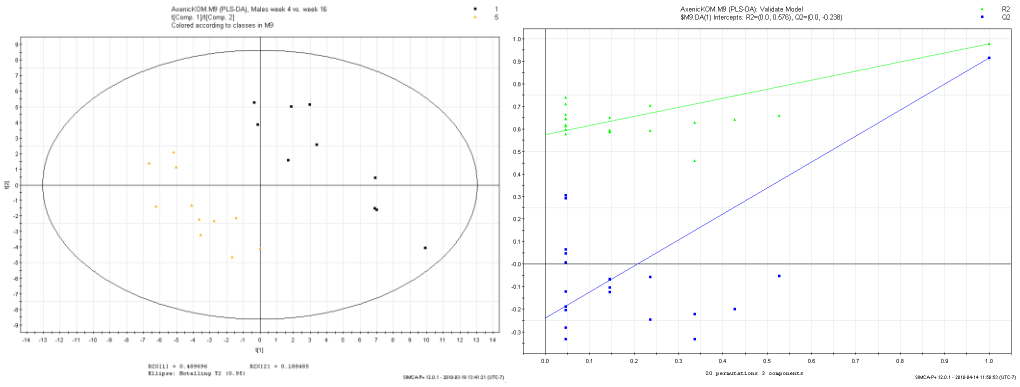

Week 4 vs. Week 20

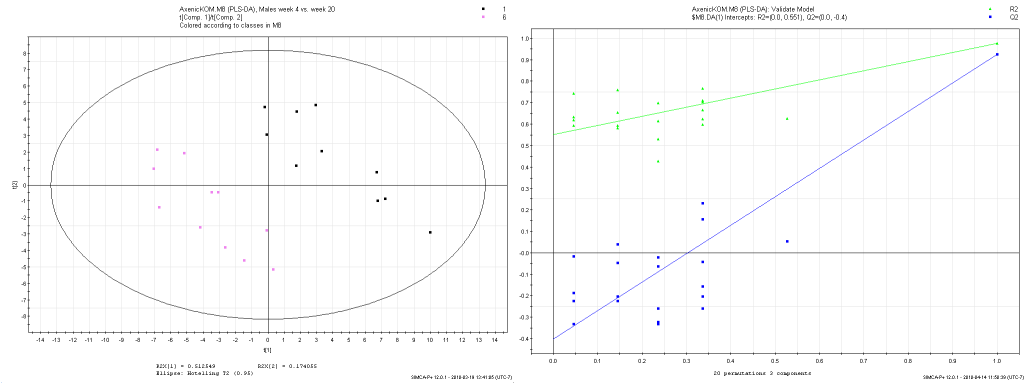

Figure 3.2.2.3 – PLS-DA plot of urine metabolomic profiles of IL-10 KO male axenic mice referenced to week 4; each group is composed of the same 10 mice from week 4 and is referenced against the other groups of 10 mice for the other weeks collected. Beside each PLS-DA plot is the corresponding validation plot.

Comparison of each individual week in reference to week 4 gives us a better idea of what is going on than does comparing them as one large group. The comparison of week 4 vs. week 6 reveals two unique clusters, one cluster for the week 4 mice and one cluster for the week 6 mice; there is no overlap between the two groups. Similar results are also observed when weeks 8, 12, 16, and 20 are compared to week 4. In each PLS-DA plot, there is complete separation between the week 4 cluster and the cluster that it is being compared to.

plot	R2Y	Q2
all weeks	0.501	0.329
4 v 6	0.97	0.928
4 v 8	0.988	0.956
4 v 12	0.979	0.944
4 v 16	0.978	0.915

4 v 20	0.975	0.926

Table 3.2.2.1 - R2Y and Q2 values for the PLS-DA plots constructed for the axenic IL-10 KO males over time.

3.2.3 IL-10 KO females: comparison of urine metabolomics over all collection weeks

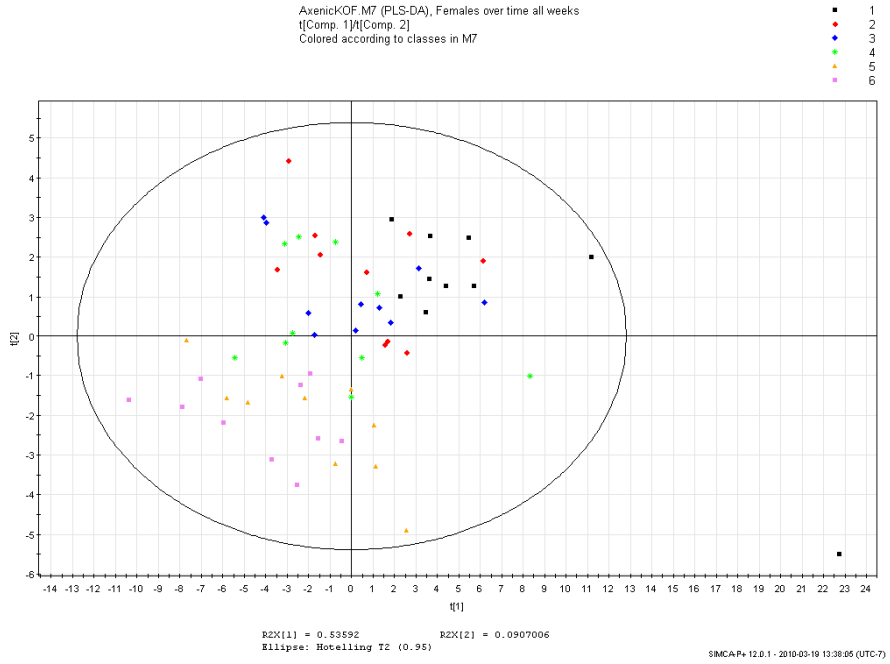

Figure 3.2.3.1– PLS-DA plot of urine metabolomic profiles of all female IL-10 KO axenic mice over all collection time points. Each week is constructed from 10 points and is

displayed in a different color: week 4 (black), week 6 (red), week 8 (blue), week 12 (green), week 16 (yellow), week 20 (purple). This plot shows the progression of the urine metabolomic profile of female wild-type mice as they grow in an axenic environment. Below the PLS-DA plot is the validation plot.

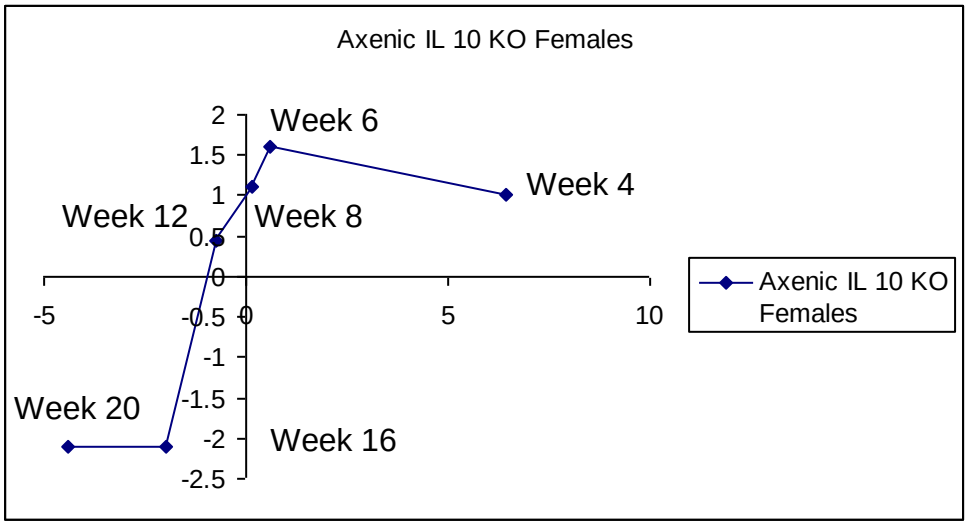

Figure 3.2.3.2– Metabolic trajectory of the axenic IL-10 KO females; the plot was constructed by taking the coordinates of all the points for each week and calculating a single mean coordinate for each week.

Figure 3.2.3.1 is the PLS-DA for all the axenic female IL-10 KO mice. Similar to what was seen with the IL-10 KO male PLS-DA, it is difficult to identify any groupings or movement of the groups in the graph. The one outlier occurring at week 4 is due to a low volume of urine collected. Analysis of the metabolic trajectories plot (figure 3.2.3.2) shows a similar trend to what was observed for the IL-10 KO males. The largest movements in the plot occur between week 4 and 6 and weeks 12-16. Once again, the movement from week 4 to week 6 is most likely due to

growth, dietary changes, and development. To further investigate the interaction of the different clusters, we referenced the other weeks against week 4.

Week 4 vs. Week 6

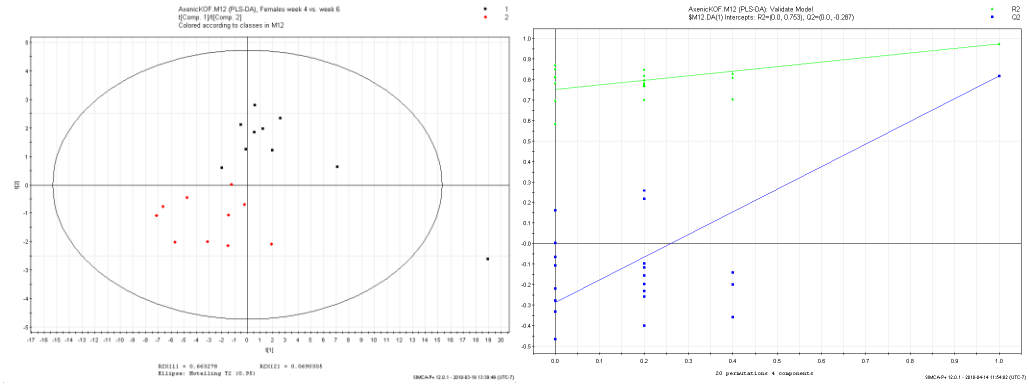

Week 4 vs. Week 8

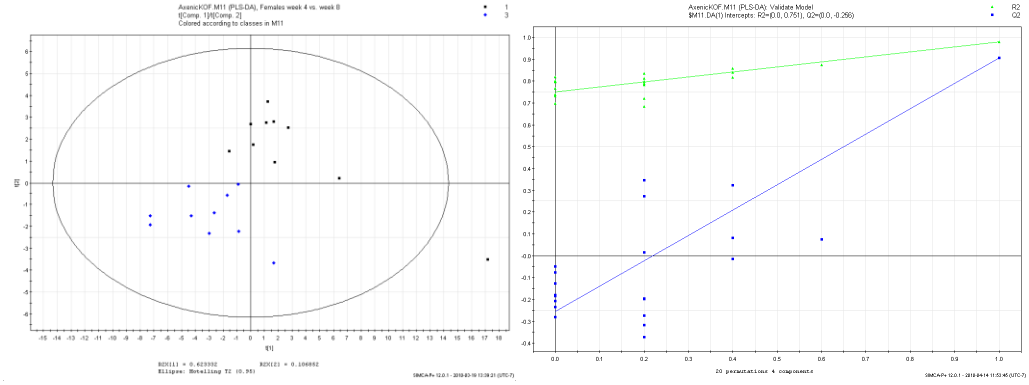

Week 4 vs. Week 12

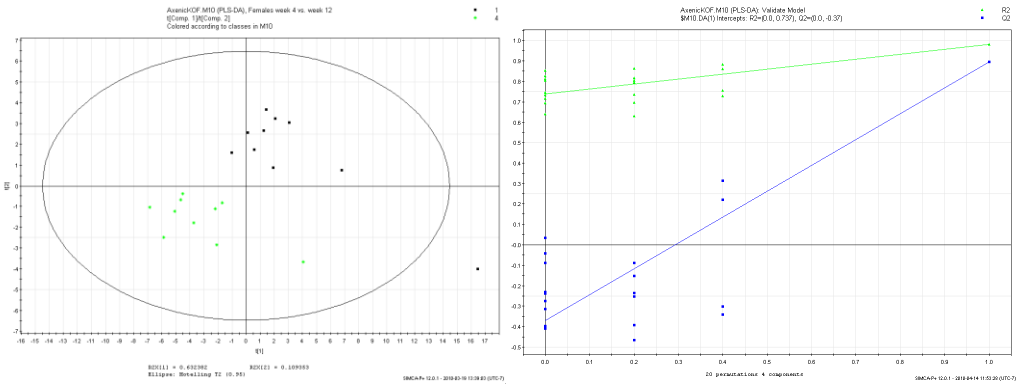

Week 4 vs. Week 16

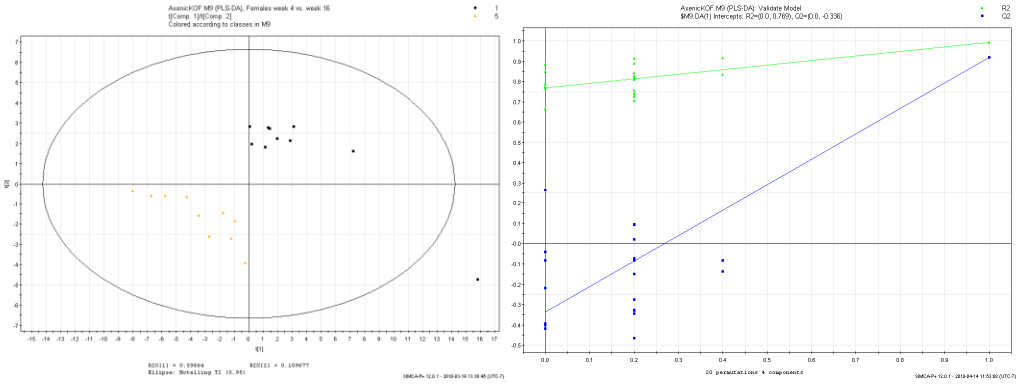

Week 4 vs. Week 20

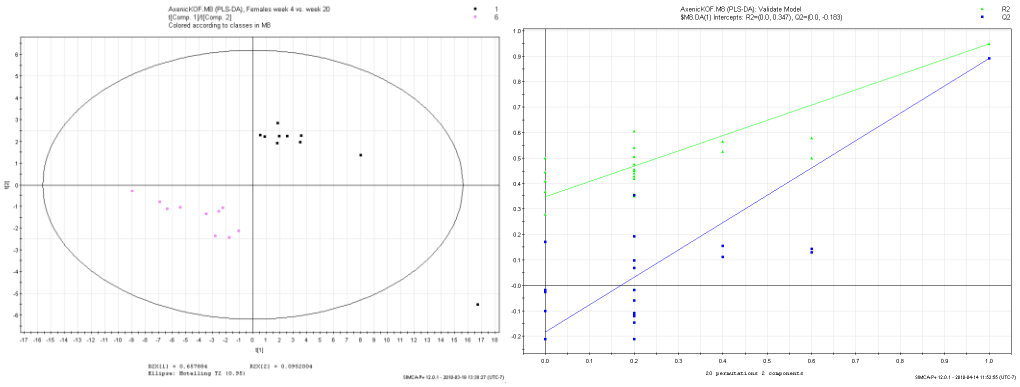

Figure 3.2.3.3 – PLS-DA plot of urine metabolomic profiles of IL-10 KO female axenic mice referenced week 4; each group is composed of the same 10 mice from week 4 and is referenced against the other groups of 10 mice that comprise the other weeks collected. Beside each PLS-DA plot is the corresponding validation plot.

Once again, comparing each week to week 4 gives a better idea of how the metabolites in the female IL-10 KO mouse change over time. Starting at week 6, two separate clusters begin to be formed, one cluster for the week 4 mice and one cluster for the week 6 mice. Weeks 8, 12 16, and 20 also show the same clustering, wherein week 4 clusters together and the week being referenced to it makes its own cluster. We can also see that there is no overlapping between any of the clusters. As the weeks progress, we also see the clusters moving farther apart. At week 6, the clusters are very close to each other and almost overlapping; at week 8 they are a little farther apart, and they are even farther at week 12. Weeks 16 and 20 appear to be about the same distance from the week 4 cluster.

plot	R2Y	Q2
all weeks	0.36	0.233
4 v 6	0.975	0.817
4 v 8	0.981	0.906
4 v 12	0.979	0.894
4 v 16	0.992	0.92
4 v 20	0.949	0.891

Table 3.2.3.1 - R2Y and Q2 values for the PLS-DA plots constructed for the axenic IL-10 KO females over time.

3.3 WT vs. KO: comparison of axenic wild-type mice vs. IL-10 KO mice

3.3.1 Male population

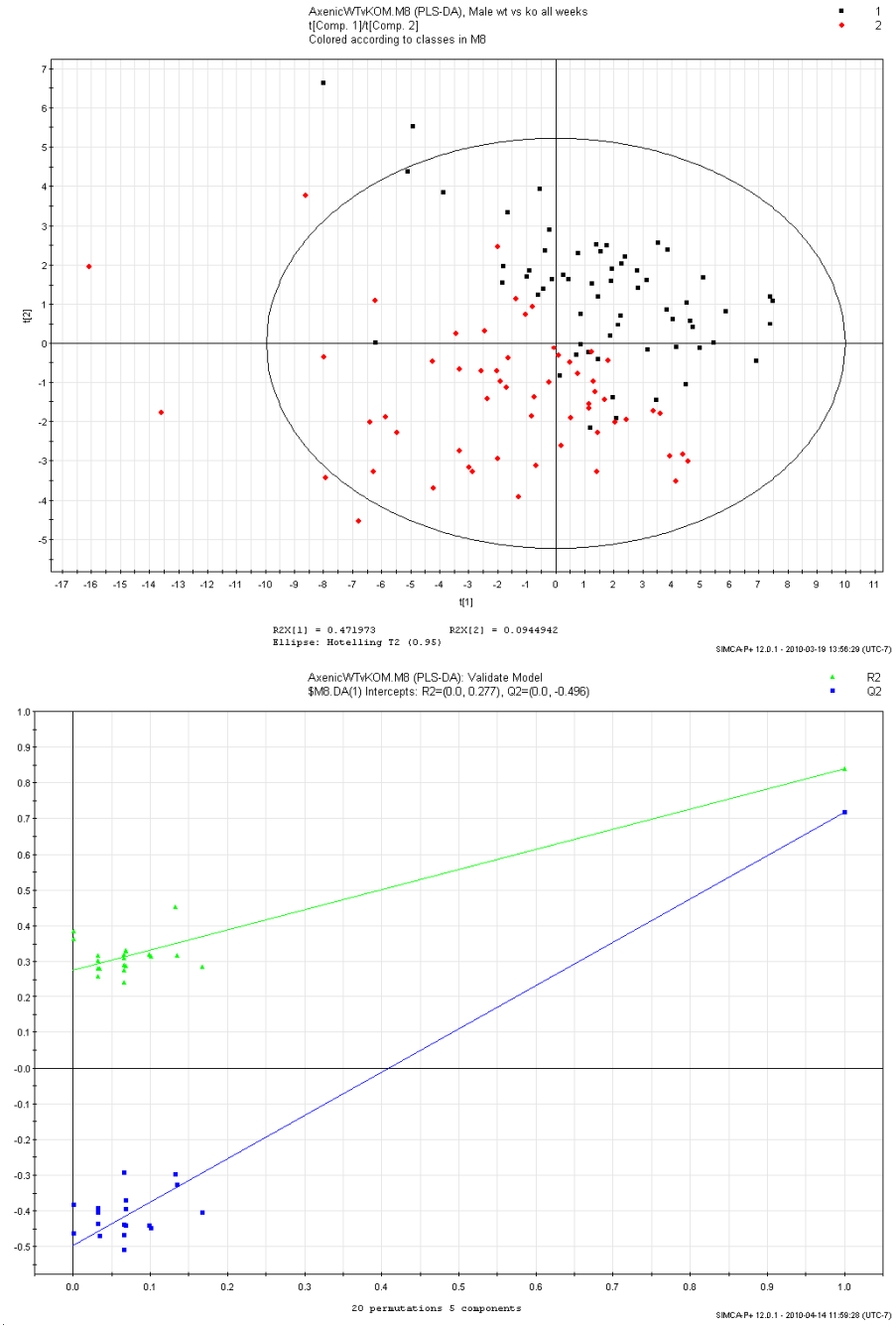

Figure 3.3.1.1 – PLS-DA plot of the urine metabolomic profiles of all male wild-type and IL-10 KO axenic mice (collected from the axenic environments) at weeks 4, 6, 8, 12, 16,

and 20 of age. The wild-type and IL-10 KO groups have 60 data points each (10 points per week). Wild-type mice are shown in red, and IL-10 KO mice are shown in black. Below the PLS-DA plot is the validation plot.

Figure 3.3.1.1 is a PLS-DA for all males comparing wild-type vs. IL-10 KO. Once again, a few outliers have occurred due to low volumes of urine collected. Analysis of the plot reveals that, although two clusters have formed, one cluster for the wild-type mice and one cluster for the IL-10 KO mice, there is also an overlap between data for the wild-type mice and that IL-10 KO mice. To investigate this overlap, we decided to look at the interactions of the clusters by week.

Week 4

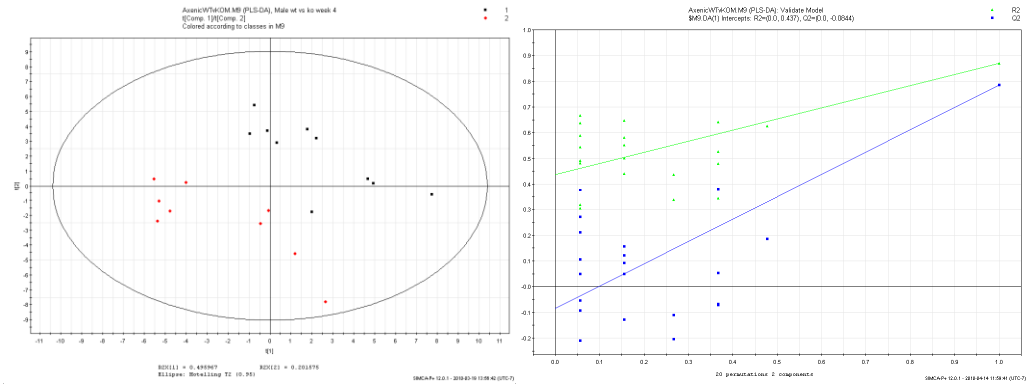

Week 6

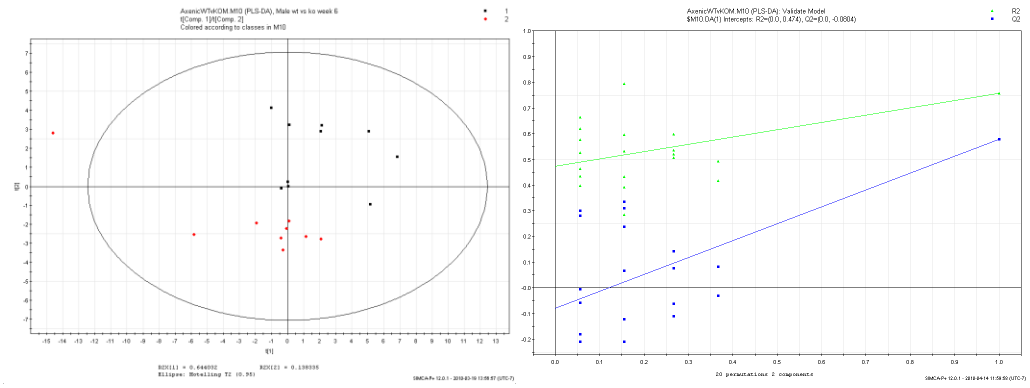

Week 8

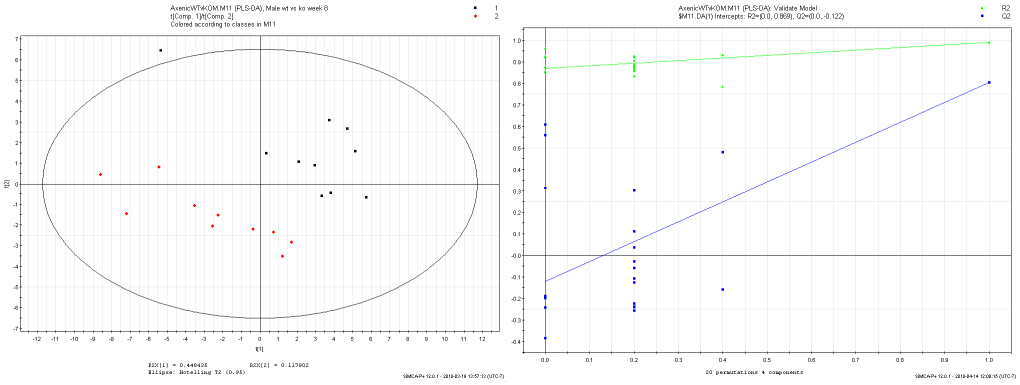

Week 12

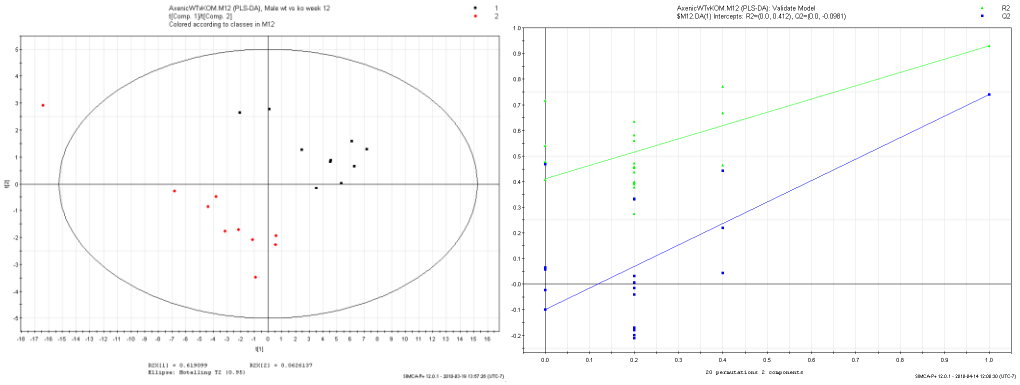

Week 16

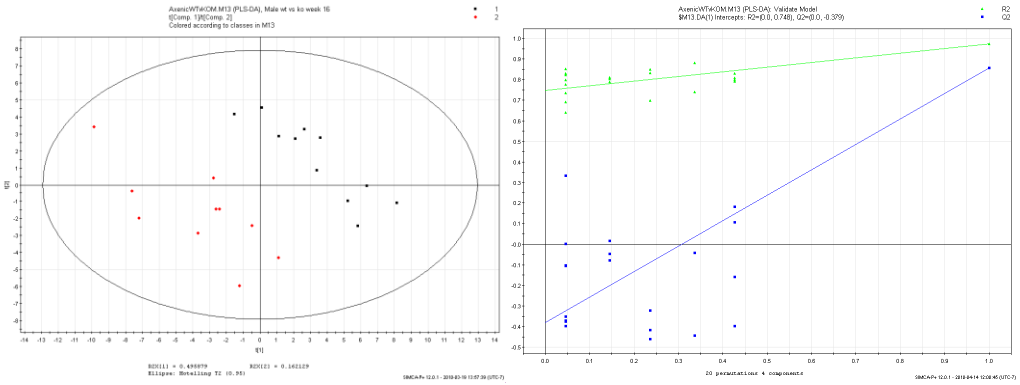

Week 20

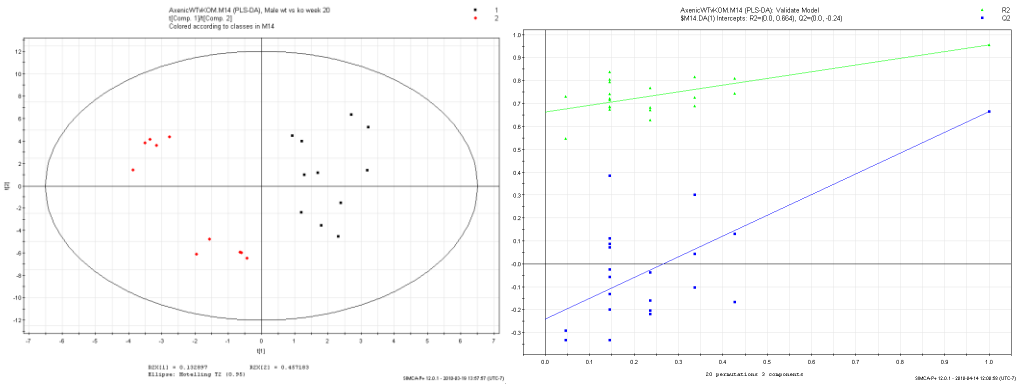

Figure 3.3.1.2 – PLS-DA plots of the urine metabolomic profiles of axenic male wild-type and IL-10 KO mice broken up by weeks of urine collection; wild-type are displayed in red, and IL-10 KO are displayed in black. Each week plots data for 10 wild-type and 10 IL-10 KO mice. Beside each PLS-DA plot is the corresponding validation plot.

A week-by-week comparison of wild-type vs. IL-10 KO axenic males also reveals that there is separation between the two groups. At each time point, there are two clusters, one cluster for the wild-type mice and the other cluster for the IL-10 KO mice. A separation between the two clusters can also be observed for each week.

plot	R2Y	Q2
All weeks	0.84	0.719
week 4	0.869	0.785
week 6	0.757	0.579
week 8	0.988	0.805
week 12	0.93	0.74
week 16	0.974	0.856
week 20	0.957	0.665

Table 3.3.1.1 - R2Y and Q2 values for the PLS-DA plots constructed for the axenic wild-type males vs. the axenic IL-10 KO males.

3.3.2 Female population

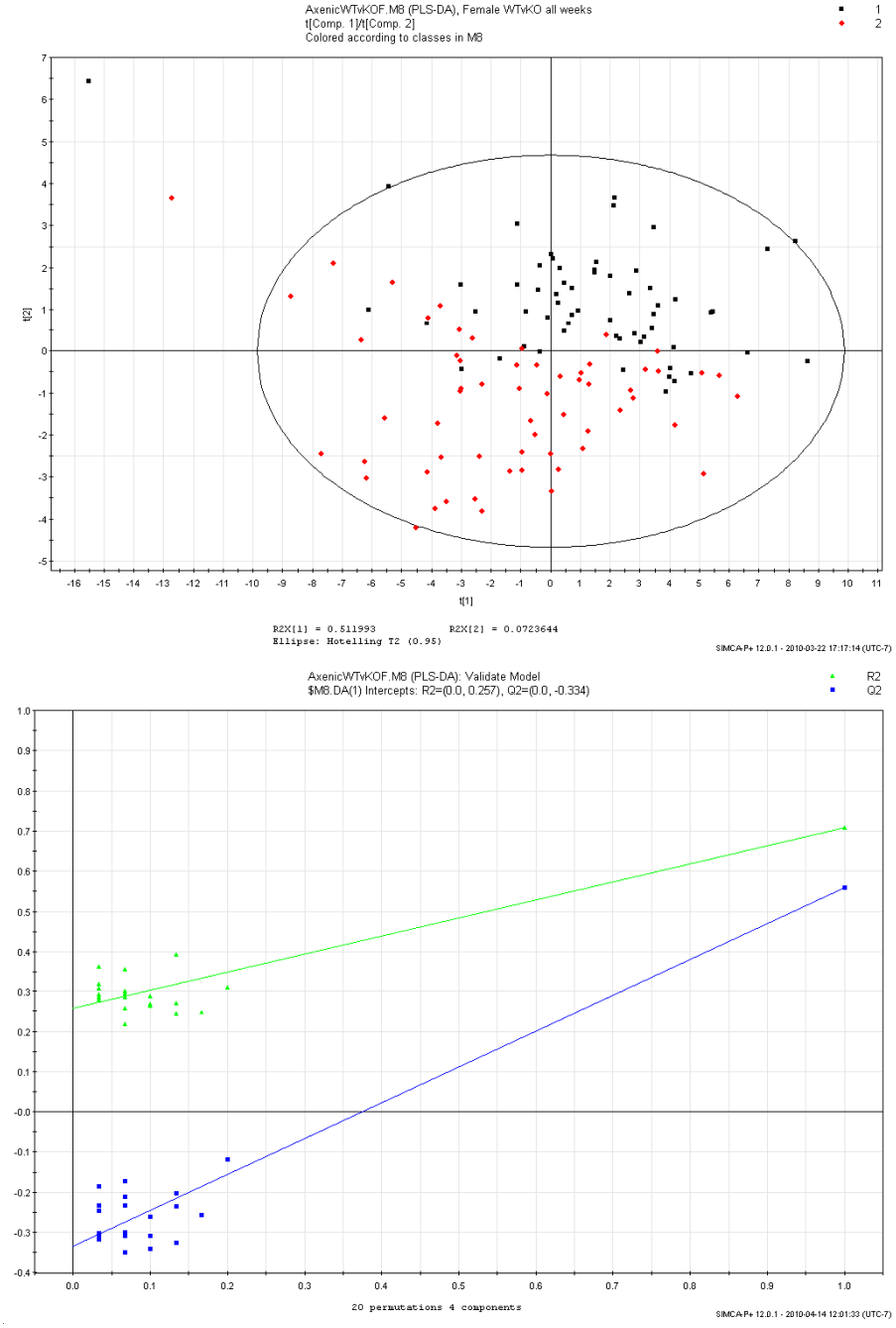

Figure 3.3.2.1 – PLS-DA plot of the urine metabolomic profiles of all female wild-type and IL-10 KO axenic mice (collected from their axenic environments) at weeks 4, 6, 8, 12, 16, and 20 of age. The wild-type and IL-10 KO groups are composed of 60 data points each (10 points per week). Wild-type mice are shown in red, and IL-10 KO mice are shown in black. Beside each PLS-DA plot is the corresponding validation plot.

Similar to the male axenic population plot, in this plot, although two clusters are formed, one cluster for the wild-type mice and one cluster for the IL-10 KO mice, there is also an overlap between the points for the wild-type mice and those for the IL-10 KO mice. The PLS-DA plot also shows a few outliers in this group, again due to low volume of urine collection in the initial collection set. To investigate the overlap, we again looked at the interactions of each cluster by week.

Week 4

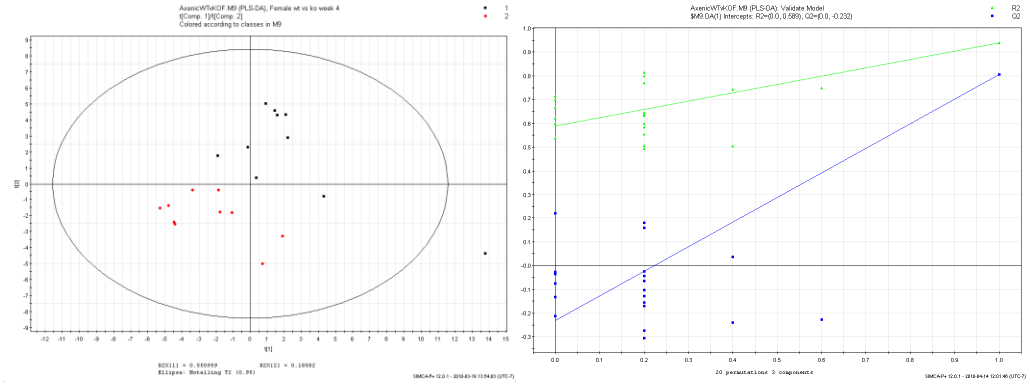

Week 6

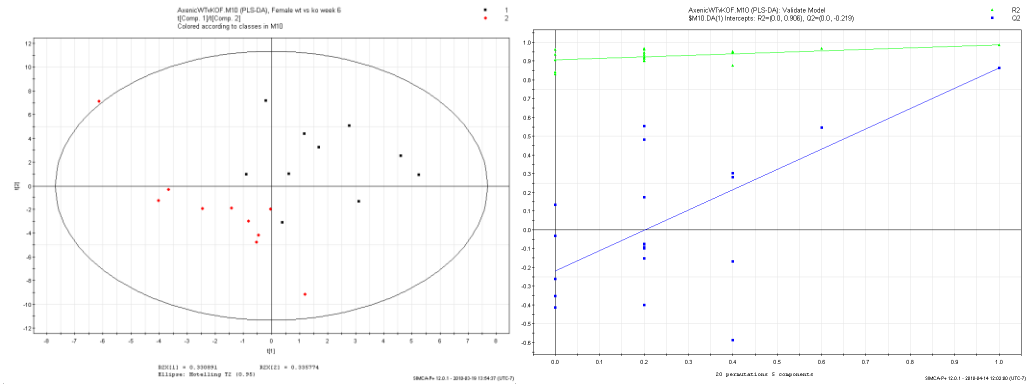

Week 8

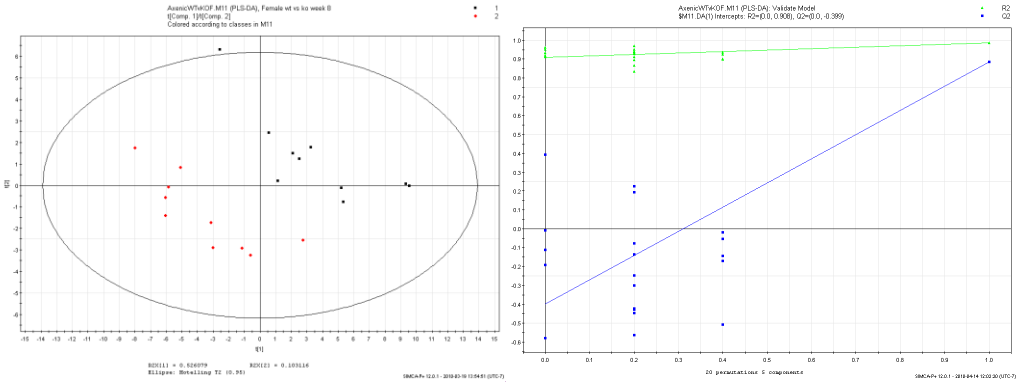

Week 12

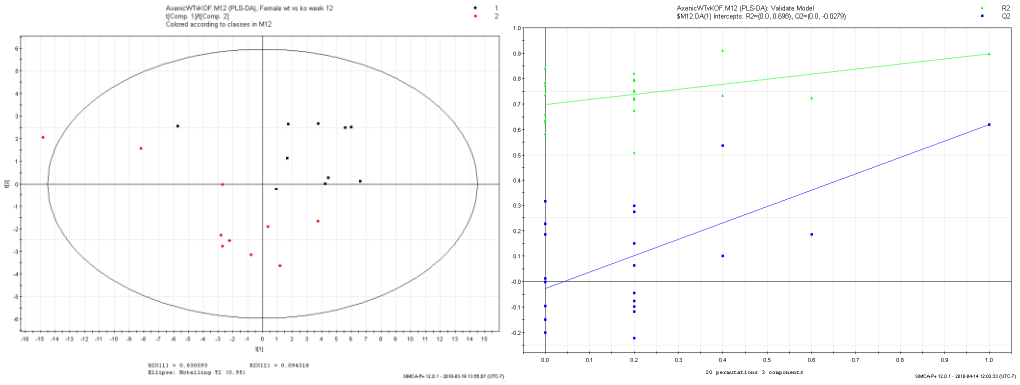

Week 16

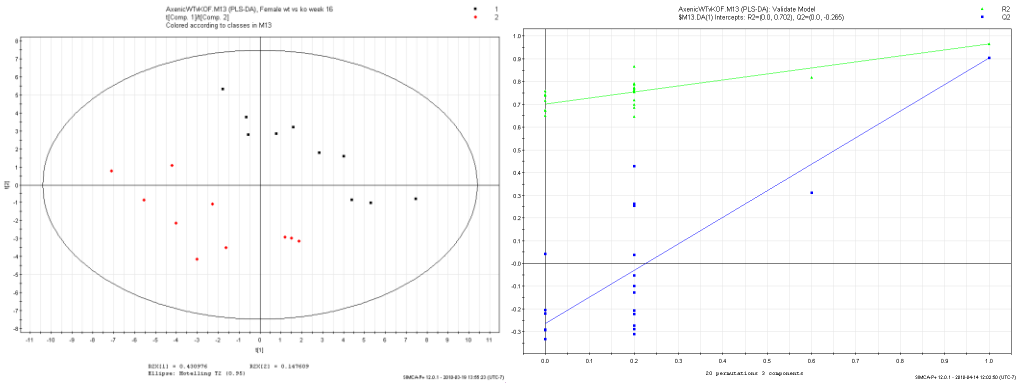

Week 20

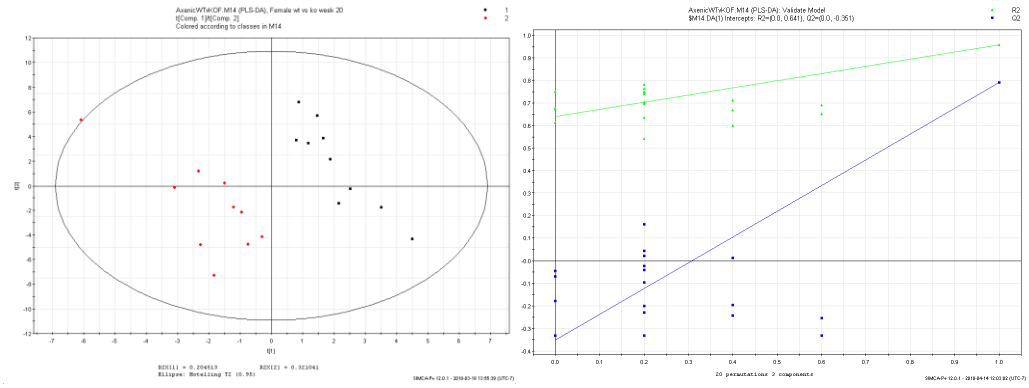

Figure 3.3.2.2 – PLS-DA plots of the urine metabolomic profiles of the axenic female wild-type and IL-10 KO mice broken up by week of urine collection; wild-type are displayed in red, and IL-10 KO are displayed in black. Each week is composed of 10 wild-type and 10 IL-10 KO. Beside each PLS-DA plot is the corresponding validation plot.

Week-by-week comparisons of wild-type axenic females vs. IL-10 KO axenic females shows separation between the wild-type mice and the IL-10 KO mice. Weeks 4, 8, 16, and 20 show a clear separation. Week 12 also shows separation, but the separation is not as large as those observed at other weeks. Week 6 shows two clusters with a very slight overlap between the two groups.

plot	R2Y	Q2
All weeks	0.709	0.561
week 4	0.94	0.807
week 6	0.988	0.865
week 8	0.987	0.884
week 12	0.898	0.618
week 16	0.967	0.904
week 20	0.959	0.792

Table 3.3.2.1 - R2Y and Q2 values for the PLS-DA plots constructed for axenic wild-type females vs. axenic IL-10 KO females.

Chapter 4 - Conventional Mice

4.1 Wild-type population

4.1.1 Wild-type population: comparison of male and female at various ages

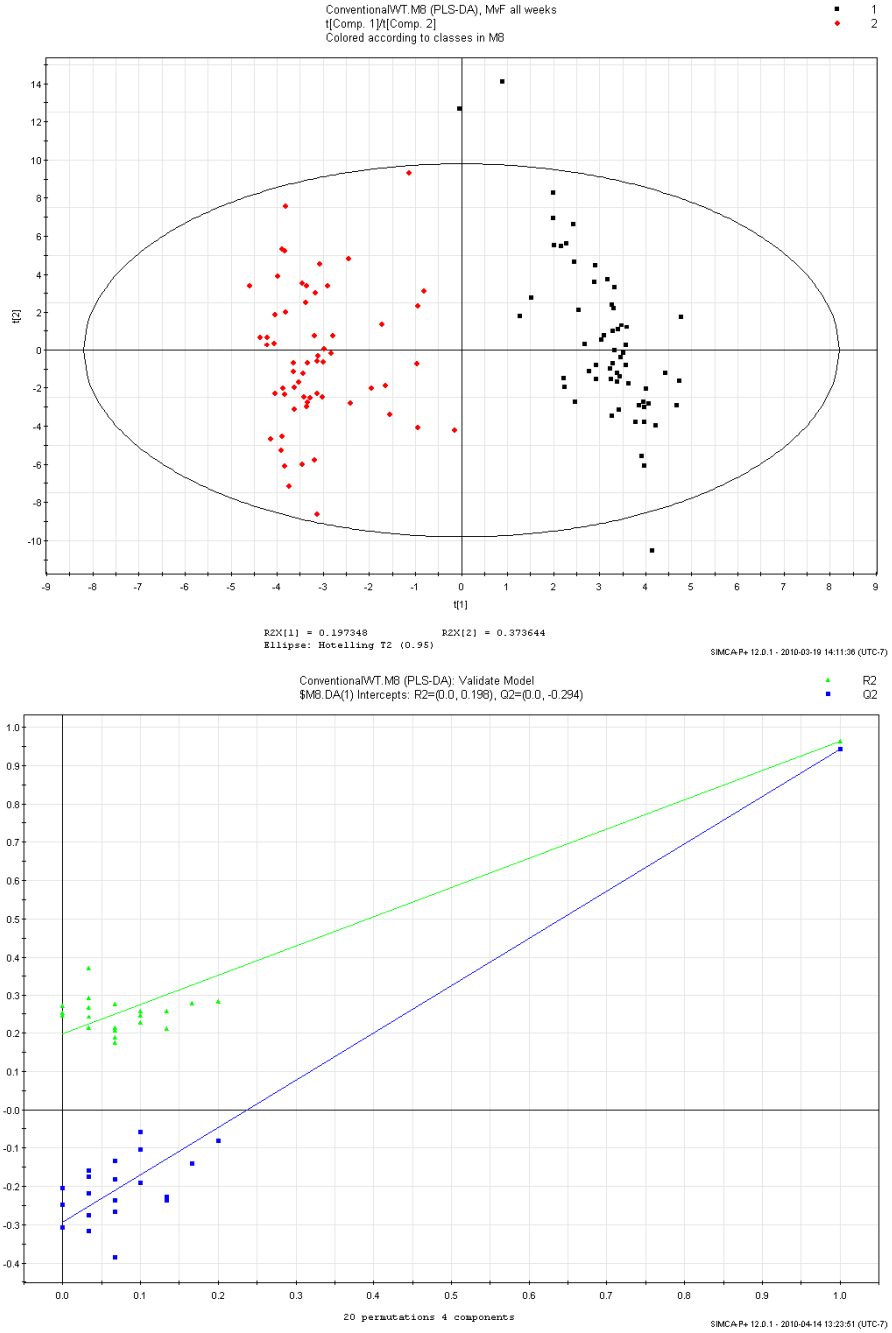

Figure 4.1.1.1 – PLS-DA plot of the urine metabolomic profiles of all male and female conventional wild-type mice (collected from their conventional environments) on weeks 4,

6, 8, 12, 16, and 20 of age. The male and female groups each comprises 60 data points (10 points per week). Male mice are shown in red, and female mice are shown in black. Although a few outliers do appear, a clear separation between the two groups can be observed. Below the PLS-DA plot is the validation plot.

Figure 4.1.1.1 is a PCA plot showing data from wild-type males and wild-type females raised in a conventional environment. This plot clearly shows the clustering of the male group (red) as completely separate from the clustering of the female group (black). Other than the 3 outliers, the clustering of these groups also appears to be fairly tight. Although the female group has 3 outliers, their data seems to group together more tightly than does that of the male group.

Week 4

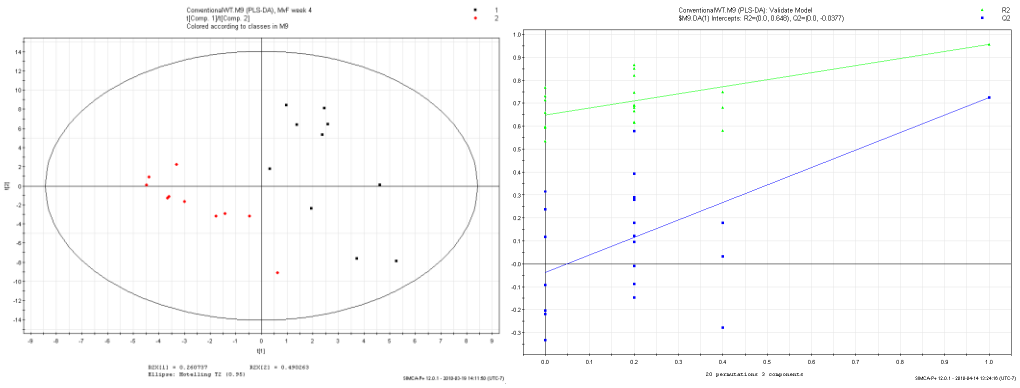

Week 6

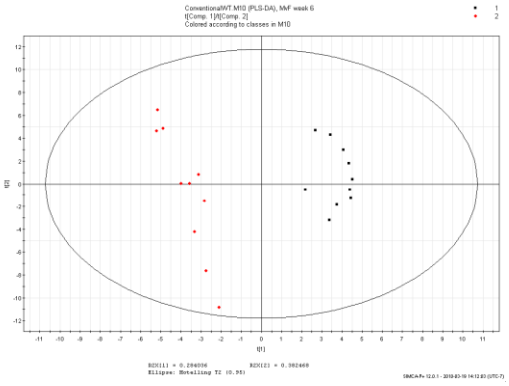

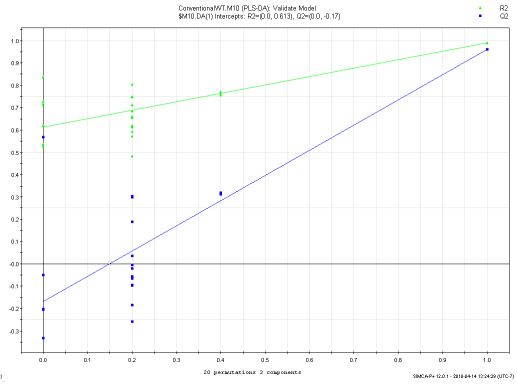

Week 8

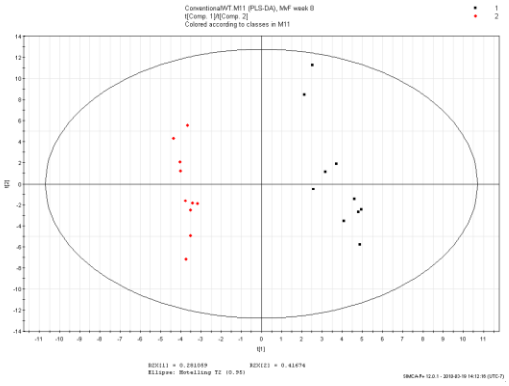

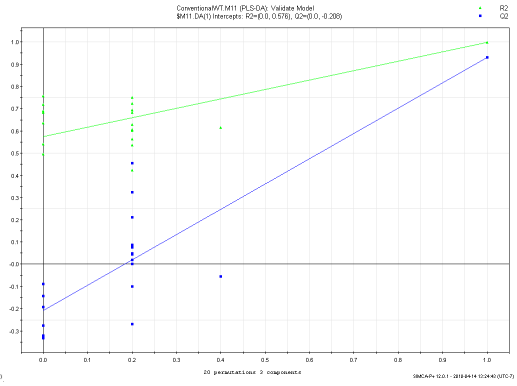

Week 12

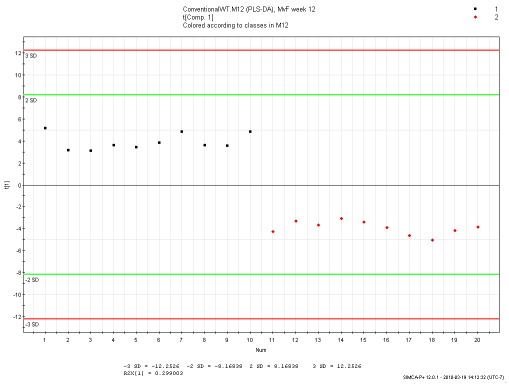

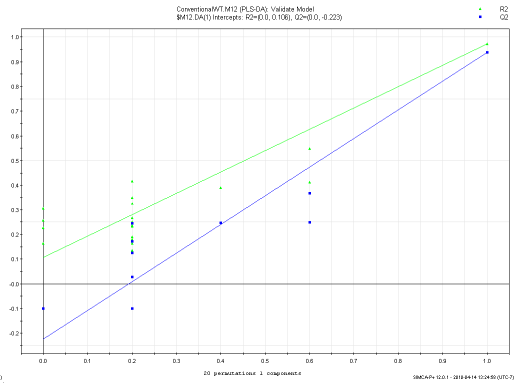

Week 16

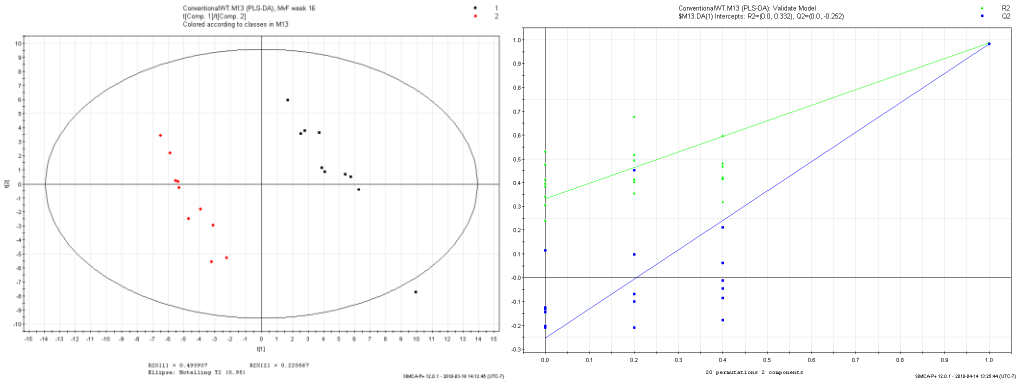

Week 20

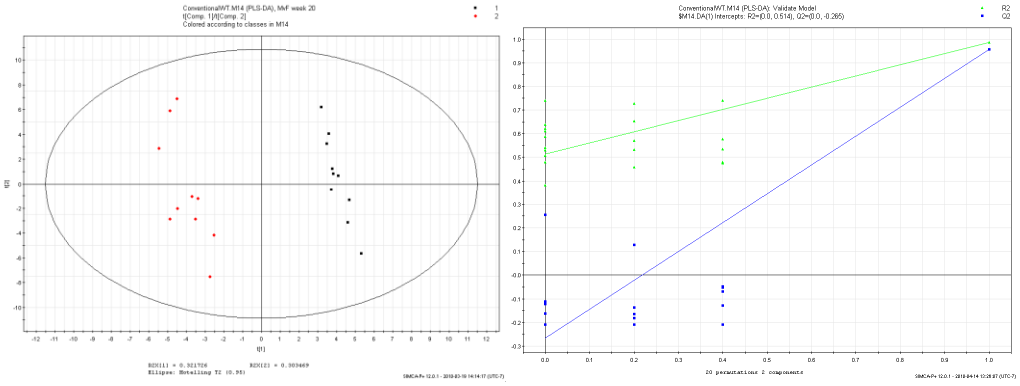

Figure 4.1.1.2 – PLS-DA plots of the urine metabolomic profiles of the conventional wild-type mice broken up according to week of urine collection; males are displayed in red, and females are displayed in black. Each week comprised 10 male and 10 female data points. Beside each PLS-DA plot is the corresponding validation plot.

A week-by-week comparison confirms what we saw in the above figure. There is very clear separation between males and females at every time point. Week 4 is the only time point at which the male and female clusters come close to overlapping, and even at week 4 it is quite apparent that two separate clusters have been formed. All subsequent weeks show a very clear clustering of males as distinct from females, and the separation

between the two groups is very clear. One interesting note is that, at week 12, only one component was used to separate the males from the females; a second component was initially constucted, but it was discarded from analysis as it created a model that was not as accurate as the original single-component model.

plot	R2Y	Q2
All weeks	0.965	0.944
week 4	0.955	0.725
week 6	0.991	0.96
week 8	0.977	0.931
week 12	0.974	0.938
week 16	0.988	0.983
week 20	0.985	0.957

Table 4.1.1.1 - R2Y and Q2 values for the PLS-DA plots constructed for the conventional wild-type male vs. conventional wild-type female plots.

4.1.2 Wild-type males: comparison of urine metabolomics over all collection weeks

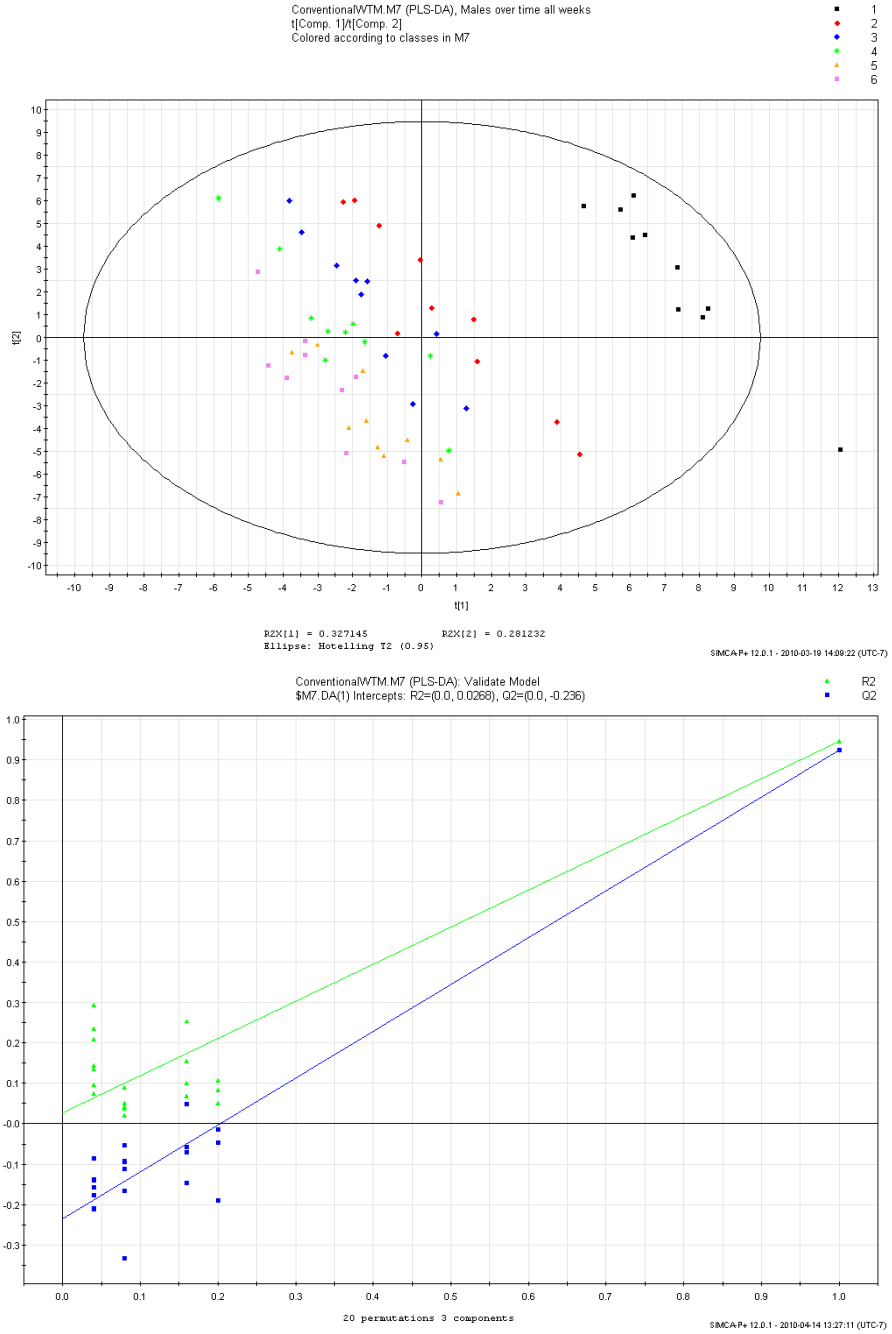

Figure 4.1.2.1– PLS-DA plot of urine metabolomic profiles of all wild-type male conventional mice over all collection time points. Each week is constructed from 10 points and is displayed in a different color: week 4 (black), week 6 (red), week 8 (blue), week 12 (green), week 16 (yellow), week 20 (purple). This plot shows the progression of the urine

metabolomic profiles of male wild-type mice as they grow in a conventional environment. Below the PLS-DA plot is the validation plot.

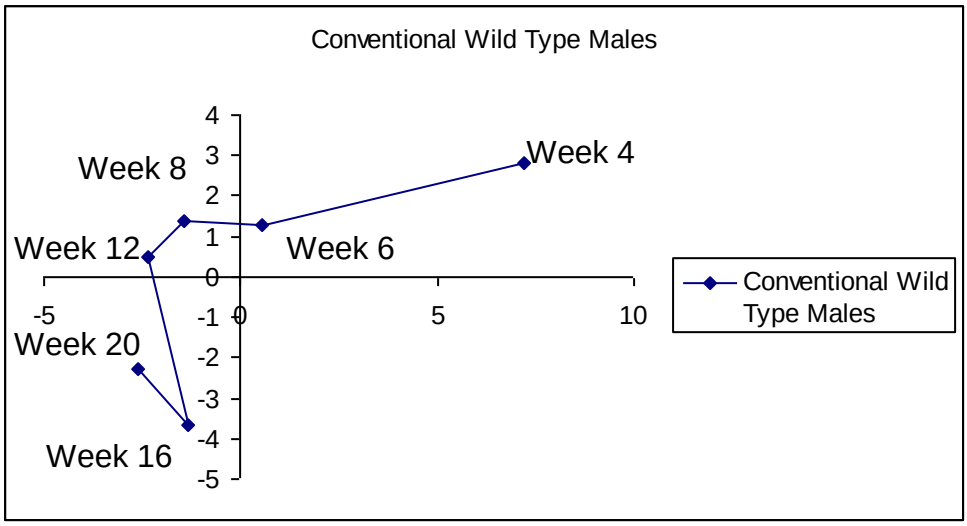

Figure 4.1.2.2– Metabolic trajectory of the conventional wild-type males; the plot was constructed by taking the coordinates of all the points for each week and calculating a single mean coordinate for each week.

Figure 4.1.2.1 is a PLS-DA for all of the conventional wild-type males over all the collected time points. Here, we can clearly see that the largest difference between any two consecutive time points occurs between week 4 and week 6; the gap between the clusters at week 4 and week 6 is larger than that for any other separation. Although not as large as that for week 4 and 6, the separation between weeks 6 and 8 also appears to have only the slightest of overlap. Week 8 to week 12 also shows some separation between clusters, although the overlap is a little more apparent than in the weeks before. However, though the clusters of week 12, 16 and 20 do not show any real horizontal movement, they do show some

vertical movement on the plot. Analysis of the metabolic trajectories plot (Figure 4.1.2.2) confirms the observations that we made from the PLS-DA plot.

Week 4 vs. Week 6

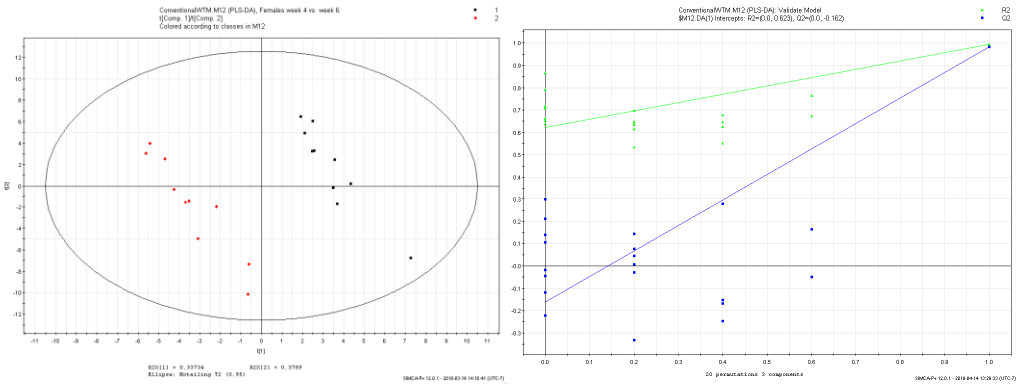

Week 4 vs. Week 8

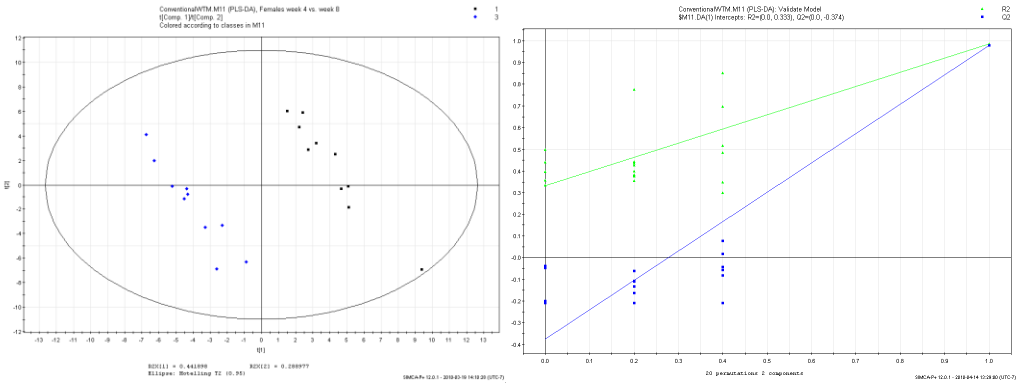

Week 4 vs. Week 12

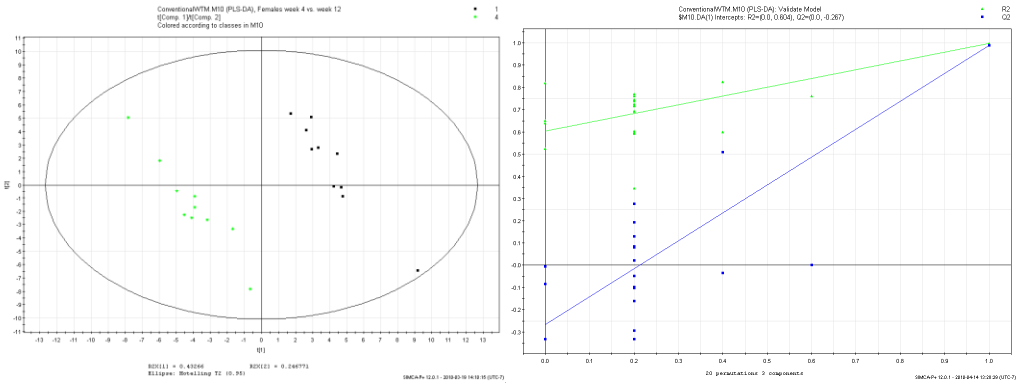

Week 4 vs. Week 16

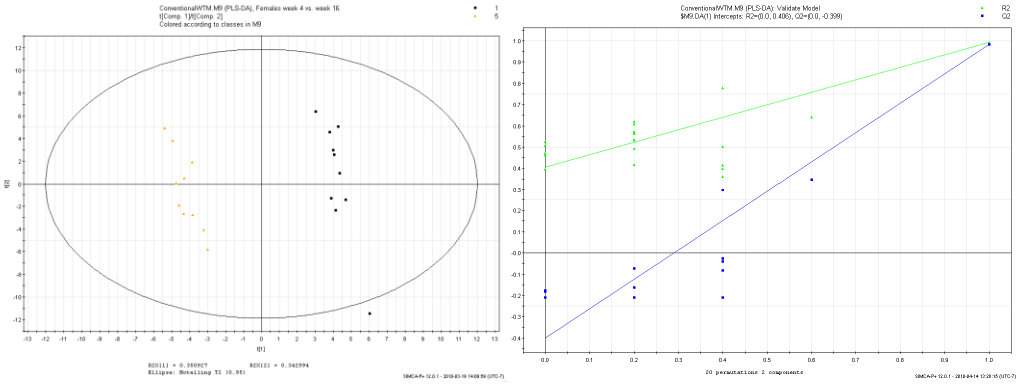

Week 4 vs. Week 20

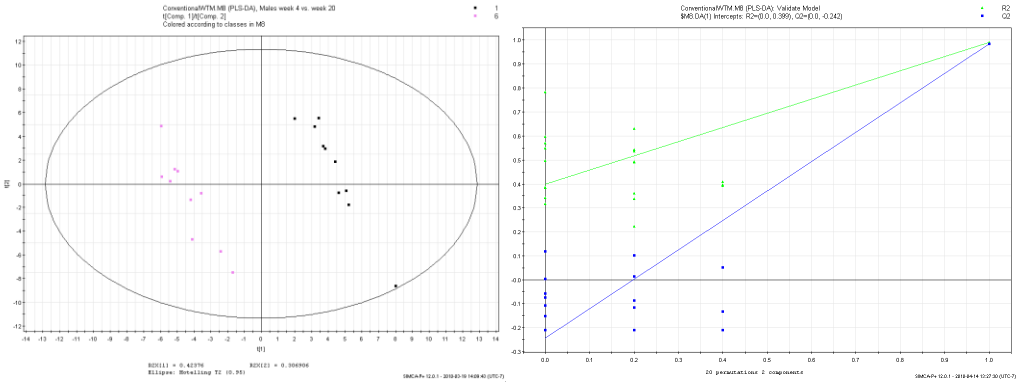

Figure 4.1.2.3 – PLS-DA plot of urine metabolomic profiles of wild-type male conventional mice in reference to week 4; each group is made up of the same 10 mice from week 4 and the week 4 data is used as reference for the groups of 10 mice that comprise the other weeks collected. Beside each PLS-DA plot is the corresponding validation plot.

Week-by-week analysis in reference to week 4, shows each week to be unique and different from week 4. For these PLS-DA plots, there are two distinct clusters formed, and the clusters do not overlap at all. In the week 4 cluster, there is one outlier, and, depending on which dataset it is compared to, it is either beyond the limit of the circle or just on the outer limit. Although all the clusters appear to be grouped together, the

groupings are a little tighter at weeks 16 and 20 than they are at weeks 6, 8, and 12.

plot	R2Y	Q2
all weeks	0.378	0.317
4 v 6	0.993	0.984
4 v 8	0.987	0.979
4 v 12	0.997	0.989
4 v 16	0.991	0.982
4 v 20	0.989	0.983

Table 4.1.2.1 - R2Y and Q2 values for the PLS-DA plots constructed for the conventional wild-type males over time.

4.1.3 Wild-type females: comparison of urine metabolomics over all collection weeks

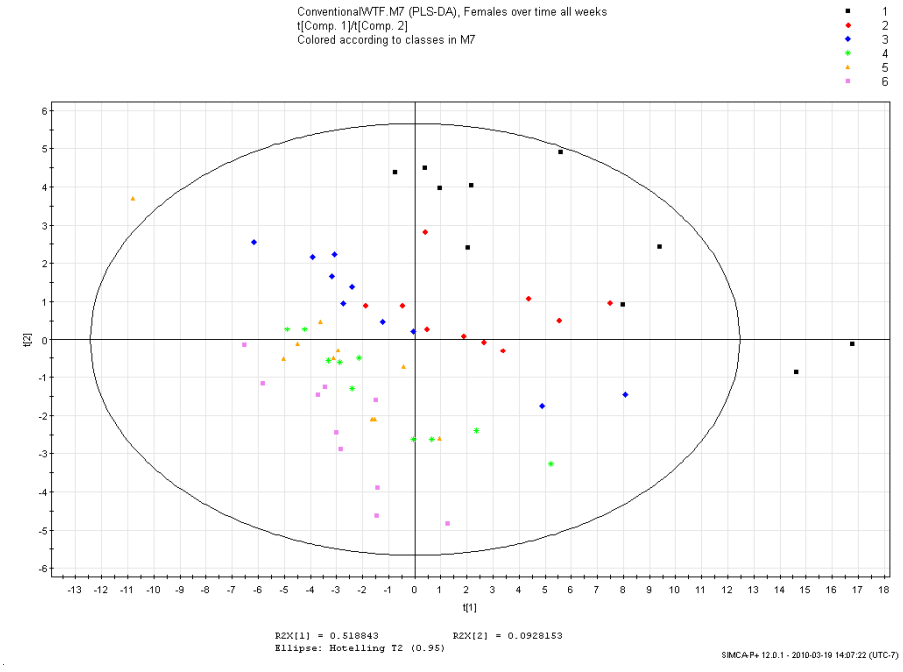

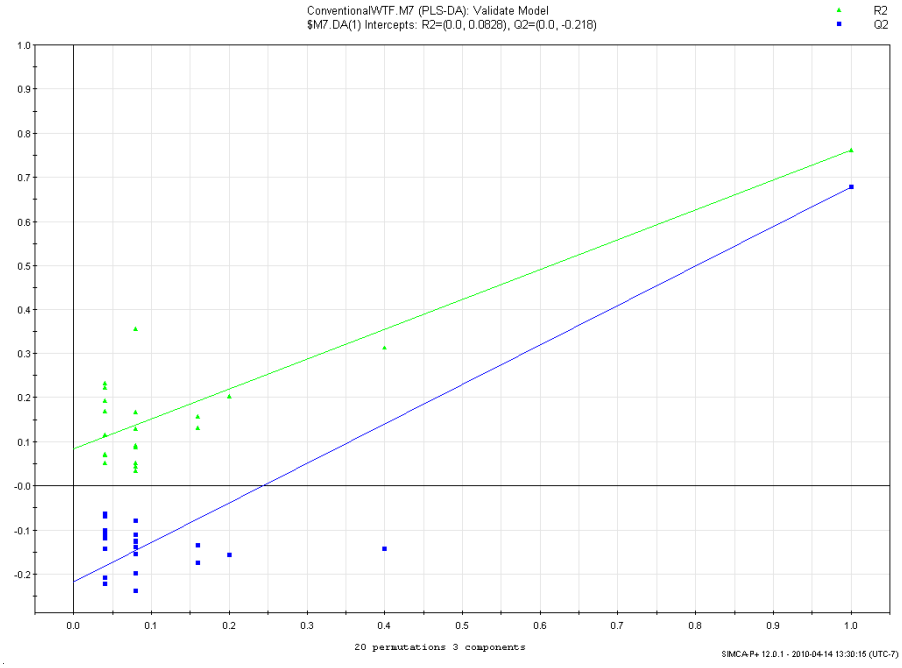

Figure 4.1.3.1– PLS-DA plot of urine metabolomic profiles of all wild-type female conventional mice over all collection time points. Each week is constructed from 10 points and is displayed in a different color: week 4 (black), week 6 (red), week 8 (blue), week 12 (green), week 16 (yellow), week 20 (purple). This plot shows the progression of the urine metabolomic profile of female wild-type mice as they grow in a conventional environment. Below the PLS-DA plot is the validation plot.

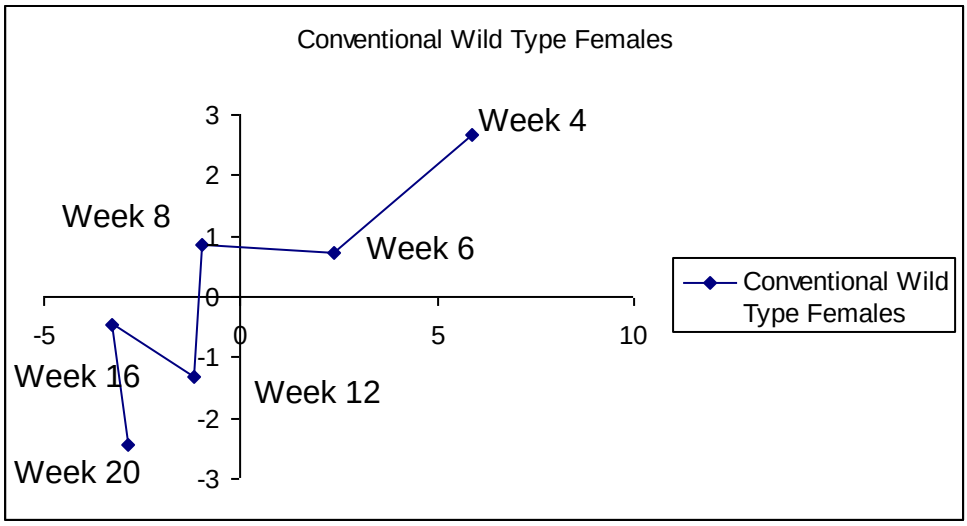

Figure 4.1.3.2– Metabolic trajectory of the conventional wild-type females; plot was constructed by taking the coordinates of all the points for each week and calculating a single mean coordinate for each week.

Figure 4.1.3.1 is a PLS-DA of conventional wild-type females over all collection time-points. Unlike those for the males, the female clusters do not seem to group together as tightly; this difference is especially evident in the earlier weeks of collection. The data points for weeks 4, 6, and 8 appear to be spread over a large area of the plot, and clustering is not clearly evident. It is not until weeks 12, 16, and 20 that we are able to see the groups beginning to cluster together, but at this point there is no real gap between the clusters that have formed. Analysis of the metabolic trajectories plot (Figure 4.1.3.2) confirms the observations from the PLS-DA plot. The largest movement along the plot occurs between weeks 4 and 6, while the other weeks appear to have about the same magnitude of movement on the plot with variation occurring in terms of the trajectory.

Week 4 vs. Week 6

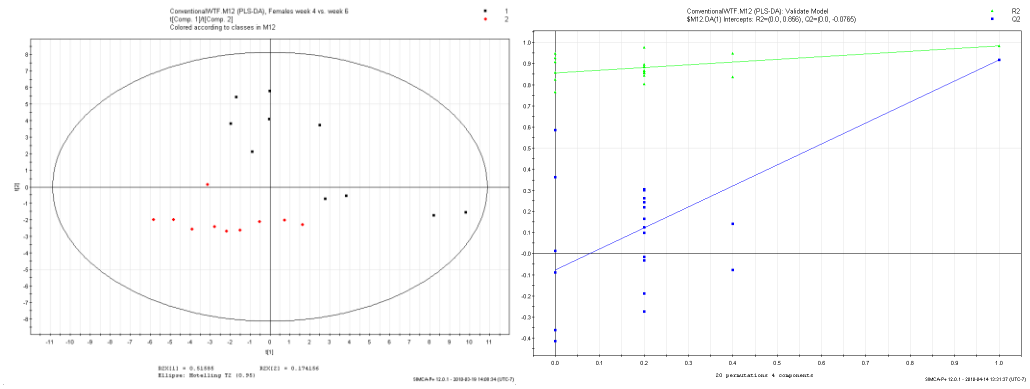

Week 4 vs. Week 8

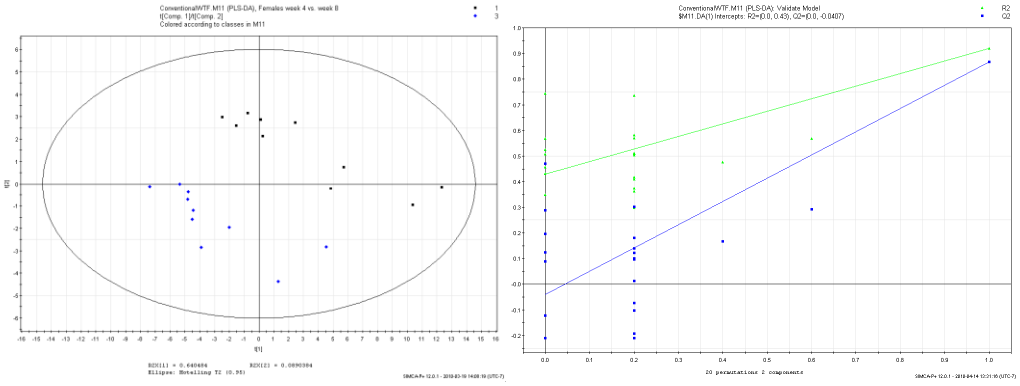

Week 4 vs. Week 12

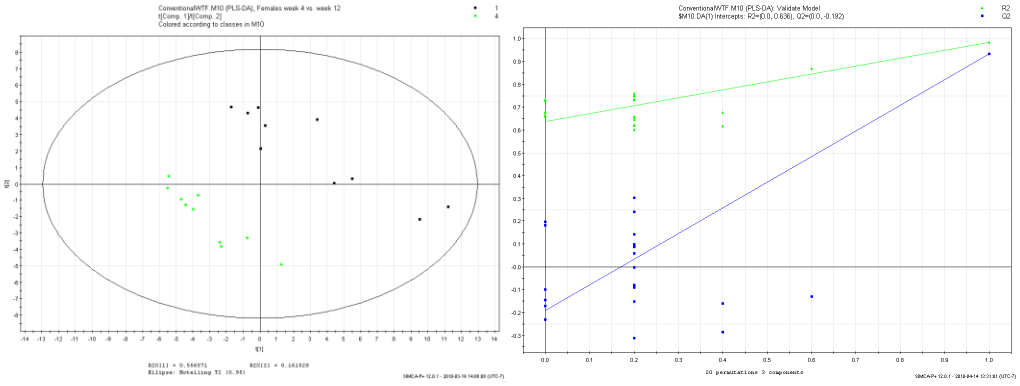

Week 4 vs. Week 16

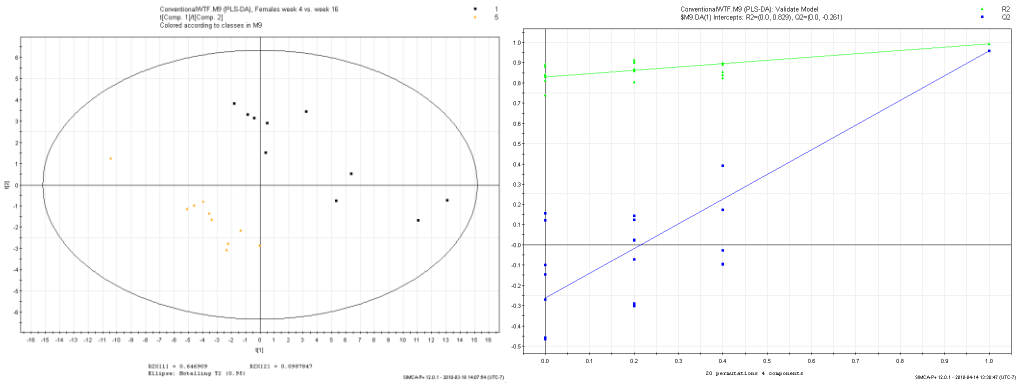

Week 4 vs. Week 20

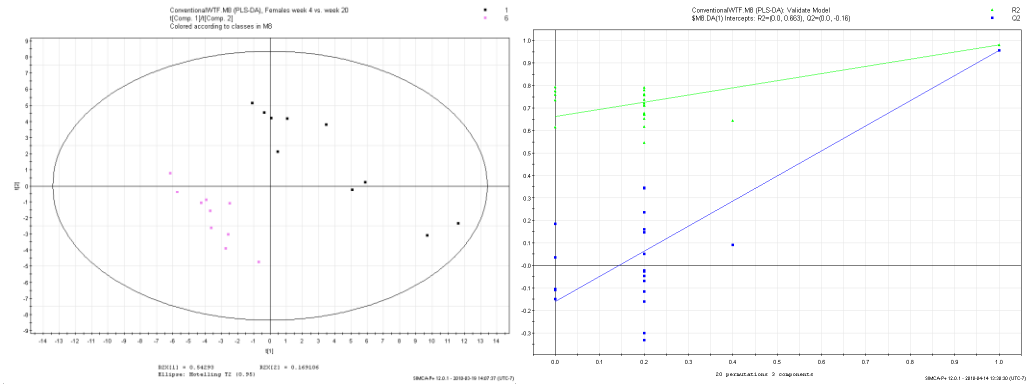

Figure 4.1.3.3 – PLS-DA plot of urine metabolomic profiles of wild-type female conventional mice referenced to week 4; each group is composed of the same 10 mice from week 4 and that data is referenced against the other groups of 10 mice that comprise the other weeks collected. Beside each PLS-DA plot is the corresponding validation plot.

Week-by-week comparisons to week 4 give us a better idea of what was happening in the PLS-DA plot above for the earlier weeks of the female mice. When compared to the week 4 cluster, the week 6 cluster does separate, and a distinct cluster is formed; although there is no overlap between the two groups, there is also little space between the two clusters. A similar trend is observed for week 8 compared to week 4. Once again, the weeks form two separate groups, and the distance between the two clusters has increased. At week 12, we see that the separation has become very large. The PLS-DA at week 4 vs. week 12 shows clustering of two separate groups, and a gap has formed between the two clusters. This is also observed in the plots for weeks 16 and 20.

plot	R2Y	Q2
all weeks	0.323	0.218
4 v 6	0.985	0.917
4 v 8	0.919	0.867
4 v 12	0.982	0.934
4 v 16	0.994	0.959
4 v 20	0.982	0.956

Table 4.1.3.1 - R2Y and Q2 values for the PLS-DA plots constructed for the conventional wild-type females over time.

4.2 IL-10 KO population

4.2.1 IL-10 KO population: comparison of male and female at various ages

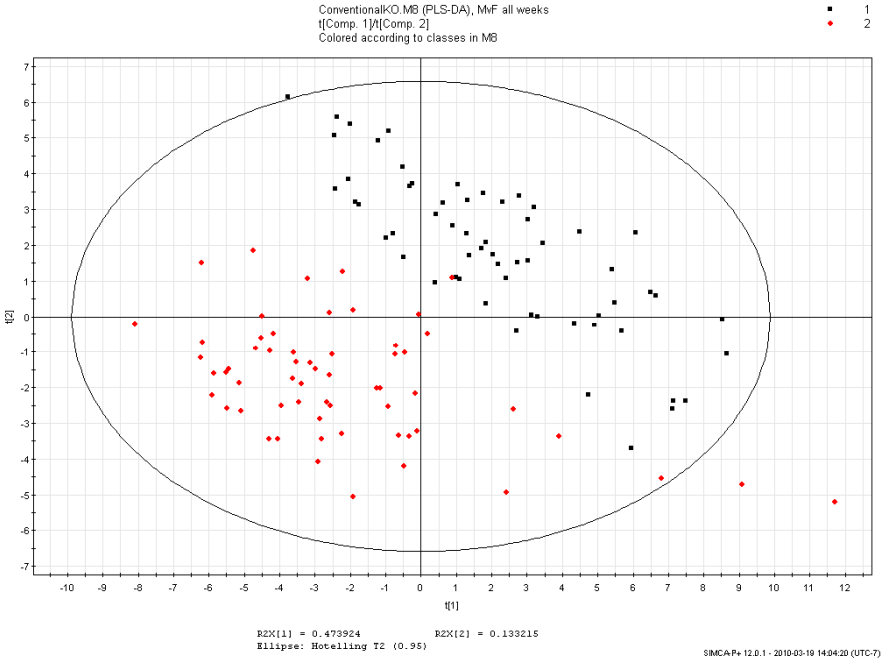

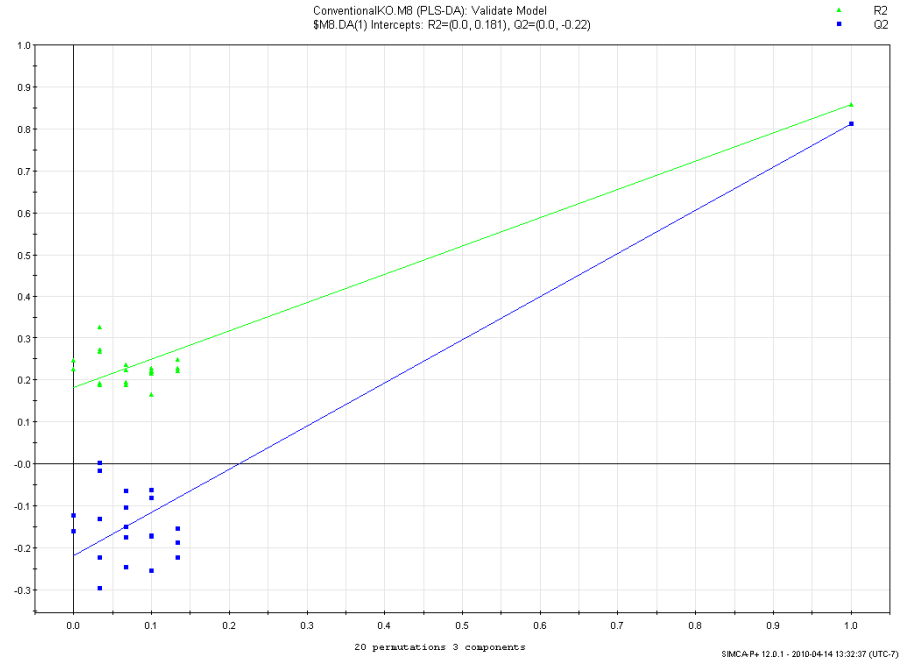

Figure 4.2.1.1 – PLS-DA plot of the urine metabolomic profiles of all male and female conventional IL-10 KO mice (collected fom their conventional environments) on weeks 4, 6, 8, 12, 16, and 20 of age. Each of the male and female groups is composed of 60 data points (10 points per week). Male mice are shown in red, and female mice are shown in black. Below the PLS-DA plot is the validation plot.

Figure 4.2.1.1 is a PLS-DA plot of all conventional IL-10 KO mice; it compares male vs. female. In this plot, we can see that there are two clusters formed, one cluster for the male group and one cluster for the female group. The two clusters separate, with the exception of 3 male points overlapping with the female cluster. This plot also shows a couple of outliers in the data. Week-by-week analysis was then performed to examine how the two clusters interact at each week.

Week 4

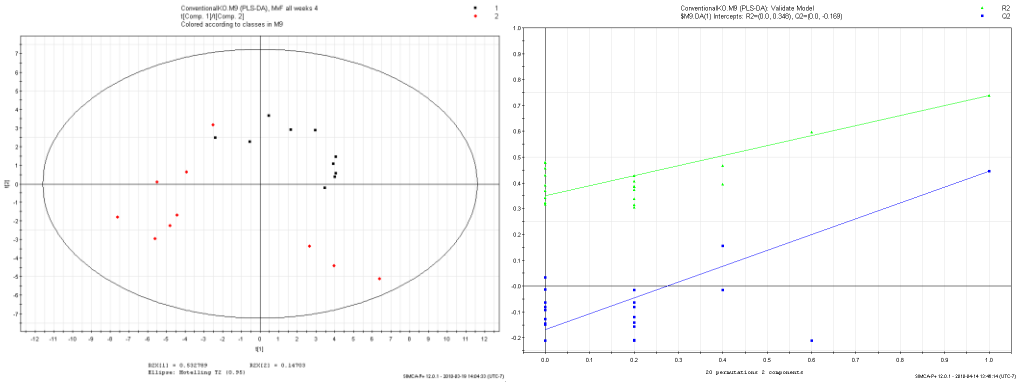

Week 6

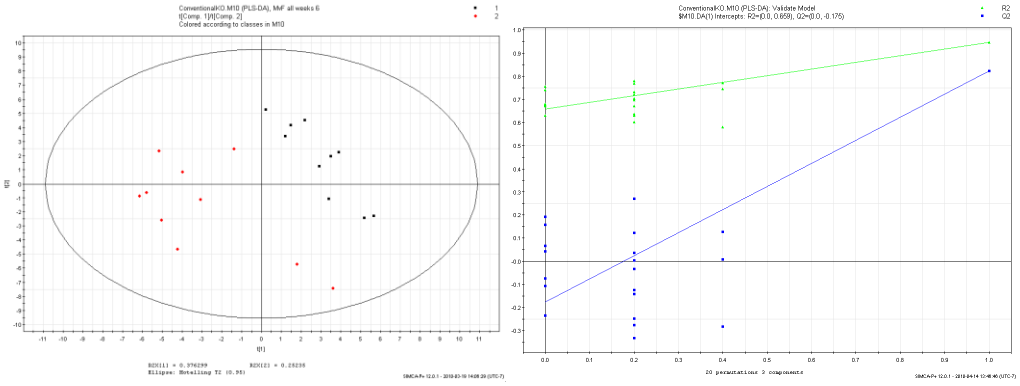

Week 8

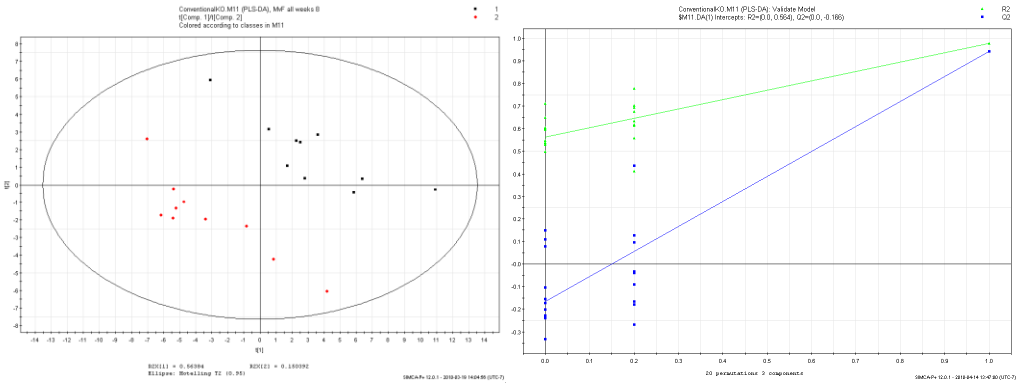

Week 12

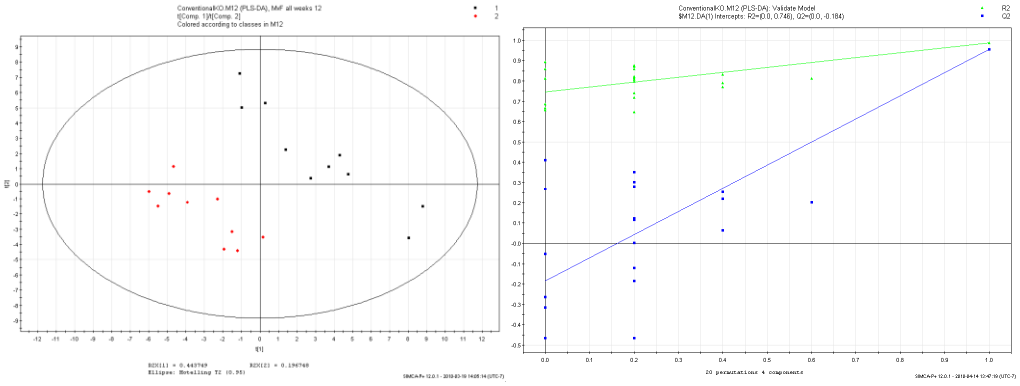

Week 16

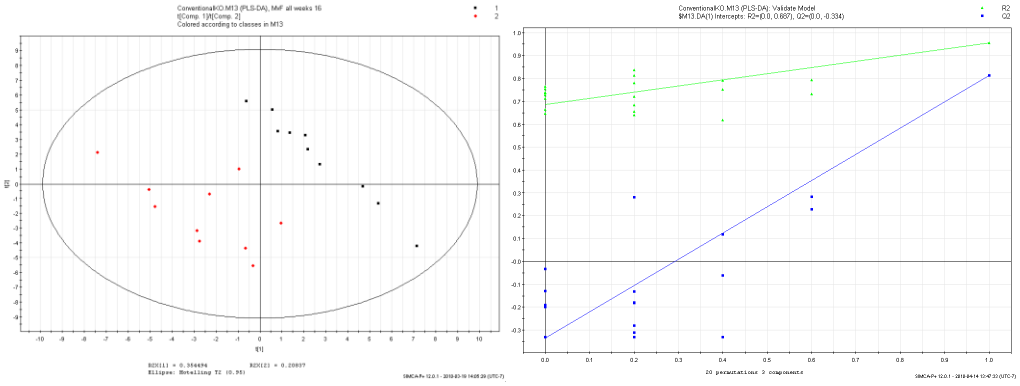

Week 20

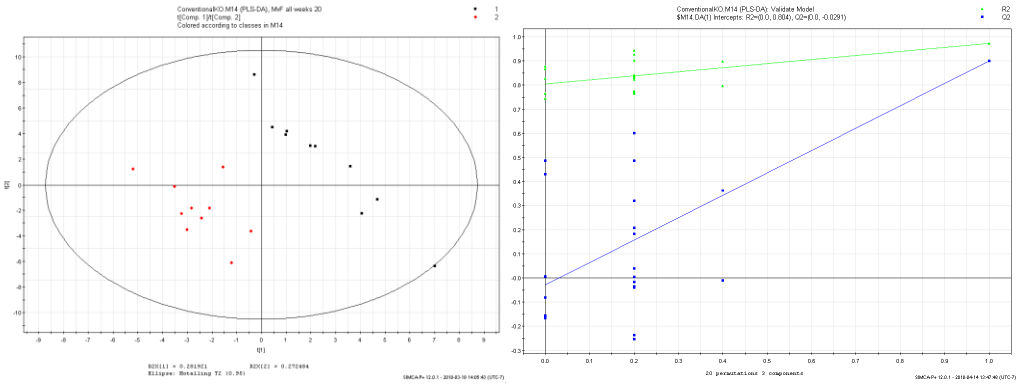

Figure 4.2.1.2 – PLS-DA plots of the urine metabolomic profiles of the conventional IL-10 KO mice broken up by weeks of urine collection; males are displayed in red and females are displayed in black. Each week comprises 10 males and 10 females. Beside each PLS-DA plot is the corresponding validation plot.

Week-by-week comparison of the conventional IL-10 KO mice shows basically the same progress we observed in the large PCA plot above. Analysis by week shows that, at each time point, two clusters have formed, one cluster for the males and one cluster for the females. At week 4, there is a slight overlap between the male and female clusters. At week 6, the two clusters have separated completely, and the gap between the two clusters is increased even more at week 8. Weeks 12, 16, and 20 show similar results to those observed at week 8, with the gap between the two clusters remaining constant.

All weeks	0.858	0.813
week 4	0.738	0.445
week 6	0.946	0.823
week 8	0.976	0.941
week 12	0.988	0.956
week 16	0.957	0.813
week 20	0.972	0.9

Table 4.2.1.1 - R2Y and Q2 values for the PLS-DA plots constructed for the conventional IL-10 KO male vs. conventional IL-10 KO female plots.

4.2.2 IL-10 KO males: comparison of urine metabolomics over all collection weeks

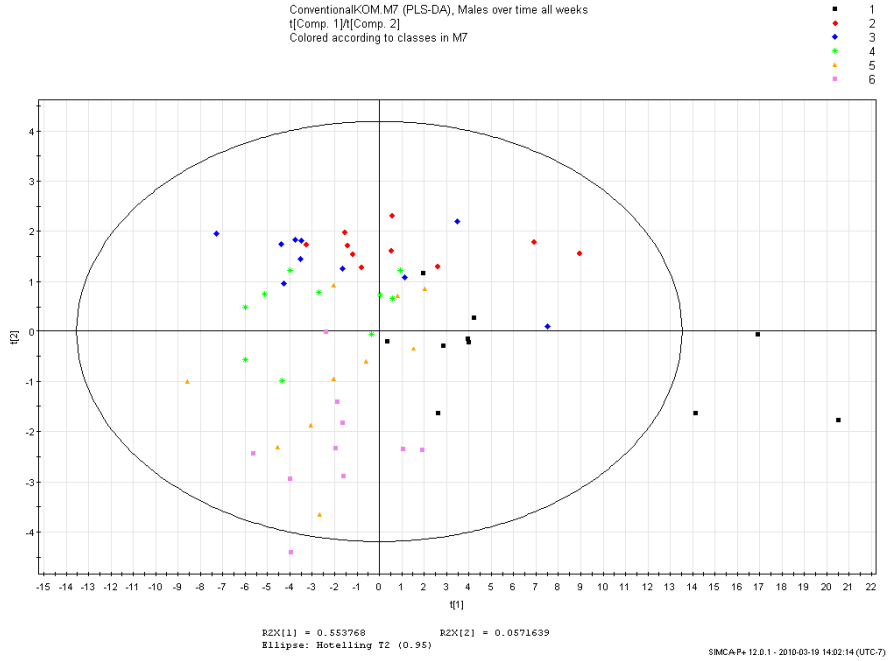

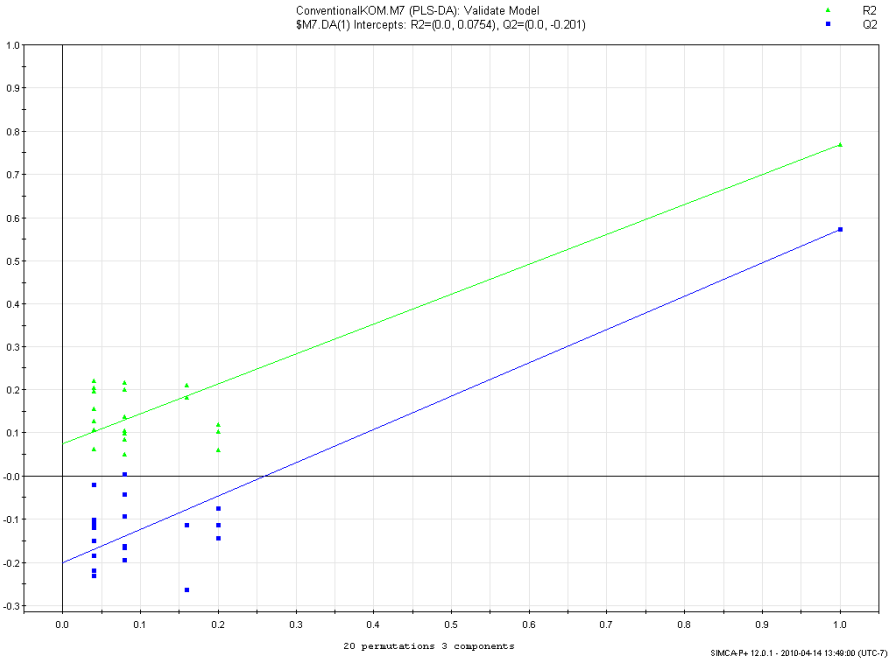

Figure 4.2.2.1– PLS-DA plot of urine metabolomic profiles of all IL-10 KO male conventional mice over all collection time-points. Each week is constructed from 10 points and is displayed in a different color: week 4 (black), week 6 (red), week 8 (blue), week 12 (green), week 16 (yellow), week 20 (purple). This plot shows the progression of

the urine metabolomic profile of male wild-type mice as the mice grow in a conventional environment. Below the PLS-DA plot is the validation plot.

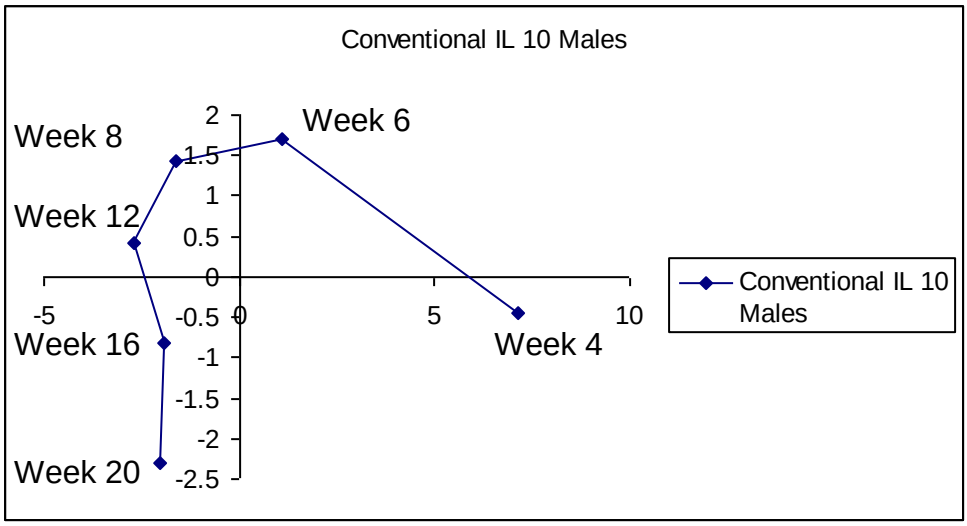

Figure 4.2.2.2– Metabolic trajectory of the conventional IL-10 KO males; the plot was constructed by taking the coordinates of all the points for each week and calculating a single mean coordinate for each week.

Figure 4.2.2.1 is a PLS-DA for all conventional IL-10 KO males over all the collection weeks. Unlike the wild-type mice, the IL-10 KO mice data do not cluster together tightly. Week 4 (black) appears to be the most spread out; this is most likely due to two main factors: age and strain. It was difficult to collect consistent samples from the week 4 mice because they are so small they naturally produce much less urine. Also, because week 4 was their first time in the metabolic cages, they were experiencing extra stress along with unfamiliar surroundings. Weeks 6 and 8 also seem to be spread throughout the plot. It is not until weeks 12, 16, and 20 that the clusters begin to group together, but the clustering is still weak, at best.

Because of the spread of the points, caution must be used when analyzing this metabolic trajectories plot (Figure 4.2.2.2). The spread could cause the mean coordinates of the group to be skewed. Although this kind of plot is useful for generalizing the movement of the clusters, it should not be over-analyzed. In order to investigate the cluster movement in this plot, we once again used week 4 as a reference for all the other weeks.

Week 4 vs. Week 6

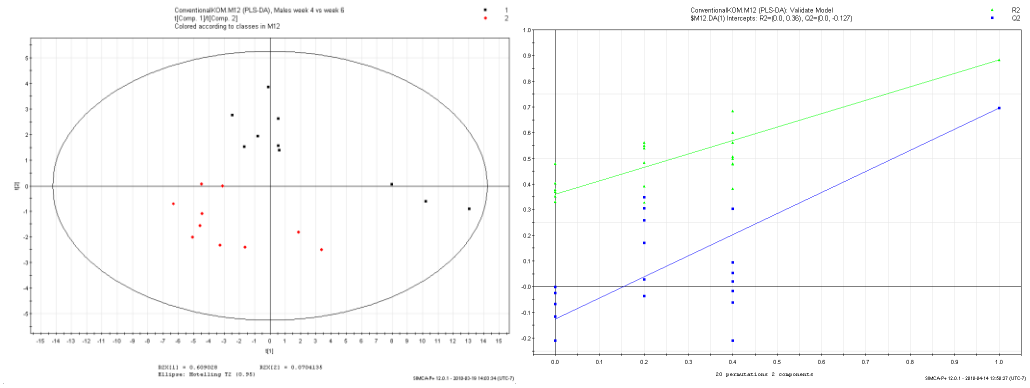

Week 4 vs. Week 8

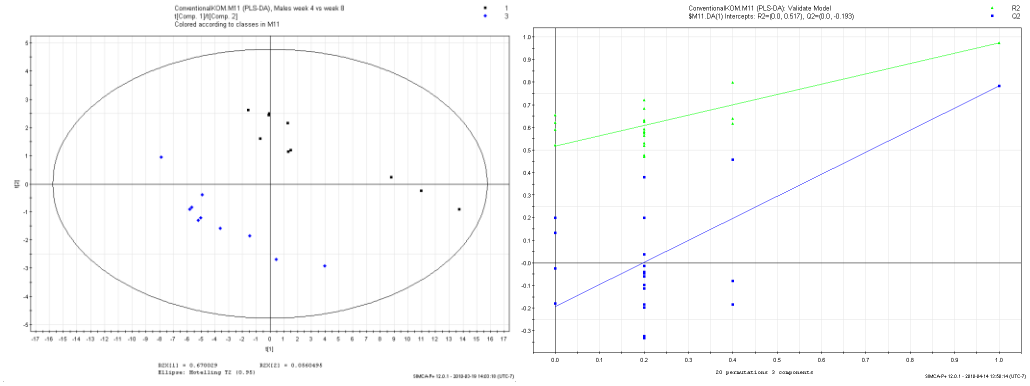

Week 4 vs. Week 12

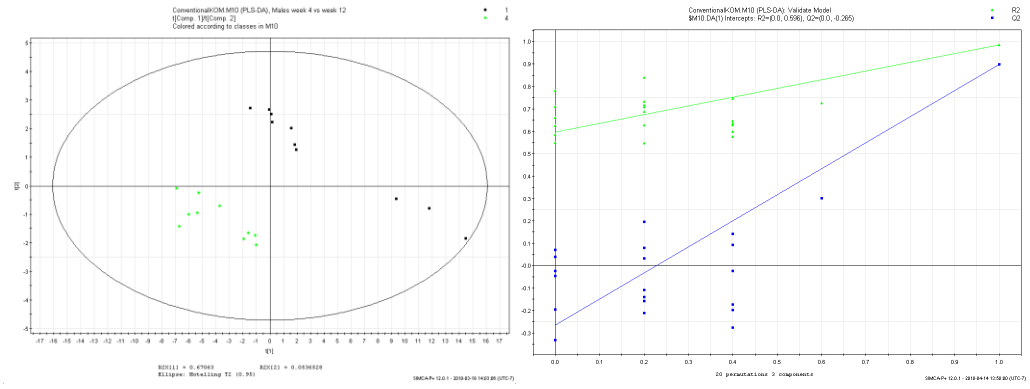

Week 4 vs. Week 16

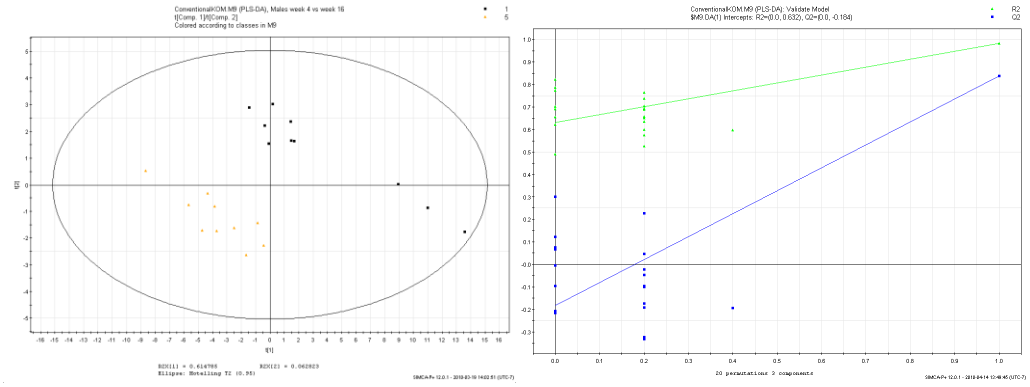

Week 4 vs. Week 20

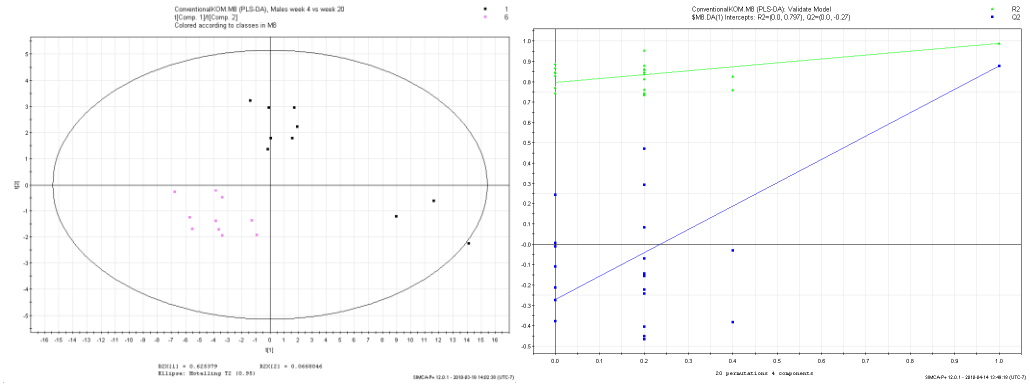

Figure 4.2.2.3 – PLS-DA plots of urine metabolomic profiles of IL-10 KO male conventional mice referenced to week 4; each group is composed of the same 10 mice from week 4, which is used to reference the other weeks collected. Beside each PLS-DA plot is the corresponding validation plot.

Similar to the results for the wild-type mice, week-by-week IL-10 KO mice-analysis results also cluster and separate according to the age group. In reference to week 4, the week 6 cluster shows complete separation. The separation of the clusters is also present for weeks 8, 12, 16, and 20. The gap between the clusters remains quite consistent for weeks 8, 12, 16, and 20, and is slightly increased over the week 6 one. One interesting note is that three points in the week 4 cluster appear to break away from the main cluster and form their own mini-cluster; these points are the same in each plot, and analysis of the concentrations reveals that these three samples were much more dilute than were the other samples.

plot	R2Y	Q2
all weeks	0.32	0.217
4 v 6	0.882	0.696
4 v 8	0.974	0.783
4 v 12	0.987	0.899
4 v 16	0.982	0.839
4 v 20	0.987	0.887

Table 4.2.2.1 - R2Y and Q2 values for the PLS-DA plots constructed for the conventional wild-type males over time.

4.2.3 IL-10 KO females: comparison of urine metabolomics over all collection weeks

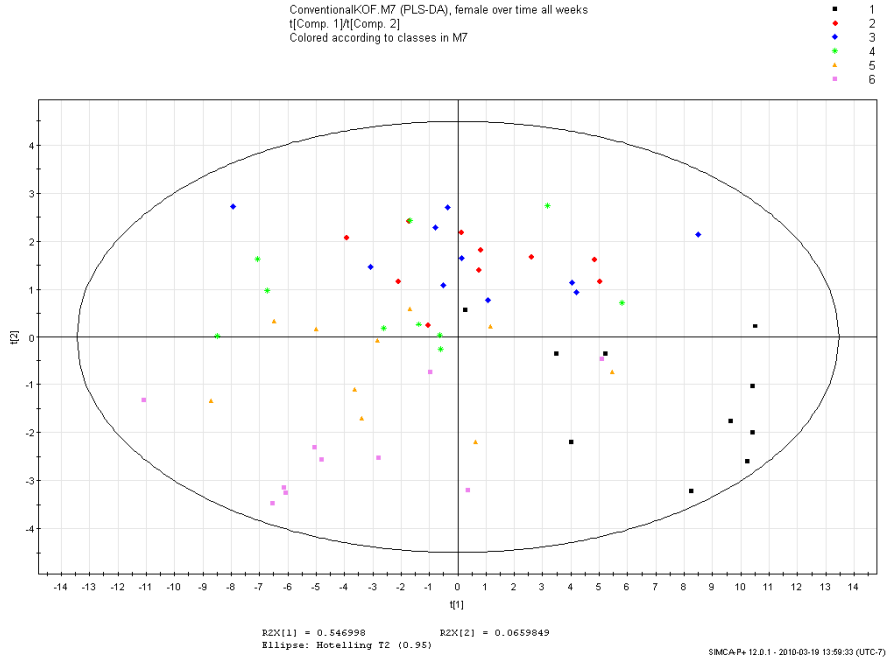

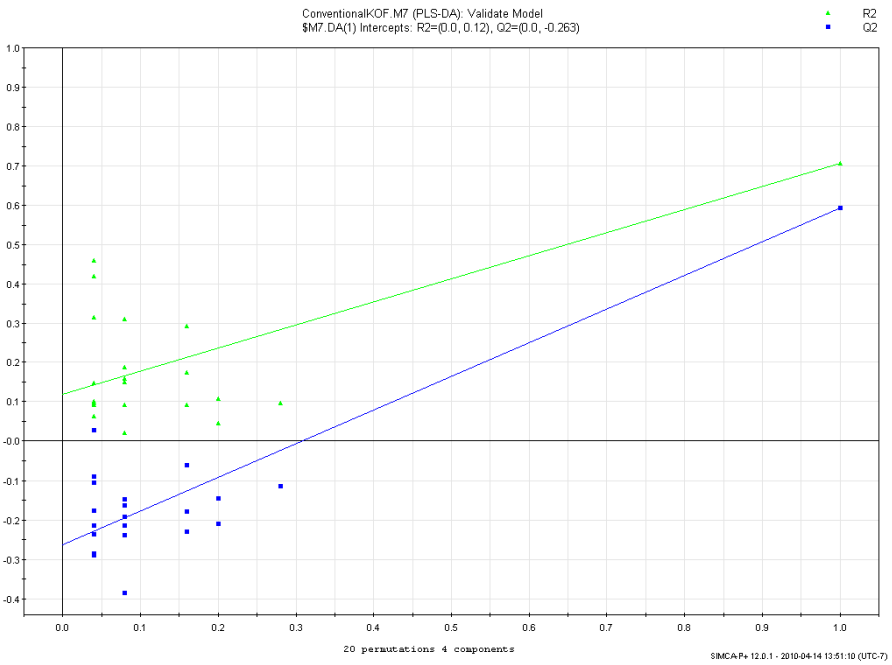

Figure 4.2.3.1 – PLS-DA plot of urine metabolomic profiles of all IL-10 KO female conventional mice over all collection time-points. Each week is constructed from 10 points and is displayed in a different color: week 4 (black), week 6 (red), week 8 (blue), week 12 (green), week 16 (yellow), week 20 (purple). This plot shows the progression of

the urine metabolomic profile of female wild-type mice as they grow in a conventional environment. Below the PLS-DA plot is the validation plot.

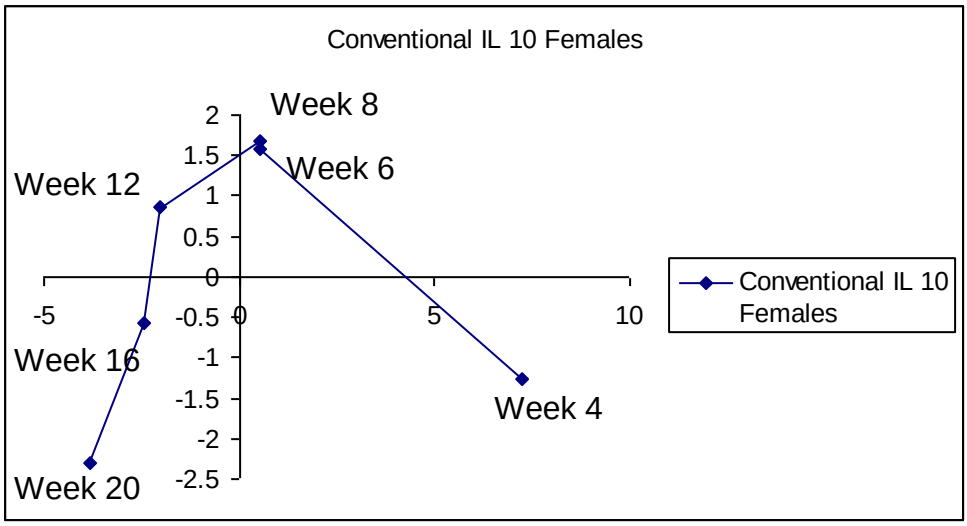

Figure 4.2.3.2 – Metabolic trajectory of the conventional IL-10 KO females; the plot was constructed by taking the coordinates of all the points for each week and calculating a single mean coordinate for each week.

Figure 4.2.3.1 is a PLS-DA for all conventional IL-10 KO females over all their collection weeks. In manner similar to the IL-10 KO male data, the IL-10 KO females' points do not group together as nicely as their wild-type counterparts' do. The lack of clustering on this plot makes it difficult to determine what exactly is occurring with respect to movement of the points along the plot. However, a metabolic trajectories plot (Figure 4.2.3.2) gives us a better idea of how the points move around on the plot. One thing we can see is that there is a general movement of the points from the lower right side of the plot towards the lower left side of the plot via a parabolic trajectory. We also see that there is quite a lot of

movement between weeks 4 and -6 and that there is not a lot of movement from week 6 to week 8. The magnitude of the movement from weeks 8 to 20 appears to be quite constant.

Week 4 vs. Week 6

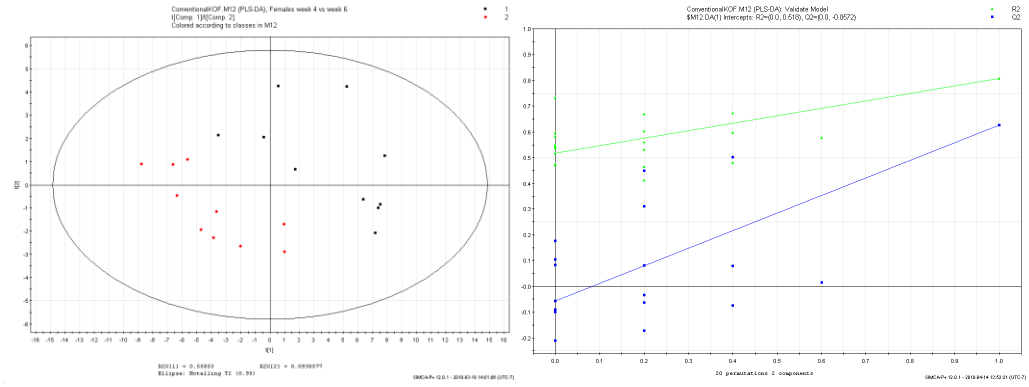

Week 4 vs. Week 8

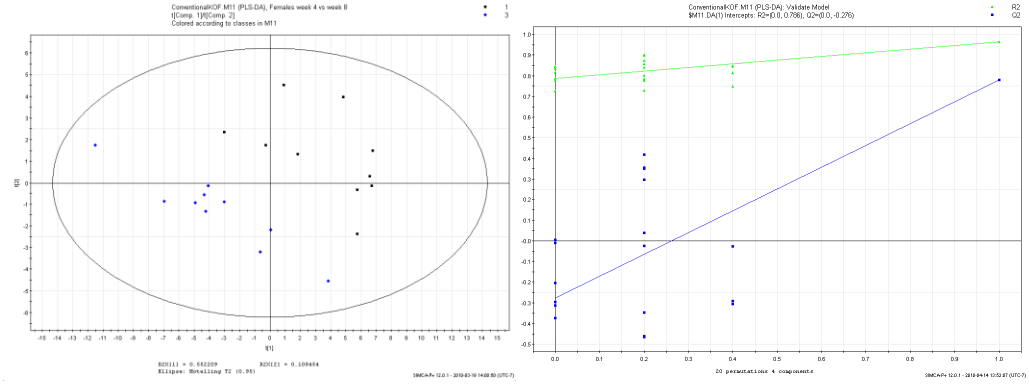

Week 4 vs. Week 12

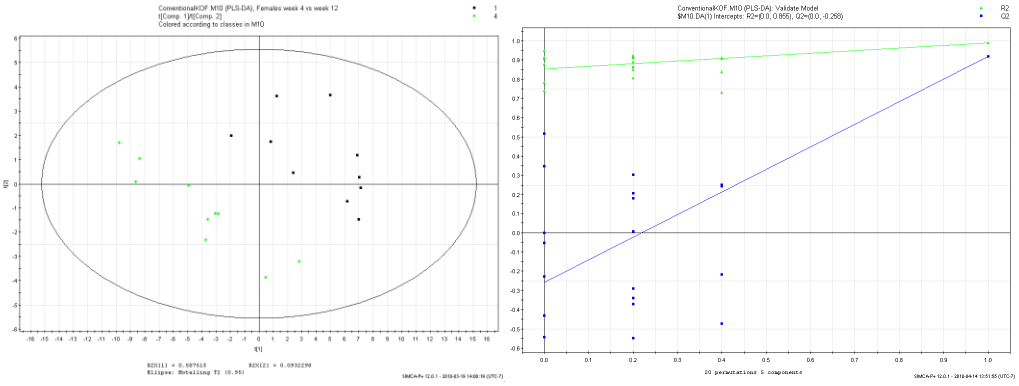

Week 4 vs. Week 16

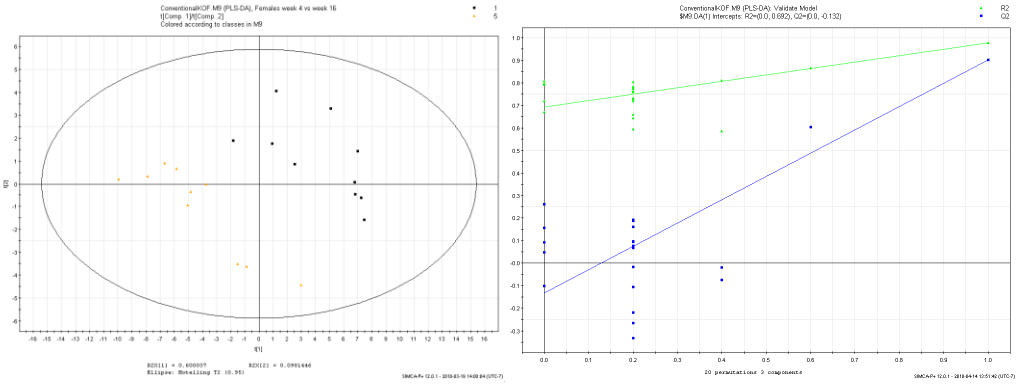

Week 4 vs. Week 20

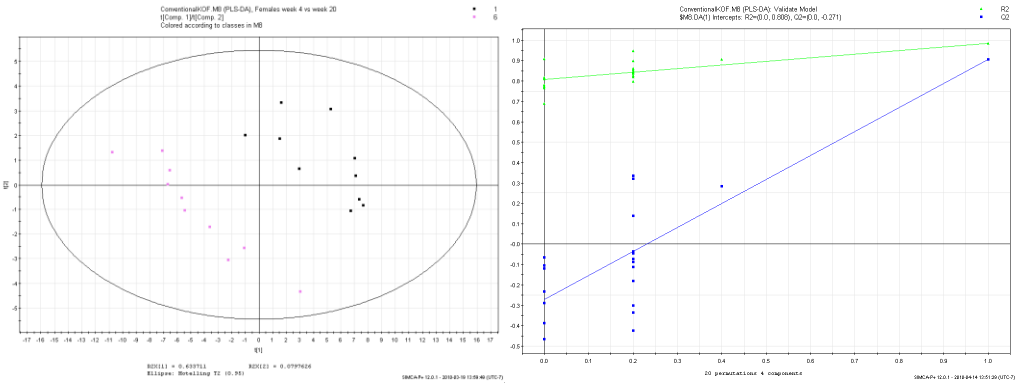

Figure 4.2.3.3 – PLS-DA plots of urine metabolomic profiles of IL-10 KO female conventional mice referenced to week 4; each group is composed of the same 10 mice from week 4 and is referenced against the other groups of 10 mice from the other weeks collected. Beside each PLS-DA plot is the corresponding validation plot.

Week-by-week comparisons of the conventional female IL-10 KO mice shows a similar trend to that for conventional male IL-10 KO mice, in that separation is seen for all the weeks when referenced against week 4. For week 6, two clusters are formed, one for the week 4 group and the other for the week 6 group. Although the clusters are close to each other, there is no overlap between the two groups.

Two separate clusters are also formed for the week 8 comparison, and the gap between the two clusters has also increased. Weeks 12, 16, and 20 also form separate clusters, and the gap between these clusters and week 4 is constant.

plot	R2Y	Q2
all weeks	0.391	0.253
4 v 6	0.807	0.627
4 v 8	0.965	0.78
4 v 12	0.99	0.919
4 v 16	0.978	0.901
4 v 20	0.983	0.905

Table 4.2.3.1 - R2Y and Q2 values for the PLS-DA plots constructed for the conventional IL-10 KO females over time.

4.3 Wild-type vs. IL-10 KO: comparison of conventional wild-type mice vs. IL-10 KO mice

4.3.1 Male population

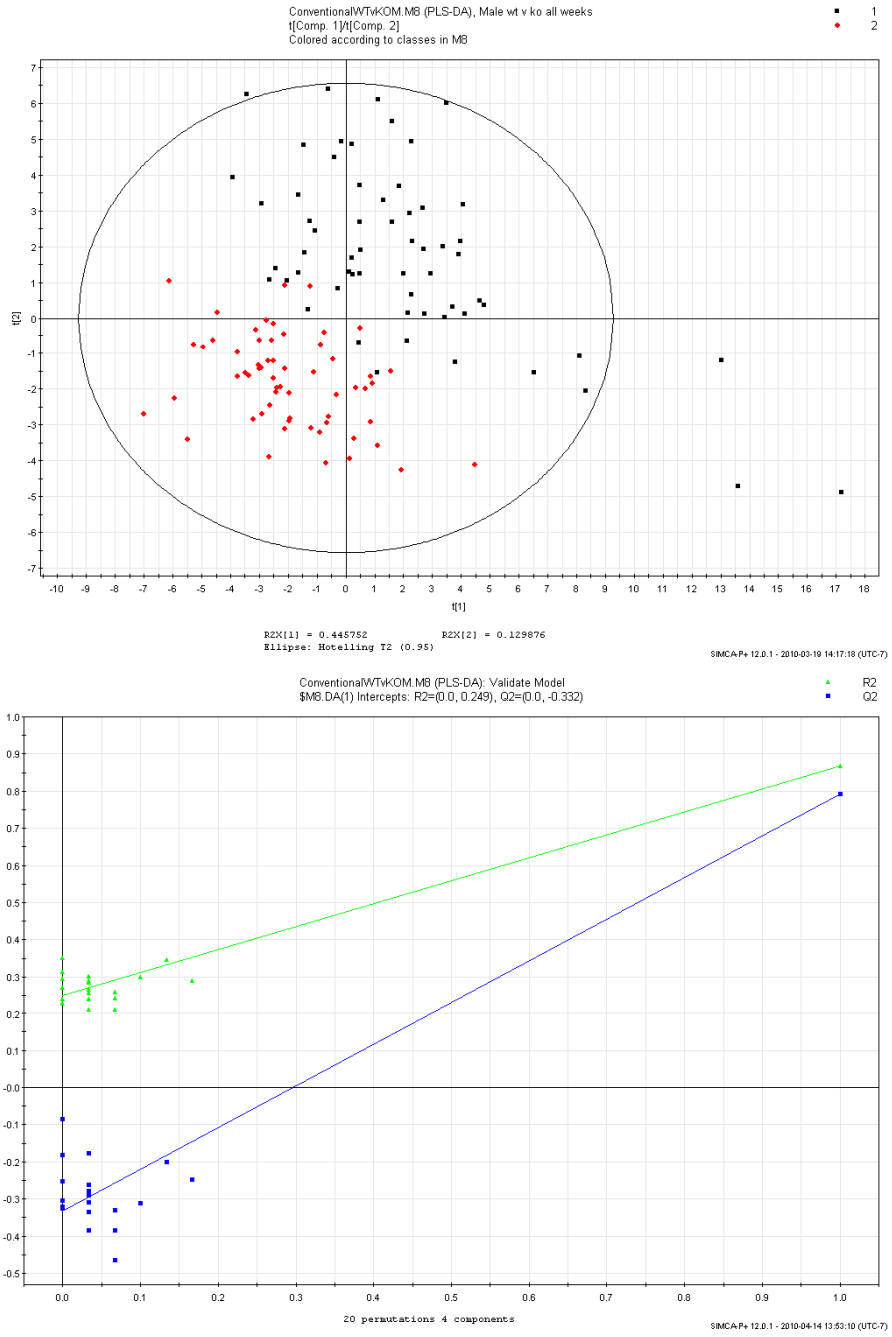

Figure 4.3.1.1 – PLS-DA plot of the urine metabolomic profiles of all male wild-type and IL-10 KO conventional mice (urine collected from mice in their conventional environments) on weeks 4, 6, 8, 12, 16, and 20 of age. Each of the wild-type and IL-10

KO groups comprises 60 data points (10 points per week). Wild-type mice are shown in red, and IL 10 mice are shown in black. Below the PLS-DA plot is the validation plot.

Figure 4.3.1.1 is a PLS-DA for all conventional males comparing wild-type mice vs. IL-10 KO mice. From this plot, we can see that two clusters have formed, one cluster for the wild-type mice and the other for the IL-10 KO mice. Since there is an overlap between the two clusters, week-by-week analysis is necessary to determine if the two groups separate out at specific weeks. This plot does show a couple of outliers in the IL-10 KO group. Three of these outliers are data points collected during week 4, and the other one was collected during week 8; once again these outliers are due to collection of low volume urine. Another general observation that can be made from this graph is that the wild-type group data (red) clusters together tighter than does the IL-10 KO group data (black).

Week 4

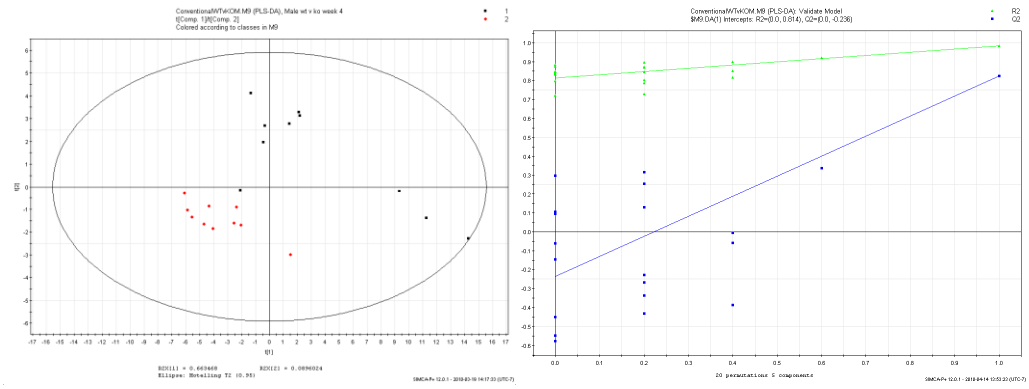

Week 6

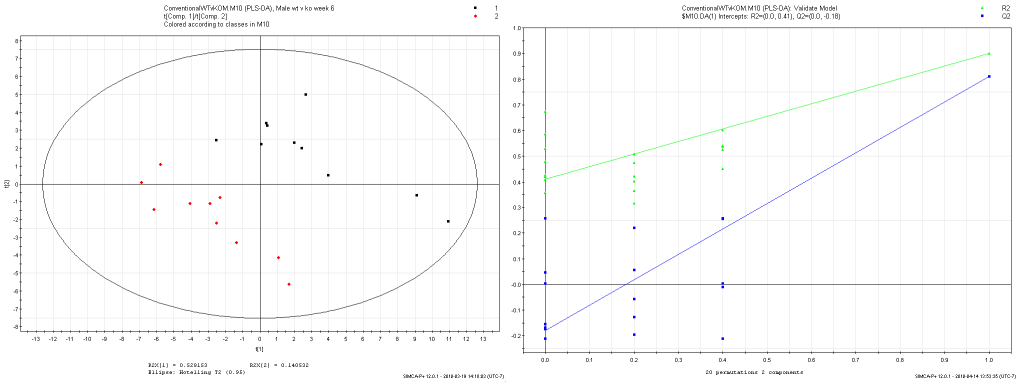

Week 8

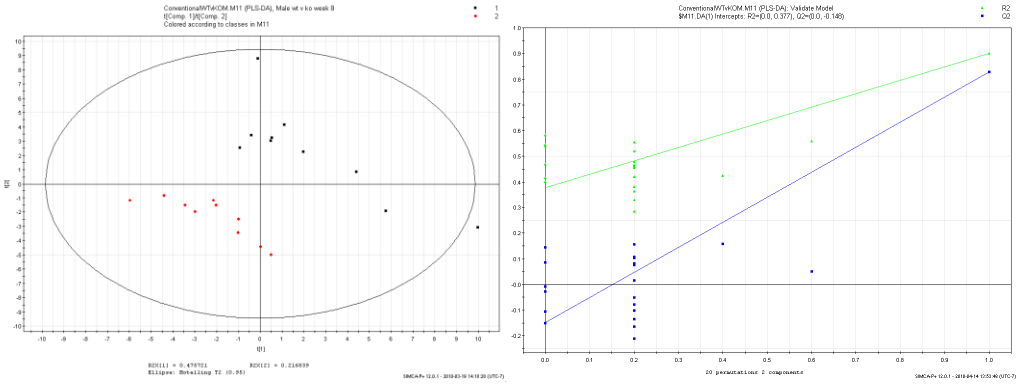

Week 12

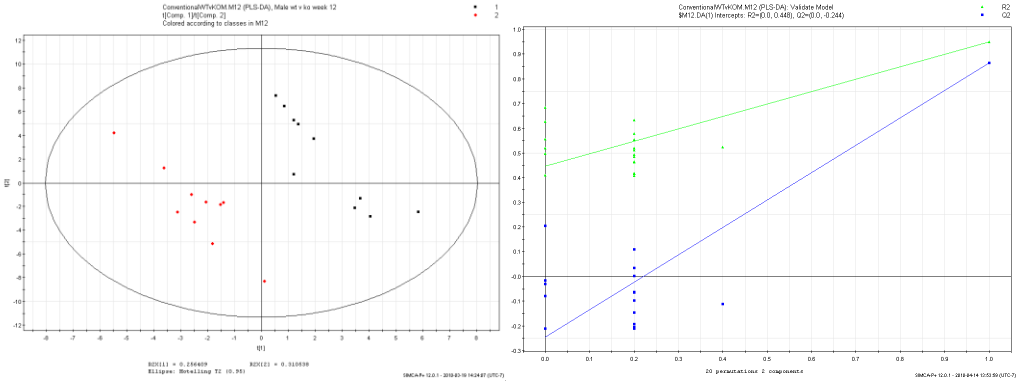

Week 16

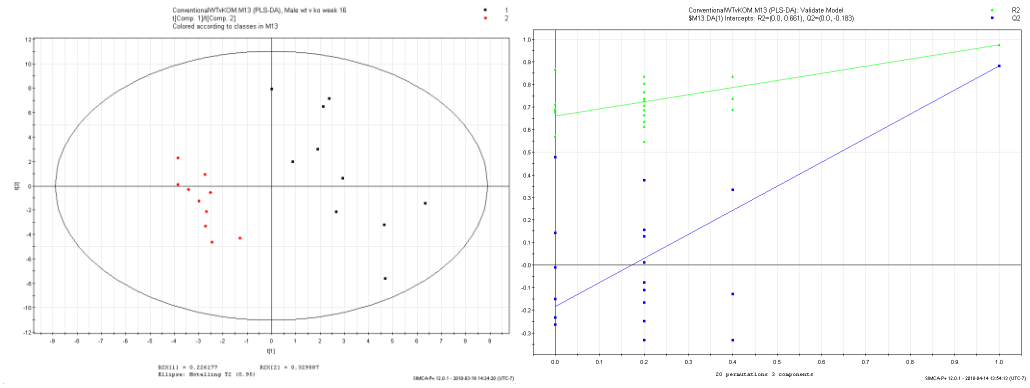

Week 20

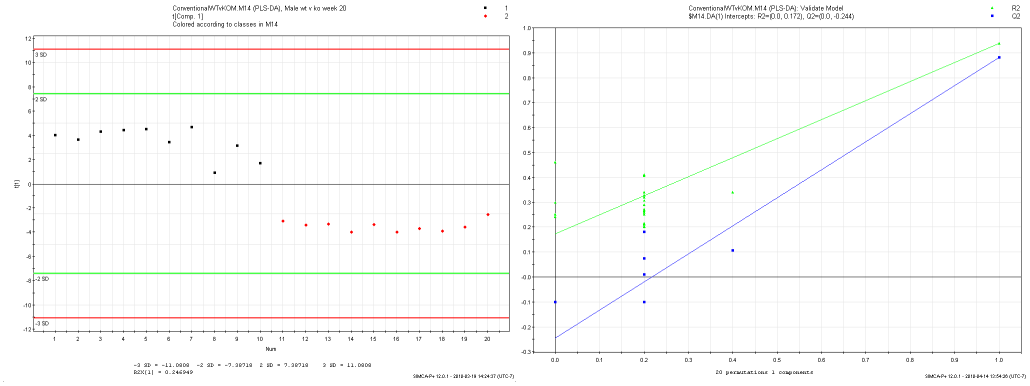

Figure 4.3.1.2 – PLS-DA plots of the urine metabolomic profiles of the conventional male wild-type and IL-10 KO mice broken up by week of urine collection; wild-type are displayed in red, and IL-10 KO are displayed in black. Each week is composed of 10 wild-type and 10 IL-10 KO. Beside each PLS-DA plot is the corresponding validation plot.

Week-by-week comparison of PCA plots of wild-type vs. IL-10 KO conventional males shows that at week 4, the cluster of the wild-type mice is very tight while the cluster of the IL-10 KO group is spread over a greater area of the plot; nevertheless, there is complete separation between the two clusters. Complete separation of the clusters continues for all the weeks analyzed. From weeks 6 to 16, the gap between the two

clusters appears to be relatively constant. Week 20 is interesting, however, because only one component was generated to separate the two clusters; a second component only resulted in a less than desirable model.

plot	R2Y	Q2
All weeks	0.867	0.793
week 4	0.985	0.824
week 6	0.901	0.81
week 8	0.901	0.828
week 12	0.951	0.865
week 16	0.976	0.882
week 20	0.938	0.881

Table 4.3.1.1 - R2Y and Q2 values for the PLS-DA plots constructed for the conventional wild-type males vs. conventional IL-10 KO males.

4.3.2 Female population

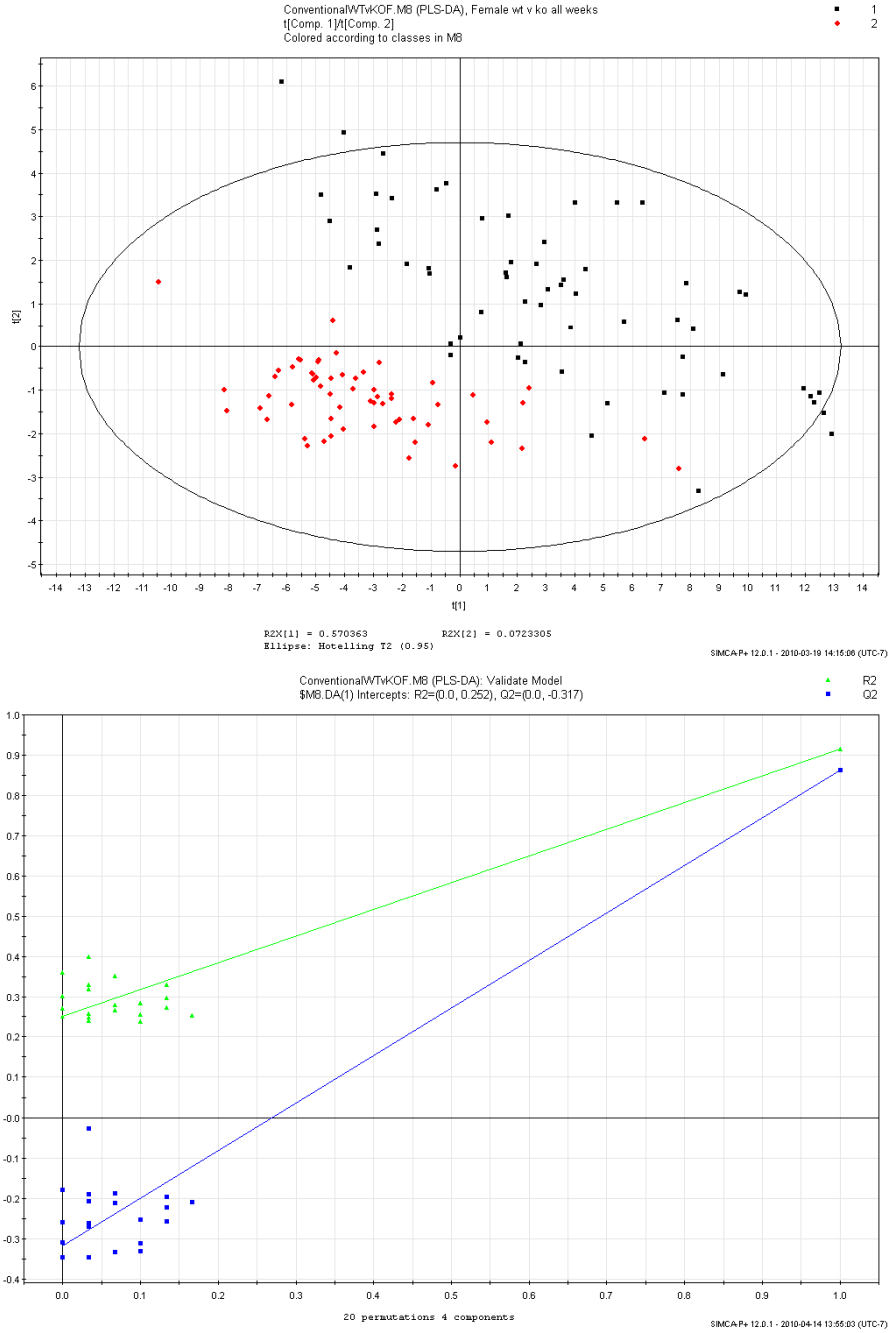

Figure 4.3.2.1 – PLS-DA plot of the urine metabolomic profiles of all female wild-type and IL-10 KO conventional mice (urine collected from mice in their conventional environments) for weeks 4, 6, 8, 12, 16, and 20 of age. Each of the wild-type and IL-10 KO groups comprises 60 data points (10 points per week). Wild-type mice are shown in red, and IL-10 KO mice are shown in black.

Figure 4.3.2.1 is a comparison of all female conventional wild-type mice vs. IL-10 KO mice. Similar to the male data, the female mice data form a wild-type cluster occupying the lower left side of the plot and an IL-10 KO cluster that is occupying the upper right side of the plot. Although two clusters have formed, there is a slight overlap between the two individual clusters. Additionally, the wild-type cluster (red) is much tighter than the IL-10 KO cluster. There also appear to be a couple of possible outliers, but their status as such needs to be confirmed through week–by-week analysis to see how they correspond with their age groups.

Week 4

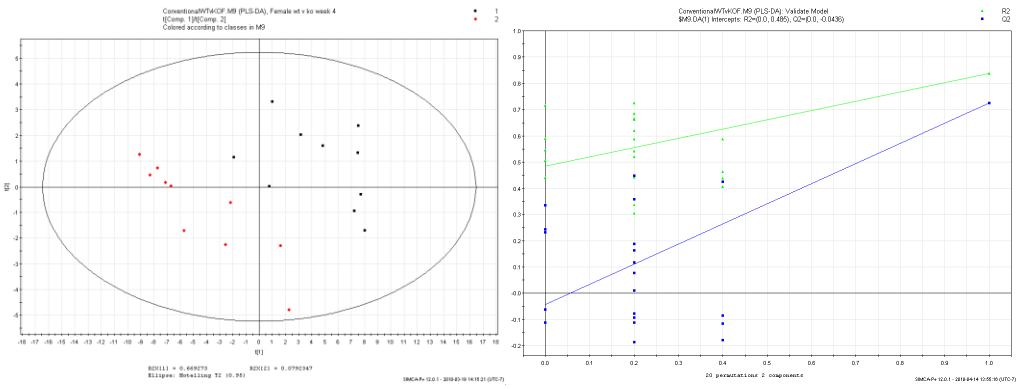

Week 6

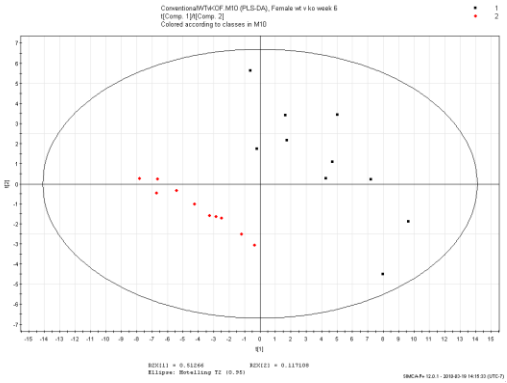

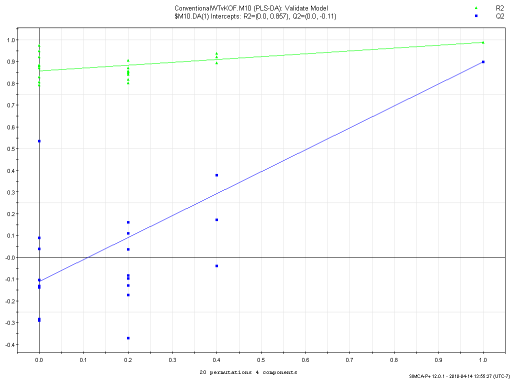

Week 8

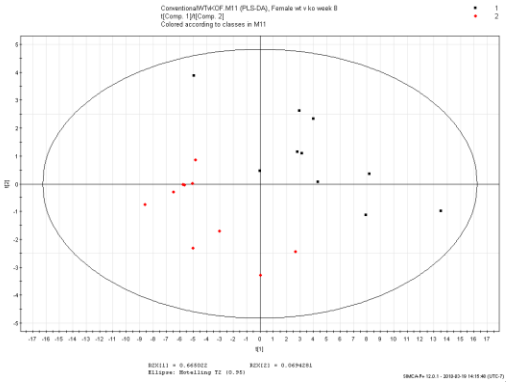

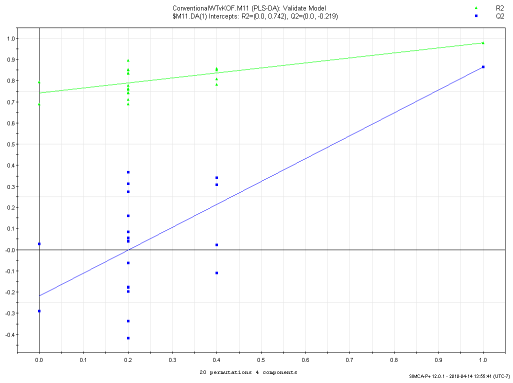

Week 12

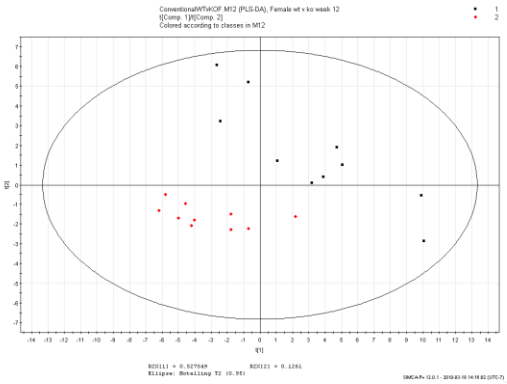

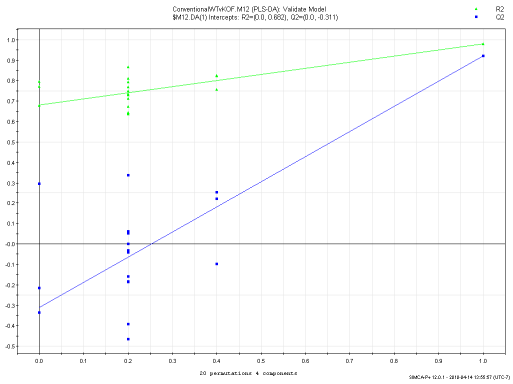

Week 16

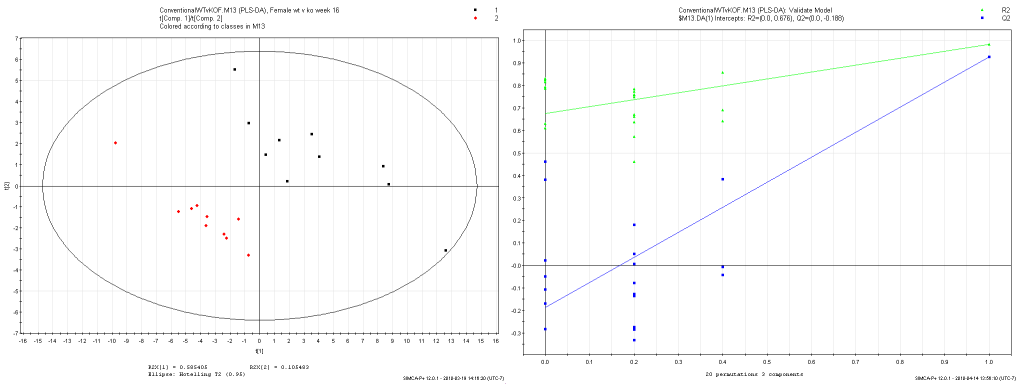

Week 20

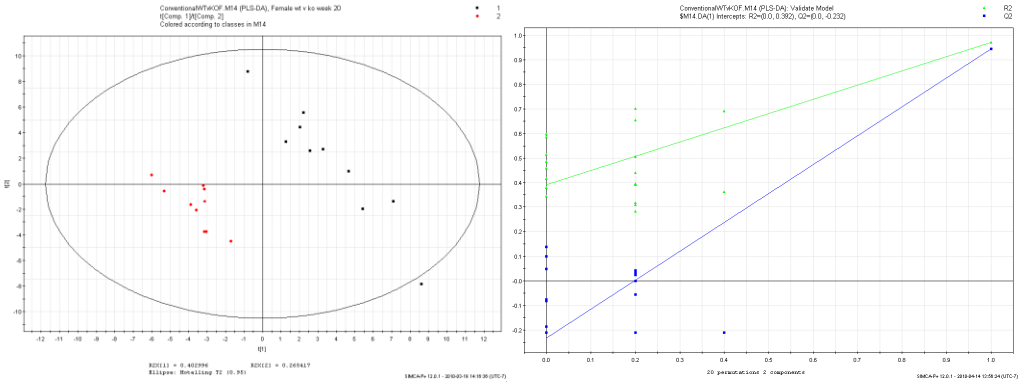

Figure 4.3.2.2 – PLS-DA plots of the urine metabolomic profiles of the conventional female wild-type and IL-10 KO mice broken up by week of urine collection; wild-type are displayed in red, and IL-10 KO are displayed in black. Each week is composed of 10 wild-type and 10 IL-10 KO. Beside each PLS-DA plot is the corresponding validation plot.

Week-by-week comparison by PCA of wild-type vs. IL-10 KO conventional females shows results that are similar to the males'. The PLS-DA plot at week 4 shows two clusters and a gap between the two formed clusters. Week 6 is interesting, in that there is complete separation and clustering of the two groups, and the gap between the two groups has increased. However, this situation does not continue: at week 8 the gap between the

two clusters is reduced. At week 12, there is a tightening of the wild-type cluster, and the gap between the wild-type and the IL-10 KO clusters remains consistent. At week 16, the gap between the two clusters once again increases. Week 20 is similar to week 16, in that two independent clusters appear and the gap between the two clusters has once again increased over that of the previous time-point.

plot	R2Y	Q2
All weeks	0.915	0.628
week 4	0.838	0.725
week 6	0.987	0.897
week 8	0.979	0.864
week 12	0.981	0.921
week 16	0.981	0.927
week 20	0.97	0.945

Table 4.3.2.1 - R2Y and Q2 values for the PLS-DA plots constructed for the conventional wild-type females vs. conventional IL-10 KO females.

Chapter 5 - Fecal Colonization

5.1 Wild-type population

5.1.1 Male: comparison of axenic mice and mice colonized with fecal bacteria

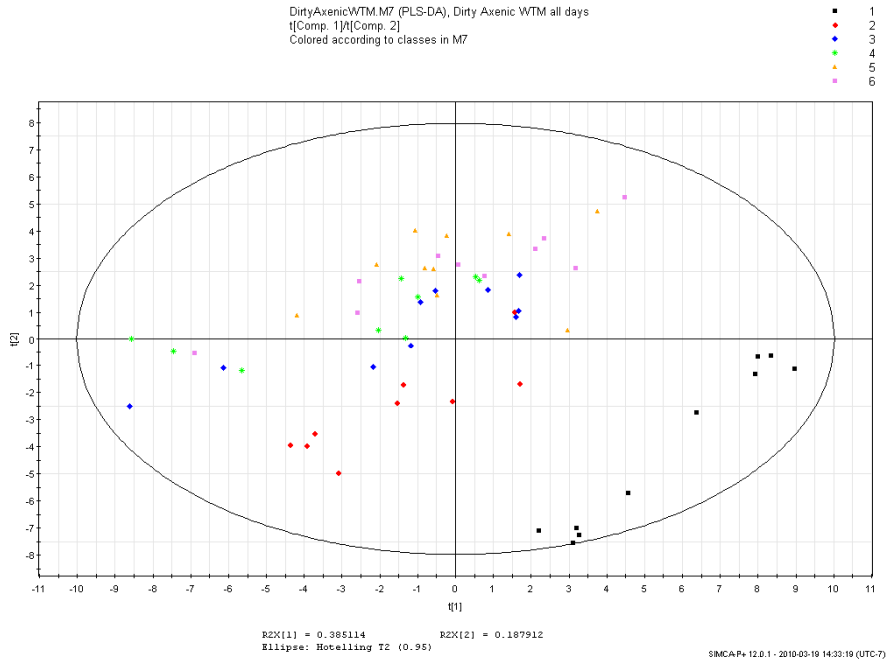

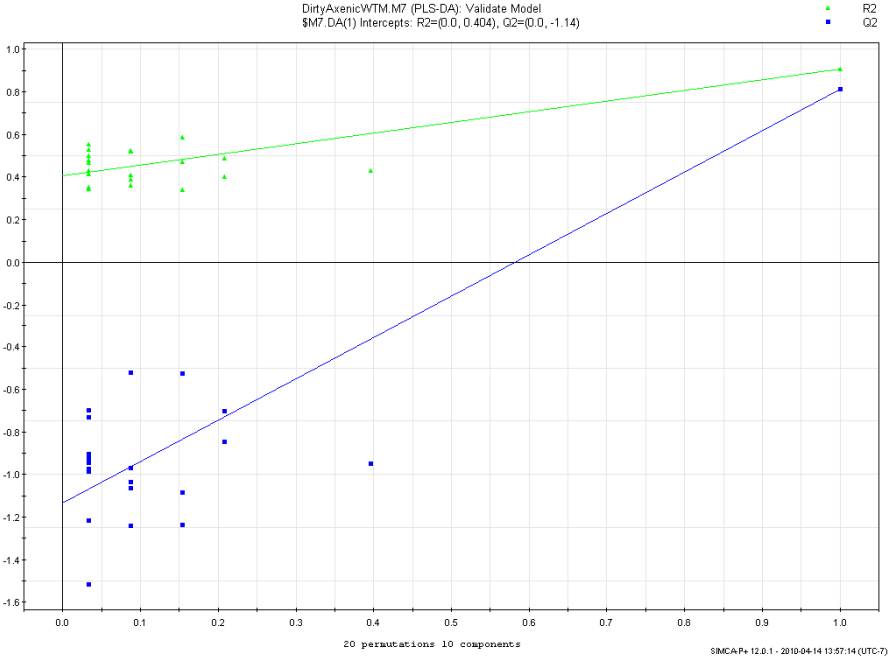

Figure 5.1.1.1 – PLS-DA of week 20 male wild-type axenic mice and mice colonized with fecal bacteria on days 1-4 and day 7 post-colonization. Axenic mice are displayed in black, colonized day 1 in red, day 2 in blue, day 3 in green, day 4 in yellow, and day 7 in pink. Below the PLS-DA plot is the validation plot.

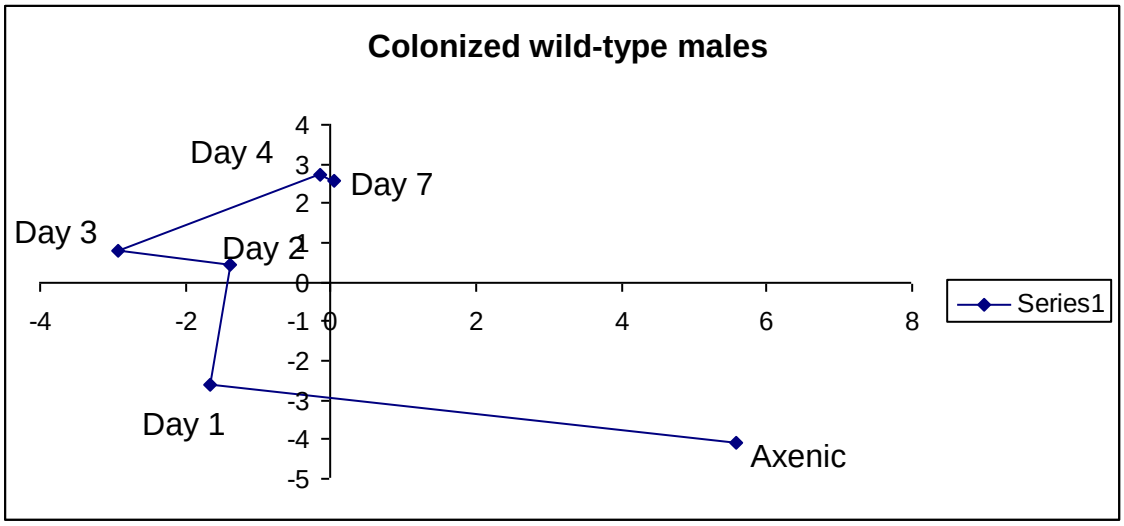

Figure 5.1.1.2– Metabolic trajectory of the colonized wild-type males; the plot was constructed by taking the coordinates of all the points for each week and calculating a single mean coordinate for each week.

Figure 5.1.1.1 is a PLS-DA of 20-week axenic mouse data combined with bacterial colonization data (from male wild-type mice) for days 1-4 and day 7. One interesting characteristic of this plot is that the data points for the colonized mice cluster together quite completely separately from the cluster that is formed by the axenic mice. Individual clusters within the colonized group show movement across the metabolic trajectories plot (Figure 5.1.1.2). The clusters appear to begin in the bottom left quadrant of the plot and, as the days progress, work their way up the plot. We can

see that the largest movement occurs between the time when the mice were axenic and day 1, and the smallest movement occurs between days 4 and 7. To further investige the post-colonization change from the axenic group, individual PLS-DA plots comparing axenic data vs. the individual colonized day data were used.

Axenic vs. Day 1

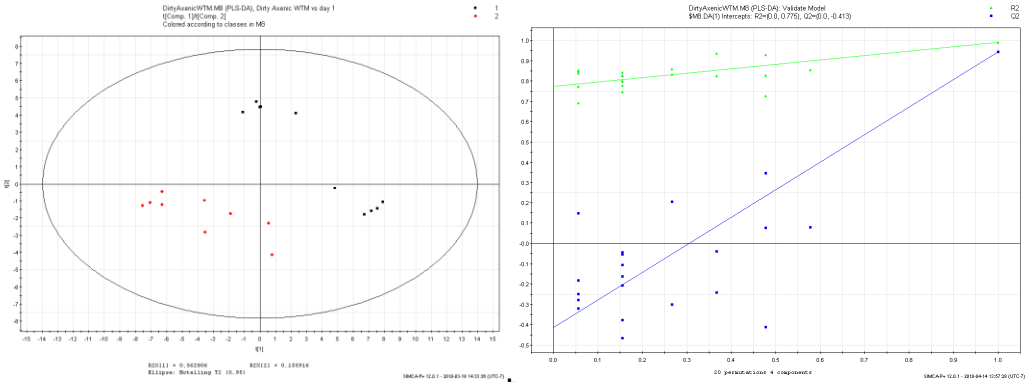

Axenic vs. Day 2

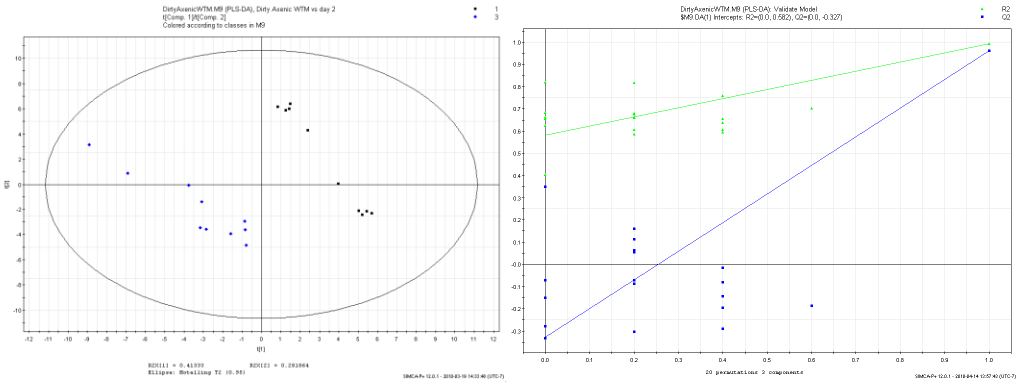

Axenic vs. Day 3

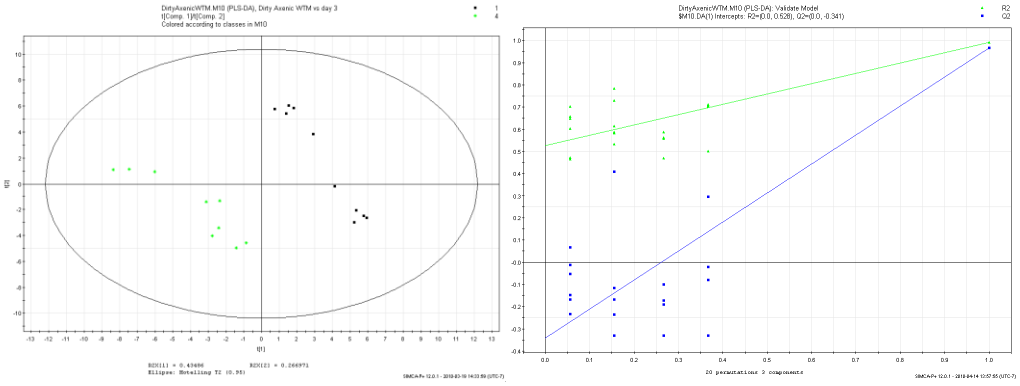

Axenic vs. Day 4

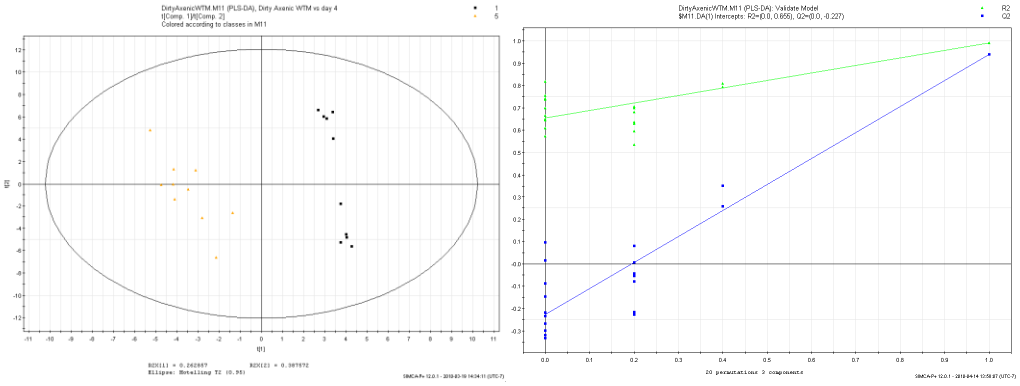

Axenic vs. Day 7

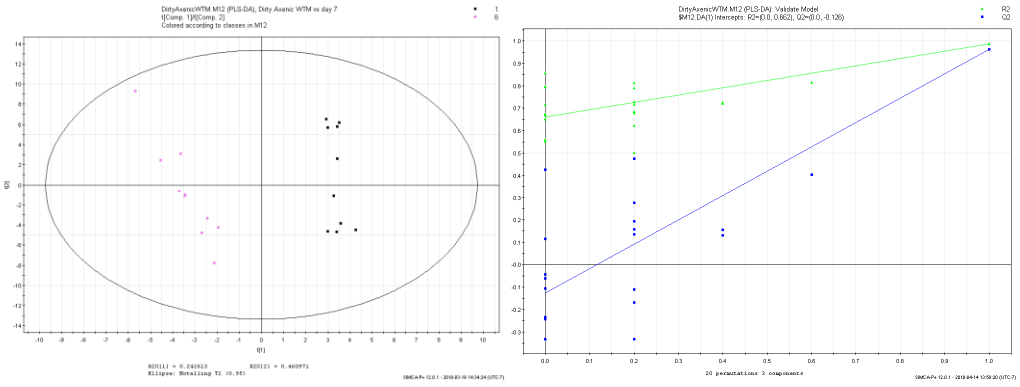

Figure 5.1.1.3 – Day by day analysis of male wild-type mice colonized with fecal bacteria, referenced to 20-week axenic mice; each plot is constructed using 10 axenic mice and 10 colonized mice that had their urine collected during the noted day after colonization. Beside each PLS-DA plot is the corresponding validation plot.

Figure 5.1.1.3 compares male wild-type mice and each of the post-colonization day urine samples referenced to data collected at 20 weeks, while the mice were still in an axenic environment. Beginning from day, 1 we see that the axenic mice and the day 1 mice have formed two separate clusters; the two clusters also completely separate, with no overlap present. Day 2 results are similar: two individual,separated clusters remain. Days 3, 4, and 7 all show two distinct clusters and the clusters are not overlapping. One interesting note about this plot is that the axenic group appears to be divided into two groups within its main cluster. These two groups were formed because the samples were collected at different times during the calendar year.

plot	R2Y	Q2
All days	0.828	0.497
ax vs. d 1	0.989	0.942
ax vs. d 2	0.994	0.961
ax vs. d 3	0.99	0.967
ax vs. d 4	0.992	0.938
ax vs. d 7	0.988	0.963

Table 5.1.1.1 - R2Y and Q2 values for the PLS-DA plots constructed for the wild-type males colonized with fecal bacteria over the days indicated.

5.1.2 Female: comparison of axenic mice and mice colonized with fecal bacteria

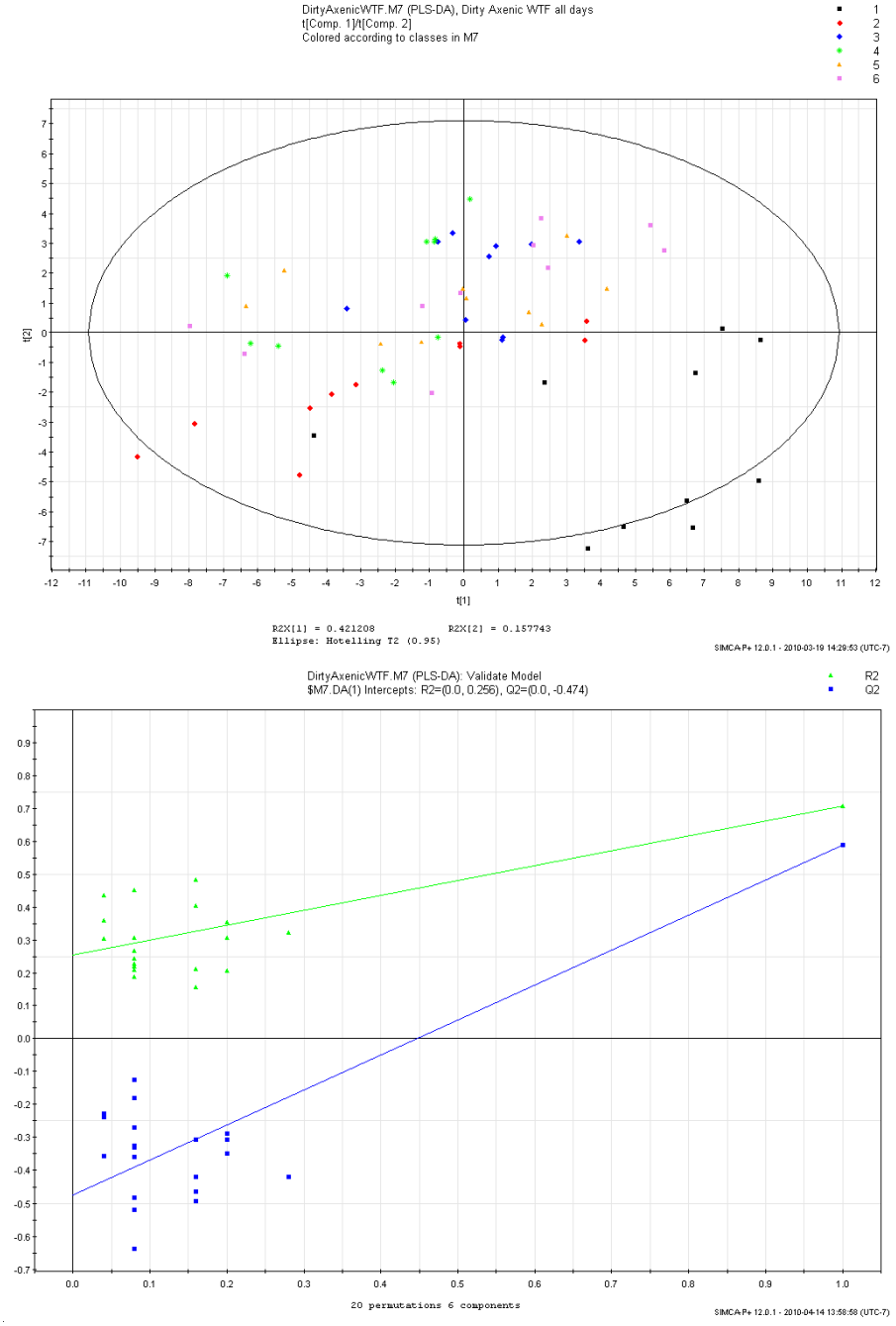

Figure 5.1.2.1 – PLS-DA of week 20 female wild-type axenic mice and mice colonized with fecal bacteria for days 1-4 and 7 post-colonization. Axenic mice are displayed in black, day 1 in red, day 2 in blue, day 3 in green, day 4 in yellow, and day 7 in pink. Below the PLS-DA plot is the validation plot.

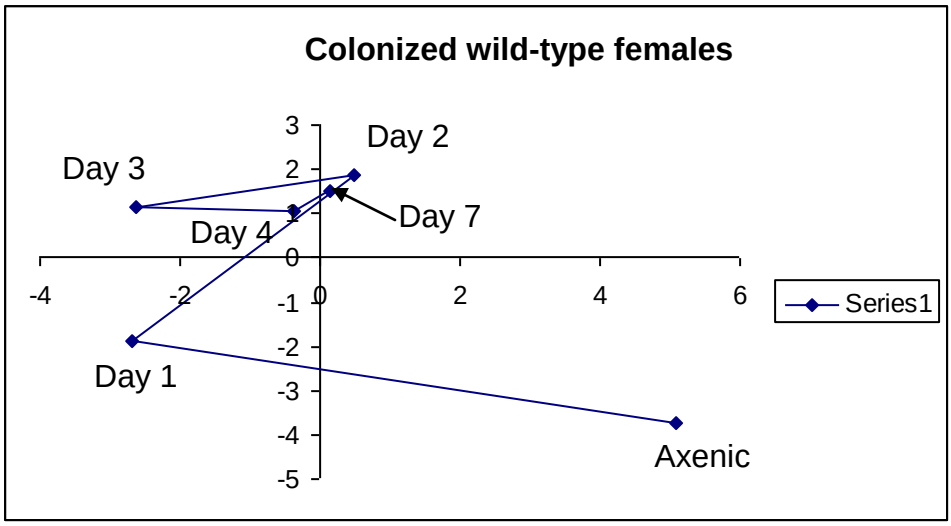

Figure 5.1.2.2– Metabolic trajectory of the colonized wild-type females; the plot was constructed by taking the coordinates of all the points for each week and calculating a single mean coordinate for each week.

Figure 5.1.2.1 is a PLS-DA of 20-week axenic data compared with bacterial colonization data from female wild-type mice collected on days 1-4 and day 7. Similar to the male data, the cluster formed by the axenic mice is distinct and there is complete separation between the axenic cluster and the colonized cluster. Analysis of the metabolic trajectories plot (Figure 5.1.2.2) shows the points moving from the lower left side of the plot towards the right side of the plot at day 2. Then the points move to the upper left side of the plot before doubling back and eventually ending up in spot similar to that of the day 2 plot. Again, the greatest movement occurs from the axenic to day 1 time-point, and the least movement occurs between days 4 and 7. Once again, the female mice data do not group together as tightly as the male groups' do. To further investigate the days'

post-colonization changes from the axenic group's state, individual PLS-DA plots comparing axenic vs. each colonized day were constructed.

Axenic vs. Day 1

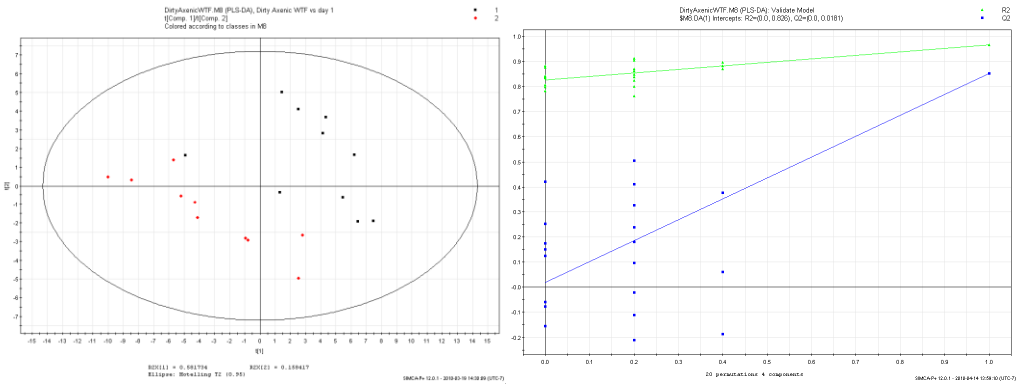

Axenic vs. Day 2

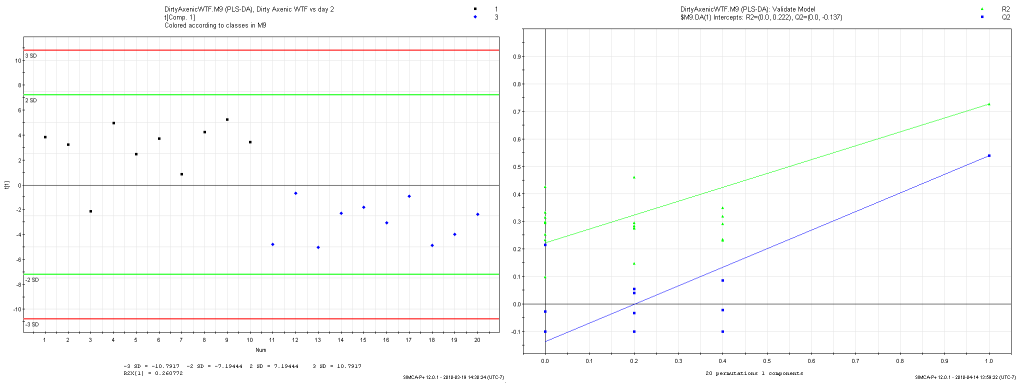

Axenic vs. Day 3

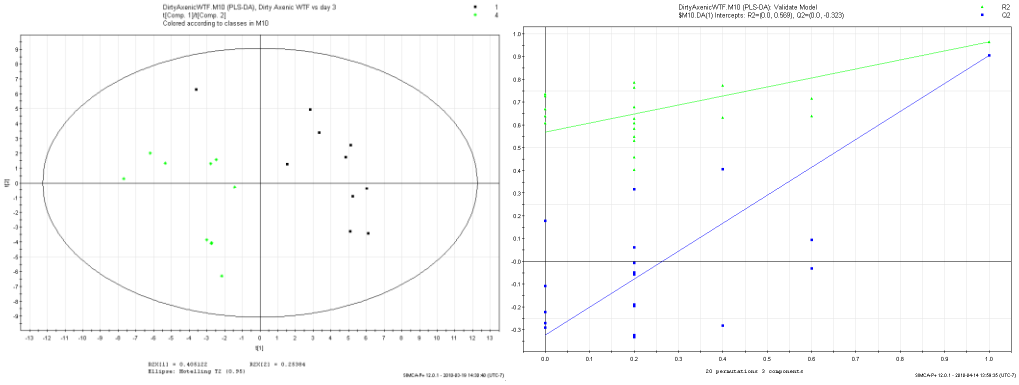

Axenic vs. Day 4

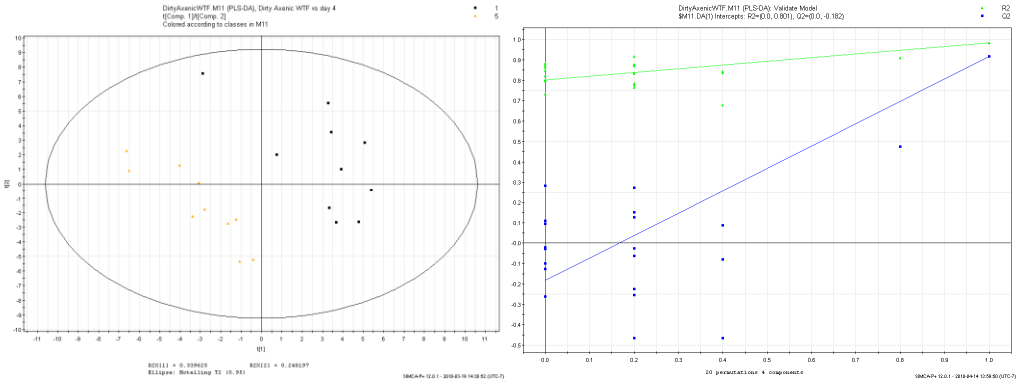

Axenic vs. Day 7

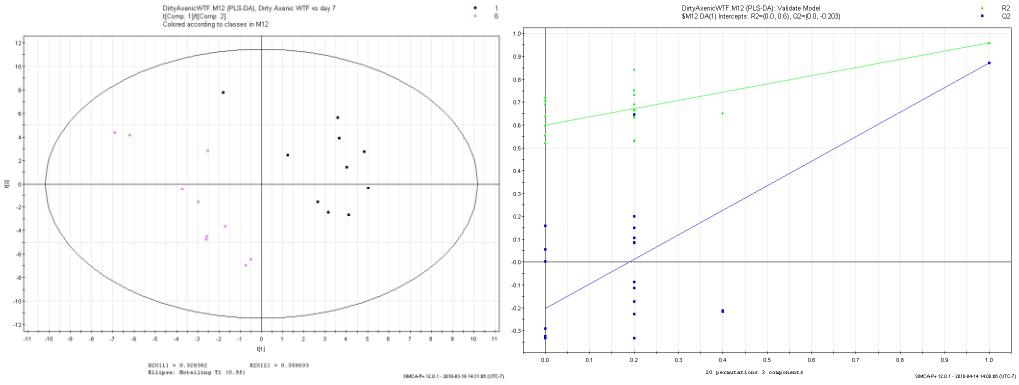

Figure 5.1.2.3 – Day-by-day analysis of female wild-type mice colonized with fecal bacteria, referenced to 20-week axenic mice; each plot is constructed for 10 axenic mice and 10 mice that had their urine collected during the corresponding day after colonization. Beside each PLS-DA plot is the corresponding validation plot.

Figure 5.1.2.3 compares female wild-type mice and each of their post-colonization day urine samples with reference to data collected at 20 weeks while the mice were still in an axenic environment. Similar to the male data, wild-type female colonization data and the axenic 20 week mice data show complete separation of groups. Right from the day 1 comparison, two distinct clusters have formed, one cluster for the 20-week

axenic mice and the other for the day-1 mice. The two clusters have no overlap. Day 2 also shows separation and two unique clusters, but what is interesting about day 2 is that only one component was generated to separate out the two groups. Days 3, 4, and 7 show similar results to those of day 1, with two distinct clusters which do not overlap.

plot	R2Y	Q2
All days	0.623	0.318
ax vs. d 1	0.967	0.853
ax vs. d 2	0.726	0.539
ax vs. d 3	0.966	0.905
ax vs. d 4	0.984	0.917
ax vs. d 7	0.96	0.871

Table 5.1.2.1 - R2Y and Q2 values for the PLS-DA plots constructed for the wild-type females colonized with fecal bacteria over the days indicated.

5.2 IL-10 KO population

5.2.1 Male: comparison of axenic mice and mice colonized with fecal bacteria

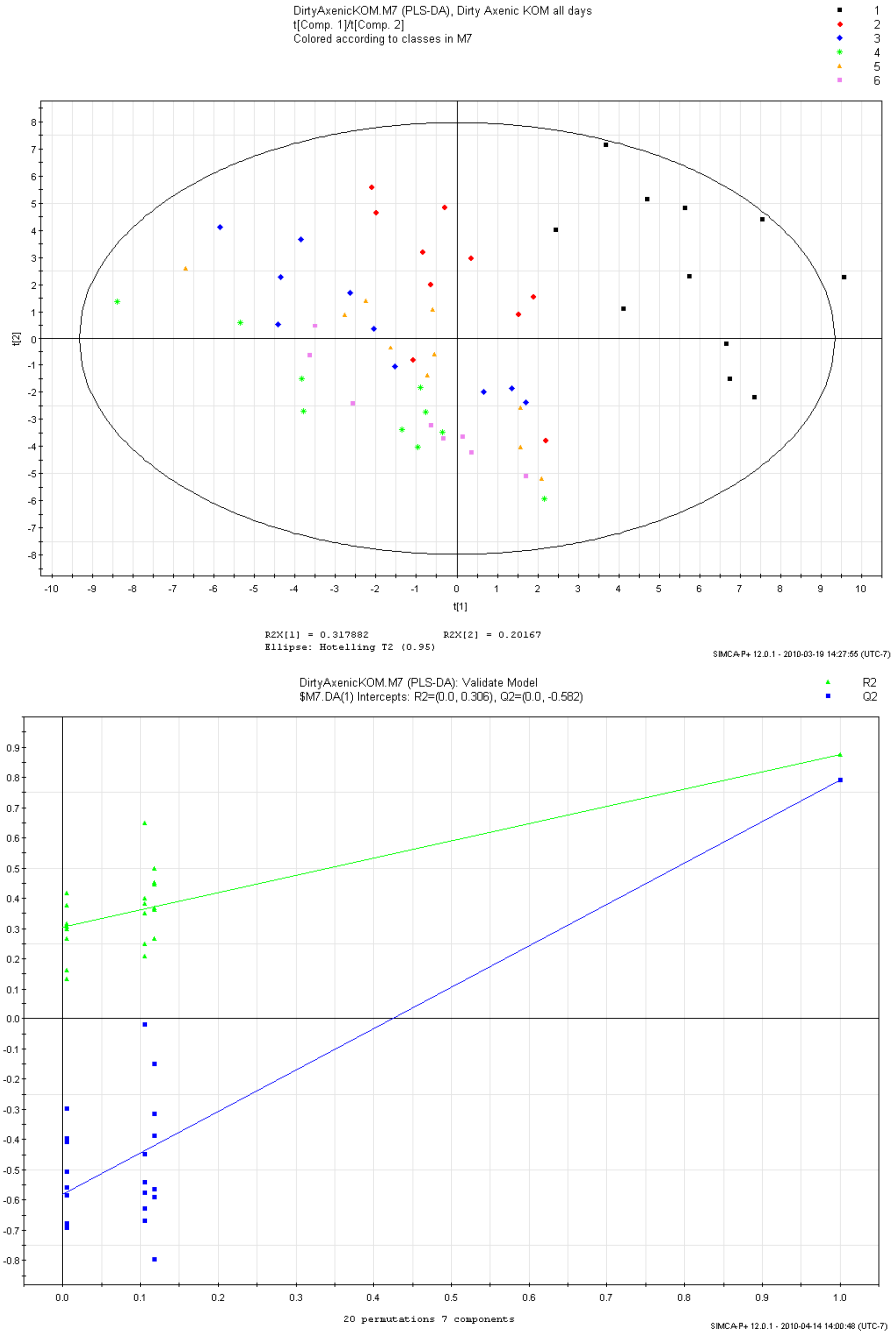

Figure 5.2.1.1 – PLS-DA of week-20 male IL-10 KO axenic mice along with mice colonized with fecal bacteria data taken on days 1-4 and 7 post-colonization. Axenic mice

are displayed in black, day 1 in red, day 2 in blue, day 3 in green, day 4 in yellow, and day 7 in pink. Below the PLS-DA plot is the validation plot.

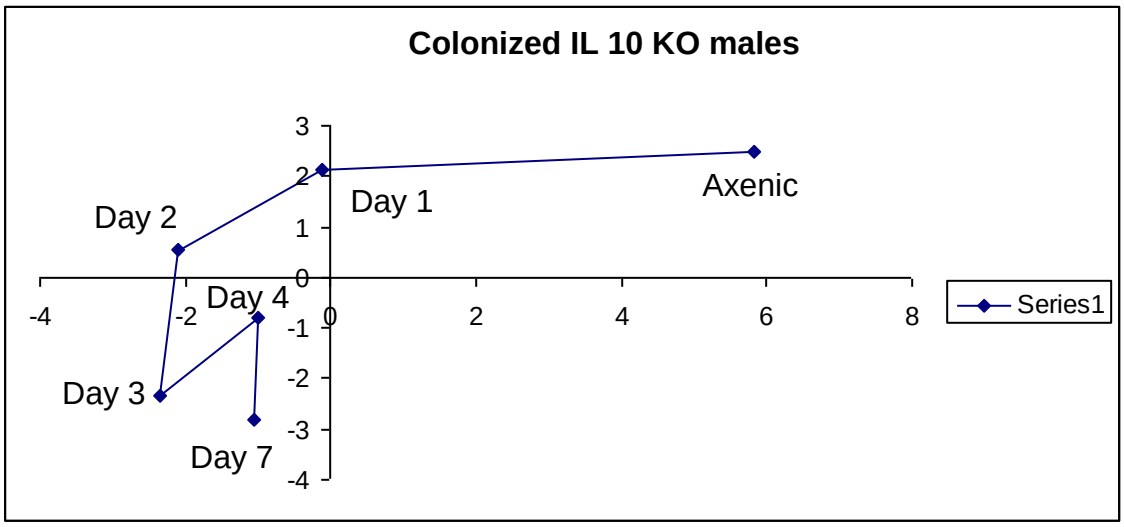

Figure 5.2.1.2– Metabolic trajectory of the colonized IL-10 KO males; the plot was constructed by taking the coordinates of all the points for each week and calculating a single mean coordinate for each week.

As with the male wild-type mice, data from the colonized IL-10 KO mice (Figure 5.2.1.1) forms its own cluster separate from the cluster formed by the 20-week axenic mice. Although the two groups are close together, there is no overlap. Just like the wild-type mice plots, the axenic cluster is in the upper right hand quadrant of the PLS-DA plot. Analysis of the metabolic trajectory plot (Figure 5.2.1.2) shows that the path of the colonized group moves from the upper middle portion of the plot and slopes down towards the left quadrant of the plot. Once again, the greatest movement occurs from the axenic to day 1 time-point. With the exception of that time-gap, the magnitude of movement is fairly consistent between the other time points.

Axenic vs. Day 1

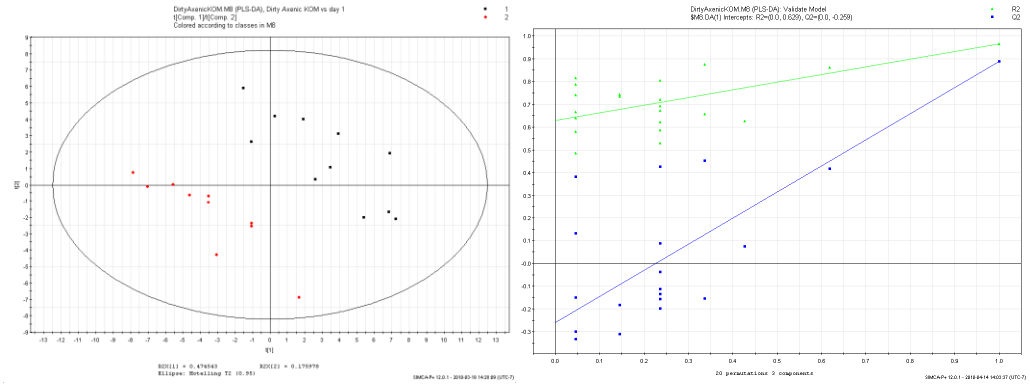

Axenic vs. Day 2

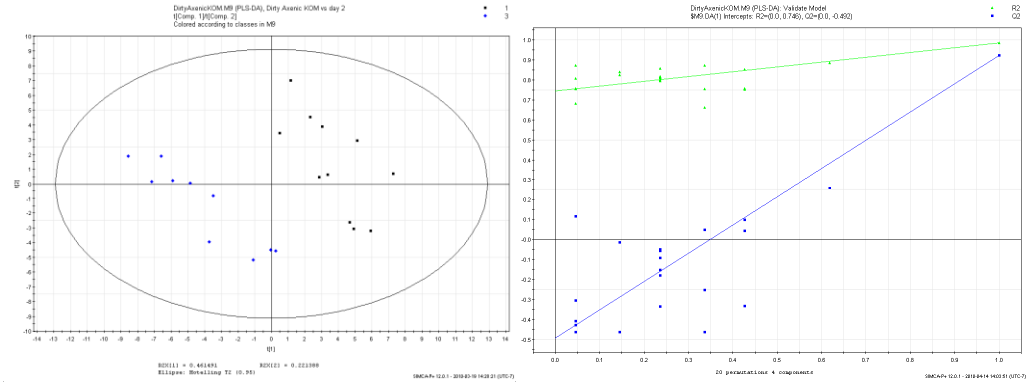

Axenic vs. Day 3

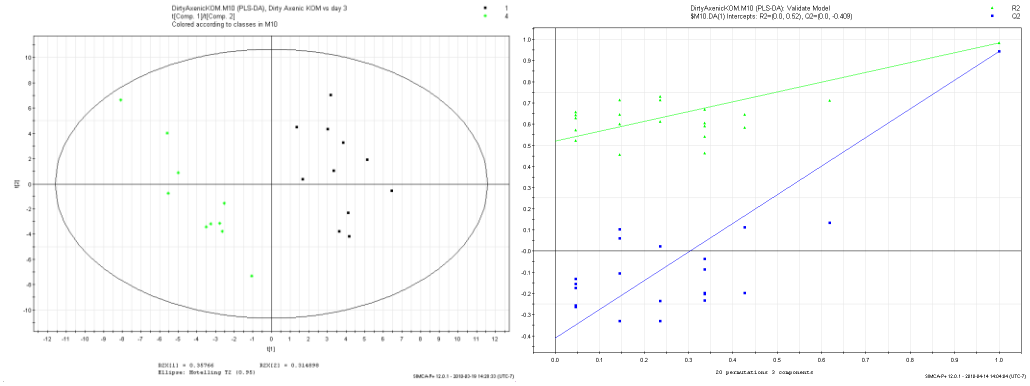

Axenic vs. Day 4

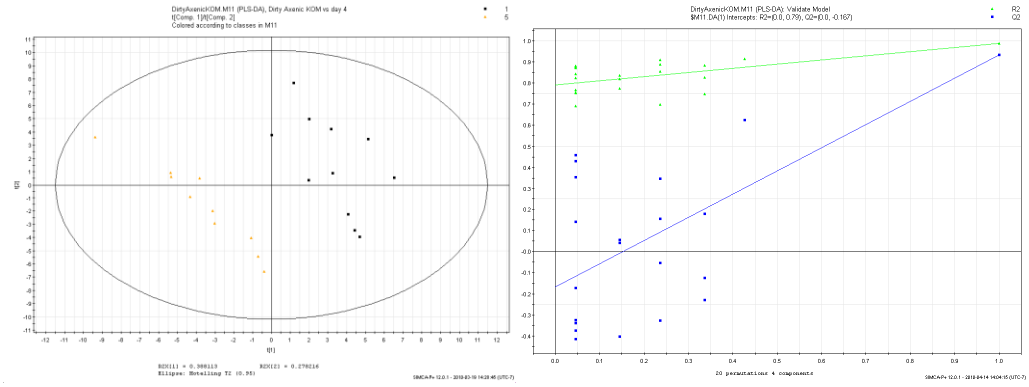

Axenic vs. Day 7

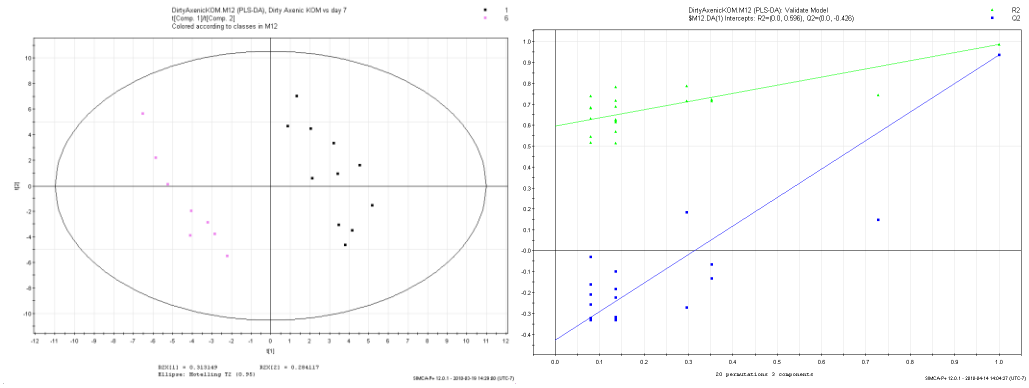

Figure 5.2.1.3 – Day-by-day analysis of male IL-10 KO mice colonized with fecal bacteria, referenced to 20-week axenic mice; each plot is constructed for 10 axenic mice and 10 mice that had their urine collected during the corresponding day after colonization. Beside each PLS-DA plot is the corresponding validation plot.

Figure 5.2.1.3 compares male IL-10 KO mice and each of their post-colonization day urine samples referenced to data collected at 20 weeks while the mice were still in an axenic environment. Right at day 1, two distinct clusters occur, one for the axenic mice and one for the day 1 mice. A separation between the axenic group and the day 1 group can be

observed. Day 2 is similar; once again two distinct clusters are formed, one by the colonized group and the other by the axenic group. The distance between the two groups also increased; it is now very obvious that there is no overlap between the two groups. Results for days 3, 4, and 7 also show two very well-defined clusters, and there is significant distance between the two clusters so that no overlap is present.

plot	R2Y	Q2
All days	0.691	0.44
ax vs. d 1	0.966	0.888
ax vs. d 2	0.987	0.922
ax vs. d 3	0.984	0.942
ax vs. d 4	0.986	0.932
ax vs. d 7	0.984	0.936

Table 5.2.1.1 - R2Y and Q2 values for the PLS-DA plots constructed for the IL-10 KO males colonized with fecal bacteria over the days indicated.

5.2.2 Female: comparison of axenic mice and mice colonized with fecal bacteria

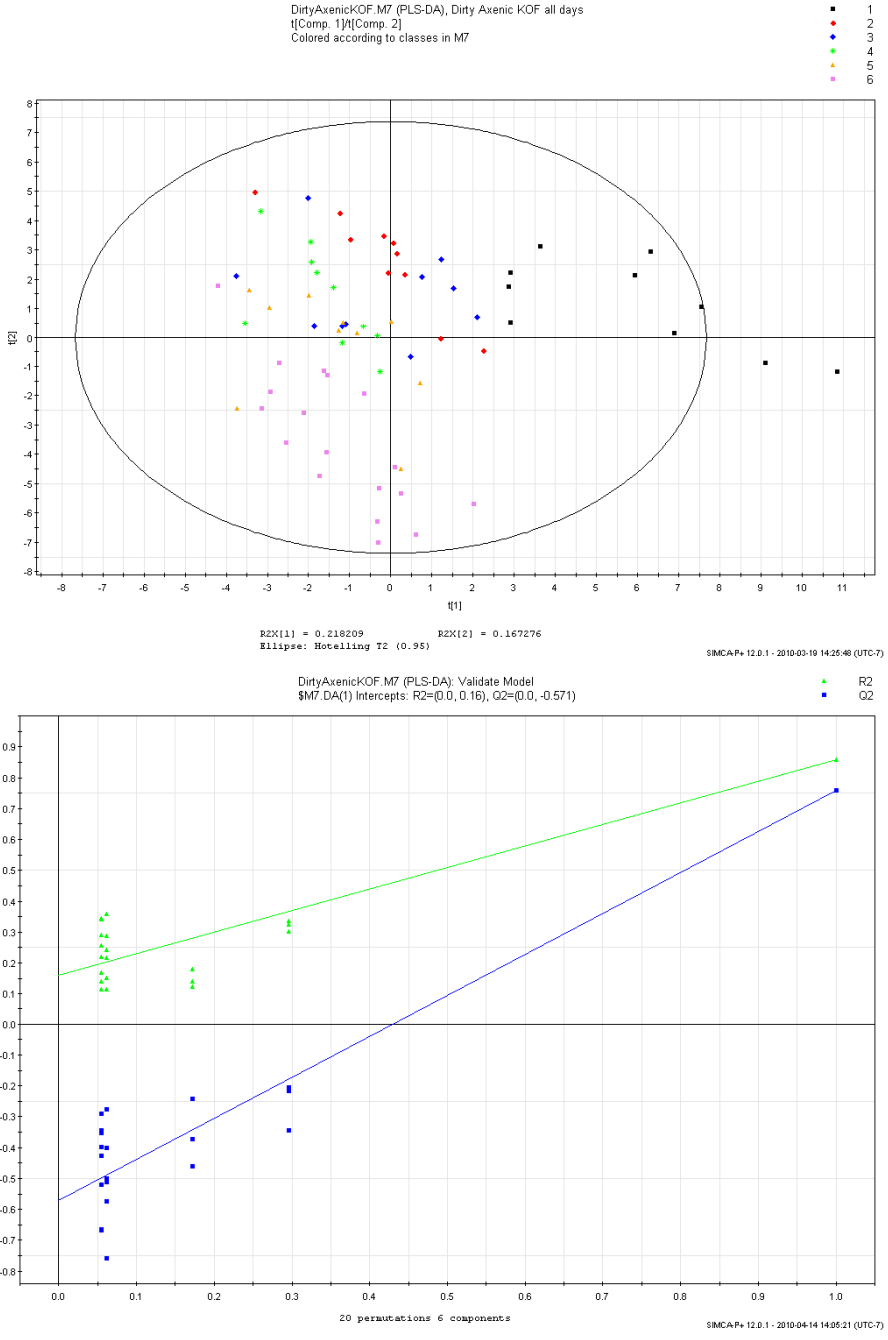

Figure 5.2.2.1– PLS-DA of week-20 female IL-10 KO axenic mice along with data from mice colonized with fecal bacteria on days 1-4 and 7 post-colonization. Axenic mice are

displayed in black, day 1 in red, day 2 in blue, day 3 in green, day 4 in yellow, and day 7 in pink. Below the PLS-DA plot is the validation plot.

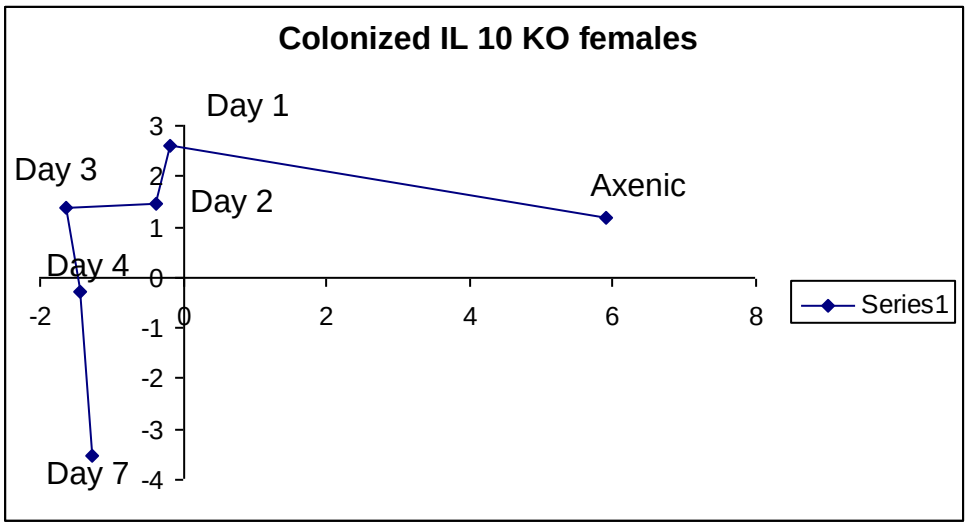

Figure 5.2.2.2– Metabolic trajectory of the colonized IL-10 KO males; the plot was constructed by taking the coordinates of all the points for each week and calculating a single mean coordinate for each week.

The female axenic IL-10 KO group (Figure 5.2.2.1) shows similar trends to the males. When compared to the axenic mice, the colonized group appears to form its own separate cluster. Analysis of the metabolic trajectories plot (Figure 5.2.2.2) shows that the female group also appears to be following a similar trend to the males with respect to the movement throughout the plot. The axenic points of the colonized group start in the upper right hand quadrant of the plot while the day 1 colonized group starts in the upper middle. As the days go by, the points move down towards the lower quadrant of the plot. Similar to the all the other groups' data, the largest movement on the plot occurs from axenic to day 1. The

magnitude of movement is fairly consistent for days 1 through 4, with the magnitude increasing from days 4 to 7.

Axenic vs. Day 1

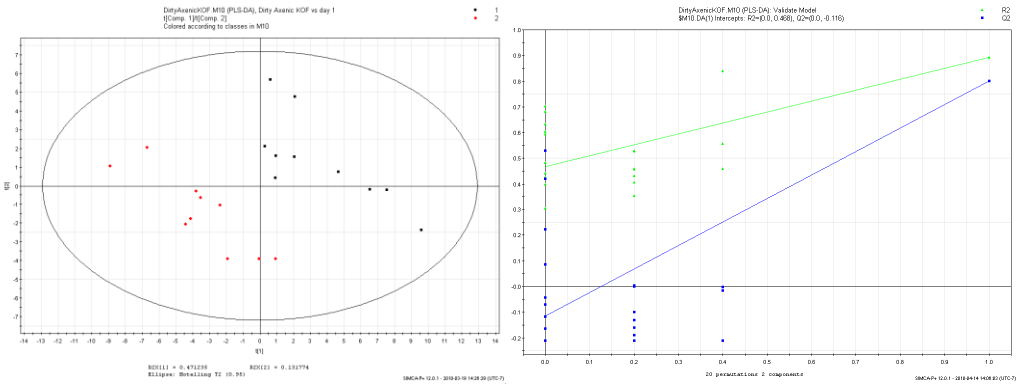

Axenic vs. Day 2

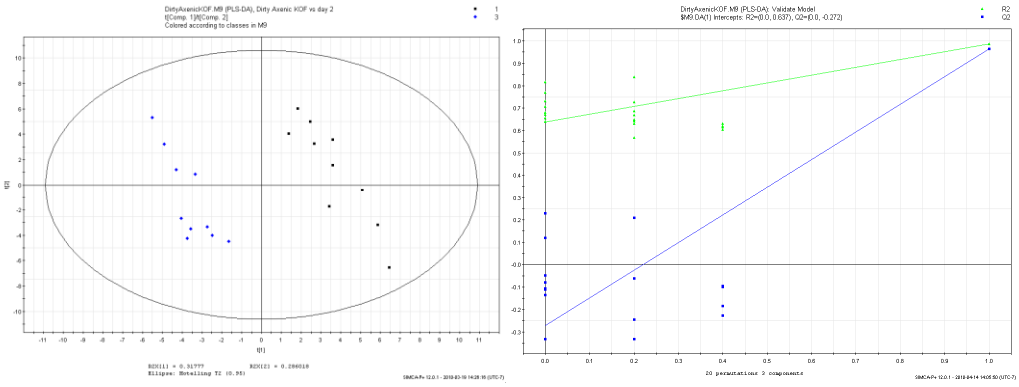

Axenic vs. Day 3

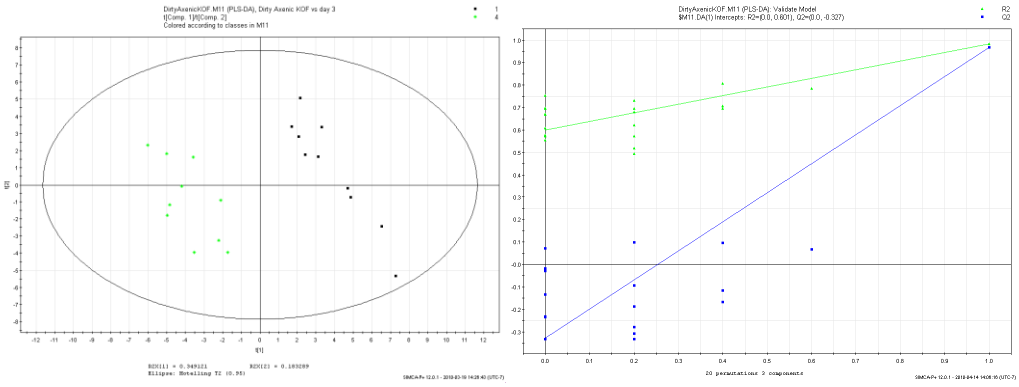

Axenic vs. Day 4

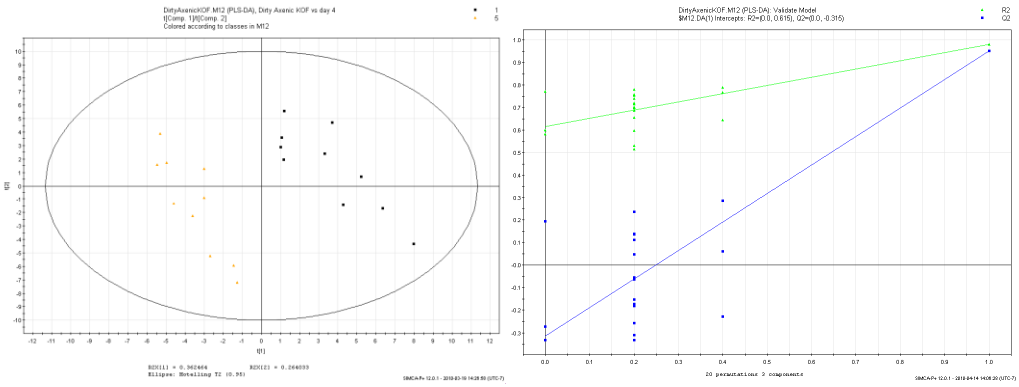

Axenic vs. Day 7

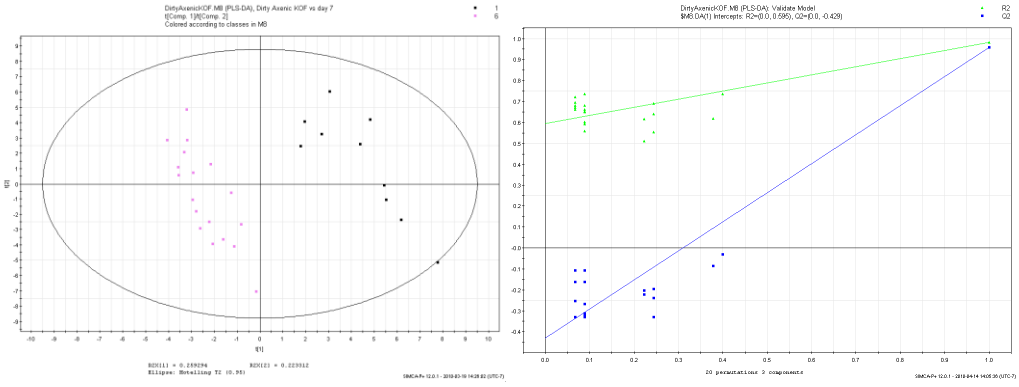

Figure 5.2.2.3 – Day-by-day analysis of female IL-10 KO mice that were colonized with fecal bacteria, reference to 20-week axenic mice; each plot is constructed using 10 axenic mice and 10 mice that had their urine collected during the corresponding day after colonization. Beside each PLS-DA plot is the corresponding validation plot.

Comparing the individual post-colonization dates to the axenic group provides a better understanding of how colonization changes the metabolic profile of the mice in reference to their axenic metabolic profiles. At day 1,the day 1 group and the axenic group appear to form their own clusters, with separation between the clusters and no overlap between the two groups. At day 2, the colonized group and the axenic group are still

distinct clusters and there is no overlap. Days 3, 4, and 7 also show similar results to what was observed at day 2. The colonized groups are all separate from the axenic group, the clustering is relatively tight, and there is no overlap between the colonized groups and the axenic groups.

plot	R2Y	Q2
All days	0.658	0.488
ax vs. d 1	0.981	0.959
ax vs. d 2	0.988	0.965
ax vs. d 3	0.893	0.802
ax vs. d 4	0.984	0.967
ax vs. d 7	0.979	0.952

Table 5.2.2.1 - R2Y and Q2 values for the PLS-DA plots constructed for the IL-10 KO females colonized with fecal bacteria over the days indicated.

5.3 Wild-type vs. IL-10 KO

5.3.1 Males – metabolic trajectory of colonized mice

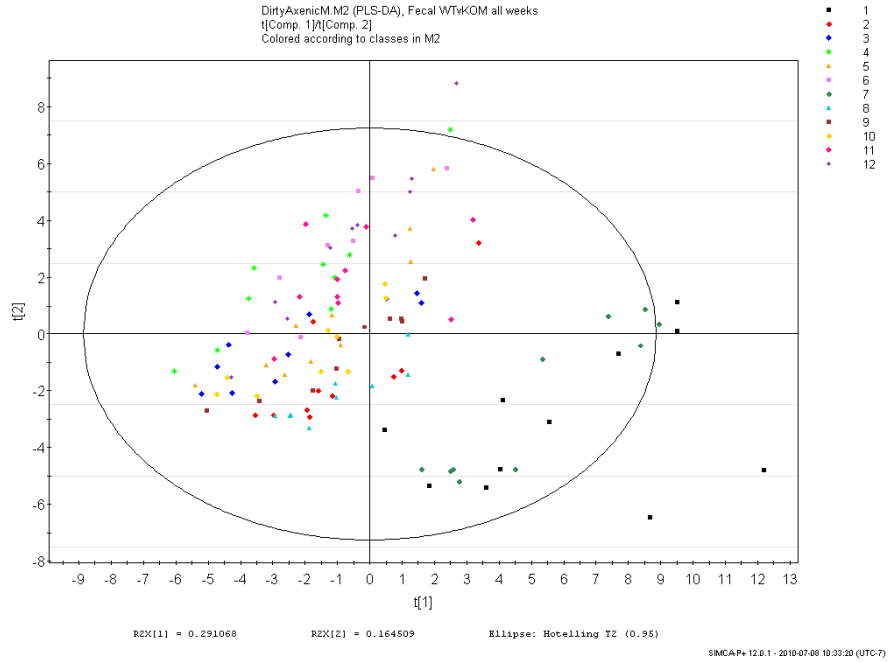

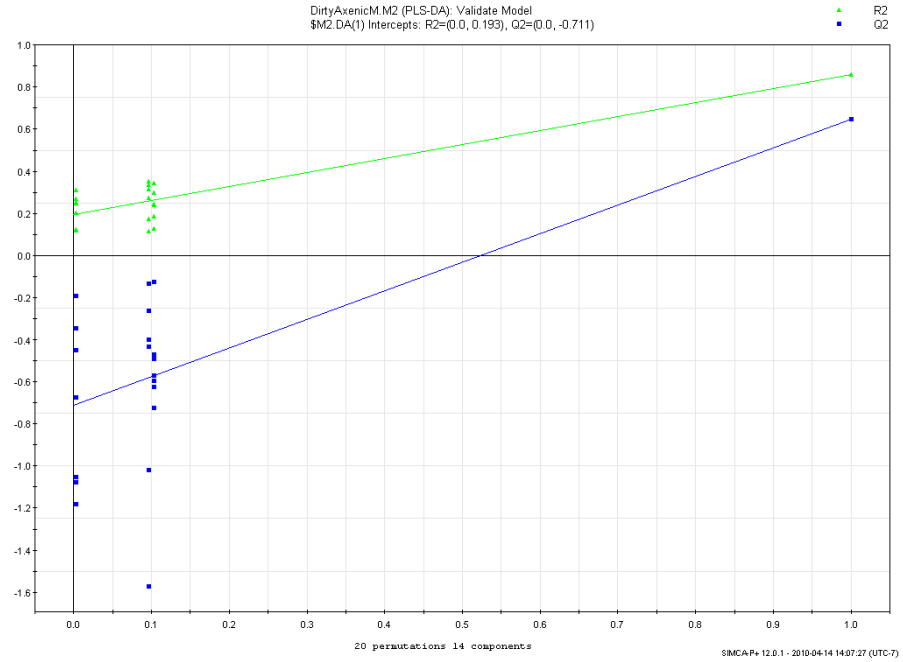

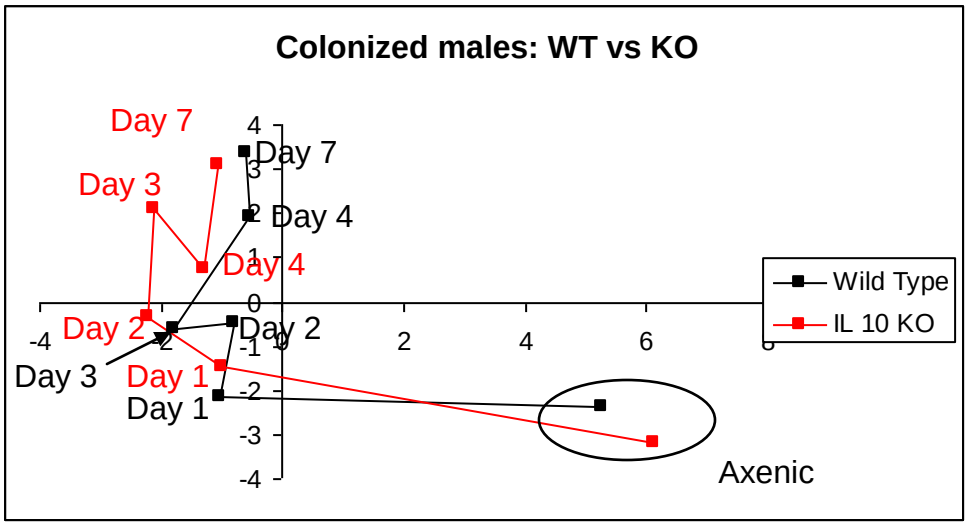

Figure 5.3.1.1 – Metabolic trajectory plot for males that have been colonized with fecal bacteria; the plot was generated by taking the individual coordinates from the PLS-DA plot (above) and generating a mean coordinate for each time-point. Wild-type mice are displayed in black, and IL-10 KO mice are displayed in red on the metabolic trajectory plot. On the PLS-DA plot, the IL-10 KO mice are numbers 1-6 and the wild-type mice are 7-12. Below the PLS-DA plot is the validation plot.

Figure 5.3.1.1 is a metabolic trajectory plot that was generated from a PLS-DA plot comparing the wild-type males which had been colonized with fecal bacteria to the IL-10 KO males which had also been colonized with fecal bacteria. The plot was generated by taking the coordinates from the original PLS-DA plot and calculating a single mean point for each time-point. From the plot, we can see that the two axenic points are very far away from all the colonization points. We can also see that the greatest change occurs between the axenic state to day 1 of fecal colonization. Although axenic to day 1 points cover the greatest distance across the plot and represents a large change from axenic to colonized, this change is

also the most similar element between data for the wild-type and the IL-10 KO mice. The wild-type mice and the IL-10 KO mice both move to basically the same location on the plot at day 1. What is interesting, however, is that from days 2-4 and day 7 the wild-type mice take an entirely different path than the IL-10 KO mice do, and eventually the two groups end up on different spots on the plot. The day 4-7 change shows distinction, in that in the wild-type there appears to be little change between days 4 and 7, while in the IL-10 KO mice there is still a large change from days 4 to 7. The differences between the paths occur because of the changes to the metabolic profiles of the mice each day. To confirm that these two groups are actually different at the end-point of day 7 a PLS-DA plot was constructed to compare the two (Figure 5.3.1.2). This PLS-DA plot shows two unique clusters, one for the wild-type mice and one for the IL-10 KO mice. There is also no overlap between the two clusters.

plot	R2Y	Q2
All days	0.447	0.194
Day 7	0.958	0.795

Table 5.3.1.1 - R2Y and Q2 values for the PLS-DA plots constructed for the wild-type colonized males vs. the IL-10 KO colonized males.

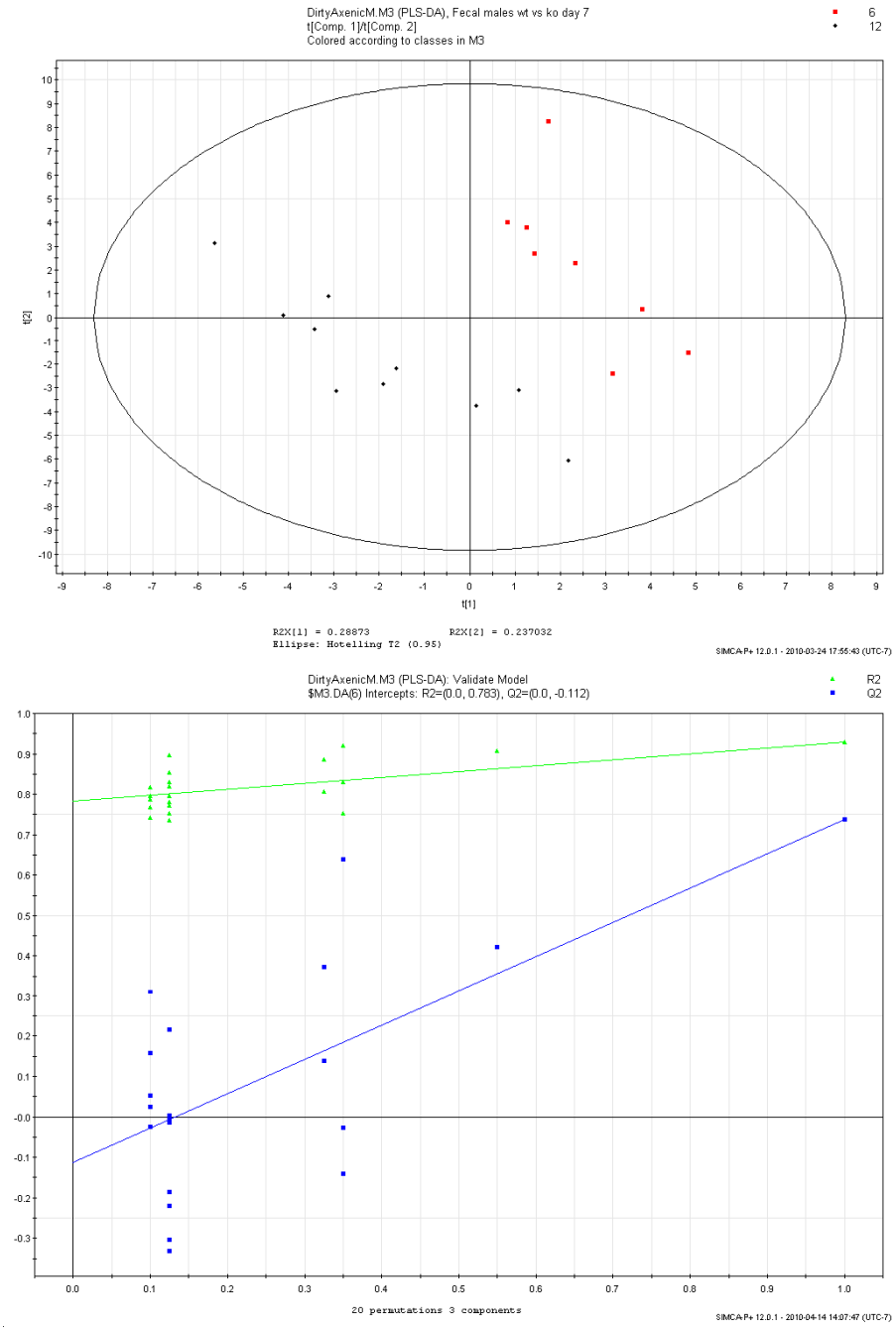

Figure 5.3.1.2 – PLS-DA plot constructed for male wild-type (black) and IL-10 KO (red) fecal-colonized mice at day 7. The wild-type group is made up of 10 points and the IL-10 KO group is made up of 8 points. Below the PLS-DA plot is the validation plot.

5.3.2 Females – metabolic trajectory of colonized mice

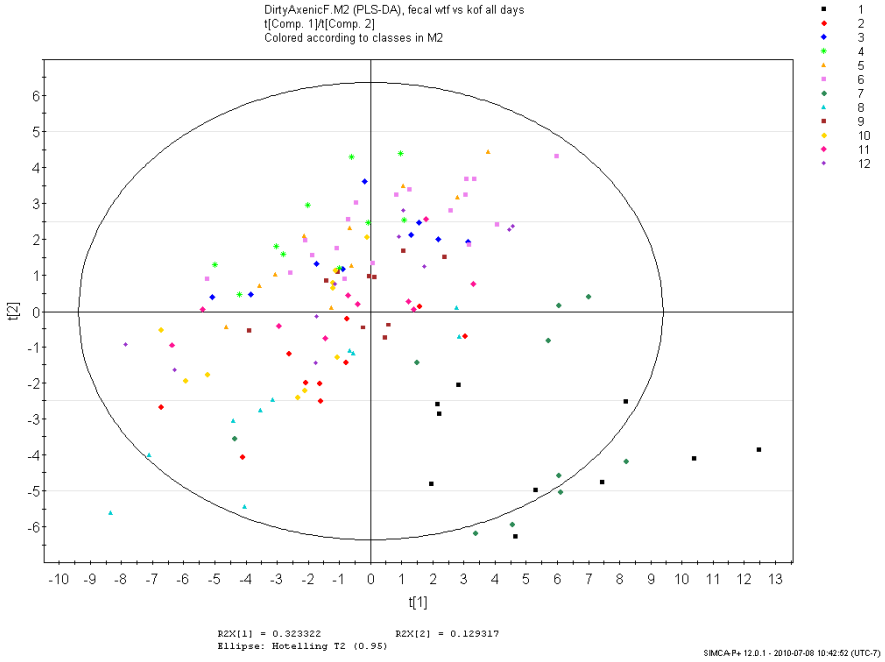

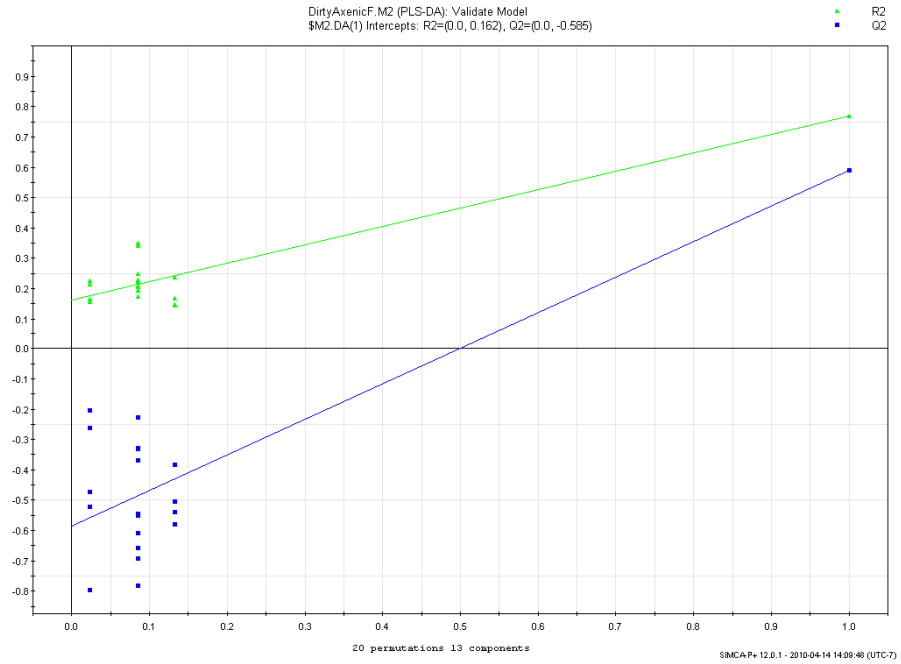

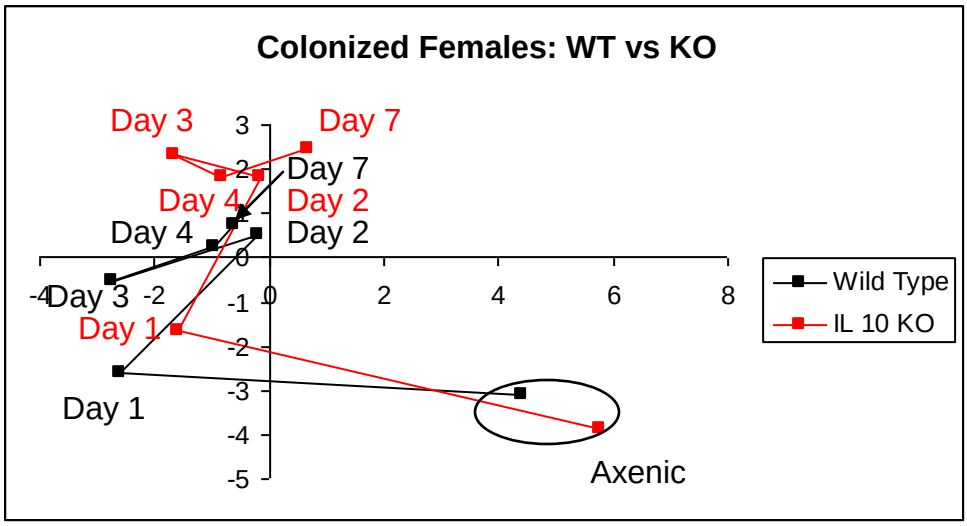

Figure 5.3.2.1 – Metabolic trajectory plot for females that have been colonized with fecal bacteria; the plot was generated by taking the individual coordinates from the PLS-DA plot (above) and generating a mean coordinate for each time-point. Wild-type mice are displayed in black and IL-10 KO mice are displayed in red in the metabolic trajectory plot. In the PLS-DA plot, the IL-10 KO mice are numbers 1-6 and the wild-type mice are 7-12. Below the PLS-DA plot is the validation plot.

Figure 5.3.2.1 is a metabolic trajectory plot once again constructed from the original PLS-DA plot (above) comparing wild-type and IL-10 KO female mice that were colonized with fecal bacteria. As with the males, the two axenic points are separated from the colonized group. Also similar is the fact that the movement from axenic to day 1 covers the greatest distance over the plot but the direction and magnitude of travel is similar between the wild-type and the IL-10 KO mice. Day 2 also shows similar magnitude and direction between the wild-type and the IL-10 KO mice. It is not until day 3 that we begin to see the path of the wild-type and the IL-10 KO mice deviate from each other. Day 4 is also interesting because the

points are once again close to each other but from completely different paths. Then, at day 7, the wild-type and the IL-10 KO mice separate and end up in different spots on the plot. To ensure that there was truly a difference between the wild-type and the IL-10 KO mice at day 7, we constructed a PLS-DA plot (figure 5.3.2.2) comparing the two group. Analysis of the PLS-DA plot shows two distinct clusters formed, one for the wild-type mice (black) and one for the IL-10 KO mice (red) with no overlap between the two clusters.

plot	R2Y	Q2
All days	0.544	0.264
Day 7	0.974	0.904

Table 5.3.2.1 - R2Y and Q2 values for the PLS-DA plots constructed for the wild-type colonized females vs. the IL-10 KO colonized females.

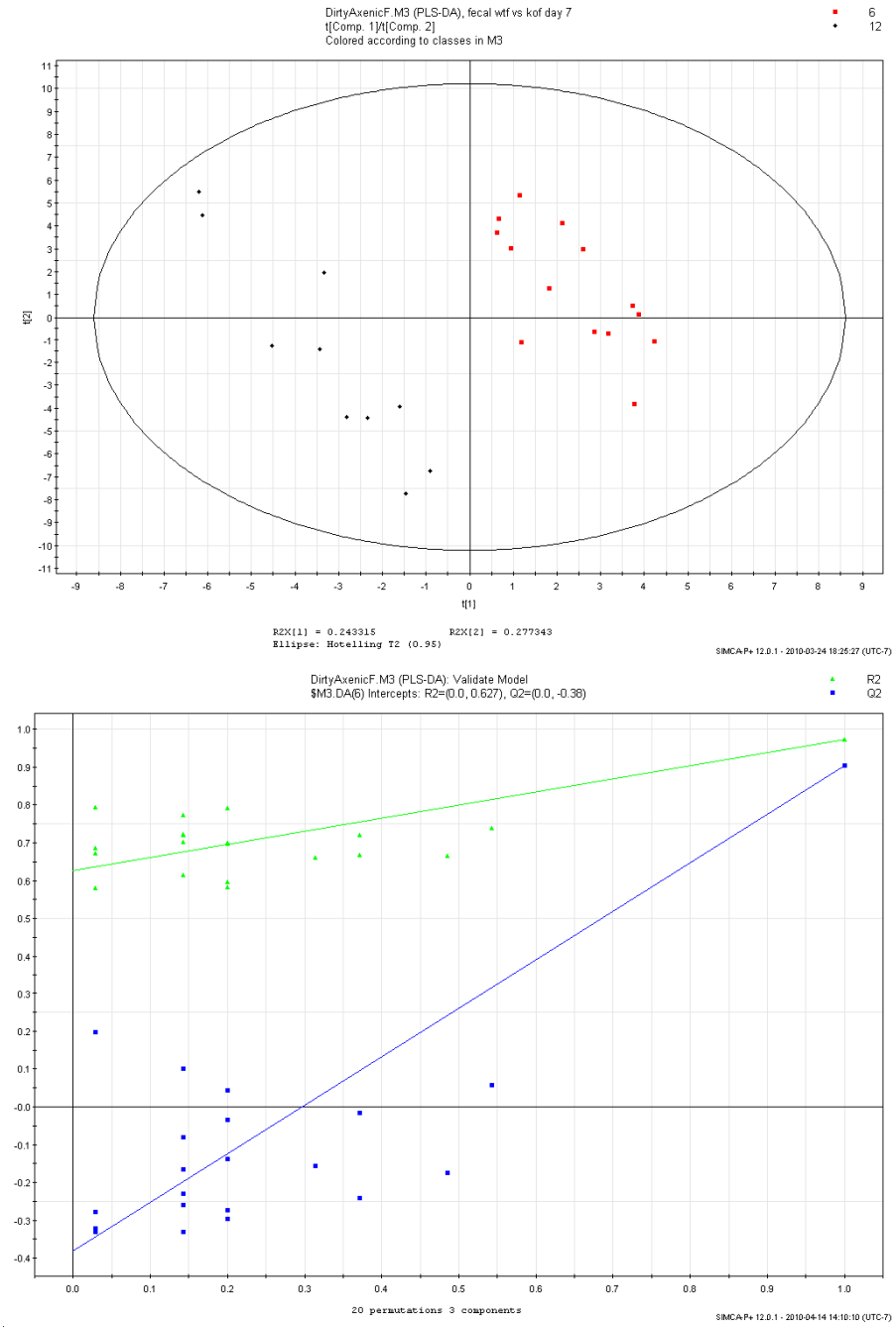

Figure 5.3.2.2 – PLS-DA plot constructed for female wild-type (black) and IL-10 KO (red) fecal-colonized mice at day 7. The wild-type group is made up of 10 points and the IL-10 KO group is made up of 14 points. Below the PLS-DA plot is the validation plot.

5.4 20-week conventional vs. day 7

5.4.1 Male population

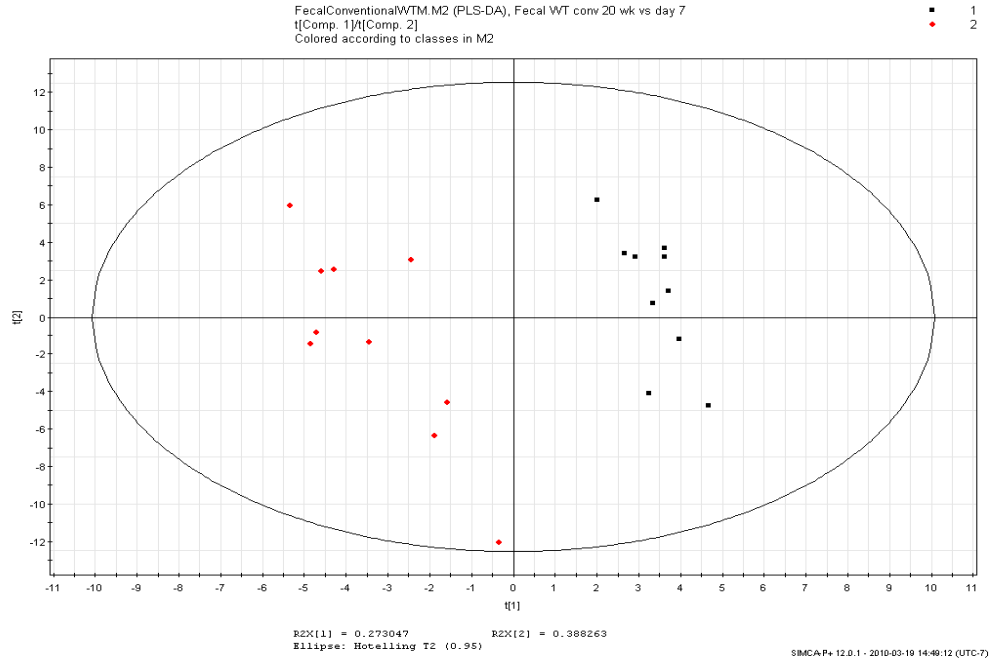

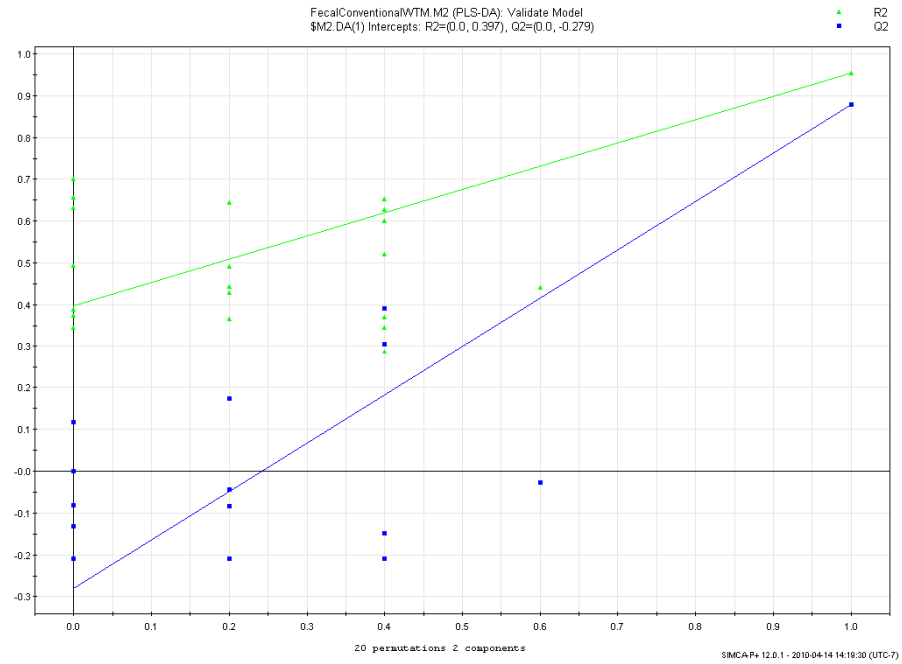

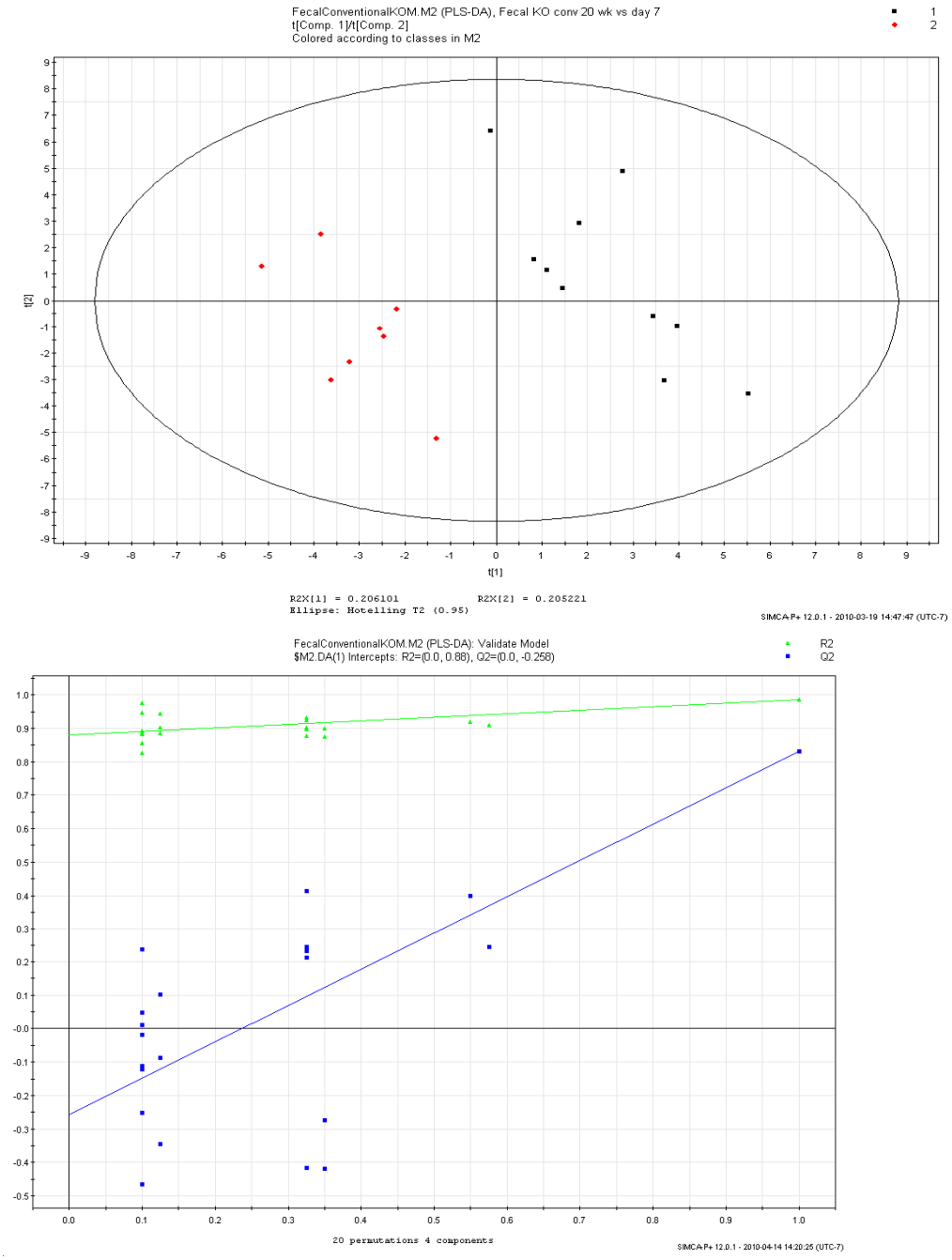

Figure 5.4.1.1 – PLS-DA plot comparing male mice that have been conventionally raised vs. male mice that had been colonized with fecal bacteria at day 7, the colonized mice are displayed in black and the conventionally raised mice are displayed in red. The top graph is the comparison for wild-type mice and the bottom graph is the comparison for the IL-10 KO mice. Below the PLS-DA plot is the corresponding validation plot.

Figure 5.4.1.1 is a PLS-DA plot comparing conventionally raised males at 20 weeks of age with 20-week-old fecally-colonized males at 7 days post-colonization. The top plot compares the wild-type mice and the bottom plot compares the IL-10 KO mice. In both plots, two clusters are formed, one cluster for the conventional 20-week-old mice and one cluster for the 7-days post-colonization group. There is also no overlap between the two groups in either plot. This plot shows that even though the IL-10 KO mice are getting sick due to the colonization process, the metabolites produced during this acute inflammation are different than in the chronic case observed in the conventional 20-week mice. The differences in the metabolite cocktail can also be observed in the wild-type mice that were colonized with fecal bacteria; even though the colonized wild-type mice do not get sick, they still form a separate group when compared to the 20-week conventional wild-type mice.

plot	R2Y	Q2
Wild-type	0.955	0.878
IL-10 KO	0.985	0.831

Table 5.4.1.1 - R2Y and Q2 values for the PLS-DA plots constructed for the week 20 vs. day 7 colonized mice for both the wild-type and the IL-10 KO males.

5.4.2 Female population

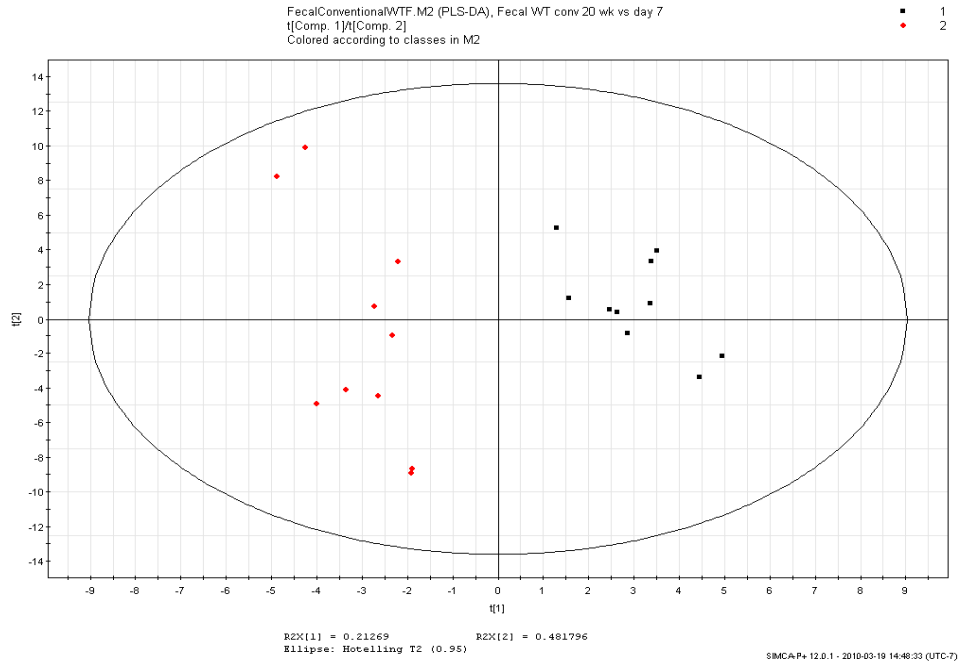

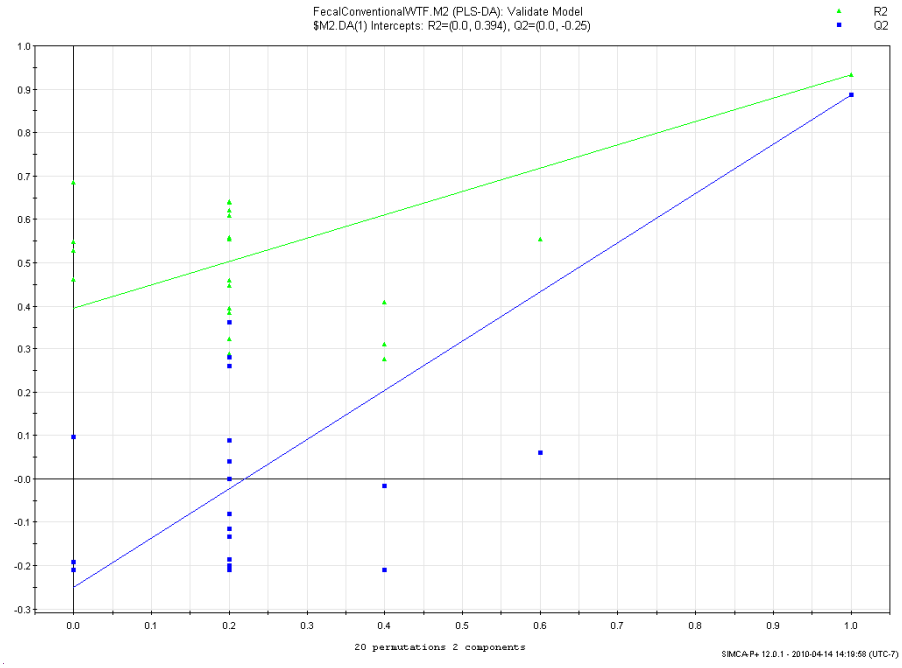

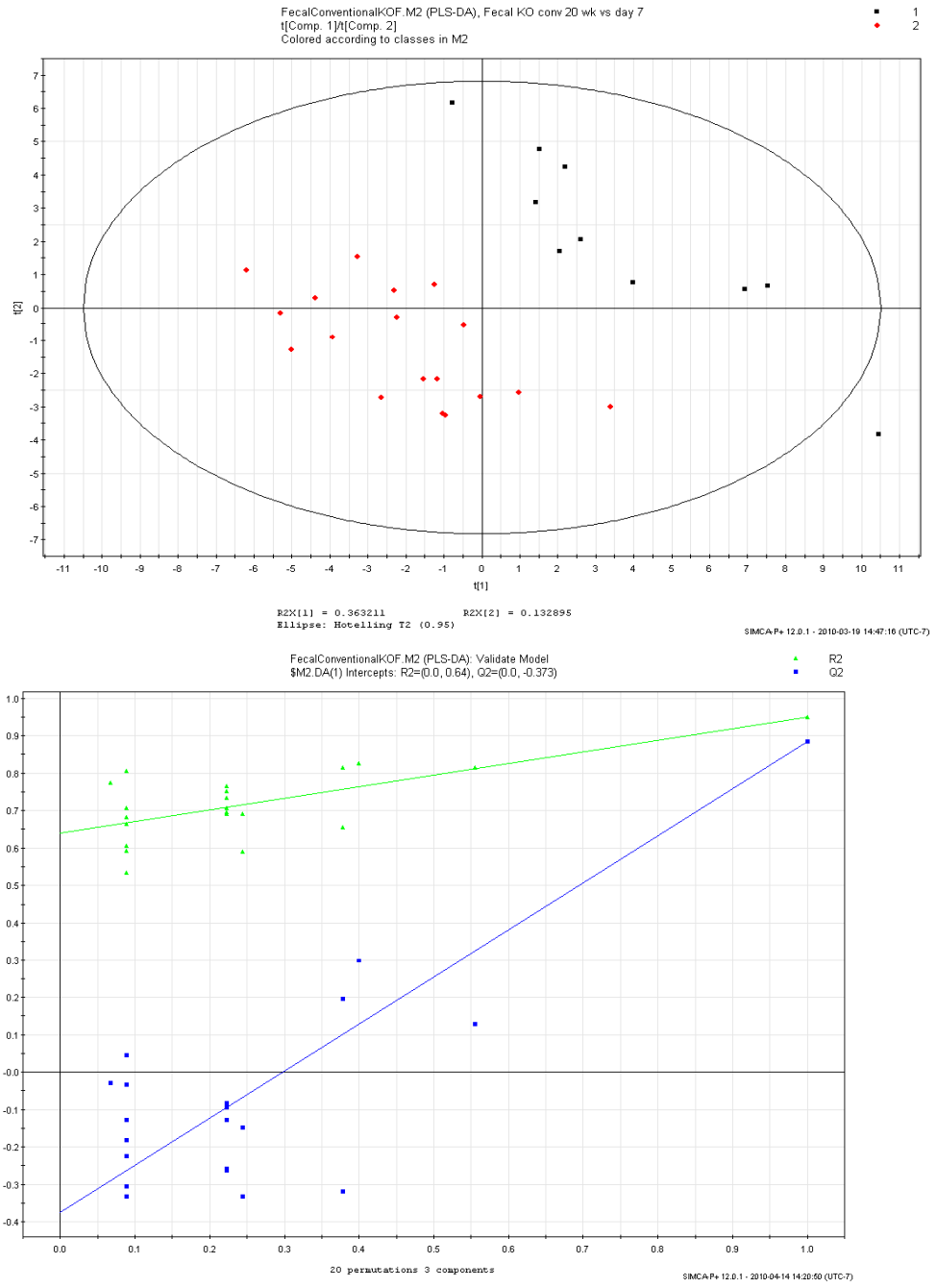

Figure 5.4.2.1 – PLS-DA plot comparing female mice that have been conventionally raised vs. female mice colonized with fecal bacteria at day 7; the colonized mice are displayed in black and the conventionally-raised mice are displayed in red. The top graph is the comparison for wild-type mice and the bottom graph is the comparison for the IL-10 KO mice. Below the PLS-DA plot is the corresponding validation plot.

Figure 5.4.2.1 is a PLS-DA plot comparing conventionally-raised females at 20 weeks of age to 20-week-old females colonized with fecal bacteria at 7 days post-colonization. The top plot compares the wild-type mice, and the bottom plot compares the IL-10 KO mice. Similar to the male plots, two clusters are formed, one cluster for the conventional 20-week-old mice and one cluster for the 7-days post-colonized group, and no overlap is present between the two groups. This plot shows that even though the IL-10 KO mice are getting sick due to the colonization process, the metabolites produced during this acute inflammation are different than the chronic case observed in the conventional 20-week mice. The differences in the metabolite cocktail can also be observed in the wild-type mice that were colonized with fecal bacteria; even though the colonized wild-type mice do not get sick, they still form a separate group when compared to the 20-week conventional wild-type mice.

plot	R2Y	Q2
Wild-type	0.933	0.888
IL-10 KO	0.951	0.885

Table 5.4.2.1 - R2Y and Q2 values for the PLS-DA plots constructed for the week 20 vs. day 7 colonized mice for both the wild-type and the IL-10 KO females.

Chapter 6 - Axenic vs. Conventional

6.1 Wild-type population

6.1.1 Male – comparison of urine metabolomics over time

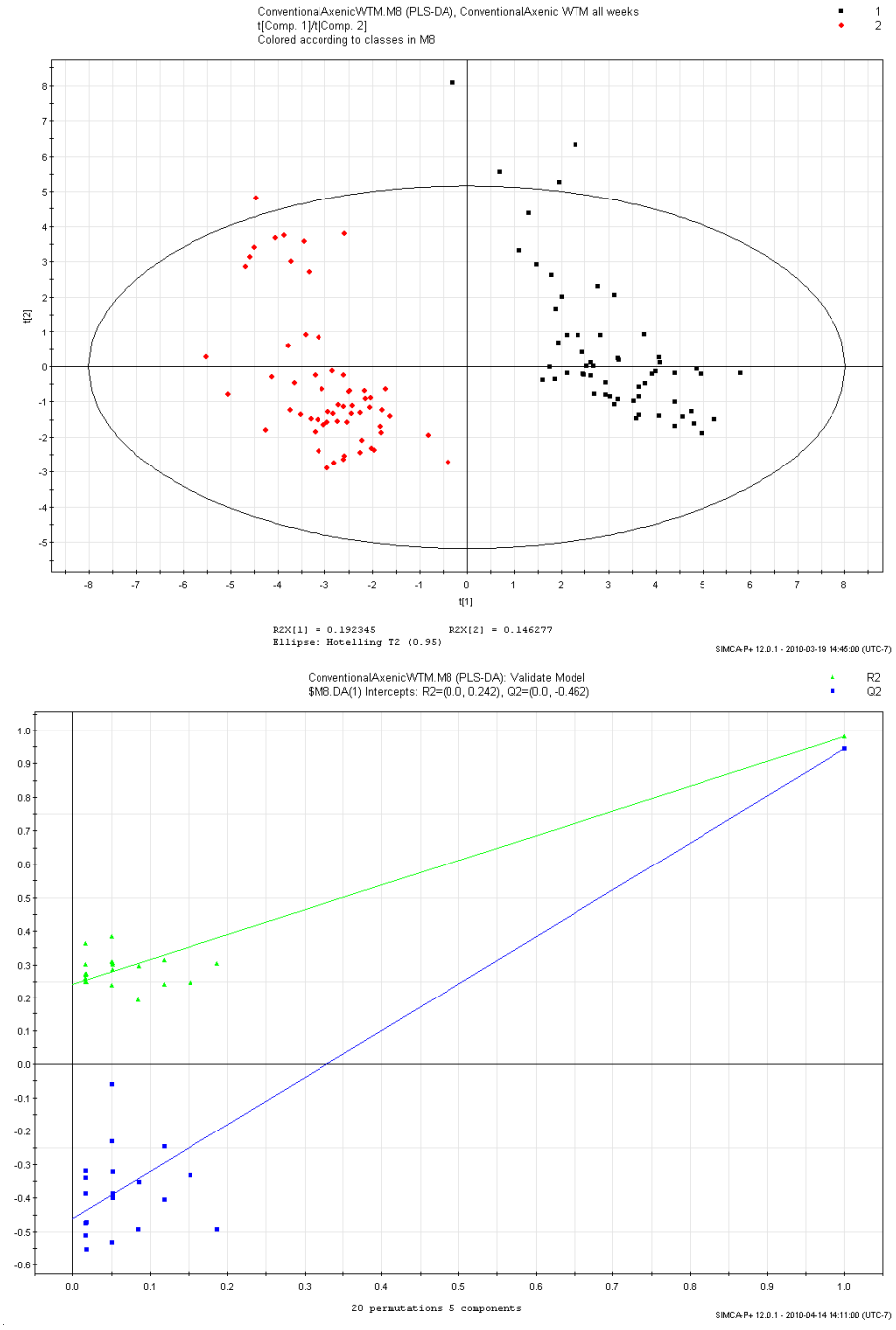

Figure 6.1.1.1 – PLS-DA plot of axenic wild-type males over all time points vs. conventional wild-type males at all time points; axenic mice are displayed in black and

conventional mice are displayed in red. Urine was collected at weeks 4, 6, 8, 12, 16, and 20, either in the germ-free bubble or in a conventional environment. 10 samples were collected at each time-point. Below the PLS-DA plot is the validation plot.

Figure 6.1.1.1 is a comparison of all wild-type axenic males and wild-type conventional males via PLS-DA plot. Right away we can see that there are two clusters formed on the plot; one cluster for the axenic wild-type mice and the other cluster for the conventional wild-type mice. Each of the clusters comprises 60 data points (10 samples x 6 collection time points). The shape of the clusters is also fairly well-defined; with the exception of 4 outliers present in the axenic group and 1 outlier from in the conventional group, they are packed together fairly tightly. The outliers are due to low-volume of urine samples collected. The two clusters also completely separate out from each other, without any overlap.

Week 4

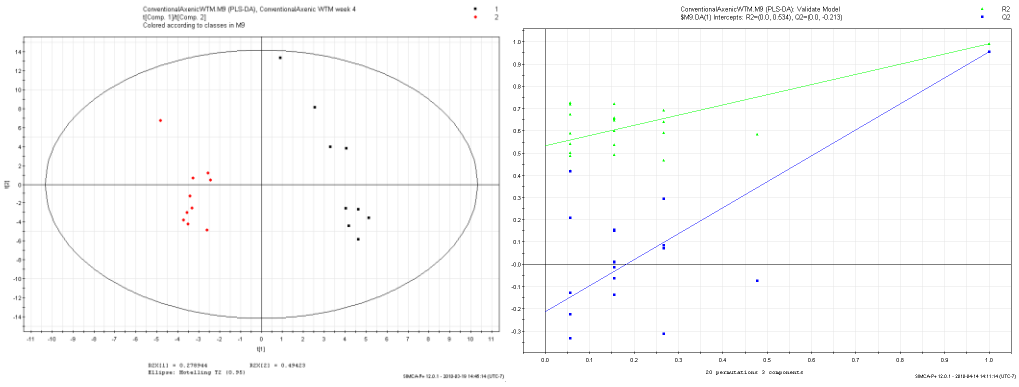

Week 6

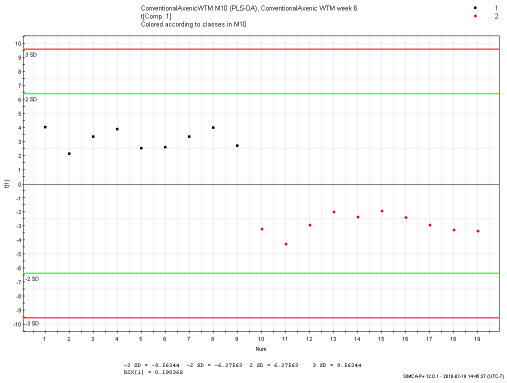

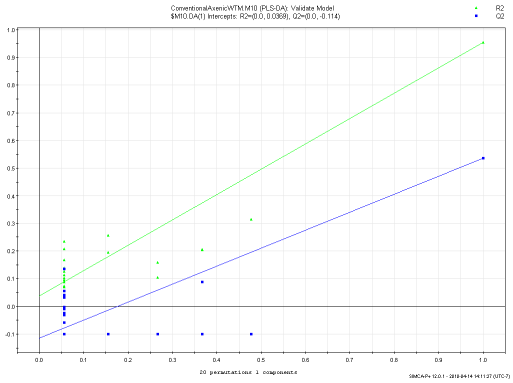

Week 8

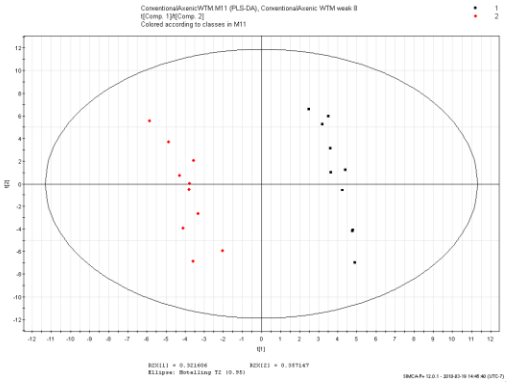

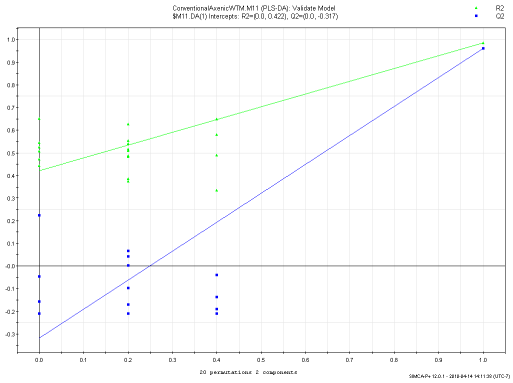

Week 12

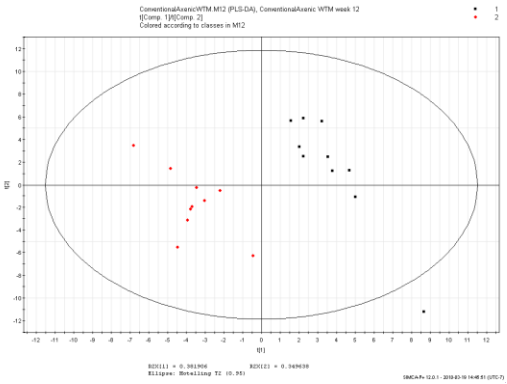

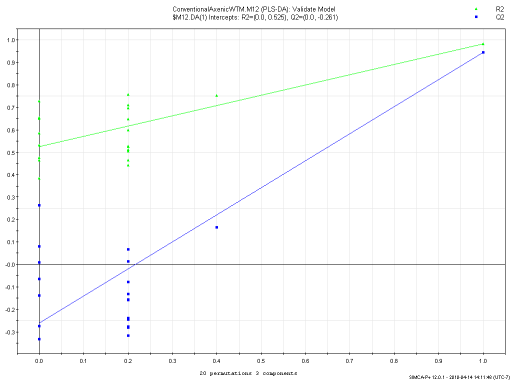

Week 16

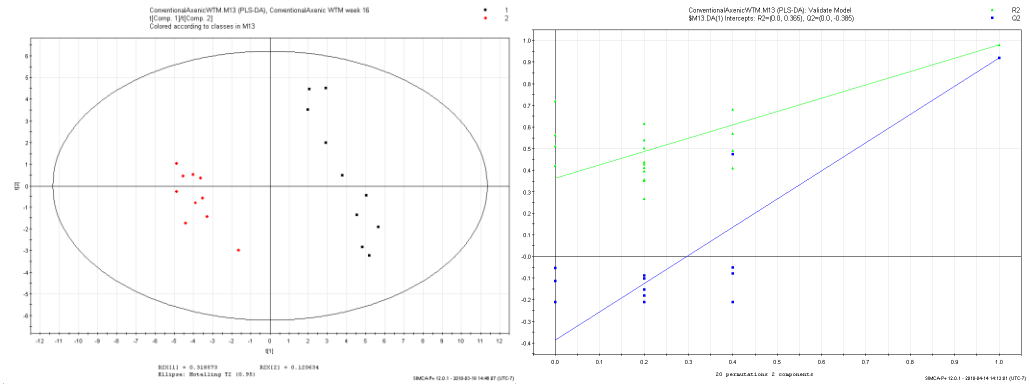

Week 20

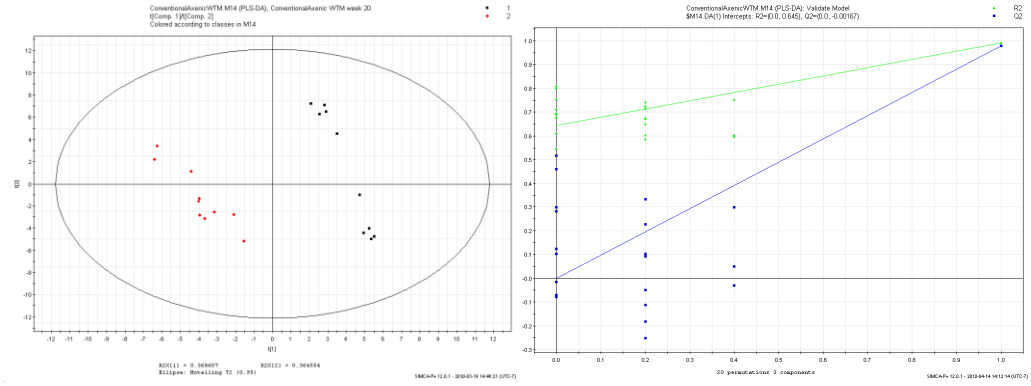

Figure 6.1.1.2 – PLS-DA plots of the urine metabolomic profiles of the axenic male wild-type and conventional male wild-type mice broken up by week of urine collection; conventional are displayed in red and axenic are displayed in black. Each week comprises 10 axenic mice and 10 conventional mice. Beside each PLS-DA plot is the corresponding validation plot.

Week-by-week comparisons of the conventional vs. axenic wild-type mice yield results similar to the single PCA plot for all the mice. At each week, we can see two completely separate clusters formed, one consisting of the conventional mice and one consisting of the axenic mice. The clusters of conventional and axenic mice do not overlap at any of the time points.

Other than the appearance of an outlier at week 12, the clusterings of both the conventional and the axenic groups remain fairly tight and bunched together. Interesting notes are that, at week 4 and week 20, the axenic cluster appears to break into two smaller groups, and that at the week 6 comparison only one component was generated to separate the conventional group from the axenic group, for the same reason as the other single component models -- forcing a second component reduces the model's predictive ability.

plot	R2Y	Q2
All weeks	0.98	0.945
week 4	0.992	0.957
week 6	0.953	0.536
week 8	0.986	0.962
week 12	0.983	0.944
week 16	0.981	0.92
week 20	0.993	0.98

Table 6.1.1.1 - R2Y and Q2 values for the PLS-DA plots constructed for the axenic wild-type males vs. the conventional wild-type males over all weeks.

6.1.2 Female – comparison of urine metabolomics over time

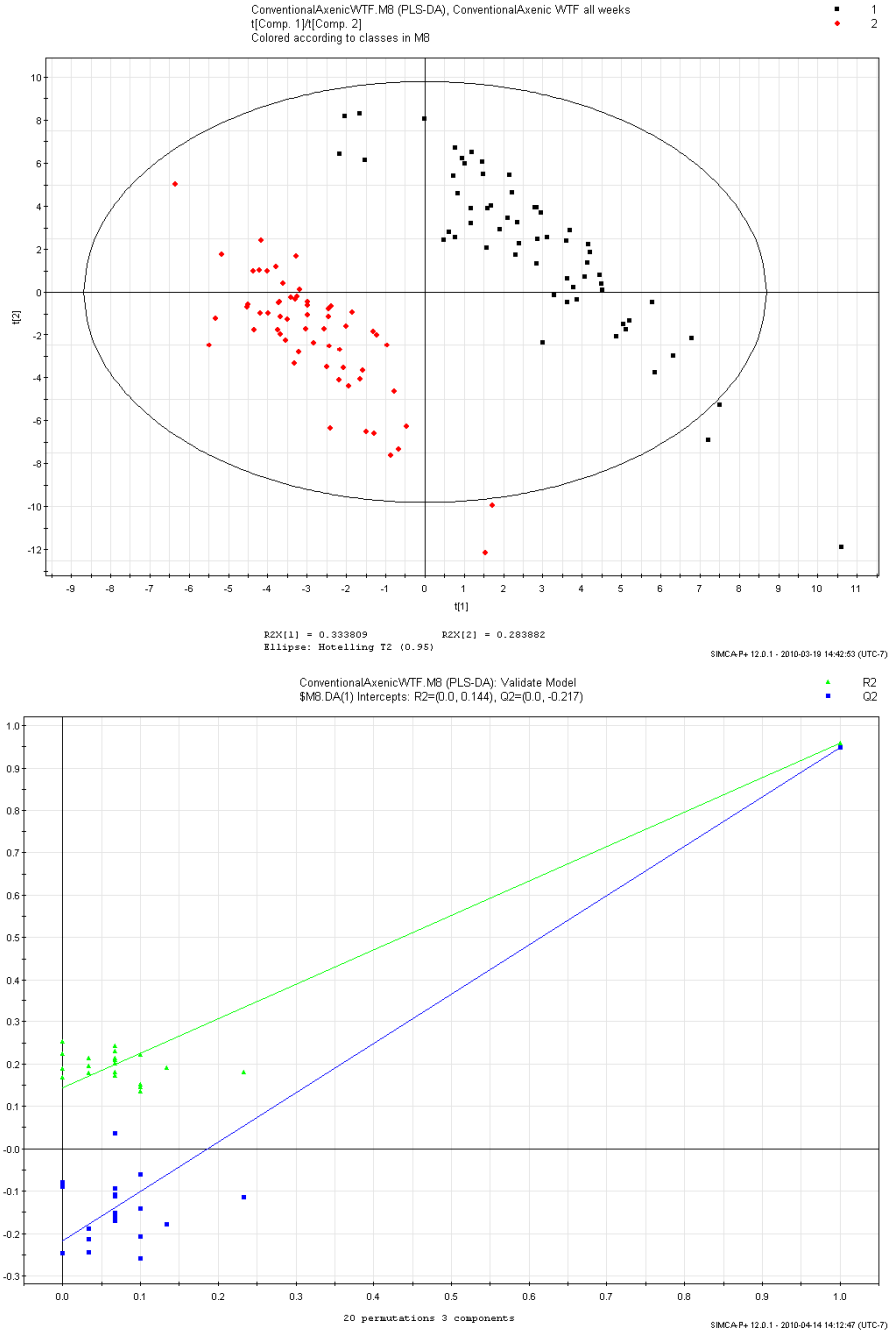

Figure 6.1.2.1 – PLS-DA plot of axenic wild-type females over all time-points vs. conventional wild-type females at all time-points; axenic mice are displayed in black and conventional mice are displayed in red. Urine was collected at weeks 4, 6, 8, 12, 16, and

20 either from the germ-free bubble or a conventional environment. 10 samples were collected at each time point. Below the PLS-DA plot is the validation plot.

Similar to the results observed for the male wild-type mice, the PCA comparison of the female wild-type conventional vs. female wild-type axenic mice produces two distinct clusters, one for conventional mice and the other for axenic mice. In addition, there is complete separation between the two clusters with a large gap present. Apart from a few outliers, which were due to low-volume urine collection during the initial collection process, the points in each cluster are bunched together in a fairly tight grouping.

Week 4

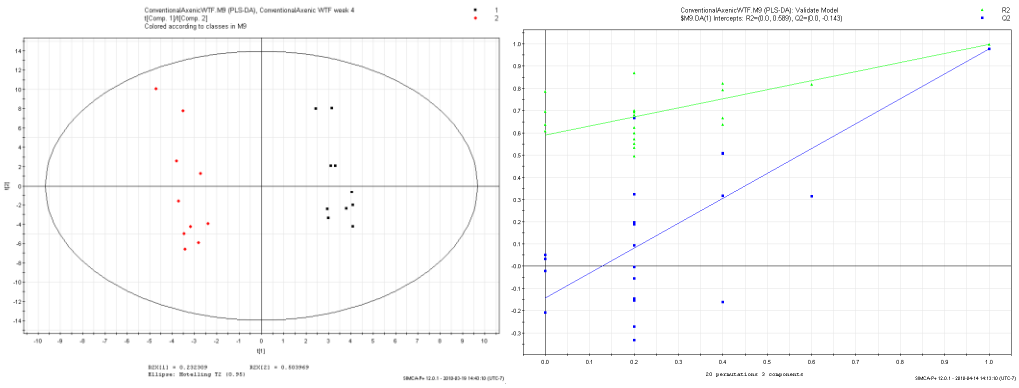

Week 6

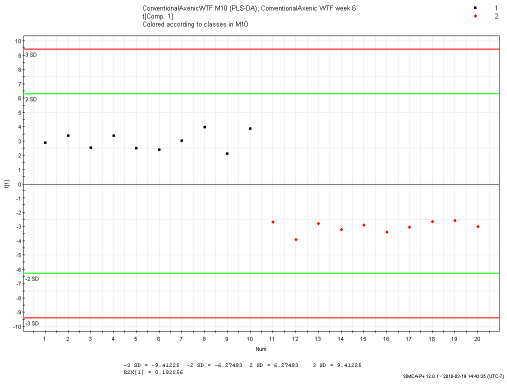

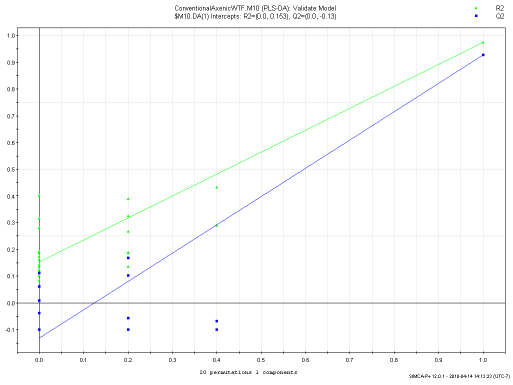

Week 8

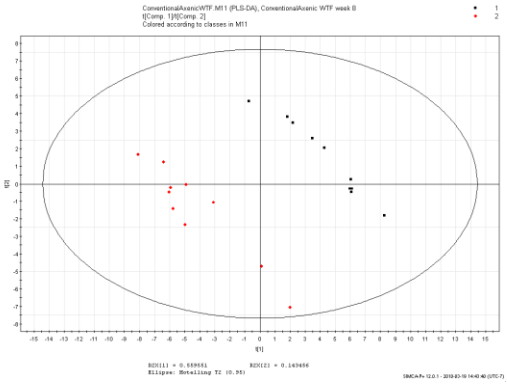

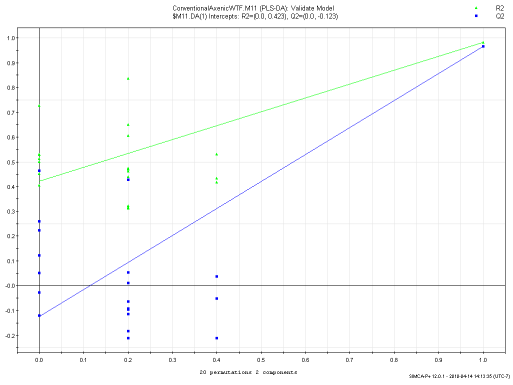

Week 12

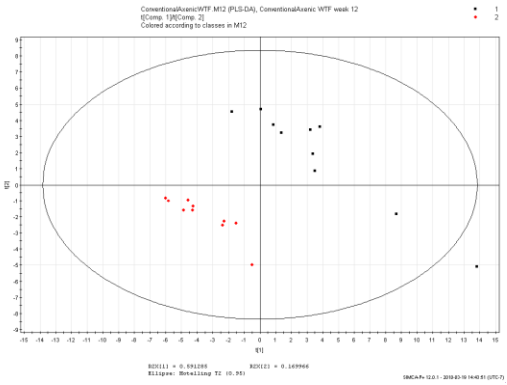

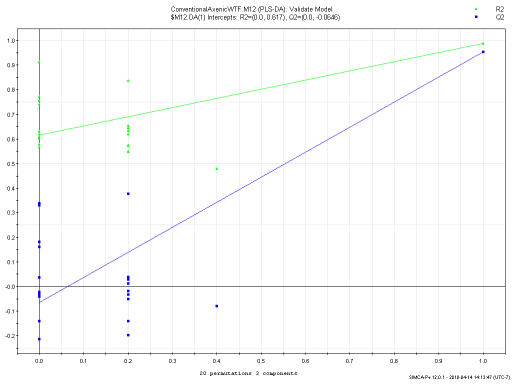

Week 16

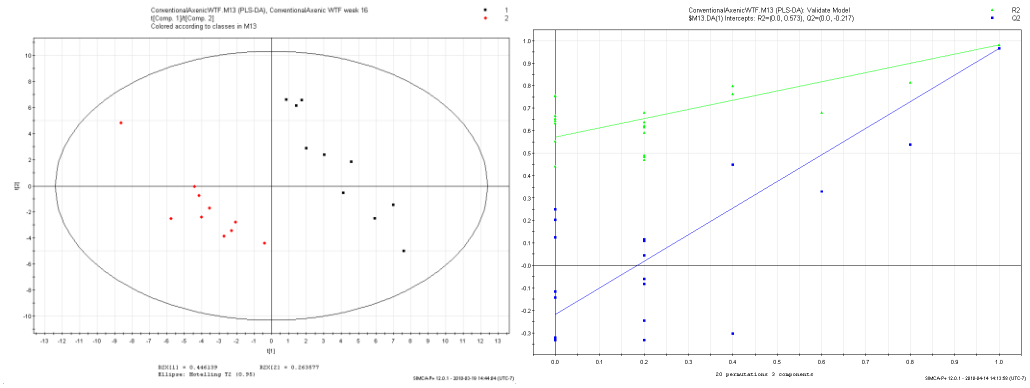

Week 20

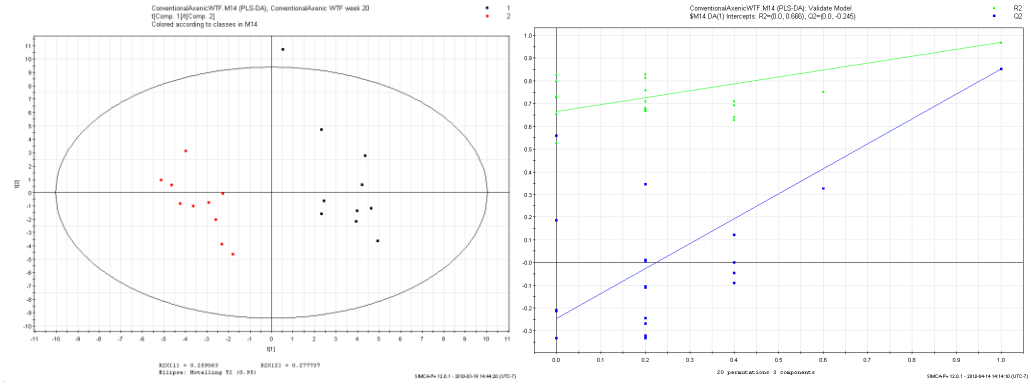

Figure 6.1.2.2 – PLS-DA plots of the urine metabolomic profiles of the axenic female wild-type and conventional female wild-type mice broken up by week of urine collection; conventional are displayed in red and axenic are displayed in black. Each week comprises 10 axenic mice and 10 conventional mice. Beside each PLS-DA plot is the corresponding validation plot.

Week-by-week comparisons of the female conventional wild-type vs. female axenic wild-type via PLS-DA also yield similar results to the ones observed in the male group. At each week, there are two separate clusters, one consisting of the conventional group and the other consisting of the axenic group. The clusters are separate at every week, with no

overlap of the clusters occurring at any of the weeks. It appears that the gap between the two clusters stays fairly constant, except in week 6, for which only one component was used to separate the conventional group from the axenic group. With the exception of a few outliers in the axenic group at week 12, the clustering within the groups is fairly tight. The clustering of the conventional group appears to be a little tighter than that for the axenic group.

plot	R2Y	Q2
All weeks	0.96	0.948
week 4	0.997	0.978
week 6	0.973	0.927
week 8	0.981	0.966
week 12	0.987	0.954
week 16	0.982	0.967
week 20	0.968	0.852

Table 6.1.2.1 - R2Y and Q2 values for the PLS-DA plots constructed for the Axenic wild-type females vs. the conventional wild-type females over all weeks.

6.2 IL-10 KO

6.2.1 Male – comparison of urine metabolomics over time

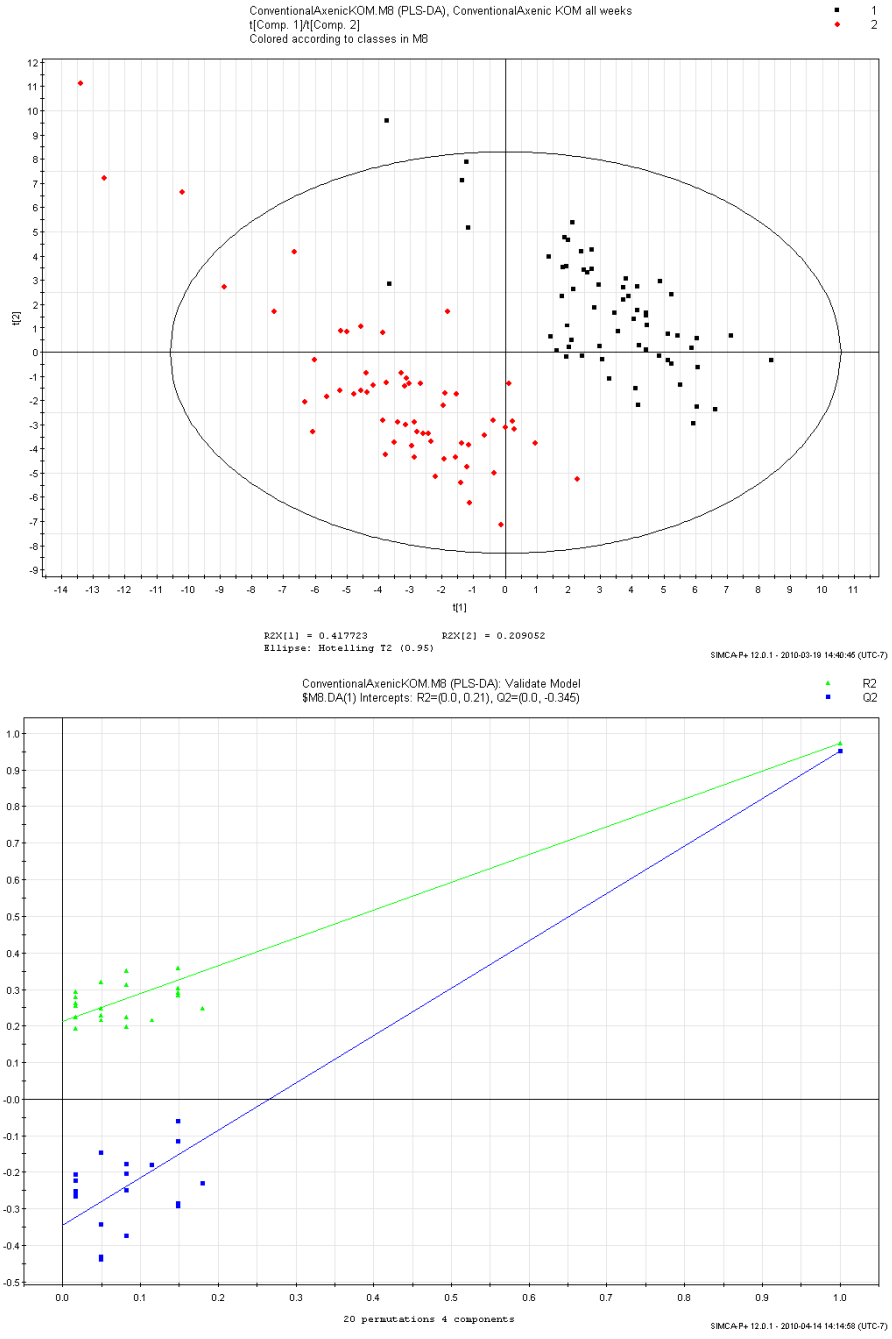

Figure 6.2.1.1 – PLS-DA plot of axenic IL-10 KO males over all time-points vs. conventional IL-10 KO males at all time–points; axenic mice are displayed in black and conventional mice are displayed in red. Urine was collected at weeks 4, 6, 8, 12, 16, and

20, either from the germ-free bubble or a conventional environment. 10 samples were collected at each time-point. Below the PLS-DA plot is the validation plot.

Figure 6.2.1.1 is a PLS-DA plot of conventional IL-10 KO male mice vs. axenic IL-10 KO male mice. Similar to the results for the wild-type comparison, there are two clusters formed on the plot, one cluster consisting of conventional mice and the other consisting of axenic mice. Further analysis of the plot shows that one of the axenic points is found in the conventional cluster. Aside from this one point there is complete separation between the axenic and the conventional clusters. This plot also reveals a few possible outliers, again due to low volume of urine collected. Even aside from the outliers, the clustering of these two groups is not as tight as the clustering that was observed in the wild-type mice, though it is tight enough for two individual groups to be formed.

Week 4

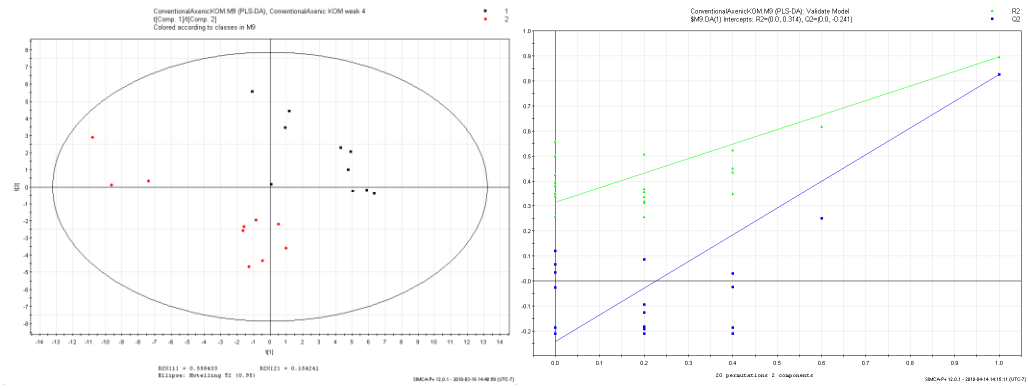

Week 6

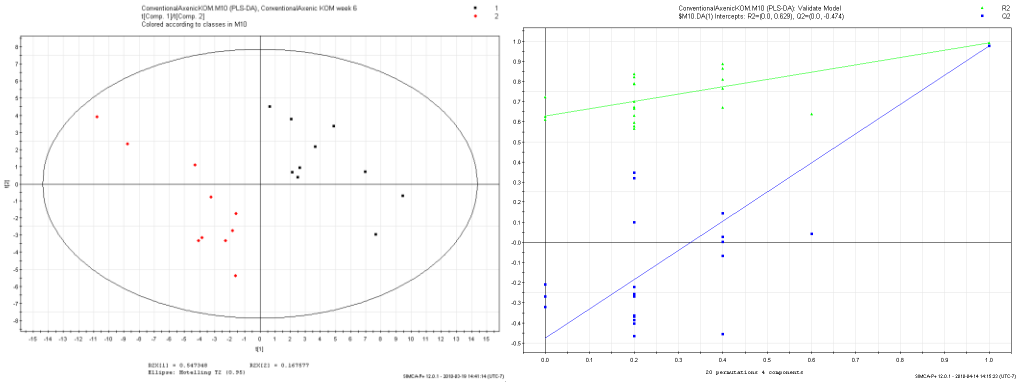

Week 8

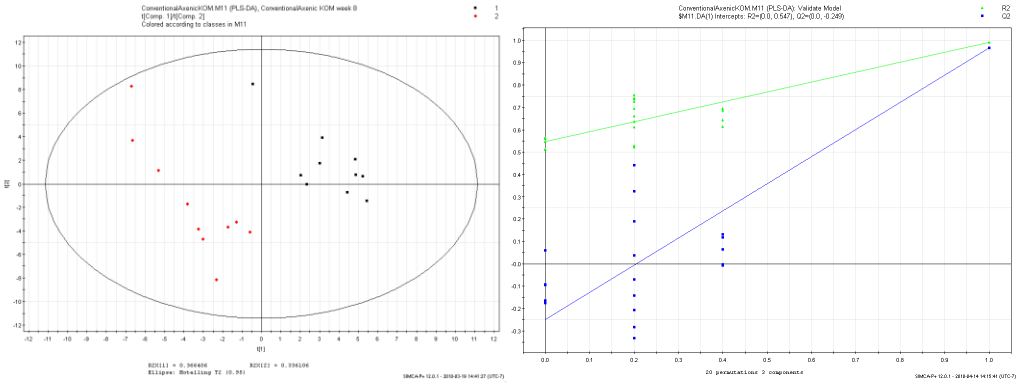

Week 12

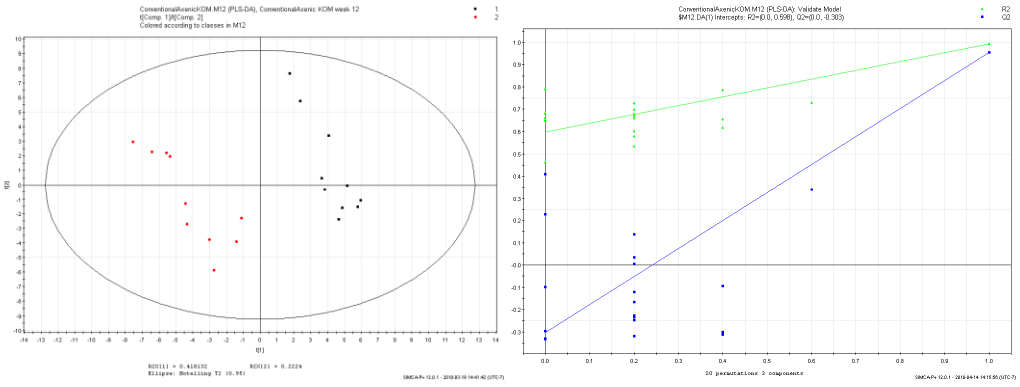

Week 16

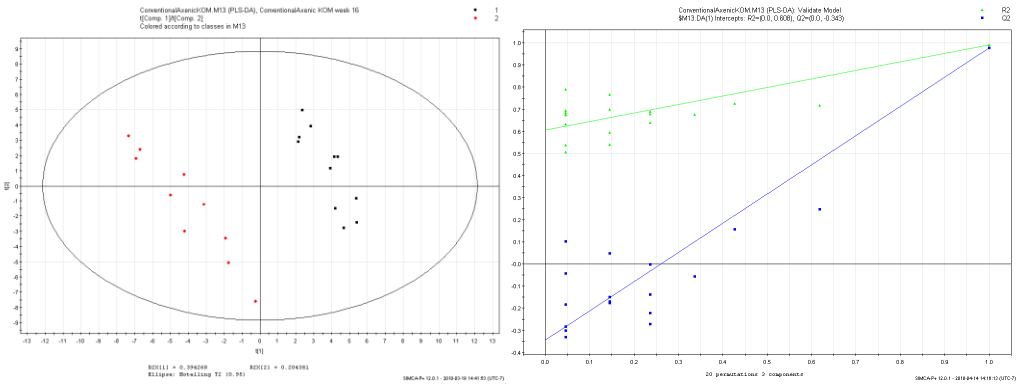

Week 20

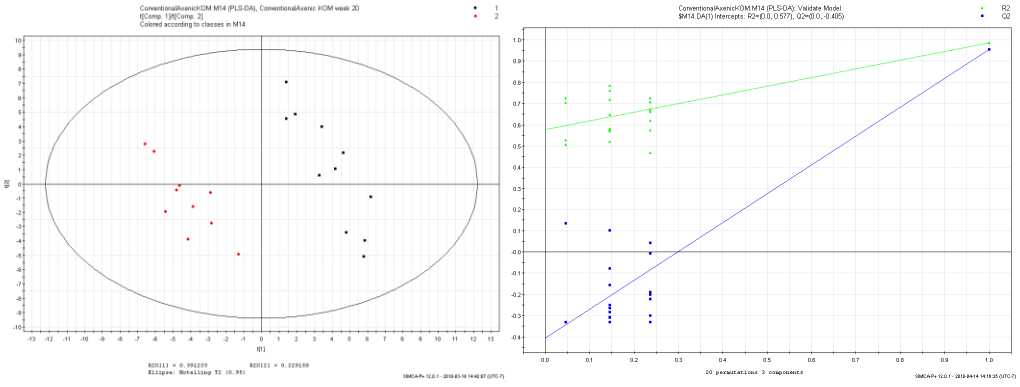

Figure 6.2.1.2 – PLS-DA plots of the urine metabolomic profiles of the axenic male IL-10 KO and conventional male IL-10 KO mice broken up by week of urine collection; conventional are displayed in red and axenic are displayed in black. Each week comprises 10 axenic mice and 10 conventional mice. Beside each PLS-DA plot is the corresponding validation plot.

Week-by-week analysis of male axenic IL-10 KO mice vs. male conventional IL-10 KO mice reveals that there is complete separation of the axenic cluster from the conventional cluster at each time-point, and none of the weeks show any overlap of the two clusters. This helps to explain the one axenic point that was found in the conventional cluster on

the PCA plot that contained all the points by showing it is not actually overlapping with any points similar to it. Once again the IL-10 KO mice do not cluster as tightly as their wild-type counterparts; the points in the IL-10 KO clusters are a greater distance from each other than the wild-type mice points. Although the clusters are not as tightly packed together as the wild-type, they are still tight enough that the two groups are separate from each other and do not overlap. The only week where the clusters are close to overlapping is week 4. However, although the clusters in these weeks are close to each other, they do not overlap.

plot	R2Y	Q2
All weeks	0.972	0.952
week 4	0.895	0.826
week 6	0.993	0.975
week 8	0.989	0.966
week 12	0.994	0.955
week 16	0.992	0.978
week 20	0.987	0.955

Table 6.2.1.1 - R2Y and Q2 values for the PLS-DA plots constructed for the axenic IL-10 KO males vs. the conventional IL-10 KO males over all weeks.

6.2.2 Female – comparison of urine metabolomics over time

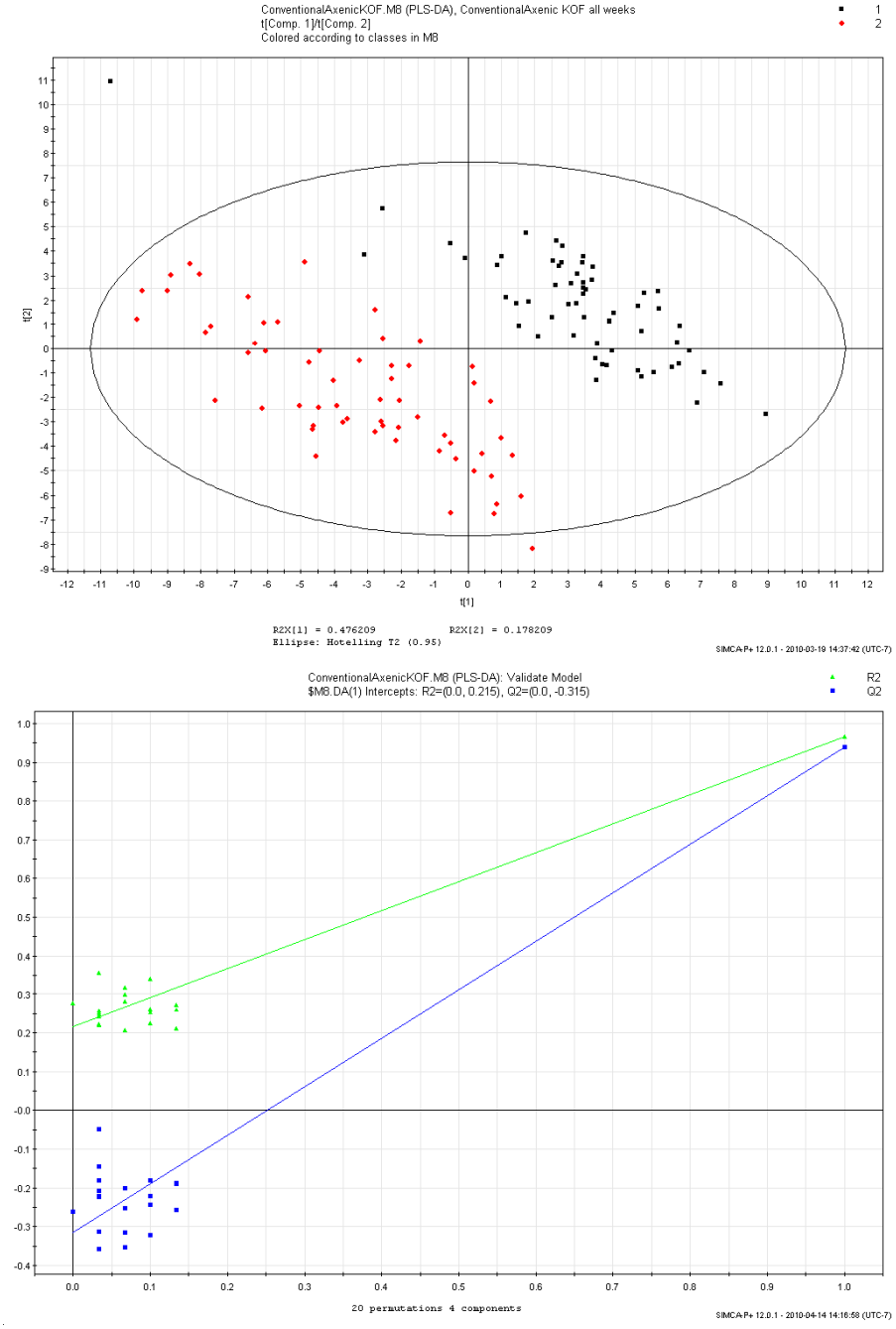

Figure 6.2.2.1 – PLS-DA plot of axenic IL-10 KO females over all time-points vs. conventional IL-10 KO females at all time-points; axenic mice are displayed in black and conventional mice are displayed in red. Urine was collected at weeks 4, 6, 8, 12, 16, and

20 either from the germ free bubble or the conventional environment. 10 samples were collected at each time-point. Below the PLS-DA plot is the validation plot.

Figure 6.2.2.1 is a PLS-DA plot comparing female axenic IL-10 KO mice vs. female conventional IL-10 KO mice. In line with what was observed with the wild-type mice and the male IL-10 KO mice, the plot shows two clusters, one cluster composed of the axenic mice and the other cluster composed of the conventional mice. As with the IL-10 KO males, there is no overlap between the axenic cluster and the conventional cluster. The clustering of the mice is also interesting, as, unlike the male clusters which were about the same shape and size, the axenic female cluster is tighter than the conventional mice one. There is also one outlier present in the axenic group and one outlier present in the conventional group, both of which can be attributed to a low volume of urine collected.

Week 4

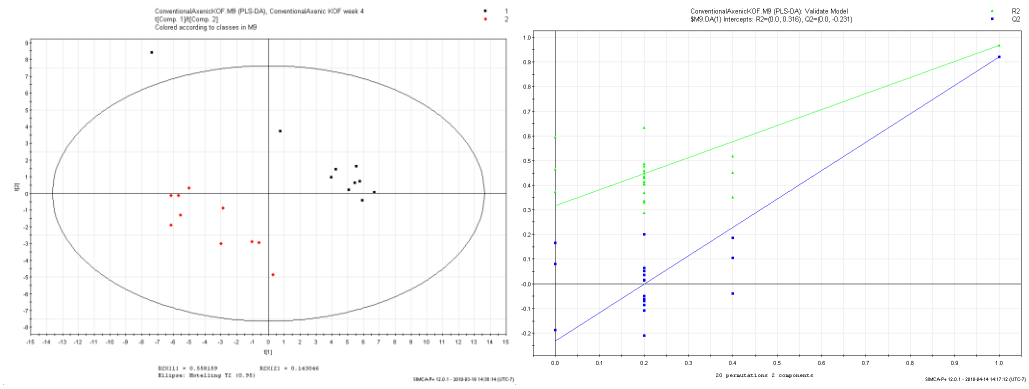

Week 6

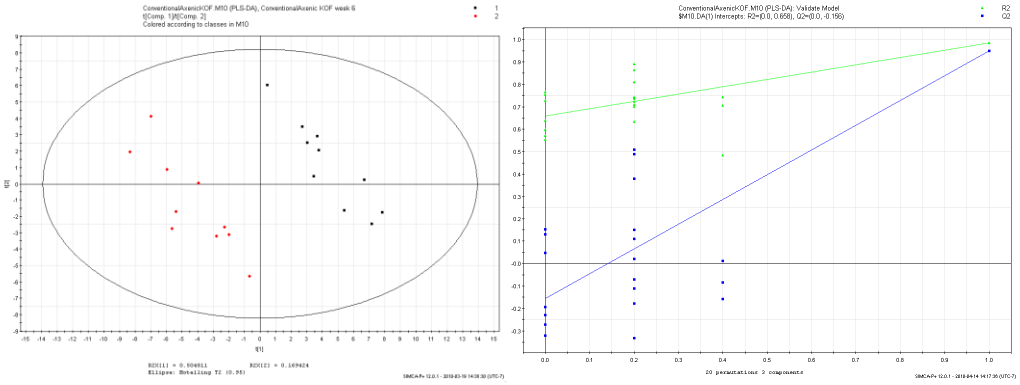

Week 8

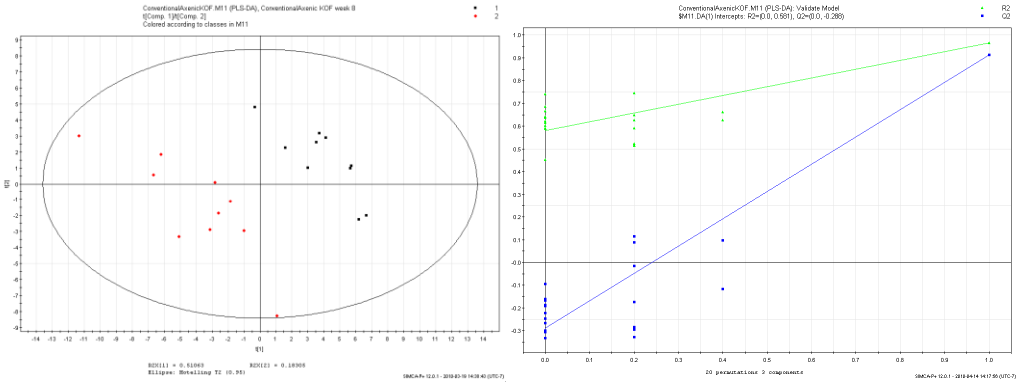

Week 12

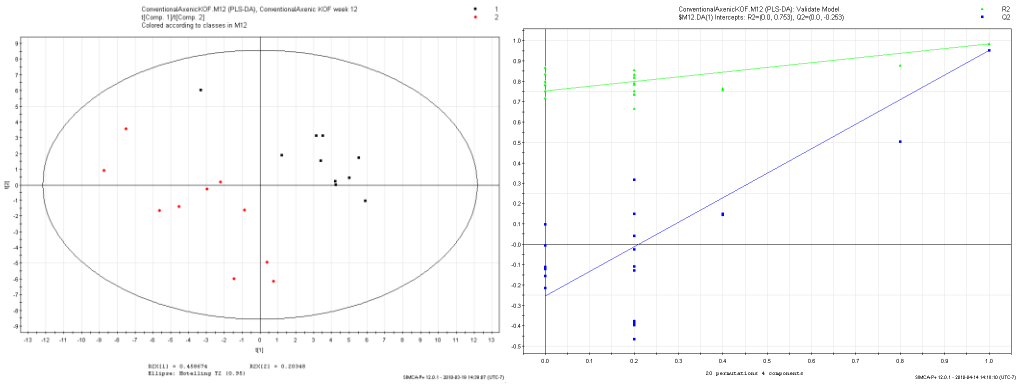

Week 16

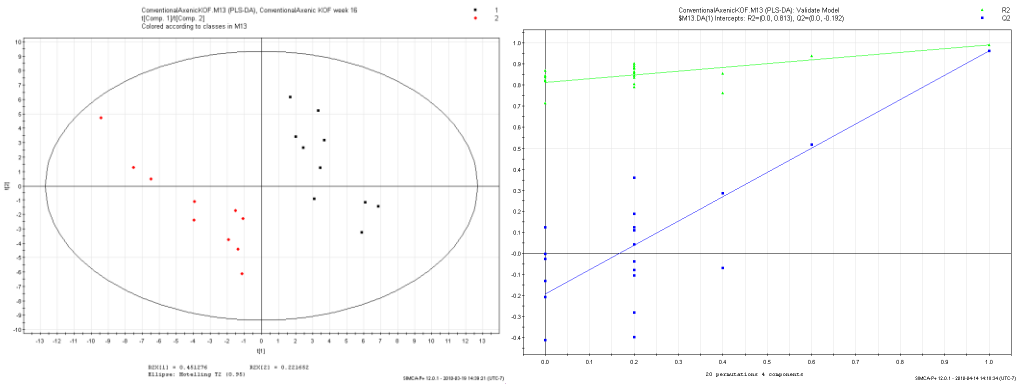

Week 20

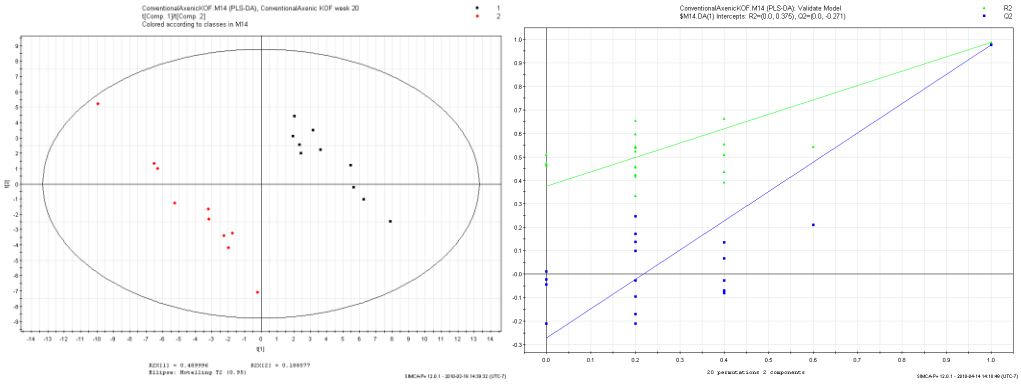

Figure 6.2.2.2 – PLS-DA plots of the urine metabolomic profiles of the axenic female IL-10 KO and conventional female IL-10 KO mice broken up by week of urine collection; conventional are displayed in red and axenic are displayed in black. Each week comprises 10 axenic mice and 10 conventional mice. Beside each PLS-DA plot is the corresponding validation plot.

Week-by-week comparison of these groups reveals results similar to the ones observed in the PLS-DA for all time-points. At each time-point here, there is complete separation between the conventional group and the axenic group. The clusterings of the axenic groups appear to be fairly tight throughout all the weeks, while the clusterings of the conventional groups

at all the other weeks also appear to be grouped tightly, with the exception of the clustering of the week 12 conventional mice. When compared to the other clusters, the cluster at week 12 is spread out over a larger area of the plot.

plot	R2Y	Q2
All weeks	0.965	0.94
week 4	0.966	0.919
week 6	0.986	0.949
week 8	0.967	0.912
week 12	0.985	0.953
week 16	0.922	0.962
week 20	0.986	0.976

Table 6.2.2.1 - R2Y and Q2 values for the PLS-DA plots constructed for the axenic IL-10 KO females vs. the conventional IL-10 KO females over all weeks.

Chapter 7 - Discussion

7.1 Axenic mice

7.1.1 Metabolites that differentiate males from females

In order to further analyze the data, we created metabolite importance charts. During each PLS-DA analysis, each metabolite used in the analysis (in our case 56) is assigned a score. This score is based on how much of an impact the particular metabolite has in shaping the particular plot; these charts allow for the identification of metabolites that significantly contribute to the separation we identified through our PLS-DA plots. Any metabolite with a score of 1 or greater on the PLS-DA chart was deemed to be an important metabolite. It is also important to note that, although the contribution of stress on the metabolic fingerprint is uniform across all groups, the stress the mice feel while being in the metabolic cages would also have an impact on their metabolic fingerprints. The stress of a new environment would be most evident in weeks 4 and 6, when the mice are still unfamiliar and uncomfortable with being in the metabolic cages.

For the male vs. female plots, a total of 17 metabolites were identified as important for the wild-type mice and IL-10 KO mice (Table 7.1.1.1). Comparison of the metabolite importance charts reveals that there are many similarities between the axenic wild-type and IL-10 KO mice when it

comes to separating them via sex. Many of the metabolites that were used to differentiate the male from the female for the axenic wild-type mice are also used to differentiate the male from the female in the IL-10 KO group. A comparison of the two charts shows that there are 8 shared metabolites (2-Aminobutyrate, Adipate, Carnitine, Isoleucine, Methylamine, N-Isovaleroylglycine, Trimethylamine, Valine) useful for differentiation of the males of wild-type and IL-10 KO mice and 6 shared metabolites (1-Methylnicotinamide, 2-Oxoisocaporate, 3-Methyl-2-oxovalerate, Glutarate, Lactate, Pyruvate) useful for differentiation of the females of wild-type and IL-10 KO mice (table 7.1.1.1) for a total of 14 metabolites used to separate males from females.

Metabolites important for male/female differentiation in Wild-type mice	Metabolites important for male/female differentiation IL-10 KO mice	Common in WT and IL-10 KO males	Common in WT and IL-10 KO females
1-Methylnicotinamide	1-Methylnicotinamide	2-Aminobutyrate	1-Methylnicotinamide
2-Aminobutyrate	2-Aminobutyrate	Adipate	2-Oxoisocaporate
2-Oxoisocaproate	2-Oxoisocaproate	Carnitine	3-Methyl-2-oxovalerate
3-Methyl-2-oxovalerate	3-Methyl-2-oxovalerate	Isoleucine	Glutarate
Adipate	Adipate	Methylamine	Lactate
Butyrate	Carnitine	N-Isovaleroylglycine	Pyruvate
Carnitine	Glutarate	Trimethylamine	
Glutarate	Isoleucine	Valine	
Guanidoacetate	Lactate		
Isoleucine	Methylamine		

Lactate	N-Isovaleroylglycine		
Methylamine	Pyruvate		
N-Carbamoyl-β-alanine	Taurine		
N-Isovaleroylglycine	Trigonelline		
Pyruvate	Trimethylamine		
Trimethylamine	Valine		
Valine	Cis-Aconitate		

Table 7.1.1.1 – List of important metabolites used to differentiate males from females in axenic wild-type and IL-10 KO mice. Columns 1 and 2 are the complete lists of important metabolites; columns 3 and 4 are the common metabolites shared between the wild-type and IL-10 KO mice

7.1.2 Metabolites that differentiate wild-type from IL-10 KO

We also see that wild-type mice and IL-10 KO mice share some common metabolites. For the male mice, a total of 15 metabolites were identified as important, and for the females a total of 20. Analysis of the important metabolites charts for this comparison shows that acetate was an important metabolite differentiating the IL-10 KO mice and 7 metabolites (1-Methylnicotinamide, Butyrate, Creatine, Glycerate, Glycolate, N-Isovalerogyglycine, Taurine) were important metabolites for differentiation of the wild-type mice (Table 7.1.2.1). We also discovered that 2-Oxoisocaporate was important to the separation of the IL-10 KO mice in the male group, but it was also important in creating to the separation of the wild-type mice in the female group.

Metabolites leading to the WT/IL-10 KO differentiation in male mice	Metabolites leading to the WT/IL-10 KO differentiation in female mice	Common in male and female wild-type mice	Common in male and female IL-10 KO mice
2-Oxoglutarate	1-Methylnicotinamide	1-Methylnicotinamide	Acetate
2-Oxoisocaproate	2-Hydroxyisobutyrate	Butyrate	
Acetate	2-Oxoisocaproate	Creatine	
Butyrate	3-Methyl-2-oxovalerate	Glycerate	
Creatine	Acetate	Glycolate	
Formate	Alanine	N-Isovaleroylglycine	
Glycerate	Allantoin	Taurine	
Glycolate	Butyrate		
Hippurate	Carnitine		
N-Isovaleroylglycine	Creatine		
Phenylacetylglycine	Creatinine		
Taurine	Glycerate		
Trimethylamine	Glycolate		
Valine	Guanidoacetate		
	Isoleucine		
	Methanol		
	N-Isovaleroylglycine		
	Taurine		
	Uracil		
	Cis-Aconitate		

Table 7.1.2.1 – List of important metabolites used to differentiate wild-type from IL-10 KO in the axenic male and female. Columns 1 and 2 are the complete lists of important metabolites; columns 3 and 4 are the common metabolites shared between the male and female mice

7.1.3 Metabolites that differentiate for the age of male mice

The comparison of growth over time between the wild-type and the IL-10 KO males does not yield as many similar metabolites as the two previous comparisons. Comparing the axenic wild-type to the axenic IL-10 KO mice, we see that there are 4 metabolites (2-Oxoisocaporate, 3-Methyl-2-oxovalerate, Isoleucine, Taurine) that were important in differentiating the older mice from the younger mice and 3 metabolites (Citrate, Uracil, Trans-Aconitate) important for the differentiation of the younger mice from the older mice. Formate was observed to identify the separation of the older mice in the wild-type group, but it was also found to be important for identifying the separation of the younger mice in the IL-10 KO group. A total of 21 metabolites was found to be important in shaping the PLS-DA plot for the growth of the axenic wild-type males, while a total of 18 metabolites was found for the axenic IL-10 KO males (Table 7.1.3.1). These metabolites had the greatest impact on creating the different clusters (each week) observed on the PLS-DA plots.

Wild-type males over time	IL-10 KO males over time	Common metabolites for younger mice	Common metabolites for older mice
2-Hydroxybutyrate	1-Methylnicotinamide	Citrate	2-Oxoisocaporate
2-Oxoisocaporate	2-Oxoisocaporate	Uracil	3-Methyl-2-oxovalerate
3-Methyl-2-oxovalerate	3-Methyl-2-oxovalerate	Trans-Aconitate	Isoleucine
Carnitine	Allantoin		Taurine
Citrate	Butyrate		

Formate	Citrate		
Glycine	Dimethylamine		
Glycolate	Formate		
Isoleucine	Fucose		
Lactate	Fumarate		
Mannose	Glutatate		
Methanol	Glycolate		
Pyruvate	Guanidoacetate		
Taurine	Isoleucine		
Trigonelline	N-Carbamoyl-β-alanine		
Trimethylamine	Taurine		
Trimethylamine N-oxide	Uracil		
Uracil	Trans-Aconitate		
Valine			
Cis-Aconitate			
Trans-Aconitate			

Table 7.1.3.1 – List of important metabolites used to differentiate younger males from older males for axenic wild-type and IL-10 KO mice. Columns 1 and 2 are the complete lists of important metabolites; columns 3 and 4 are the common metabolites shared between the younger and older mice

7.1.4 Metabolites that differentiate for the age of female mice

Comparing the important metabolite charts for the growth of the axenic wild-type females and axenic IL-10 KO females yields results similar to their equivalent male comparisons. A total of 16 metabolites was identified for the wild-type group and 14 for the IL-10 KO group. Between these groups, 4 metabolites (2-Oxoglutarate, 2-Oxoisocaporate, Phenylacetylglycine, Trimethylamine) led to the identification of the older mice and 4 metabolites (Acetate, Fucose, Trimethylamine N-oxide, Uracil) led to the differentiation of the younger mice (Table 7.1.4.1).

Wild-type females over time	IL-10 KO females over time	Common metabolites for younger mice	Common metabolites for older mice
2-Aminobutyrate	2-Oxoglutarate	Acetate	2-Oxoglutarate
2-Oxoglutarate	2-Oxoisocaporate	Fucose	2-Oxoisocaporate
2-Oxoisocaporate	3-Methyl-2-oxovalerate	Trimethylam-ine N-oxide	Phenylacetyl glycine
Acetate	Acetate	Uracil	Trimethylamine
Formate	Butyrate		
Fucose	Fucose		
Glycine	Glutartate		
Hippurate	Guanidoacetate		
Isoleucine	N-Isovaleroylglycine		
Lactate	Phenylacetylglycine		
Methanol	Taurine		
Phenylacetylglycine	Trimethylamine		
Trimethylamine	Trimethylamine N-oxide		
Trimethylamine N-oxide	Uracil		
Tyrosine			
Uracil			

Table 7.1.4.1 – List of important metabolites used to differentiate younger females from older females in axenic wild-type and IL-10 KO mice. Columns 1 and 2 are the complete lists of important metabolites; columns 3 and 4 are the common metabolites shared between the younger and older mice.

7.1.5 Summary

Our analysis of the important metabolites yielded several important findings. Firstly, the metabolites that can be used to separate male mice from female mice were very similar between the wild-type and the IL-10 KO mice. We also found that the metabolites that differentiate wild-type from IL-10 KO were very similar between the male and female mice. In the axenic mice, the greatest differences in the metabolite importance charts was found in relation to the growth and aging of the mice, since those comparisons yielded the lowest numbers of common metabolites between comparison groups.

Even though the results of this section do seem to follow logical conclusions, there are a few limitations to this part of the study. Reference to the PLS-DA plots in the results sections reveals that the data does not cluster together as tightly as does that observed in the conventional groups. This is most likely due to the fact that the urine collection was done by another source, and the quality of the collection and other factors such as storage and sample handling could not be guaranteed. Lack of consistency in the manner the samples were all collected, handled, and stored could possibly have compromised sample quality, leading to some degradation of the sample and the results obtained. Although these factors would not render the data invalid, it is possible they might have slightly altered the concentrations of some of the metabolites leading to

the slightly bigger clusters observed for the axenic mice than for the conventional mice.

7.2 Conventional mice

7.2.1 Metabolites that differentiate males from females

Similar to the observations for the axenic mice, there are many common metabolites found in the comparison of male vs. female in the conventional mice. In the wild-type mice, a total of 21 metabolites differentiated between male and female. In the IL-10 KO mice, a total of 19 metabolites were found. 10 metabolites (1-Methylnicotinamide, Formate, Trimethylamine N-oxide, 3-Methyl-2-oxovalerate, N-Carbamoyl-β-alanine, Pyruvate, Lactate, Cis-Aconitate, Glutarate, Fucose) were identified to be driving the differentiation of the female mice, and 6 metabolites (Valine, Taurine, N-Isovaleroyglycine, Methylamine, Trimethylamine, Succinate) were leading to the differentiation observed in the IL-10 KO mice (table 7.2.1.1).

Metabolites important for male/female differentiation in Wild-type mice	Metabolites important for male/female differentiation in IL-10 KO mice	Common in WT and IL-10 KO males	Common in WT and IL-10 KO females
Guanidoacetate	1-Methylnicotinamide	1-Methylnicotinamide	Valine
1-Methylnicotinamide	Lactate	Formate	Taurine
Formate	Glutarate	Trimethylamine N-oxide	N-Isovaleryglycin

			e
Trimethylamine N-oxide	Trimethylamine N-oxide	3-Methyl-2-oxovalerate	Methylamine
3-methyl-2-oxovalerate	Pyruvate	N-Carbamoyl-β-alanine	Trimethylamine
N-Carbamoyl-β-alanine	Cis-Aconitate	Pyruvate	Succinate
2-Oxoisocaporate	N-Carbamoyl-β-alanine	Lactate	
Pyruvate	3-methyl-2-oxovalerate	Cis-Aconitate	
Mannose	Fucose	Glutarate	
Lactate	3-Indoxylsulfate	Fucose	
Cis-Aconitate	Formate		
Glutarate	Trigonelline		
Fucose	Taurine		
Valine	N-Isovaleroylglycine		
Butyrate	Creatine		
Taurine	Valine		
Adipate	Methylamine		
N-Isovaleroylglycine	Trimethylamine		
Methylamine	Succinate		
Trimethylamine			
Succinate			

Table 7.2.1.1 – List of important metabolites used to differentiate males from females in conventional wild-type and IL-10 KO mice. Columns 1 and 2 are the complete lists of important metabolites; columns 3 and 4 are the common metabolites shared between the wild-type and IL-10 KO mice

7.2.2 Metabolites that differentiate wild-type from IL-10 KO

Similar to the axenic mice results, the comparison of conventional wild-type vs. IL-10 KO mice yields common metabolites that can be used to

separate the wild-type from the IL-10 KO mice. In the male mice, a total of 16 metabolites were used, and in the female mice a total of 13 metabolites were used. Of these metabolites, 4 (Hippurate, Isoleucine, Fucose, Dimethylamine) led to the differentiation of the IL-10 KO mice, and 2 (Citrate, Glutarate) led to the differentiation for the wild-type mice (table 7.2.2.1).

Metabolites important to WT/IL-10 KO differentiation in male mice	Metabolites important to WT/IL-10 KO differentiation in female mice	Common in male and female wild-type mice	Common in male and female IL-10 KO mice
Hippurate	Hippurate	Citrate	Hippurate
Isoleucine	Fucose	Glutarate	Isoleucine
Fucose	Isoleucine		Fucose
Tyrosine	Dimethylamine		Dimethylamine
Dimethylamine	Trigonelline		
Betaine	Trans-Aconitate		
Trimethylamine N-oxide	Citrate		
Glycolate	Guanidoacetate		
Trimethylamine	Methylamine		
2-Oxoglutarate	Mannose		
Succinate	N-Isovaleroylglycine		
Citrate	Glycine		
1-Methylnicotinamide	Glutarate		
Glutarate			
Fumarate			
Acetate			

Table 7.2.2.1 – List of important metabolites used to differentiate wild-type from IL-10 KO in conventional male and female mice. Columns 1 and 2 are the complete lists of

important metabolites; columns 3 and 4 are the common metabolites shared between the wild-type and IL-10 KO mice

7.2.3 Metabolites that differentiate for the age of male mice

Comparing the metabolites important for growth in the conventional males yields results similar to those seen for the axenic males. For the wild-type males there are a total of 22 metabolites used to differentiate between the younger and the older mice. For the IL-10 KO males, there are only 16 metabolites used to differentiate the young from the old mice. Of these metabolites, a total of 8 metabolites were found to be common, 4 metabolites (Trimethylamine N-oxide, Uracil, N-Carbamoyl-β-alanine, Citrate) led to differentiation of the younger mice in both groups, and 4 metabolites (3-Methyl-2-oxovalerate, Butyrate, N-Isovaleroylglycine, 2-Oxoisocaporate) led to the identification of the older mice in both groups. There was also one metabolite that was leading to the differentiation of the younger mice for the wild-type males but was actually leading to the differentiation for the older mice for the IL-10 KO group; this metabolite was fucose.

Wild-type males over time	IL-10 KO males over time	Common metabolites for younger mice	Common metabolites for older mice
Trimethylamine N-oxide	Uracil	Trimethylamine -N-oxide	3-Methyl-2-oxovalerate
Uracil	N-Carbamoyl-β-alanine	Uracil	Butyrate
Fucose	Glutarate	N-Carbamoyl-	N-Isovaleroyl glycine

		β-alanine	
N-Carbamoyl-β-alanine	Trimethylamine N-oxide	Citrate	2-Oxoisocaporate
Allantoin	Citrate		
Formate	Lactate		
Trigonelline	Tyrosine		
1-Methylnicotinamide	Succinate		
Citrate	2-oxoglutarate		
Acetate	N-Isovaleroylglycine		
Hippurate	Fucose		
2-hydroxyisobutyrate	Butyrate		
Glycolate	3-methyl-2-oxovalerate		
Creatinine	2-Oxoisocaporate		
3-methyl-2-oxovalerate	Trimethylamine		
Butyrate			
Taurine			
Carnitine			
N-Isovaleroylglycine			
Betaine			
2-Oxoisocaporate			
Valine			

Table 7.2.3.1 – List of important metabolites used to differentiate younger males from older males in conventional wild-type and IL-10 KO mice. Columns 1 and 2 are the complete lists of important metabolites; columns 3 and 4 are the common metabolites shared between the younger and older mice

7.2.4 Metabolites that differentiate between the ages of female mice

A comparison of female mice over time produces only a few metabolites that are common between the wild-type and the IL-10 KO groups. A total of 19 metabolites were used to separate the younger mice from the older mice in both the wild-type and IL-10 KO groups. Of those 19 metabolites, a total of 3 metabolites (Uracil, Trigonelline, Creatine) were found to lead towards the identification of the younger mice in both groups, 2 metabolites (Tyrosine, Butyrate) were found to lead towards the identification of the older mice, and 1 metabolite (Hippurate) was found to lead to identification of the younger wild-type mice but also to the differentiation of the older IL-10 KO mice. Finally, 1 metabolite (Lactate) was found to lead the identification of the older wild-type mice but also the younger IL-10 KO mice.

Wild-type females over time	IL-10 KO females over time	Common metabolites for younger mice	Common metabolites for older mice
Uracil	Taurine	Tyrosine	Uracil
N-Carbamoyl-β-alanine	Uracil	Butyrate	Trigonelline
Citrate	Guanidoacetate		Creatine
Formate	Creatine		
Trigonelline	Mannose		
Hippurate	Citrate		
Creatine	Lactate		
Tyrosine	Trigonelline		
Glutarate	Isoleucine		
Fumarate	Trans-Aconiate		
Butyrate	Trimethylamine		
2-Oxoglutarate	Fucose		

Glycolate	2-Hydroxyisobutyrate		
Lactate	Urea		
Creatinine	Tyrosine		
2-Aminobutyrate	Hippurate		
Betaine	Butyrate		
3-methyl-2-oxovalerate	Succinate		
2-Oxoisocaporate	3-Indoxylsulfate		

Table 7.2.4.1 – List of important metabolites used to differentiate younger females from older females in conventional wild-type and IL-10 KO mice. Columns 1 and 2 are the complete lists of important metabolites; columns 3 and 4 are the common metabolites shared between the younger and older mice

7.2.5 Summary

Analysis of the metabolites for the conventional mice yields similar results to those observed for the axenic mice. Many of the metabolites used to differentiate the males from the females in the wild-type group were also identified for the separation of the males and females in the IL-10 KO mice. We also see that many of the metabolites that differentiated the wild-type males from the IL-10 KO males were shared between the male and female mice. This shows us once again that using metabolomics to separate wild-type from IL-10 KO and also male from female is effective, and that the metabolites that are related to the separation are consistent, meaning that the main factors used to separate genetic strain differences or sex are the ones that are being utilized to separate the groups. Where

our conventional groups seemed to have the most variation was for the comparisons made due to aging. As with the axenic mice, we see that the fewest number of common metabolites is found when comparing the growth and aging of the wild-type vs. the IL-10 KO in both the males and the females.

7.3 Colonized mice

7.3.1 Day 0

Analysis of the important metabolite charts at day 0 prior to fecal colonization for both the male and female mice reveals a host of metabolites that differentiate between the wild-type and IL-10 KO mice. In the males, a total of 19 metabolites were used; 12 were found for discrimination of the IL-10 KO mice, and 7 were found for the discrimination of the wild-type mice. In the females, a total of 17 metabolites were used; 10 led to the identification of the IL-10 KO mice and 7 led to the differentiation of the wild-type mice. Within the lists of metabolites used to discriminate wild-type from IL-10 KO in each sex, there is a group of metabolites that are found to be common for both sexes (Table 7.3.1.1).

IL-10 KO	Wild-type
Formate	Trimethylamine
Tyrosine	Butyrate

Acetate	Trimethylamine N-oxide
Valine	N-Isovaleroylglycine
Mannose	

Table 7.3.1.1 – Common metabolites found to discriminate wild-type from IL-10 KO in both sexes at day 0.

7.3.2 Day 1

At day 1 post-fecal-colonization, we continue to see different metabolites which lead to the identification and separation of the two groups. For the males, a total of 19 metabolites were used to discriminate between wild-type and IL-10 KO mice; 10 led to the differentiation of the IL-10 KO and 9 led to the differentiation of the wild-type mice. For the females, 18 metabolites were used to discriminate between the wild-type and the IL-10 KO mice; 11 led to the differentiation of the IL-10 KO mice, and 7 led to the differentiation of the wild-type mice. Within the lists of metabolites used to discriminate between wild-type and IL-10 KO in each sex, once again there is a group of metabolites that are found to be common to both genders. However, when compared to the metabolites at day 0, the common metabolites at day 1 (Table 7.3.2.1) are a completely different group.

IL-10 KO	Wild-type
Carnitine	Glycine
Tyrosine	Acetate

Trigonelline	Butyrate
3-Methyl-2-oxovalerate	

Table 7.3.2.1 – Common metabolites found to discriminate between wild-type and IL-10 KO for both sexes at day 1

7.3.3 Day 2

At day 2 post-fecal-colonization, we continue to see that different metabolites separate the two groups. For the males, a total of 13 metabolites were used; 8 led to the identification of the IL-10 KO and 5 led to the identification of the wild-type mice. For the females 19 metabolites were used; 12 led to the identification of the IL-10 KO and 7 led to the identification of the wild-type mice. When compared to the common metabolites found for the sexes at day 1, the common metabolites at day 2 (Table 7.3.3.1) are once again a completely different group of shared metabolites.

IL-10 KO	Wild-type
Trimethylamine	Taurine
Trimethylamine N-oxide	Methylamine
Cis-Aconitate	Creatine
Trans-Aconitate	
2-Oxoglutarate	
Citrate	
Succinate	

Table 7.3.3.1 – Common metabolites found to discriminate between wild-type and IL-10 KO in both sexes at day 2

7.3.4 Day 3

At day 3 post-fecal-colonization we begin to see that some of the metabolites found in the previous days again indicate the separation between the two groups. For the males, a total of 23 metabolites helped to differentiate wild-type from IL-10 KO; 15 were leading to the identification of the IL-10 KO and 8 were leading to the identification of the wild-type mice. For the females, 22 metabolites were used in the same discrimination process, 12 were leading to the identification of the IL-10 KO, and 10 were leading to the identification of the wild-type mice. Some of the metabolites at day 3 (Table 7.3.4.1) were also present at day 2 (trimethylamine, trimethylamine N-oxide, succinate).

IL-10 KO	Wild-type
Fucose	Creatinine
Phenylacetylglycine	Adipate
Trimethylamine	Glycine
Pyruvate	Glycolate
Tyrosine	
Trimethylamine N-Oxide	
Betaine	
Succinate	

Table 7.3.4.1 – Common metabolites found to discriminate between wild-type and IL-10 KO in both sexes at day 3.

7.3.5 Day 4

At day 4 post-fecal-colonization, we begin to see that there are fewer metabolites shared between the males and females. For the males, a total of 24 metabolites differentiated wild-type from IL-10 KO; 13 led to the identification of the IL-10 KO and 11 led to the identification of the wild-type mice. For the females, 15 metabolites were used in the same discrimination process; 11 lead to the differentiation of the IL-10 KO and 4 led to the differentiation of the wild-type mice. Of the metabolites used at day 4 (Table 7.3.5.1), only a few (trimethylamine and glycine) were present at day 3.

IL-10 KO	Wild-type
Trigonelline	Glycine
Trimethylamine	Methylamine
Trans-Aconitate	Glutarate
Lactate	

Table 7.3.5.1 – Common metabolites found to discriminate between wild-type and IL-10 KO in both sexes at day 4

7.3.6 Day 7

At day 7 post-fecal–colonization, even fewer shared metabolites are found for males and females. For the males, a total of 16 metabolites differentiate wild-type from IL-10 KO; 8 lead to the identification of the IL-10 KO, and 8 lead to the identification of the wild-type mice. For the females, 17 metabolites were used for the same discrimination process; 10 led to the defferentiation of the IL-10 KO and 7 led to the differentiation of the wild-type mice. Once again, when compared to the metabolites used at day 4, only two day 7metabolites (trimethylamine, glutarate) are the same (Table 7.3.6.1).

IL-10 KO	Wild-type
Trimethylamine	Glutarate
N-Carbamoyl-β-alanine	Phenylacetylglycine
Alanine	

Table 7.3.6.1 – Common metabolites found to discriminate between wild-type and IL-10 KO in both sexes at day 7

Comparing the metabolites shared between the males and females allows us to determine which metabolites are most likely to be associated with the disease and helps to eliminate the possibility that the metabolites may also be sex-specific; this is not to say that other metabolites are not important to the disease.

Along with the shared metabolites found for the males and females in the wild-type vs. IL-10 KO comparison, we also saw that several of the metabolites that led to the identification of the wild-type mice while in the axenic environment are now leading to the identification of the IL-10 KO mice after bacterial colonization. In the males, some these changes were observed right from day 1, while others were not seen until later days. Similar observations were made for the females with the exception that changes were not observed until day 2 (Table 7.3.6.2). The shifting of these metabolites may also provide clues about the gut's interactions with the colonizing bacteria.

Male	Female
Trimethylamine	Trimethylamine
Glycine	Trimethylamine N-oxide
Acetate	Butyrate
Trimethylamine N-oxide	Mannose
Phenylacetylglycine	Guanidoacetate
Fumarate	Formate
Hippurate	Valine
	Creatine
	Tyrosine

Table 7.3.6.2 – Metabolites that were originally up-regulated in the axenic mice at day 0, and later found to be up-regulated in the colonized mice after bacterial colonization

To confirm the disease state in both the wild-type and IL-10 KO mice, histological sections were also taken at day 7 (post-sacrifice). Data for both IL-10 KO groups reached statistical significance when compared to their wild-type counterparts, confirming that disease was present in the IL-10 KO mice and not in the wild-type mice (Figure 7.3.6.1)

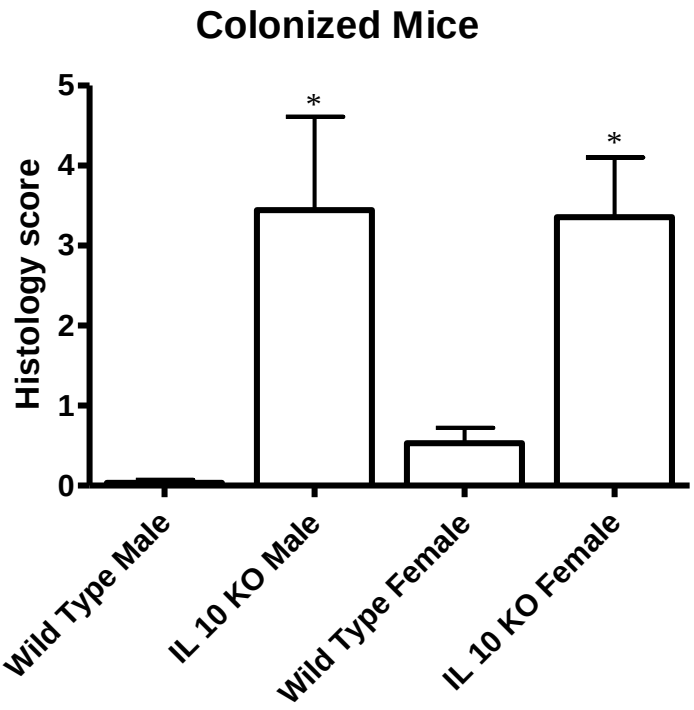

Figure 7.3.6.1 – Histology scores for all mice that were colonized with fecal bacteria

*p <0.05

7.4 Axenic vs. Conventional

7.4.1 Axenic wild-type males vs. conventional wild-type males

Comparison of the important metabolite charts for axenic vs. conventional mice at each time-point shows a recurring group of metabolites that are common to the axenic animals and a different set of metabolites common to the conventional animals. For this dataset, 4 comparisons were made. Axenic wild-type males were compared to conventional wild-type males; and the females were also compared. Axenic IL-10 KO males were compared to the conventional IL-10 KO males, and this comparison was also done for the females. For the wild-type males, a total of 17 metabolites separated the axenic mice from the conventional mice. Of those 17, 7 led to the identification of the axenic mice, and 10 were led to the identification of the conventional mice (Table 7.4.1.1)

Axenic	Conventional
Glycolate	Cis-Aconitate
Creatinine	Isoleucine
Formate	2-Oxoglutarate
Carnitine	Citrate
Lactate	Trans-Aconitate
Acetate	Succinate
Glutarate	Phenylacetylglycine

	Trimethylamine
	Trimethylamine N-oxide
	Methylamine

Table 7.4.1.1 – Important metabolites used to separate axenic wild-type males from conventional wild-type males

7.4.2 Axenic wild-type females vs. conventional wild-type females

For the wild-type females, a total of 15 metabolites were used to separate the axenic mice from the conventional mice. Of those 15 metabolites, 4 led to the identification of the axenic animals, and 11 led to the identification of the conventional animals (Table 7.4.2.1).

Axenic	Conventional
Glycolate	Fucose
Taurine	Phenylacetylglycine
Creatinine	N-Carbamoyl-β-alanine
Carnitine	Trans-Aconitate
	Cis-Aconitate
	2-Oxoglutarate
	Trimethylamine
	Glutarate

	Trimethylamine N-oxide
	Methylamine
	Citrate

Table 7.4.2.1 – Important metabolites used to separate axenic wild-type females from conventional wild-type females

7.4.3 Axenic IL-10 KO males vs. conventional IL-10 KO males

For the IL-10 KO males, a total of 20 metabolites were used to separate the axenic animals from the conventional animals. These metabolites separated into 10 metabolites leading to the identification of the axenic animals and 10 metabolites leading to the identification of the conventional animals (Table 7.4.3.1).

Axenic	Conventional
Acetate	Xylose
Formate	Alanine
Glycolate	Trimethylamine
Lactate	Trans-Aconitate
Carnitine	Citrate
Creatinine	Fucose
Adipate	Trimethylamine N-oxide
Glucose	Taurine

Glycerate	Methylamine
Glycine	Hippurate

Table 7.4.3.1 – Important metabolites used to separate axenic IL-10 KO males from conventional IL-10 KO males

7.4.4 Axenic IL-10 KO females vs. conventional IL-10 KO females

For the female IL-10 KO mice, a total of 15 metabolites separated the axenic animals from the conventional animals; 7 metabolites led to the identification of the axenic animals while the remaining 8 led to the identification of the conventional animals (Table 7.4.4.1).

Axenic	Conventional
Acetate	Trans-Aconitate
Formate	Trimethylamine
Glucose	Trimethylamine N-oxide
Lactate	Fucose
Creatinine	Citrate
Adipate	Methylamine
Trigonelline	Hippurate
	Isoleucine

Table 7.4.4.1 – Important metabolites used to separate axenic IL-10 KO females from conventional IL-10 KO females

Comparison of all the important metabolite lists reveals that, in the conventional group, a number of metabolites were consistently present. The presence of these metabolites on all our important metabolite lists indicates that they could play in integral roles in the interaction between the host and the gut microbes in conventional wild-type and IL-10 KO mice for both sexes. Whether these metabolites are the by-product of the gut microbes themselves, or a cellular by-product of the interaction of the cell and the gut microbes is unclear at this point. Metabolites in this group include trimethylamine, trimethylamine N-oxide, methylamine, and trans-aconitate.

In addition to these common metabolites, there are some metabolites that are specific to certain strains of mice. In the wild-type group, phenylacetylglycine, citrate, and 2-oxoglutarate are present in the important metabolite lists for both sexes, but these metabolites are not present in any of the important metabolite lists for the IL-10 KO mice. We also see that hippurate is present in both sexes for the IL-10 KO mice but not present for either sex for the wild-type mice.

In the axenic mice, some common metabolites are also present; creatinine appears for both sexes and strains of mouse, while glycolate only appears to be present in the male axenic mice and not the female axenic mice.

While a few metabolites are present in all the lists, others are specific to certain groups. For instance, creatinine was present throughout the axenic group. Within the axenic group, glycolate was only present in the males and not the females. Unfortunately, these were the only two metabolites that were found to be common in the axenic mice. One possible explanation for the lack of common metabolites in the axenic group could be that the mice are simply not that similar, but a more reasonable explanation once again refers to the problems identified with the sample collection and storage, which could have had an impact on the quality of the urine samples and the possible degradation of metabolites.

Histology samples were also taken from these mice at 20 weeks of age after the last urine collection. These were also used to confirm disease presence in the IL-10 KO mice and to show that no disease was present in the wild-type mice. Once again, the histology scores for both IL-10 KO groups reach significance when compared to those of their wild-type counterparts (Figure 7.4.4.1).

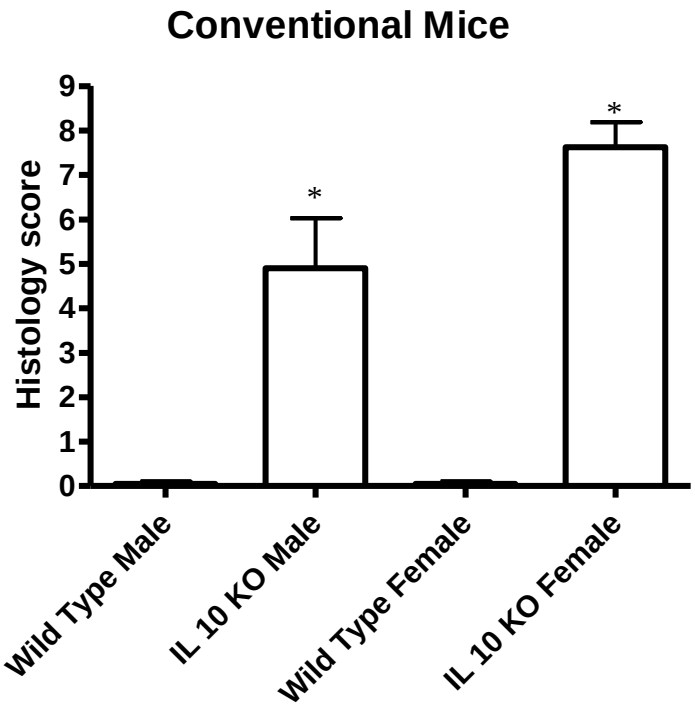

Figure 7.4.4.1 – Histology scores for all the conventional wild-type and IL-10 KO mice

*p<0.05

7.5 Important Metabolites

Throughout the analysis of the important metabolite lists, several important metabolites make frequent appearances. Some of these metabolites appear to be unique to small and specific groups, while others appear in larger and more general groups.

One of the more specific metabolites identified was acetate. Acetate was observed only in the axenic IL-10 KO mice. In the colon, large amounts of acetate are present (Cook and Sellin 1998). Acetate is a short chain-fatty acid (SCFA) and other SCFA's such as butyrate have been shown to have

anti-inflammatory properties and beneficial effects in IBD (Scheppach, Sommer et al. 1992). However, acetate does not share the beneficial effects of butyrate as a SCFA. Lewis et al. showed that, unlike butyrate, acetate was unable to prevent increased translocation across a treated monolayer and was unable to block NF-κB activation (Tedelind, Westberg et al. 2007; Lewis, Lutgendorff et al. 2009). Other groups have also shown that, when compared to SCFSs like butyrate and propionate, acetate is the least potent at inhibiting activation of the NF- κB pathway (Tedelind, Westberg et al. 2007). The increased presence of acetate in the axenic IL-10 KO animals could be a factor contributing towards disease.

Hippurate is another metabolite that was specific to a very small group. Hippurate was only found to be important in the conventional IL-10 KO groups. Hippurate excretion in urine is the result of the microbial metabolism of aromatic amine acids like tyrosine or other aromatic compounds such as purines (Williams, Cox et al. 2009). The gut microbial population has also been shown to have the ability to modulate the concentration of hippurate excreted in urine (Williams, Eyton-Jones et al. 2002; Nicholls, Mortishire-Smith et al. 2003). The presence of hippurate in our conventional IL-10 KO mice may provide a clue to the differences in the microbiota of the wild-type and the IL-10 KO mice.

Several metabolites were also identified as unique to the conventional wild-type mice. Phenylacetylglycine, citrate, and 2-oxoglutarate were observed in the wild-type lists of all the conventional mice but did not appear in the conventional IL-10 KO mice. In rodents, phenylacetylglycine is the end-product of phenylalanine metabolism and the precursors to phenylacetlyglycine are products of the gut microflora (James, Smith et al. 1972; Delaney, Neville et al. 2004). Intermediates from the Kreb's cycle, including citrate and 2-oxoglutarate, may also warrant further investigation (Wei, Liao et al. 2008).

While some metabolites were found in very specific groups, others were found to be present in very large and general groups. 4 metabolites were observed in all the conventional and colonized mouse groups. These metabolites are trimethylamine, trimethylamine N-oxide, methylamine, and trans-aconitate. Trimethylamine is usually present in urine, along with its metabolic-oxidation product trimethylamine N-oxide. Experiments have shown that the urine of conventional mice contains both trimethylamine and trimethylamine N-oxide, while in the case of germ-free animals, only very small amounts of these metabolites are found, thus indicating that intestinal microflora are essential for the excretion of these metabolites in urine (al-Waiz, Mikov et al. 1992). Along with trimethylamine and trimethylamine N-oxide, methylamine is another bacterial metabolite produced during the degradation of food products (Smith, Wishnok et al.

1994; Seibel and Walsh 2002). While these metabolites are all associated with microbes and microbial products, trans-aconitate has been linked to energy metabolism and the effects of stress-related differences in energy metabolism (Martin, Rezzi et al. 2009).

Chapter 8 - Summary & Future Directions

For axenic and conventional mice, we identified that metabolomics data could not only but used effectively for separating the wild-type mice from the IL-10 KO mice, but we were also able to use it to separate the male mice from the female mice. Along with differentiating wild-type mice from IL-10 KO mice and male from female, we were able to follow the mice as they aged and observe the changes in metabolic profiles over an established period of time.

We determined that there are many metabolites common to the males and females of each group that could be used to distinguish the wild-type mice from the IL-10 KO mice. This sex-related finding helped us to confirm that these shared metabolites were related to the differences between the genetic profiles of the wild-type mice and the IL-10 KO mice and not to simple male/female differences. In addition, we identified shared metabolites that differentiated between males and females for both the wild-type and IL-10 KO groups. These shared metabolites helped to confirm that the metabolites used to identify the separation were indeed sex-related and not due to the genetic differences of the wild-type and IL-10 KO mice.

These observations also held true when the same comparisons were made with conventional mice; this is important, because it shows that

even though gut microbes are present in the conventional group, they do not interfere with or inhibit the ability to discriminate between male and female or wild-type and IL-10 KO.

We were able to identify changes in the colonized mice's metabolic profiles during the colonization of these germ-free animals with fecal bacteria. Following the mice over days 1-4 and 7 allowed us to identify metabolites present during colonization with bacteria, as well as metabolites that may lead to information about how colonization may play a role in the development of inflammation in the IL-10 KO mice.

The comparison of the axenic mice to the conventional mice yielded metabolites similar to the ones identified in the colonization experiments. This similarity helped to reaffirm that the production of these metabolites is due either to the bacteria in the gut themselves or to the bacterial stimulation of the cells in the gut. Either way, the presence of these metabolites may play an important role in distinguishing possible biomarkers, pathways of interaction, or even bacteria that may be causing and perpetuating disease.

The comparison of IL-10 KO mice and wild-type mice in the axenic environment provided information on the differences in metabolism that occur when IL 10 is not present. The comparison of IL-10 KO mice and

wild-type mice in the conventional environment, conversely, provided information on the differences in metabolism that occur when IL 10 is not present but gut microbes are, with the eventual onset of disease in the IL-10 KO mice. The comparison of axenic to conventional mice in both the IL-10 KO and wild-type mice provided information on the differences in metabolism between a gut with and a gut without microbes. The comparison of groups that were colonized with fecal bacteria showed us how such colonization can alter the metabolism of both the IL-10 KO and the wild-type mice.

In conclusion, this study has shown that metabolomics can be used as an effective tool for monitoring metabolic changes associated with growth and aging as well as with the onset of disease. The targeted profiling methods used to identify specific metabolites and the multivariate statistical analysis identified several metabolites of interest. Many of these metabolites result from the interaction between the microbial population and the gut. Whether these metabolites modulate immune responses or are causing changes to metabolic pathways will require further exploration.

As for future work, it would be interesting to add a urine sample at week 14. This is because the separation between the wild-type and the IL-10 KO clusters on the PLS-DA plots appears to occur between week 12 and week 16. If a sample were taken at week 14, it would provide a more

detailed picture of how the metabolites are changing between the two groups. It would also be interesting to take the wild-type mice and possibly the IL-10 KO mice that were colonized with fecal bacteria and follow the animals for 2, 3, or 4 weeks, taking weekly samples to see if their metabolic fingerprints ever reach patterns similar to those observed in the mice raised in a conventional environment for their whole lives. Although it would require a lot more animals, time, and money, it would be beneficial to sacrifice conventional animals at each week time-point and the colonized mice at each day time-point for histology; this approach would allow for comparison between the information gathered from the metabolic profiles and the histological scores, helping to correlate the separation of the clusters observed on the PLS-DA plots with the histological scores.

Combining the data of this study with future experiments will help us to understand how intestinal microbiota initiate and perpetuate intestinal inflammation in the IL-10 KO mouse. This type of metabolomics information could provide information about important host and bacterial metabolic pathways that play integral roles not only in the case of disease, but also in the overall interaction of the gut immune system with its microbial neighbours.

Bibliography

Abubakar, I., D. J. Myhill, et al. (2007). "A case-control study of drinking water and dairy products in Crohn's Disease--further investigation of the possible role of Mycobacterium avium paratuberculosis." Am J Epidemiol **165**(7): 776-83.

Afdhal, N. H., A. Long, et al. (1991). "Controlled trial of antimycobacterial therapy in Crohn's disease. Clofazimine versus placebo." Dig Dis Sci **36**(4): 449-53.

al-Waiz, M., M. Mikov, et al. (1992). "The exogenous origin of trimethylamine in the mouse." Metabolism **41**(2): 135-6.

Allen, J., H. M. Davey, et al. (2003). "High-throughput classification of yeast mutants for functional genomics using metabolic footprinting." Nat Biotechnol **21**(6): 692-6.

Awasthi, A., Y. Carrier, et al. (2007). "A dominant function for interleukin 27 in generating interleukin 10-producing anti-inflammatory T cells." Nat Immunol **8**(12): 1380-9.

Barbara, G., V. Stanghellini, et al. (2005). "Interactions between commensal bacteria and gut sensorimotor function in health and disease." Am J Gastroenterol **100**(11): 2560-8.

Barrett, J. C., S. Hansoul, et al. (2008). "Genome-wide association defines more than 30 distinct susceptibility loci for Crohn's disease." Nat Genet **40**(8): 955-62.

Bauer, H., R. E. Horowitz, et al. (1963). "The response of the lymphatic tissue to the microbial flora. Studies on germfree mice." Am J Pathol **42**: 471-83.

Berg, D. J., N. Davidson, et al. (1996). "Enterocolitis and colon cancer in interleukin-10-deficient mice are associated with aberrant cytokine production and CD4(+) TH1-like responses." J Clin Invest **98**(4): 1010-20.

Bergman, E. N. (1990). "Energy contributions of volatile fatty acids from the gastrointestinal tract in various species." Physiol Rev **70**(2): 567-90.

Bernstein, C. N. and J. F. Blanchard (2000). "Viruses and inflammatory bowel disease: is there evidence for a causal association?" Inflamm Bowel Dis **6**(1): 34-9.

Bernstein, C. N., P. Rawsthorne, et al. (2007). "Population-based case-control study of measles, mumps, and rubella and inflammatory bowel disease." Inflamm Bowel Dis **13**(6): 759-62.

Bertin, J., Y. Guo, et al. (2000). "CARD9 is a novel caspase recruitment domain-containing protein that interacts with BCL10/CLAP and activates NF-kappa B." J Biol Chem **275**(52): 41082-6.

Bettelli, E., T. Korn, et al. (2008). "Induction and effector functions of T(H)17 cells." Nature **453**(7198): 1051-7.

Brandwein, S. L., R. P. McCabe, et al. (1997). "Spontaneously colitic C3H/HeJBir mice demonstrate selective antibody reactivity to antigens of the enteric bacterial flora." J Immunol **159**(1): 44-52.

Bry, L., P. G. Falk, et al. (1996). "A model of host-microbial interactions in an open mammalian ecosystem." Science **273**(5280): 1380-3.
Cadwell, K., J. Y. Liu, et al. (2008). "A key role for autophagy and the autophagy gene Atg16l1 in mouse and human intestinal Paneth cells." Nature **456**(7219): 259-63.
Caligiuri, G., M. Rudling, et al. (2003). "Interleukin-10 deficiency increases atherosclerosis, thrombosis, and low-density lipoproteins in apolipoprotein E knockout mice." Mol Med **9**(1-2): 10-7.
Chen, W., D. Li, et al. (2002). "Detection of Chlamydia pneumoniae by polymerase chain reaction-enzyme immunoassay in intestinal mucosal biopsies from patients with inflammatory bowel disease and controls." J Gastroenterol Hepatol **17**(9): 987-93.
Chiodini, R. J., H. J. Van Kruiningen, et al. (1984). "Possible role of mycobacteria in inflammatory bowel disease. I. An unclassified Mycobacterium species isolated from patients with Crohn's disease." Dig Dis Sci **29**(12): 1073-9.
Collazo, C. M., G. S. Yap, et al. (2001). "Inactivation of LRG-47 and IRG-47 reveals a family of interferon gamma-inducible genes with essential, pathogen-specific roles in resistance to infection." J Exp Med **194**(2): 181-8.
Cong, Y., S. L. Brandwein, et al. (1998). "CD4+ T cells reactive to enteric bacterial antigens in spontaneously colitic C3H/HeJBir mice: increased T helper cell type 1 response and ability to transfer disease." J Exp Med **187**(6): 855-64.
Cook, S. I. and J. H. Sellin (1998). "Review article: short chain fatty acids in health and disease." Aliment Pharmacol Ther **12**(6): 499-507.
Darfeuille-Michaud, A., J. Boudeau, et al. (2004). "High prevalence of adherent-invasive Escherichia coli associated with ileal mucosa in Crohn's disease." Gastroenterology **127**(2): 412-21.
Darfeuille-Michaud, A., C. Neut, et al. (1998). "Presence of adherent Escherichia coli strains in ileal mucosa of patients with Crohn's disease." Gastroenterology **115**(6): 1405-13.
De Lisle, R. C., W. Xu, et al. (2008). "Effects of Muclin (Dmbt1) deficiency on the gastrointestinal system." Am J Physiol Gastrointest Liver Physiol **294**(3): G717-27.
de Waal Malefyt, R., J. Abrams, et al. (1991). "Interleukin 10(IL-10) inhibits cytokine synthesis by human monocytes: an autoregulatory role of IL-10 produced by monocytes." J Exp Med **174**(5): 1209-20.
Delaney, J., W. A. Neville, et al. (2004). "Phenylacetylglycine, a putative biomarker of phospholipidosis: its origins and relevance to phospholipid accumulation using amiodarone treated rats as a model." Biomarkers **9**(3): 271-90.
Elson, C. O. and Y. Cong (2002). "Understanding immune-microbial homeostasis in intestine." Immunol Res **26**(1-3): 87-94.
Elson, C. O., R. B. Sartor, et al. (1995). "Experimental models of inflammatory bowel disease." Gastroenterology **109**(4): 1344-67.

Farrell, R. J. and J. T. LaMont (2002). "Microbial factors in inflammatory bowel disease." Gastroenterol Clin North Am **31**(1): 41-62.
Feng, C. G., L. Zheng, et al. (2008). "The immunity-related GTPase Irgm1 promotes the expansion of activated CD4+ T cell populations by preventing interferon-gamma-induced cell death." Nat Immunol **9**(11): 1279-87.
Fiehn, O. (2002). "Metabolomics--the link between genotypes and phenotypes." Plant Mol Biol **48**(1-2): 155-71.
Fuss, I. J., M. Neurath, et al. (1996). "Disparate CD4+ lamina propria (LP) lymphokine secretion profiles in inflammatory bowel disease. Crohn's disease LP cells manifest increased secretion of IFN-gamma, whereas ulcerative colitis LP cells manifest increased secretion of IL-5." J Immunol **157**(3): 1261-70.
Galli, S. J., M. Tsai, et al. (2008). "The development of allergic inflammation." Nature **454**(7203): 445-54.
Gordon, J. I., L. V. Hooper, et al. (1997). "Epithelial cell growth and differentiation. III. Promoting diversity in the intestine: conversations between the microflora, epithelium, and diffuse GALT." Am J Physiol **273**(3 Pt 1): G565-70.
Gross, O., A. Gewies, et al. (2006). "Card9 controls a non-TLR signalling pathway for innate anti-fungal immunity." Nature **442**(7103): 651-6.
Gui, G. P., P. R. Thomas, et al. (1997). "Two-year-outcomes analysis of Crohn's disease treated with rifabutin and macrolide antibiotics." J Antimicrob Chemother **39**(3): 393-400.
Hilsden, R. J., J. B. Meddings, et al. (1996). "Intestinal permeability changes in response to acetylsalicylic acid in relatives of patients with Crohn's disease." Gastroenterology **110**(5): 1395-403.
Hollander, D., C. M. Vadheim, et al. (1986). "Increased intestinal permeability in patients with Crohn's disease and their relatives. A possible etiologic factor." Ann Intern Med **105**(6): 883-5.
Hooper, L. V., T. Midtvedt, et al. (2002). "How host-microbial interactions shape the nutrient environment of the mammalian intestine." Annu Rev Nutr **22**: 283-307.
Horning, E. C., Horning, MG (1971). "Human metabolic profiles obtained by GC and GC/MS." Journal Chromatographic Science **9**: 129-140.
Hsu, Y. M., Y. Zhang, et al. (2007). "The adaptor protein CARD9 is required for innate immune responses to intracellular pathogens." Nat Immunol **8**(2): 198-205.
Hugot, J. P., M. Chamaillard, et al. (2001). "Association of NOD2 leucine-rich repeat variants with susceptibility to Crohn's disease." Nature **411**(6837): 599-603.
Husebye, E., P. M. Hellstrom, et al. (1994). "Intestinal microflora stimulates myoelectric activity of rat small intestine by promoting cyclic initiation and aboral propagation of migrating myoelectric complex." Dig Dis Sci **39**(5): 946-56.

Ibbotson, J. P., J. R. Lowes, et al. (1992). "Mucosal cell-mediated immunity to mycobacterial, enterobacterial and other microbial antigens in inflammatory bowel disease." Clin Exp Immunol **87**(2): 224-30.
James, M. O., R. L. Smith, et al. (1972). "The conjugation of phenylacetic acid in man, sub-human primates and some non-primate species." Proc R Soc Lond B Biol Sci **182**(66): 25-35.
Kandori, H., K. Hirayama, et al. (1996). "Histochemical, lectin-histochemical and morphometrical characteristics of intestinal goblet cells of germfree and conventional mice." Exp Anim **45**(2): 155-60.
Kell, D. B. (2002). "Metabolomics and machine learning: explanatory analysis of complex metabolome data using genetic programming to produce simple, robust rules." Mol Biol Rep **29**(1-2): 237-41.
Koutroubakis, I. E., D. Drygiannakis, et al. "Antiglycan Antibodies in Greek Patients with Inflammatory Bowel Disease." Dig Dis Sci.
Kuballa, P., A. Huett, et al. (2008). "Impaired autophagy of an intracellular pathogen induced by a Crohn's disease associated ATG16L1 variant." PLoS One **3**(10): e3391.
Kuhn, R., J. Lohler, et al. (1993). "Interleukin-10-deficient mice develop chronic enterocolitis." Cell **75**(2): 263-74.
Lewis, K., F. Lutgendorff, et al. (2009). "Enhanced translocation of bacteria across metabolically stressed epithelia is reduced by butyrate." Inflamm Bowel Dis.
Lievin-Le Moal, V. and A. L. Servin (2006). "The front line of enteric host defense against unwelcome intrusion of harmful microorganisms: mucins, antimicrobial peptides, and microbiota." Clin Microbiol Rev **19**(2): 315-37.
Lin, H. M., S. I. Edmunds, et al. (2009). "Nontargeted urinary metabolite profiling of a mouse model of Crohn's disease." J Proteome Res **8**(4): 2045-57.
Linskens, R. K., X. W. Huijsdens, et al. (2001). "The bacterial flora in inflammatory bowel disease: current insights in pathogenesis and the influence of antibiotics and probiotics." Scand J Gastroenterol Suppl(234): 29-40.
Liu, Y., H. J. van Kruiningen, et al. (1995). "Immunocytochemical evidence of Listeria, Escherichia coli, and Streptococcus antigens in Crohn's disease." Gastroenterology **108**(5): 1396-404.
Liu, Y., P. Zhang, et al. (2008). "A critical function for TGF-beta signaling in the development of natural CD4+CD25+Foxp3+ regulatory T cells." Nat Immunol **9**(6): 632-40.
Marchesi, J. R., E. Holmes, et al. (2007). "Rapid and noninvasive metabonomic characterization of inflammatory bowel disease." J Proteome Res **6**(2): 546-51.
Martin, F. P., S. Rezzi, et al. (2009). "Metabolic effects of dark chocolate consumption on energy, gut microbiota, and stress-related metabolism in free-living subjects." J Proteome Res **8**(12): 5568-79.

Martin, F. P., S. Rezzi, et al. (2009). "Metabolic assessment of gradual development of moderate experimental colitis in IL-10 deficient mice." J Proteome Res **8**(5): 2376-87.
May, G. R., L. R. Sutherland, et al. (1993). "Is small intestinal permeability really increased in relatives of patients with Crohn's disease?" Gastroenterology **104**(6): 1627-32.
McCarroll, S. A., A. Huett, et al. (2008). "Deletion polymorphism upstream of IRGM associated with altered IRGM expression and Crohn's disease." Nat Genet **40**(9): 1107-12.
Mizushima, N., B. Levine, et al. (2008). "Autophagy fights disease through cellular self-digestion." Nature **451**(7182): 1069-75.
Mourelle, M., A. Salas, et al. (1998). "Stimulation of transforming growth factor beta1 by enteric bacteria in the pathogenesis of rat intestinal fibrosis." Gastroenterology **114**(3): 519-26.
Murdoch, T. B., H. Fu, et al. (2008). "Urinary metabolic profiles of inflammatory bowel disease in interleukin-10 gene-deficient mice." Anal Chem **80**(14): 5524-31.
Neish, A. S. (2009). "Microbes in gastrointestinal health and disease." Gastroenterology **136**(1): 65-80.
Nicholls, A. W., R. J. Mortishire-Smith, et al. (2003). "NMR spectroscopic-based metabonomic studies of urinary metabolite variation in acclimatizing germ-free rats." Chem Res Toxicol **16**(11): 1395-404.
O'Garra, A., B. Stockinger, et al. (2008). "Differentiation of human T(H)-17 cells does require TGF-beta!" Nat Immunol **9**(6): 588-90.
Ogura, Y., D. K. Bonen, et al. (2001). "A frameshift mutation in NOD2 associated with susceptibility to Crohn's disease." Nature **411**(6837): 603-6.
Oliver, S. G., M. K. Winson, et al. (1998). "Systematic functional analysis of the yeast genome." Trends Biotechnol **16**(9): 373-8.
Paganelli, R., F. Pallone, et al. (1985). "Isotypic analysis of antibody response to a food antigen in inflammatory bowel disease." Int Arch Allergy Appl Immunol **78**(1): 81-5.
Peltekova, V. D., R. F. Wintle, et al. (2004). "Functional variants of OCTN cation transporter genes are associated with Crohn disease." Nat Genet **36**(5): 471-5.
Reinhard, C. and J. D. Rioux (2006). "Role of the IBD5 susceptibility locus in the inflammatory bowel diseases." Inflamm Bowel Dis **12**(3): 227-38.
Rennick, D. M. and M. M. Fort (2000). "Lessons from genetically engineered animal models. XII. IL-10-deficient (IL-10(-/-) mice and intestinal inflammation." Am J Physiol Gastrointest Liver Physiol **278**(6): G829-33.
Rolhion, N. and A. Darfeuille-Michaud (2007). "Adherent-invasive Escherichia coli in inflammatory bowel disease." Inflamm Bowel Dis **13**(10): 1277-83.
Rosenstiel, P., C. Sina, et al. (2007). "Regulation of DMBT1 via NOD2 and TLR4 in intestinal epithelial cells modulates bacterial recognition and invasion." J Immunol **178**(12): 8203-11.

Saemann, M. D., G. A. Bohmig, et al. (2002). "Short-chain fatty acids: bacterial mediators of a balanced host-microbial relationship in the human gut." Wien Klin Wochenschr **114**(8-9): 289-300.
Saitoh, T., N. Fujita, et al. (2008). "Loss of the autophagy protein Atg16L1 enhances endotoxin-induced IL-1beta production." Nature **456**(7219): 264-8.
Sartor, R. B. (1997). "Review article: Role of the enteric microflora in the pathogenesis of intestinal inflammation and arthritis." Aliment Pharmacol Ther **11 Suppl 3**: 17-22; discussion 22-3.
Sartor, R. B. (2000). "Microbial factors in the pathogenesis of Crohn's disease, ulcerative colitis, and experimental intestinal inflammation." Inflamm Bowel Dis **5**: 153-178.
Savage, D. C. (1986). "Gastrointestinal microflora in mammalian nutrition." Annu Rev Nutr **6**: 155-78.
Savage, D. C., J. E. Siegel, et al. (1981). "Transit time of epithelial cells in the small intestines of germfree mice and ex-germfree mice associated with indigenous microorganisms." Appl Environ Microbiol **42**(6): 996-1001.
Scheppach, W., H. Sommer, et al. (1992). "Effect of butyrate enemas on the colonic mucosa in distal ulcerative colitis." Gastroenterology **103**(1): 51-6.
Schuller, J. L., J. Piket-van Ulsen, et al. (1979). "Antibodies against Chlamydia of lymphogranuloma-venereum type in Crohn's disease." Lancet **1**(8106): 19-20.
Seibel, B. A. and P. J. Walsh (2002). "Trimethylamine oxide accumulation in marine animals: relationship to acylglycerol storage." J Exp Biol **205**(Pt 3): 297-306.
Seong, S. Y. and P. Matzinger (2004). "Hydrophobicity: an ancient damage-associated molecular pattern that initiates innate immune responses." Nat Rev Immunol **4**(6): 469-78.
Shanahan, F. (2000). "Probiotics and inflammatory bowel disease: is there a scientific rationale?" Inflamm Bowel Dis **6**(2): 107-15.
Shkoda, A., P. A. Ruiz, et al. (2007). "Interleukin-10 blocked endoplasmic reticulum stress in intestinal epithelial cells: impact on chronic inflammation." Gastroenterology **132**(1): 190-207.
Sibartie, S., P. Scully, et al. "Mycobacterium avium subsp. Paratuberculosis (MAP) as a modifying factor in Crohn's disease." Inflamm Bowel Dis **16**(2): 296-304.
Silverberg, M. S., R. H. Duerr, et al. (2007). "Refined genomic localization and ethnic differences observed for the IBD5 association with Crohn's disease." Eur J Hum Genet **15**(3): 328-35.
Simon, G. L. and S. L. Gorbach (1984). "Intestinal flora in health and disease." Gastroenterology **86**(1): 174-93.
Smith, J. L., J. S. Wishnok, et al. (1994). "Metabolism and excretion of methylamines in rats." Toxicol Appl Pharmacol **125**(2): 296-308.
Stappenbeck, T. S., L. V. Hooper, et al. (2002). "Developmental regulation of intestinal angiogenesis by indigenous microbes via Paneth cells." Proc Natl Acad Sci U S A **99**(24): 15451-5.

Stoll, M., B. Corneliussen, et al. (2004). "Genetic variation in DLG5 is associated with inflammatory bowel disease." Nat Genet **36**(5): 476-80.
Strandberg, K., G. Sedvall, et al. (1966). "Effect of some biologically active amines on the cecum wall of germfree rats." Proc Soc Exp Biol Med **121**(3): 699-702.
Swidsinski, A., A. Ladhoff, et al. (2002). "Mucosal flora in inflammatory bowel disease." Gastroenterology **122**(1): 44-54.
Swidsinski, A., J. Weber, et al. (2005). "Spatial organization and composition of the mucosal flora in patients with inflammatory bowel disease." J Clin Microbiol **43**(7): 3380-9.
Tabaqchali, S., D. P. O'Donoghue, et al. (1978). "Escherichia coli antibodies in patients with inflammatory bowel disease." Gut **19**(2): 108-13.
Tedelind, S., F. Westberg, et al. (2007). "Anti-inflammatory properties of the short-chain fatty acids acetate and propionate: a study with relevance to inflammatory bowel disease." World J Gastroenterol **13**(20): 2826-32.
Thomas, G. A., G. L. Swift, et al. (1998). "Controlled trial of antituberculous chemotherapy in Crohn's disease: a five year follow up study." Gut **42**(4): 497-500.
Tlaskalova-Hogenova, H., R. Stepankova, et al. (2004). "Commensal bacteria (normal microflora), mucosal immunity and chronic inflammatory and autoimmune diseases." Immunol Lett **93**(2-3): 97-108.
Topping, D. L. and P. M. Clifton (2001). "Short-chain fatty acids and human colonic function: roles of resistant starch and nonstarch polysaccharides." Physiol Rev **81**(3): 1031-64.
Tsuji, S., J. Uehori, et al. (2001). "Human intelectin is a novel soluble lectin that recognizes galactofuranose in carbohydrate chains of bacterial cell wall." J Biol Chem **276**(26): 23456-63.
Van de Merwe, J. P., P. I. Schmitz, et al. (1981). "Antibodies to Eubacterium and Peptostreptococcus species and the estimated probability of Crohn's disease." J Hyg (Lond) **87**(1): 25-33.
Van de Merwe, J. P., J. H. Stegeman, et al. (1983). "The resident faecal flora is determined by genetic characteristics of the host. Implications for Crohn's disease?" Antonie Van Leeuwenhoek **49**(2): 119-24.
Van Limbergen, J., R. K. Russell, et al. (2007). "Genetics of the innate immune response in inflammatory bowel disease." Inflamm Bowel Dis **13**(3): 338-55.
Van Limbergen, J., R. K. Russell, et al. (2007). "The genetics of inflammatory bowel disease." Am J Gastroenterol **102**(12): 2820-31.
Van Limbergen, J., D. C. Wilson, et al. (2009). "The genetics of Crohn's disease." Annu Rev Genomics Hum Genet **10**: 89-116.
Walmsley, R. S., J. P. Ibbotson, et al. (1996). "Antibodies against Mycobacterium paratuberculosis in Crohn's disease." Qjm **89**(3): 217-21.
Wang, Q. Z., C. Y. Wu, et al. (2006). "Integrating metabolomics into a systems biology framework to exploit metabolic complexity: strategies and applications in microorganisms." Appl Microbiol Biotechnol **70**(2): 151-61.

Wei, L., P. Liao, et al. (2008). "Toxicological effects of cinnabar in rats by NMR-based metabolic profiling of urine and serum." Toxicol Appl Pharmacol **227**(3): 417-29.
Weljie, A. M., J. Newton, et al. (2006). "Targeted profiling: quantitative analysis of 1H NMR metabolomics data." Anal Chem **78**(13): 4430-42.
Williams, H. R., I. J. Cox, et al. (2009). "Characterization of inflammatory bowel disease with urinary metabolic profiling." Am J Gastroenterol **104**(6): 1435-44.
Williams, R. E., H. W. Eyton-Jones, et al. (2002). "Effect of intestinal microflora on the urinary metabolic profile of rats: a (1)H-nuclear magnetic resonance spectroscopy study." Xenobiotica **32**(9): 783-94.
Wine, E., J. C. Ossa, et al. (2009). "Adherent-invasive Escherichia coli, strain LF82 disrupts apical junctional complexes in polarized epithelia." BMC Microbiol **9**: 180.
Wrackmeyer, U., G. H. Hansen, et al. (2006). "Intelectin: a novel lipid raft-associated protein in the enterocyte brush border." Biochemistry **45**(30): 9188-97.
Xavier, R. J. and D. K. Podolsky (2007). "Unravelling the pathogenesis of inflammatory bowel disease." Nature **448**(7152): 427-34.
Yamanaka, T., L. Helgeland, et al. (2003). "Microbial colonization drives lymphocyte accumulation and differentiation in the follicle-associated epithelium of Peyer's patches." J Immunol **170**(2): 816-22.
Zampa, A., S. Silvi, et al. (2004). "Effects of different digestible carbohydrates on bile acid metabolism and SCFA production by human gut micro-flora grown in an in vitro semi-continuous culture." Anaerobe **10**(1): 19-26.
Zoetendal, E. G., E. E. Vaughan, et al. (2006). "A microbial world within us." Mol Microbiol **59**(6): 1639-50.

Appendix 1

Axenic Mice

Wild-type population

Wild-type population: comparison of male and female at various ages

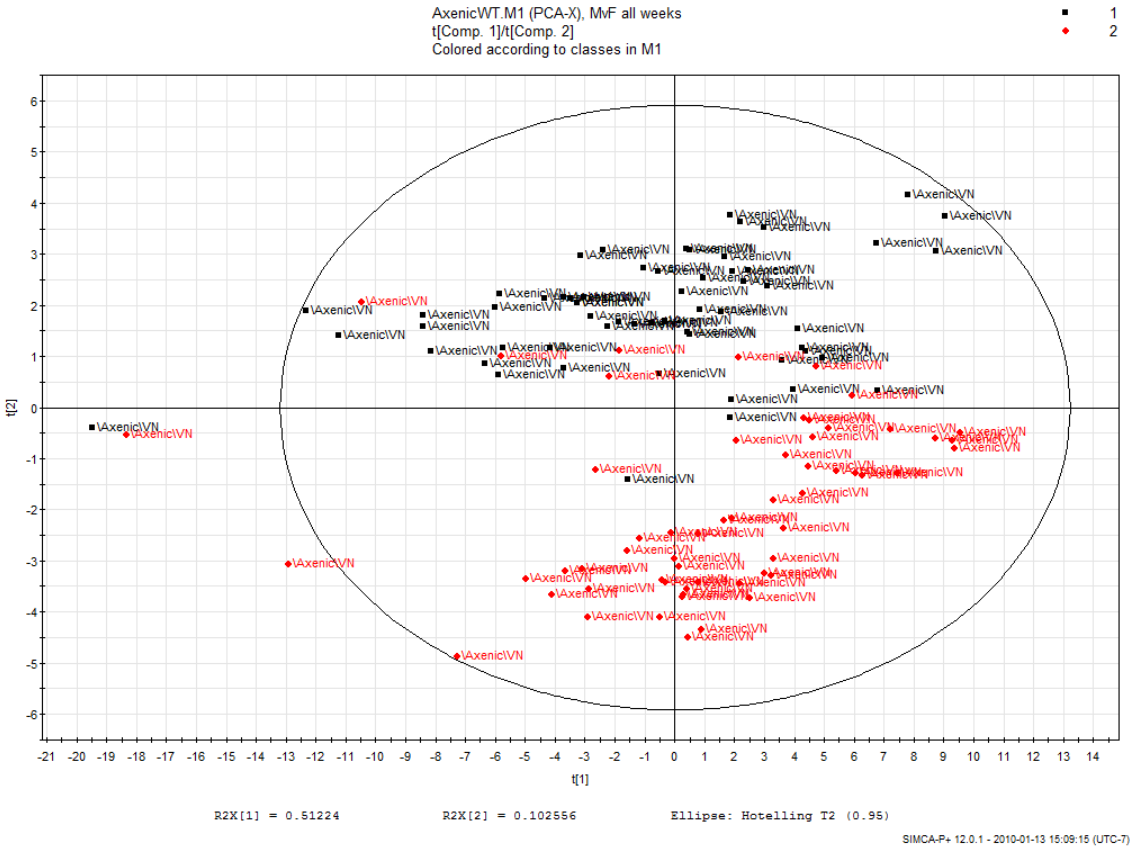

Fig. 1 – PCA plot of the urine metabolomic profiles of all male and female axenic wild-type mice collected in their axenic environments on weeks 4, 6, 8, 12, 16, and 20 of age. Each of the male and female groups is composed of 60 data points (10 points per week). Male mice are shown in red and female mice are shown in black. Despite a slight overlap and a few outliers, there is a clear separation between the two groups.

Week-by-week comparison

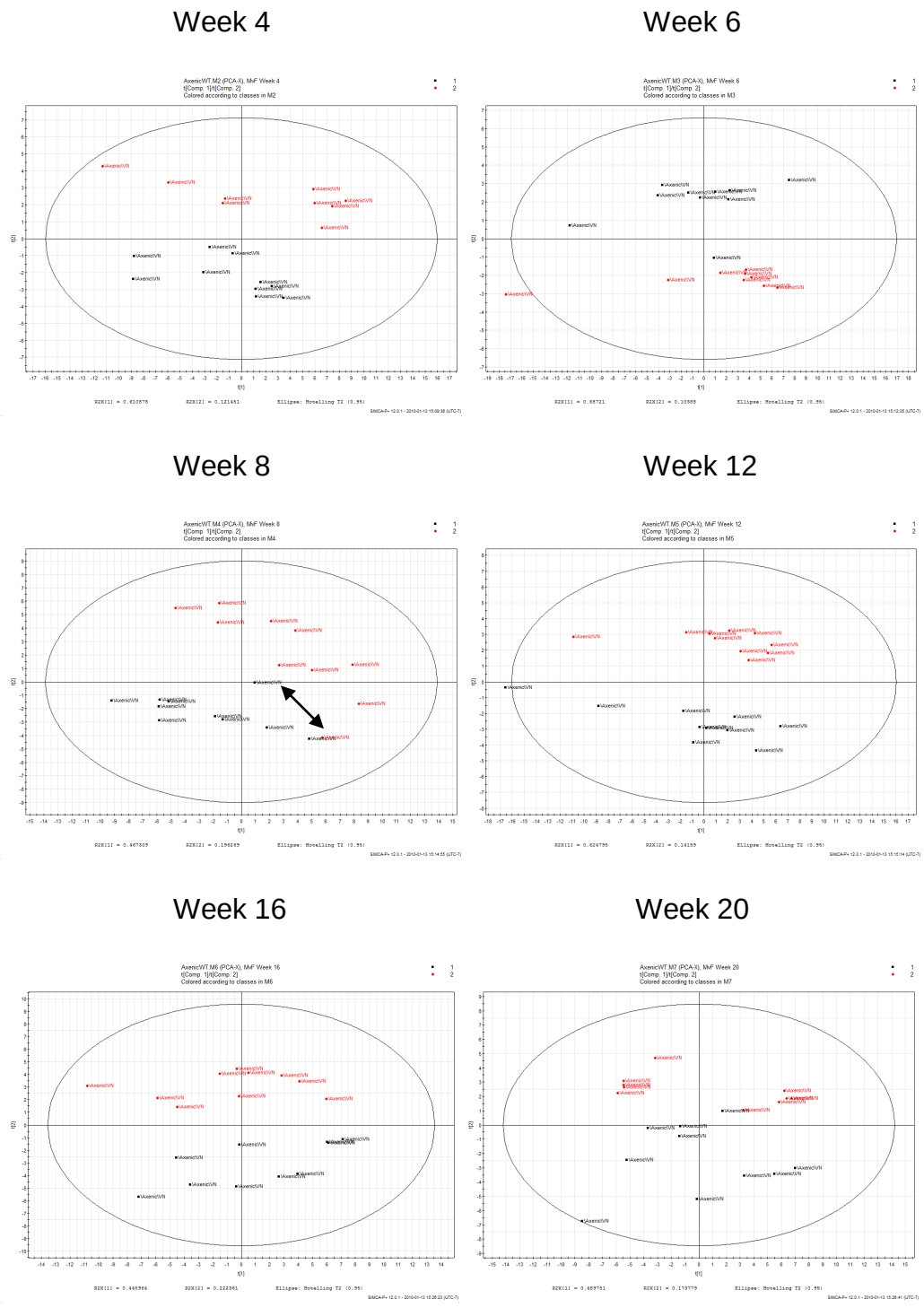

Fig. 2 – PCA plots of the urine metabolomic profiles of the axenic wild-type mice broken up by week of urine collection; males are displayed in red and females are displayed in black. Each week is composed of 10 males and 10 females.

Wild-type males: comparison of urine metabolomics over all collection weeks

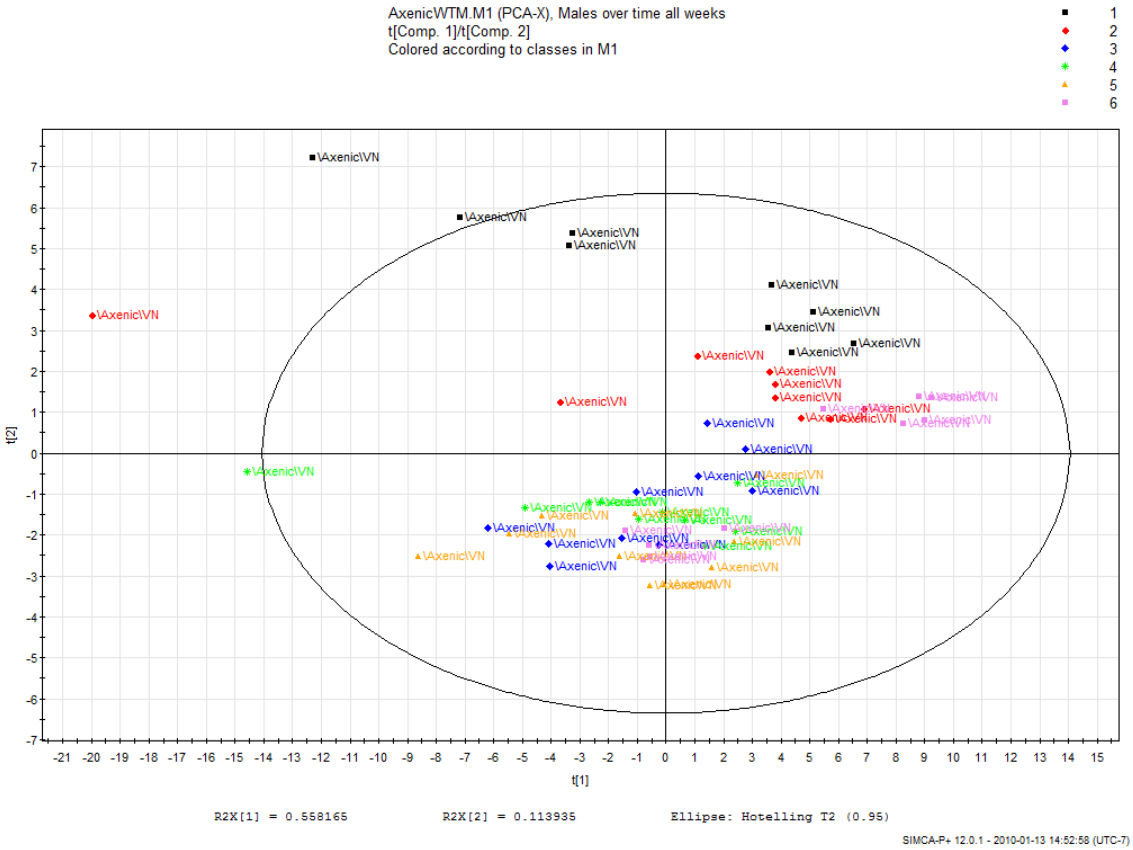

Fig. 3– PCA plot of urine metabolomic profiles of all male wild-type axenic mice over all collection time-points. Each week is constructed from 10 points and is displayed in a different color: week 4 (black), week 6 (red), week 8 (blue), week 12 (green), week 16 (yellow), week 20 (purple). This plot shows the progression of the urine metabolomic profile of male wild-type mice as they grow in an axenic environment.

Reference to week 4 comparison

Week 4 vs. Week 6

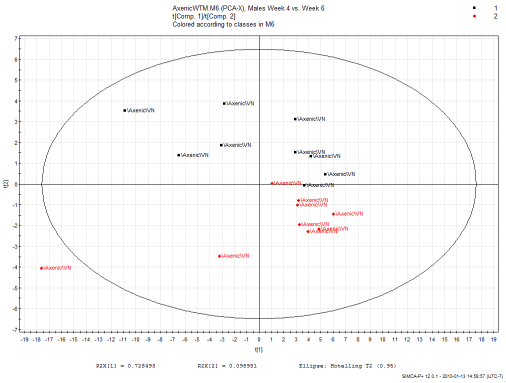

Week 4 vs. Week 8

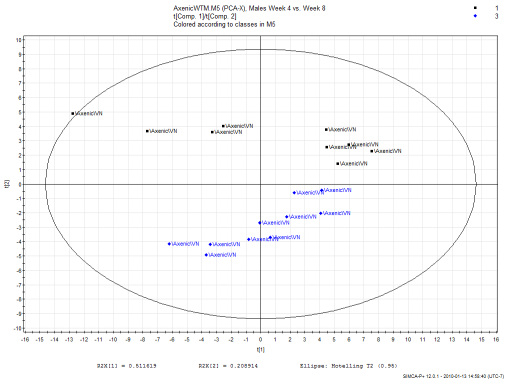

Week 4 vs. Week 12

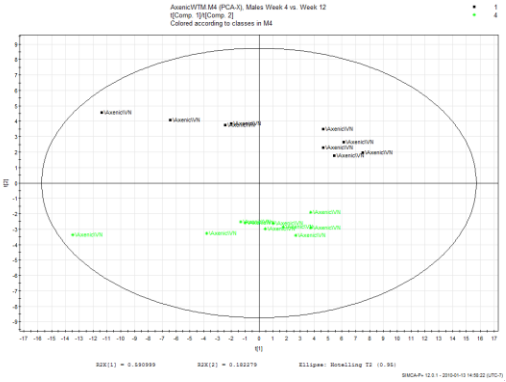

Week 4 vs. Week 16

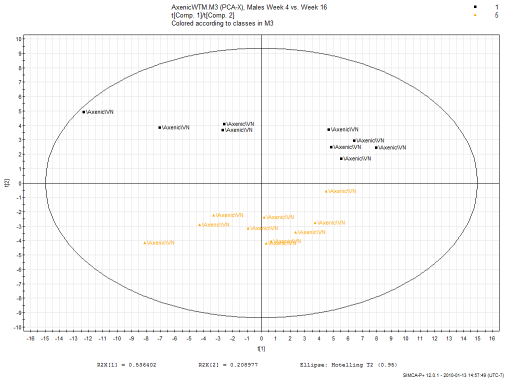

Week 4 vs. Week 20

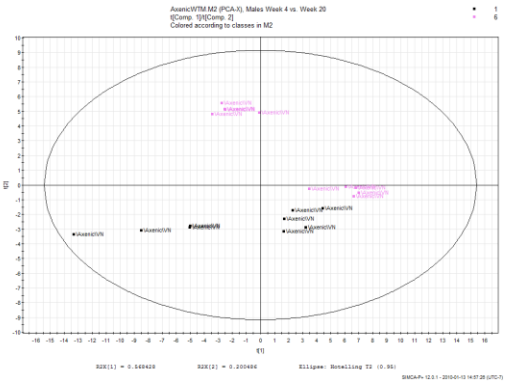

Fig. 4– PCA plot of urine metabolomic profiles of wild-type male axenic mice referenced to week 4; each group is composed of the same 10 mice from week 4 and is referenced against the other groups of 10 mice that comprise the other weeks collected.

Wild-type females: comparison of urine metabolomics over all collection weeks

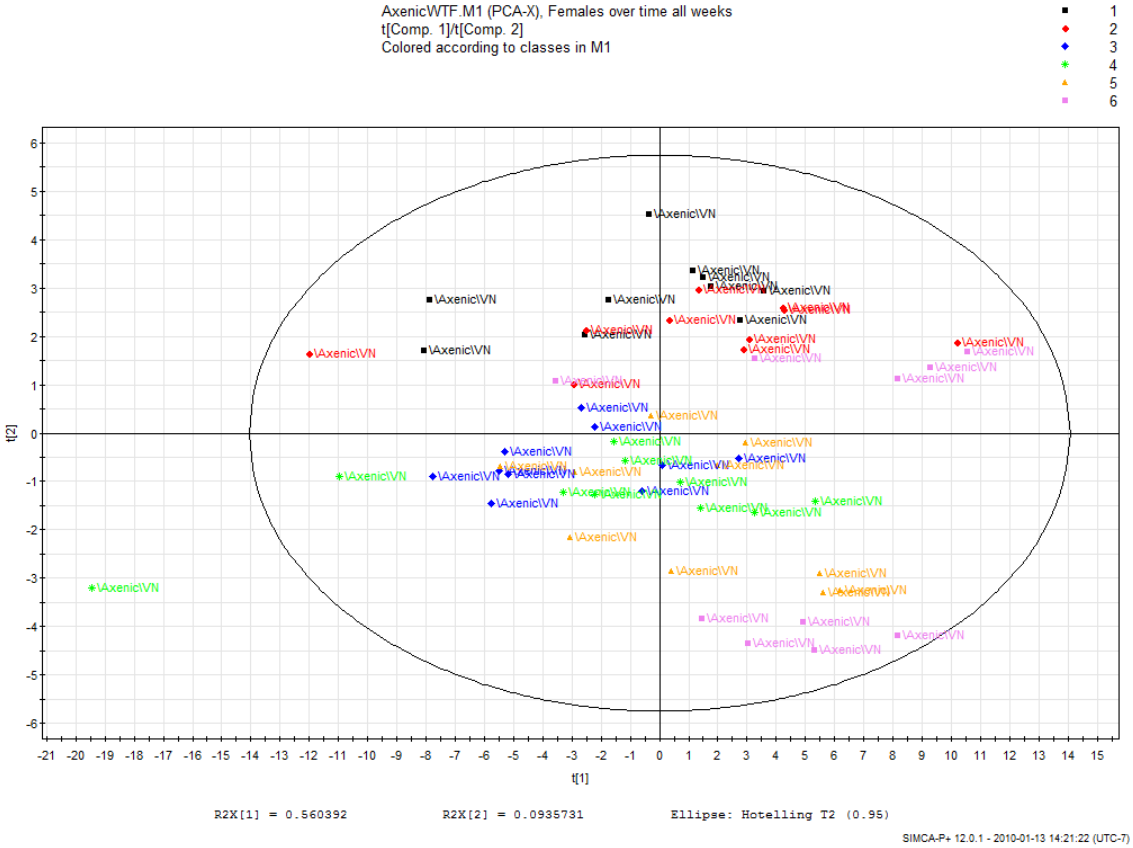

Fig. 5– PCA plot of urine metabolomics profile of all female wild-type axenic mice over all collection time-points. Each week is constructed from 10 points and is displayed in a different color: week 4 (black), week 6 (red), week 8 (blue), week 12 (green), week 16 (yellow), week 20 (purple). This plot shows the progression of the urine metabolomic profile of female wild-type mice as they grow in an axenic environment.

Reference to week 4 comparison

Week 4 vs. Week 6

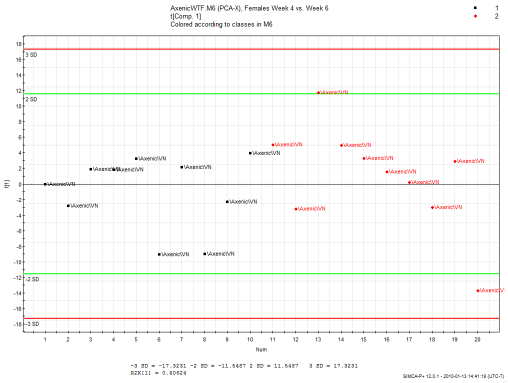

Week 4 vs. Week 8

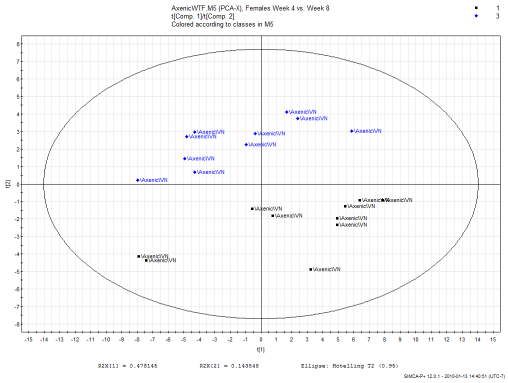

Week 4 vs. Week 12

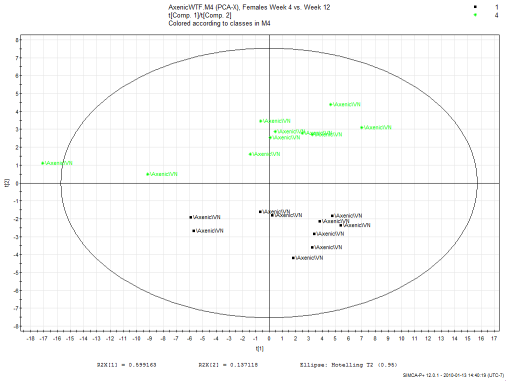

Week 4 vs. Week 16

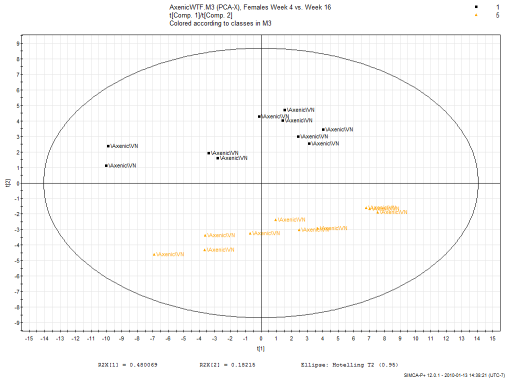

Week 4 vs. Week 20

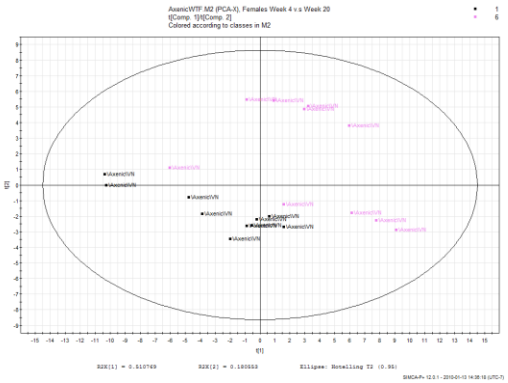

Fig. 6 – PCA plots of urine metabolomic profiles of female wild-type axenic mice in reference to week 4; each group is composed of the same 10 mice from week 4 and is referenced against the other groups of 10 mice that comprise the other weeks collected.

IL-10 KO population

IL-10 KO population: comparison of male and female at various ages

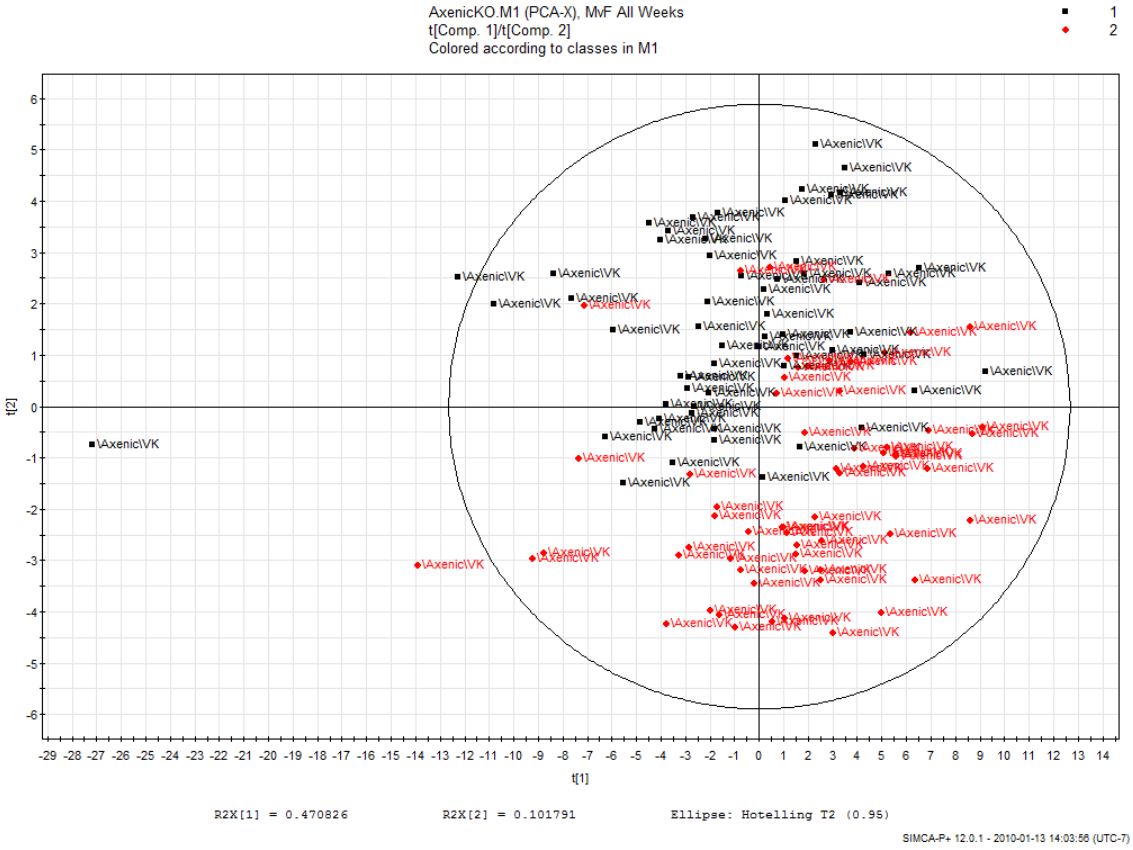

Fig 7- PCA plot of the urine metabolomic profiles of all male and female IL-10 KO axenic mice (urine collected in their axenic environments on weeks 4, 6, 8, 12, 16, and 20 of age). Each of the male and female groups is composed of 60 data points (10 points per week). Male mice are shown in red and female mice are shown in black. Unlike the wild-type mice, there is quite a bit more overlap between the two groups.

Reference to week 4 comparison

Week 4

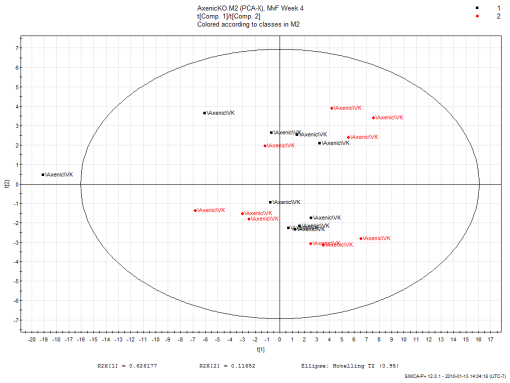

Week 6

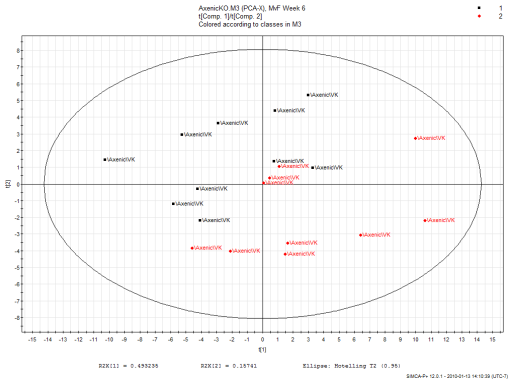

Week 8

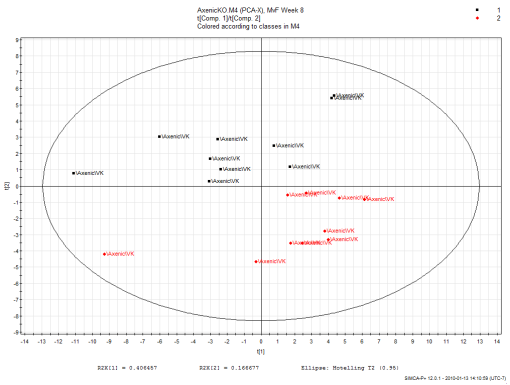

Week 12

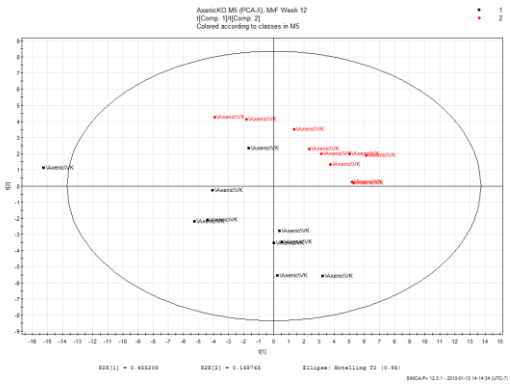

Week 16

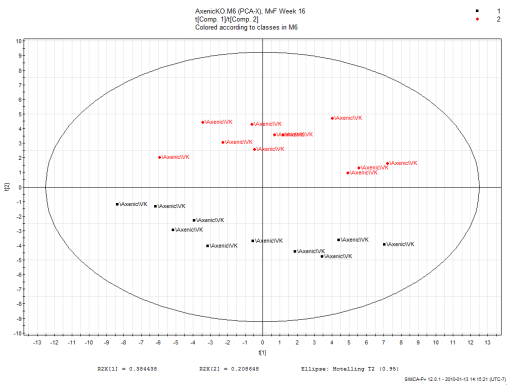

Week 20

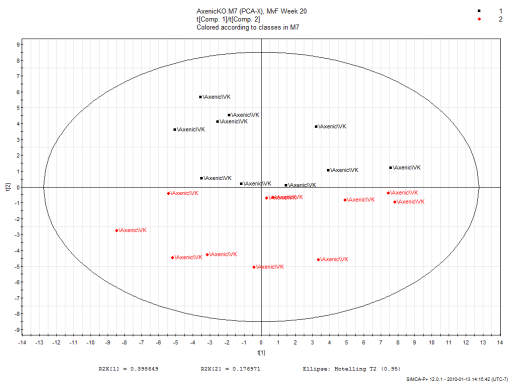

Fig. 8 – PCA plots of the urine metabolomic profiles of the axenic IL-10 KO mice broken up by week of urine collection; males are displayed in red and females are displayed in black. Each week comprises 10 males and 10 females.

IL-10 KO males: comparison of urine metabolomics over all collection weeks

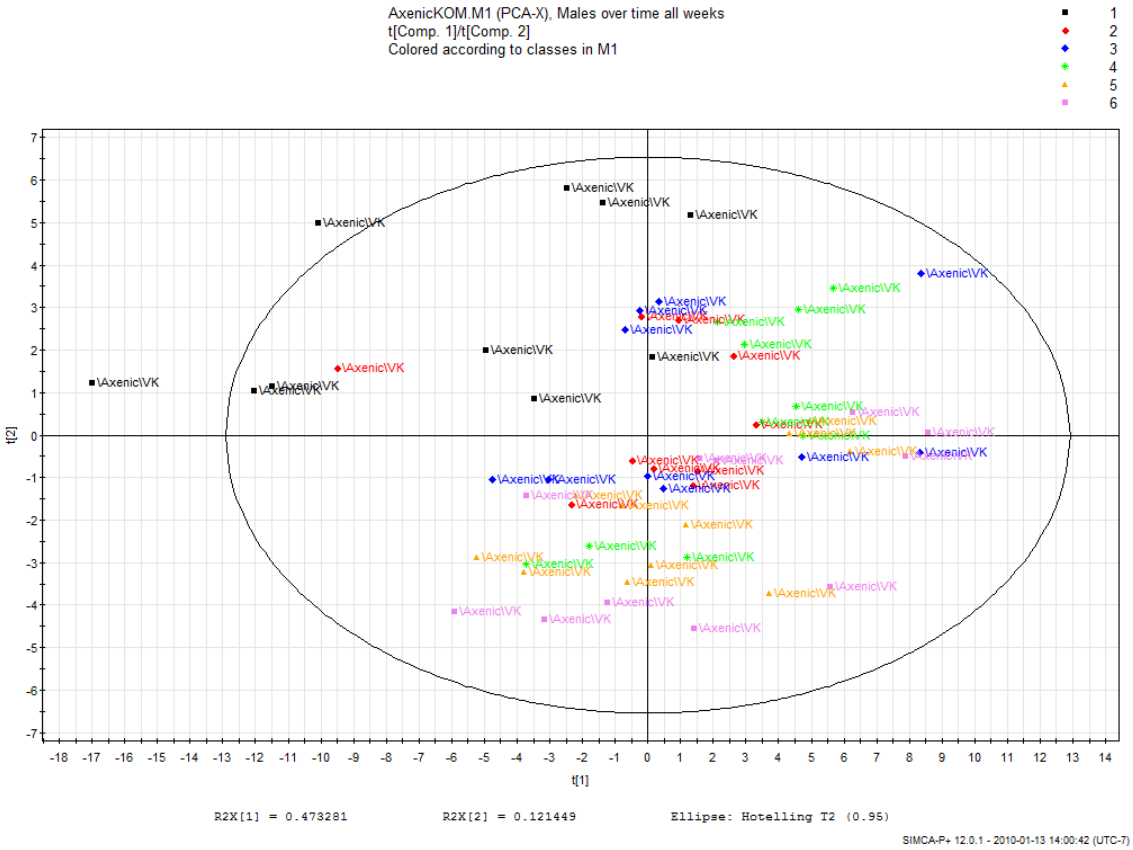

Fig. 9– PCA plot of urine metabolomic profiles of all male IL-10 KO axenic mice over all collection time-points. Each week is constructed from 10 points and is displayed in a different color: week 4 (black), week 6 (red), week 8 (blue), week 12 (green), week 16 (yellow), week 20 (purple). This plot shows the progression of the urine metabolomic profile of male wild-type mice as they grow in an axenic environment.

Reference to week 4 comparison

Week 4 vs. Week 6

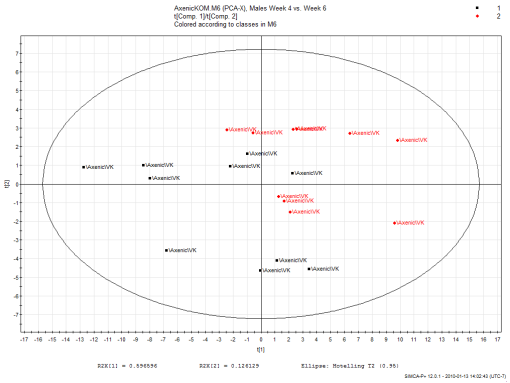

Week 4 vs. Week 8

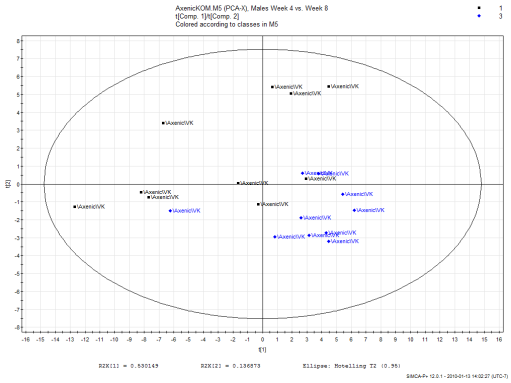

Week 4 vs. Week 12

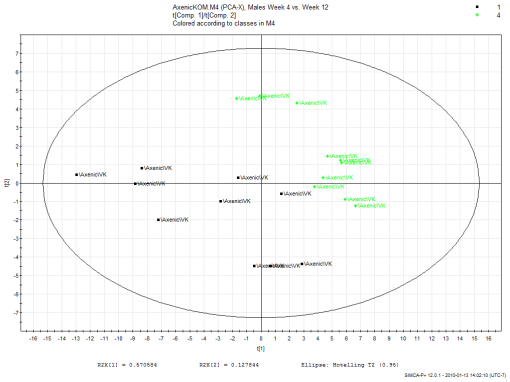

Week 4 vs. Week 16

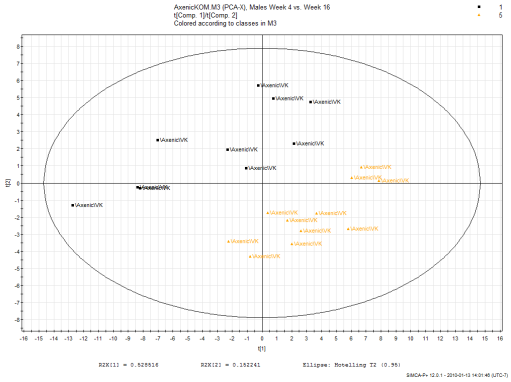

Week 4 vs. Week 20

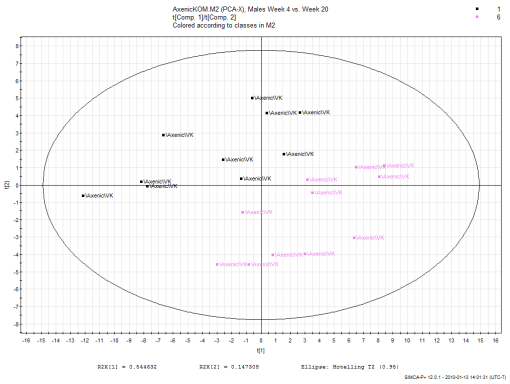

Fig. 10 – PCA plots of urine metabolomic profiles of IL-10 KO male axenic mice in reference to week 4; each group is composed of the same 10 mice from week 4 and is referenced against the other groups of 10 mice that comprise the other weeks collected.

IL-10 KO females: comparison of urine metabolomics over all collection weeks

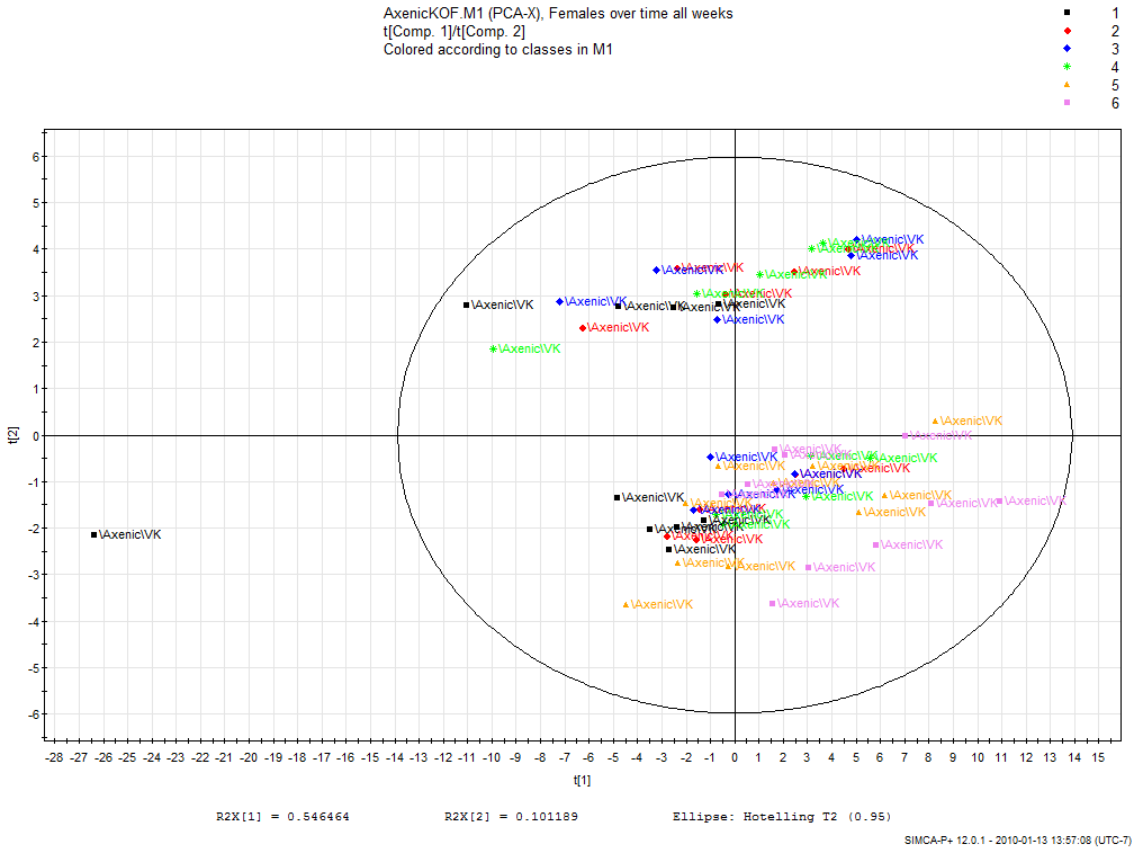

Fig. 11– PCA plot of urine metabolomics profiles of all female IL-10 KO axenic mice over all collection time-points. Each week is constructed from 10 points and is displayed in a different color: week 4 (black), week 6 (red), week 8 (blue), week 12 (green), week 16 (yellow), week 20 (purple). This plot shows the progression of the urine metabolomic profile of female wild-type mice as they grow in an axenic environment.

Reference to week 4 comparison

Week 4 vs. Week 6

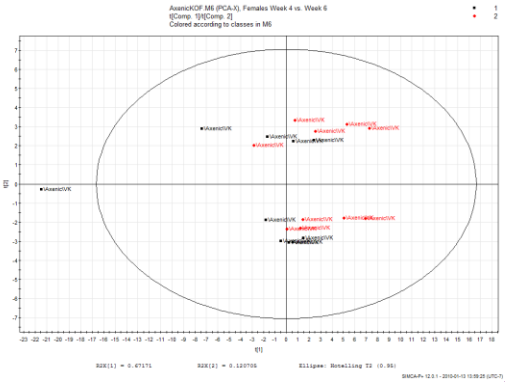

Week 4 vs. Week 8

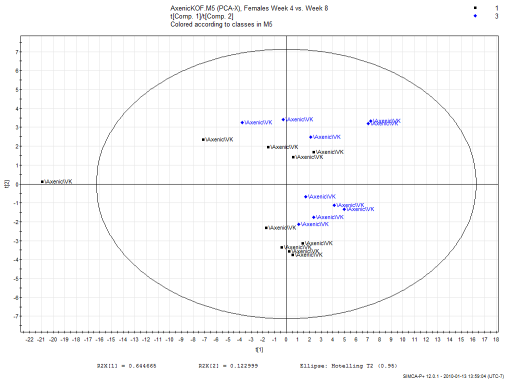

Week 4 vs. Week 12

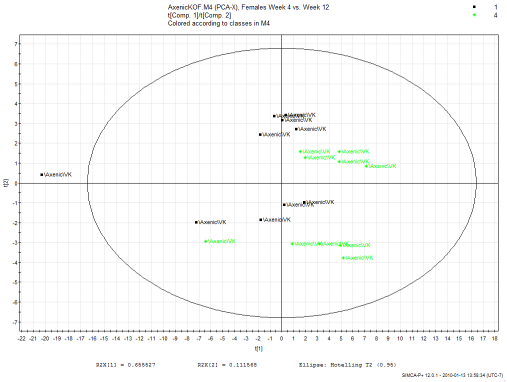

Week 4 vs. Week 16

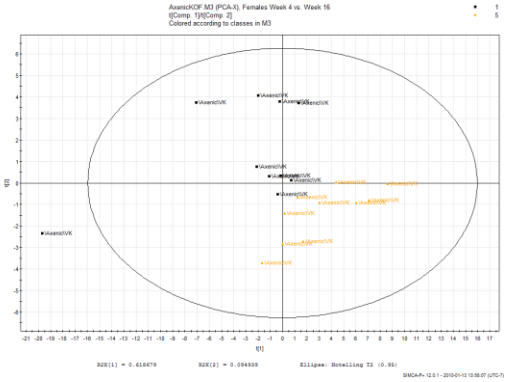

Week 4 vs. Week 20

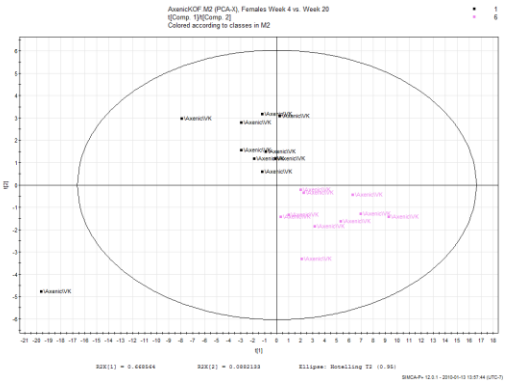

Fig. 12 – PCA plots of urine metabolomic profiles of IL-10 KO female axenic mice referenced to week 4; each group is comprised of the same 10 mice from week 4 and is referenced against the other groups of 10 mice that comprise the other weeks collected.

Wild-type vs. IL-10 KO: comparison of axenic wild-type mice vs. IL-10 KO mice

Male population

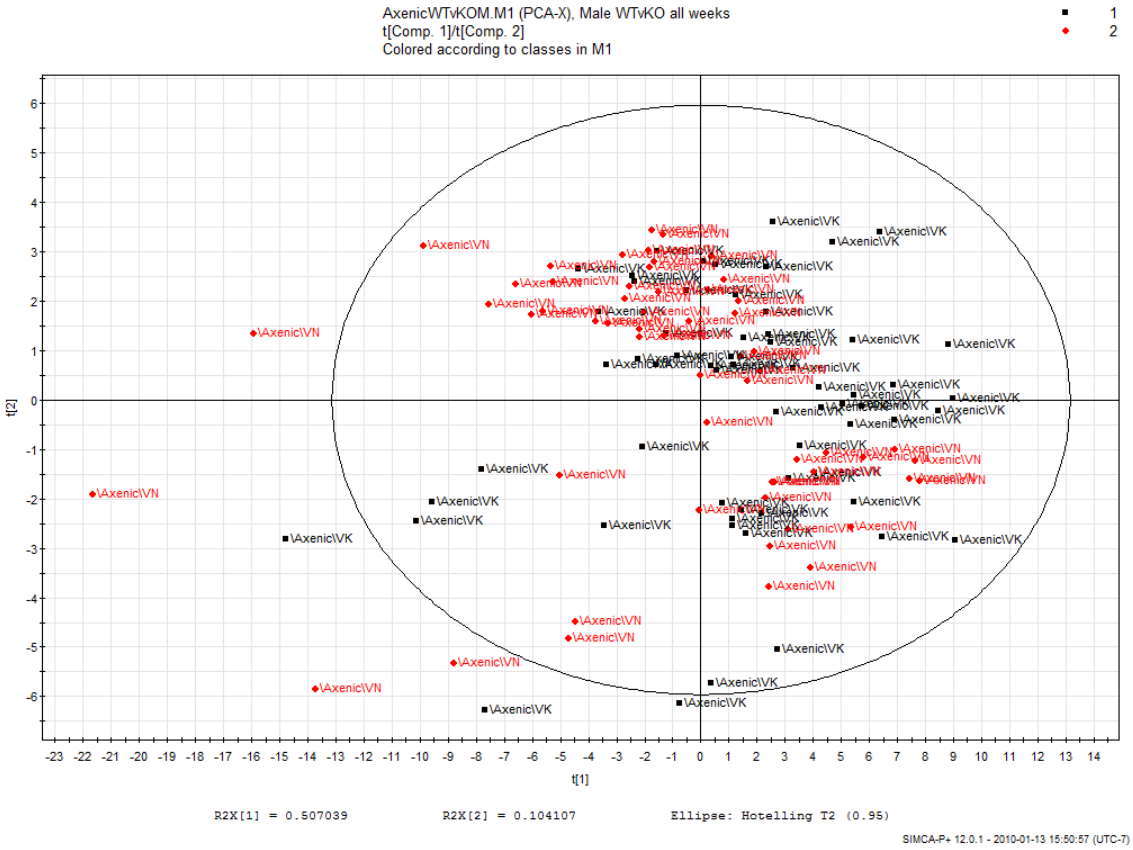

Fig 13 - PCA plot of the urine metabolomic profiles of all male wild-type and IL-10 KO axenic mice (urine collected from their axenic environments on weeks 4, 6, 8, 12, 16, and 20 of age). Each of the wild-type and IL-10 KO groups comprises 60 data points (10 points per week). Wild-type mice are shown in red and IL-10 KO mice are shown in black.

Week-by-week comparison referenced to week 4

comparison

Week 4

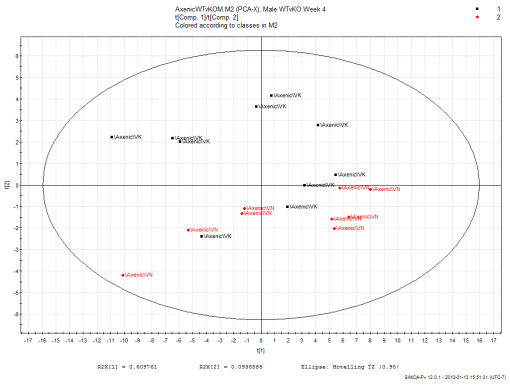

Week 6

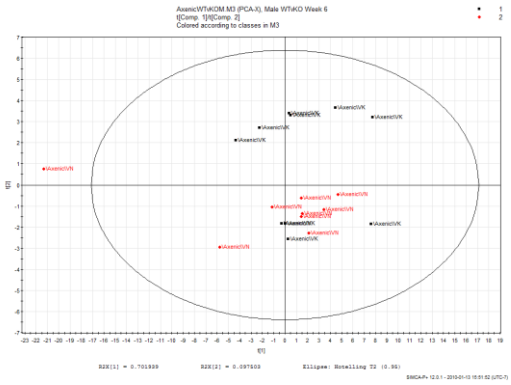

Week 8

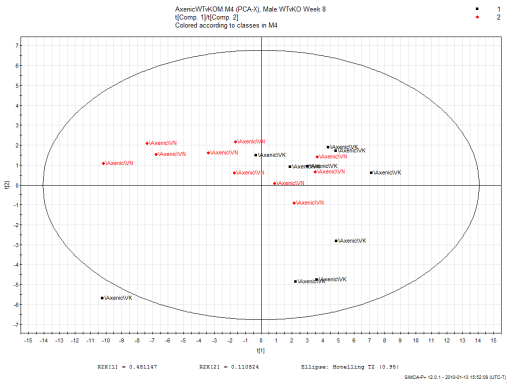

Week 12

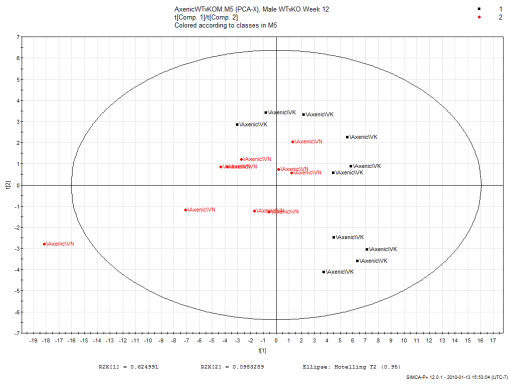

Week 16

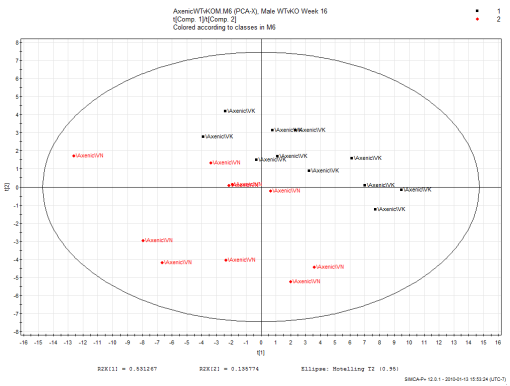

Week 20

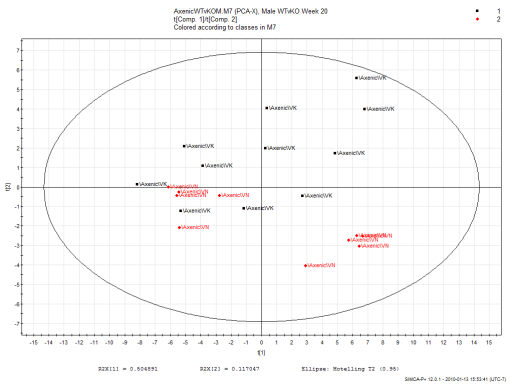

Fig. 14 – PCA plots of the urine metabolomic profiles of the axenic male wild-type and IL-10 KO mice broken up by weeks of urine collection; wild-type are displayed in red and IL-10 KO are displayed in black. Each week is composed of 10 wild-type and 10 IL-10 KO.

Female population

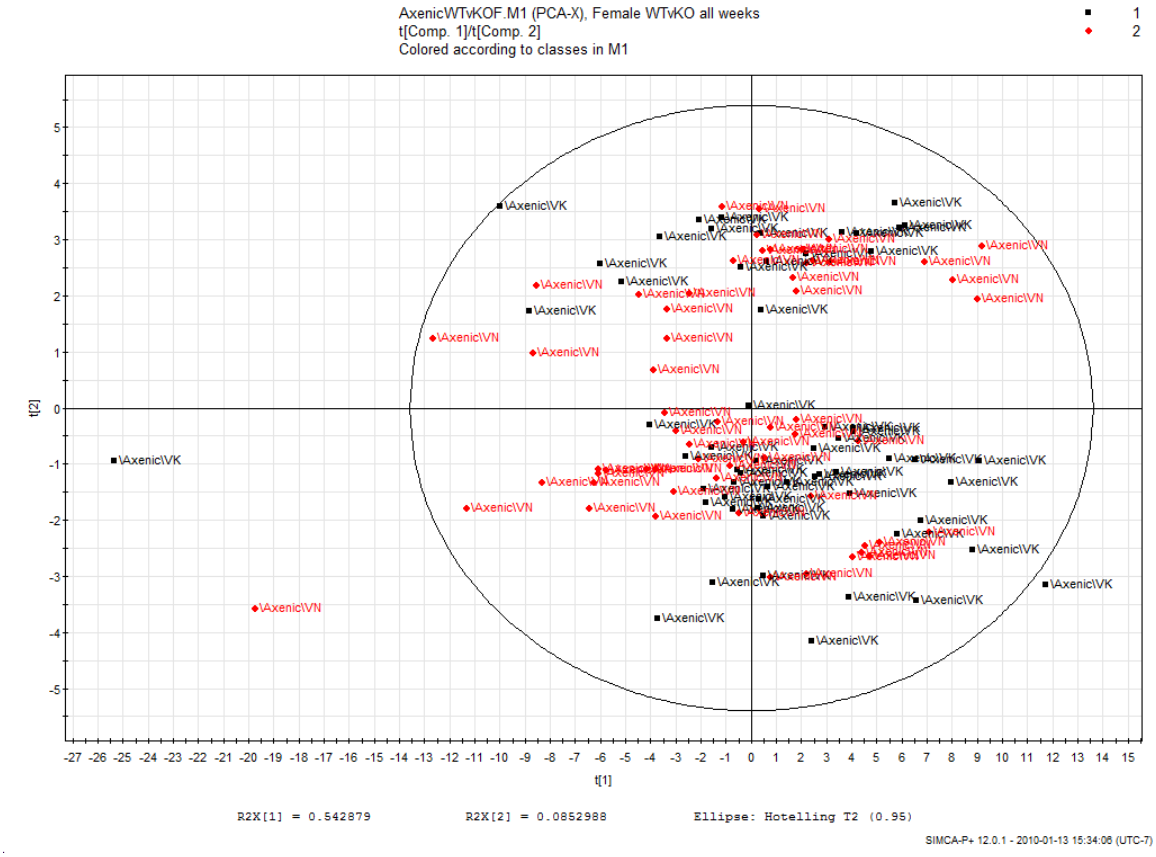

Fig 15 - PCA plot of the urine metabolomic profiles of all female wild-type and IL-10 KO axenic mice (urine collected from their axenic environments on weeks 4, 6, 8, 12, 16, and 20 of age). Each of the wild-type and IL-10 KO groups is composed of 60 data points (10 points per week). Wild-type mice are shown in red and IL 10 mice are shown in black.

Week-by-week comparison

Week 4

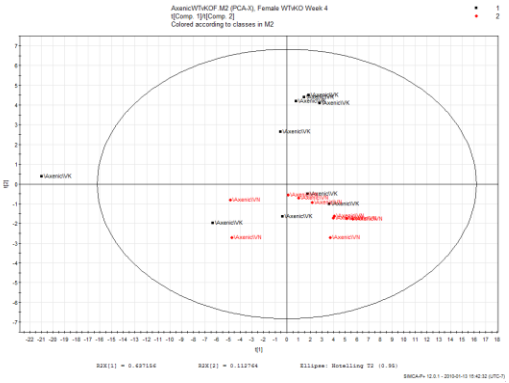

Week 6

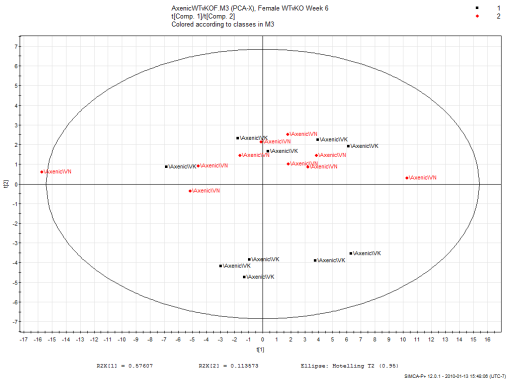

Week 8

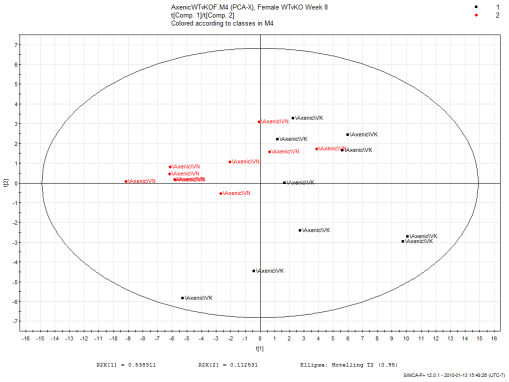

Week 12

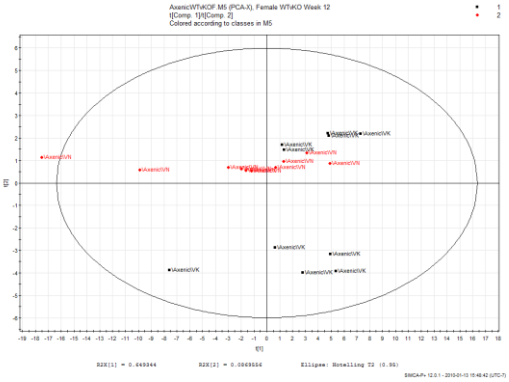

Week 16

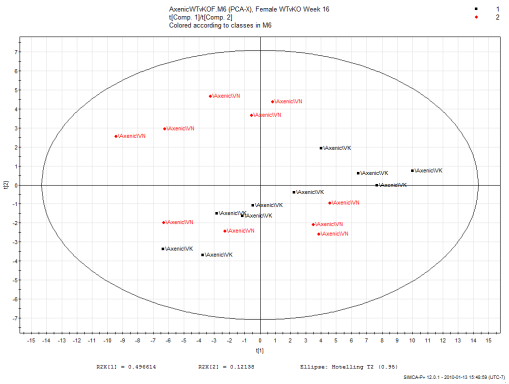

Week 20

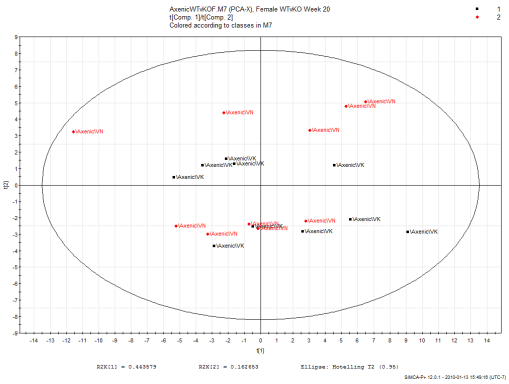

Fig. 16 – PCA plots of the urine metabolomic profiles of the axenic female wild-type and IL-10 KO mice broken up by week of urine collection; wild-type are displayed in red and IL-10 KO are displayed in black. Each week comprises 10 wild-type and 10 IL-10 KO.

Conventional Mice

Wild-type population

Wild-type population: comparison of male and female at various ages

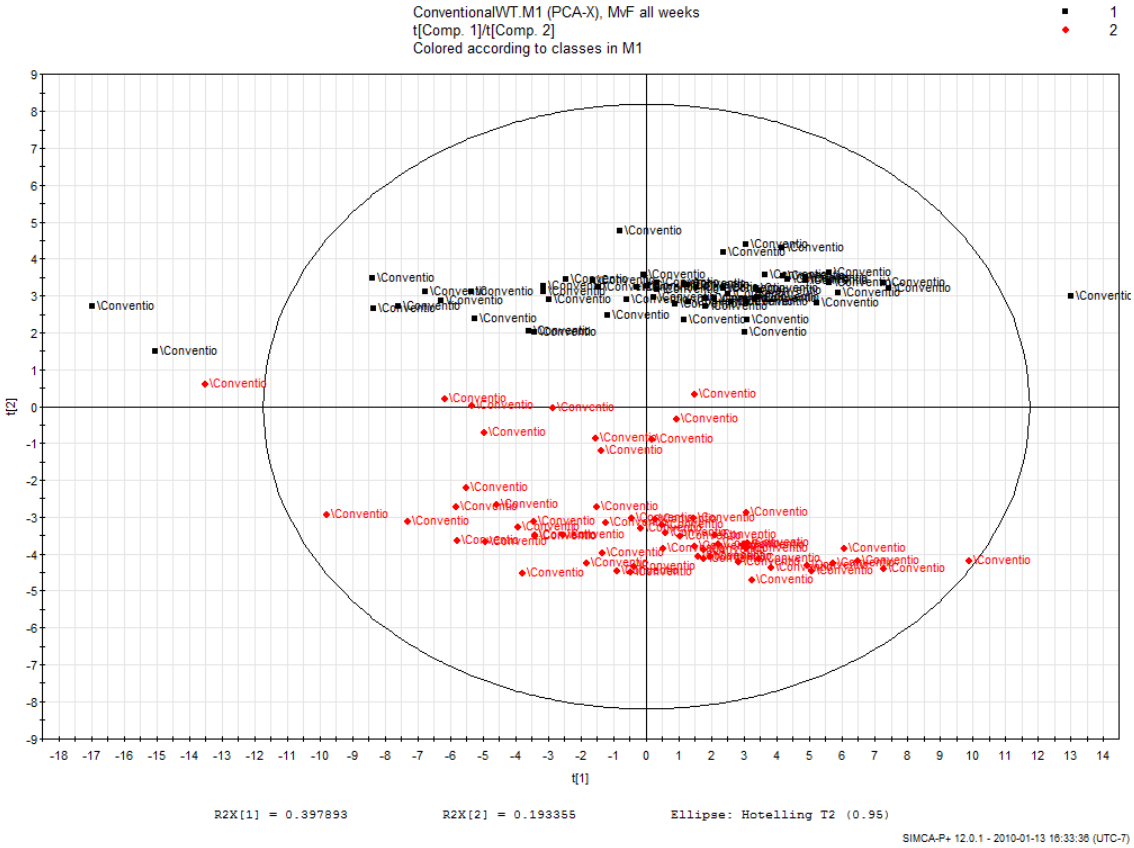

Fig. 17 – PCA plot of the urine metabolomic profiles of all male and female conventional wild-type mice (urine collected from their conventional environments on weeks 4, 6, 8, 12, 16, and 20 of age).Each of the male and female groups are composed of 60 data points (10 points per week). Male mice are shown in red and female mice are shown in black. Although a few outliers do appear, a clear separation between the two groups can be observed.

Week-by-week comparison

Week 4

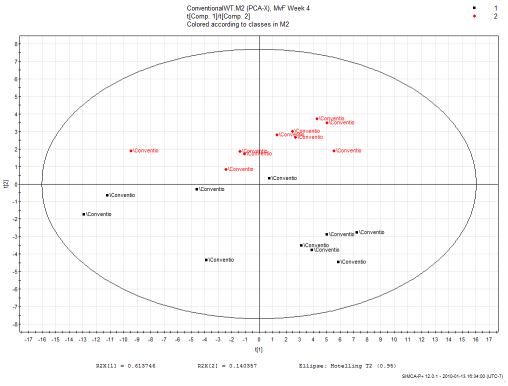

Week 6

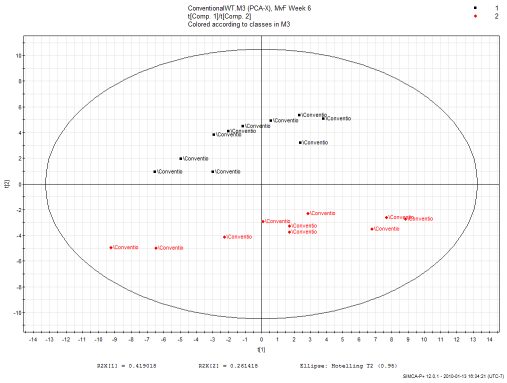

Week 8

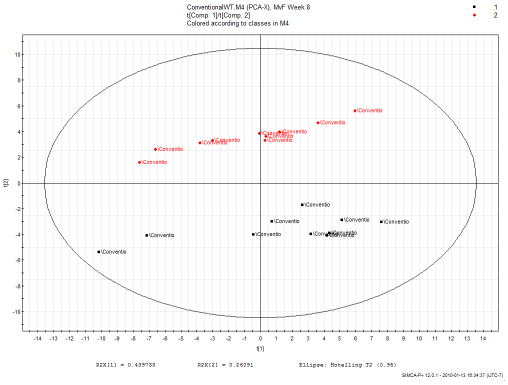

Week 12

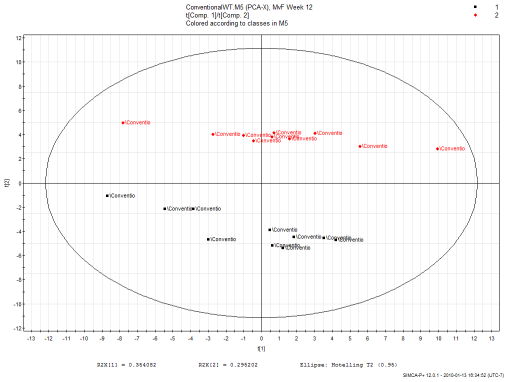

Week 16

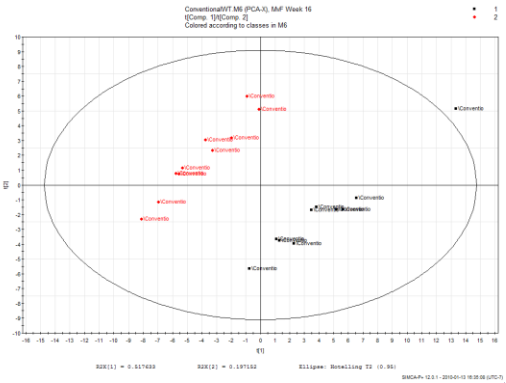

Week 20

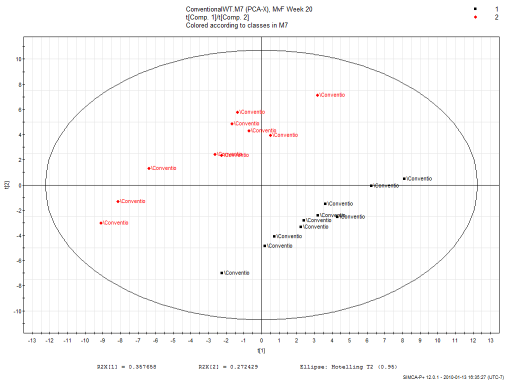

Fig. 18 – PCA plots of the urine metabolomic profiles of the conventional wild-type mice broken up by week of urine collection; males are displayed in red and females are displayed in black. Each week is composed of 10 males and 10 females.

Wild-type males: comparison of urine metabolomics over all collection weeks

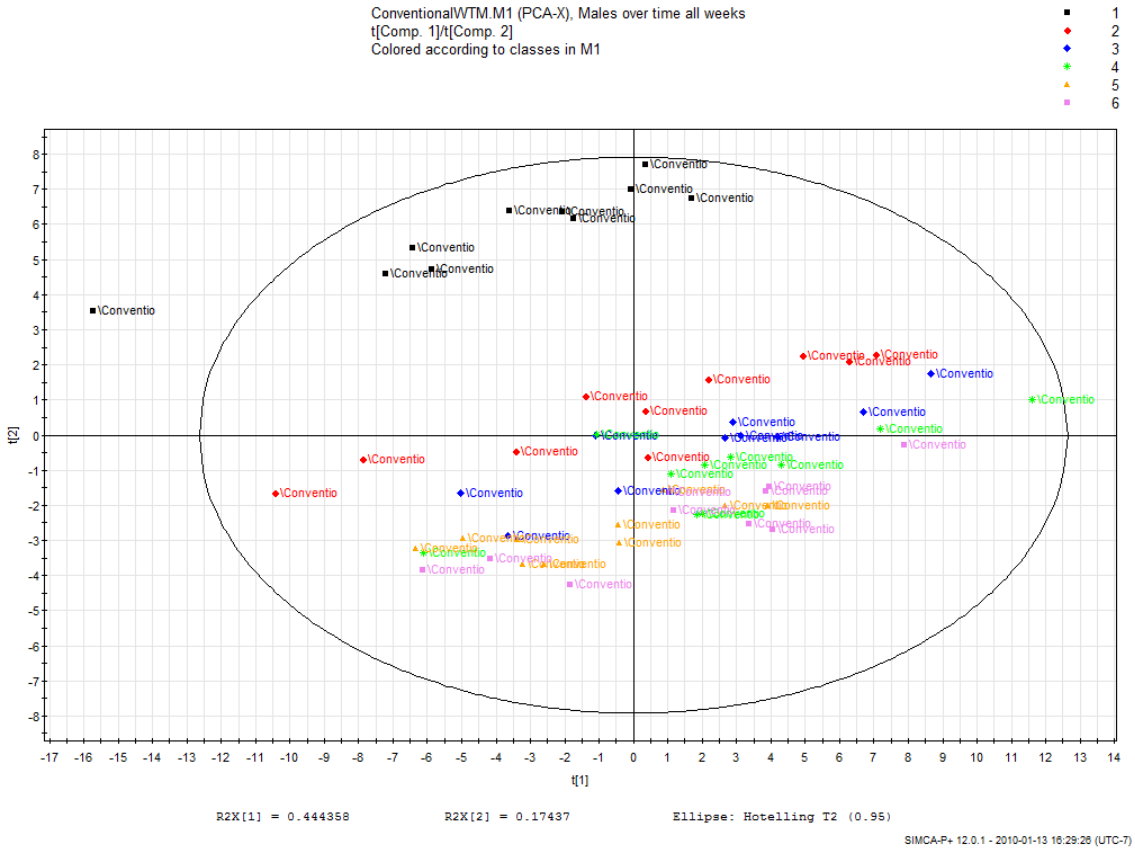

Fig. 19– PCA plot of urine metabolomics profiles of all wild-type male conventional mice over all collection time points. Each week is constructed from 10 points and is displayed in a different color: week 4 (black), week 6 (red), week 8 (blue), week 12 (green), week 16 (yellow), week 20 (purple). This plot shows the progression of the urine metabolomic profile of male wild-type mice as they grow in a conventional environment.

Reference to week 4 comparison

Week 4 vs. Week 6

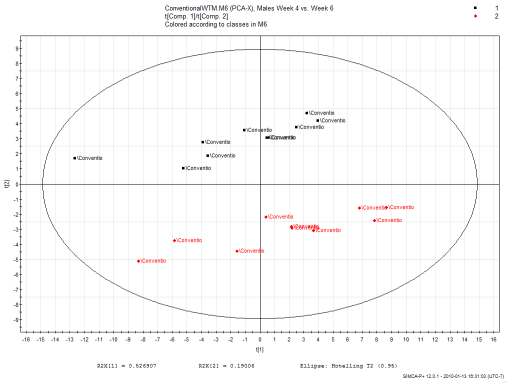

Week 4 vs. Week 8

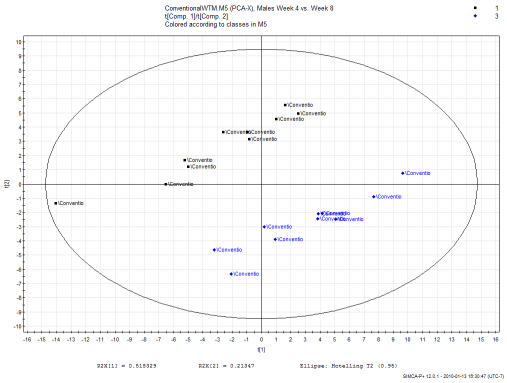

Week 4 vs. Week 12

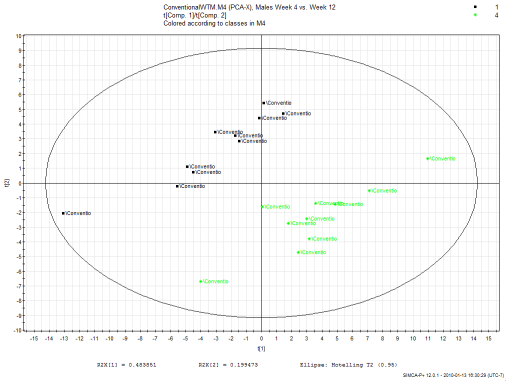

Week 4 vs. Week 16

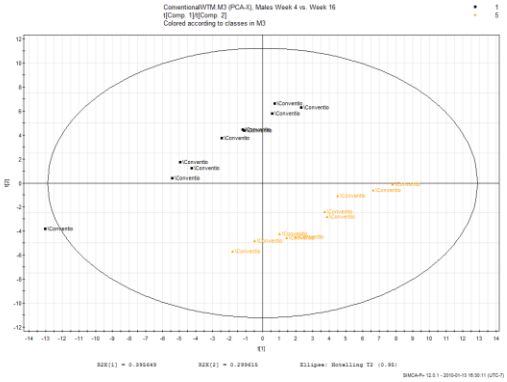

Week 4 vs. Week 20

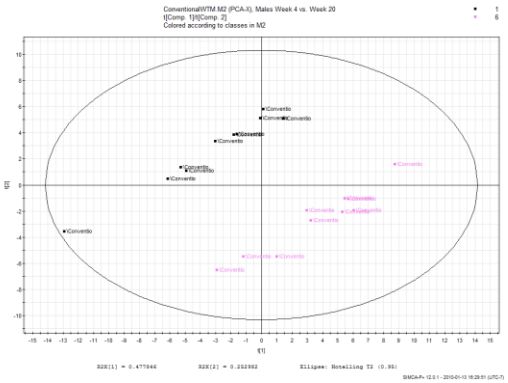

Fig. 20 – PCA plot of urine metabolomics profiles of wild-type male conventional mice in reference to week 4; each group is composed of the same 10 mice from week 4 and is referenced against the other groups of 10 mice that comprise the other weeks collected.

Wild-type females: comparison of urine metabolomics over all collection weeks

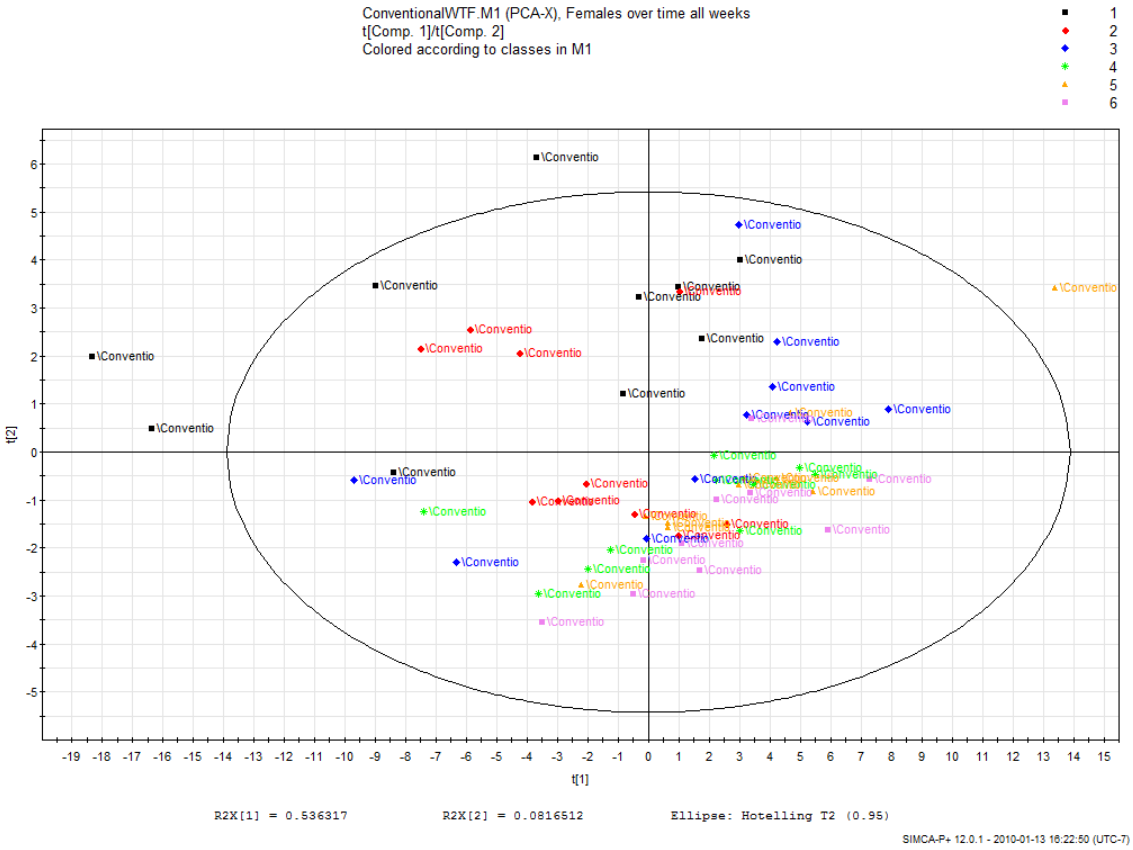

Fig. 21– PCA plot of urine metabolomic profiles of all wild-type female conventional mice over all collection time points. Each week is constructed from 10 points and is displayed in a different color: week 4 (black), week 6 (red), week 8 (blue), week 12 (green), week 16 (yellow), week 20 (purple). This plot shows the progression of the urine metabolomic profile of male wild-type mice as they grow in a conventional environment.

Reference to week 4 comparison

Week 4 vs. Week 6

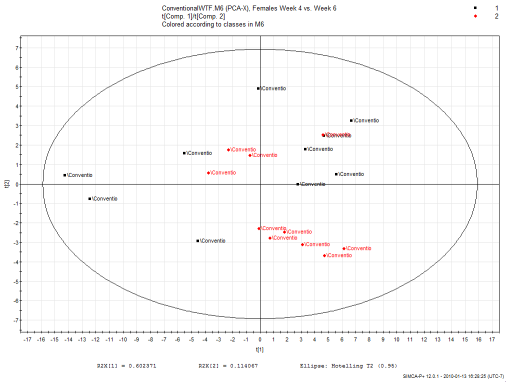

Week 4 vs. Week 8

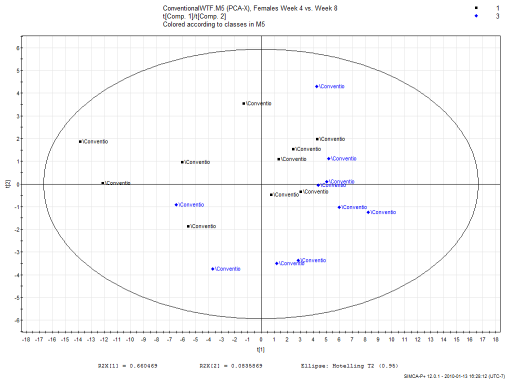

Week 4 vs. Week 12

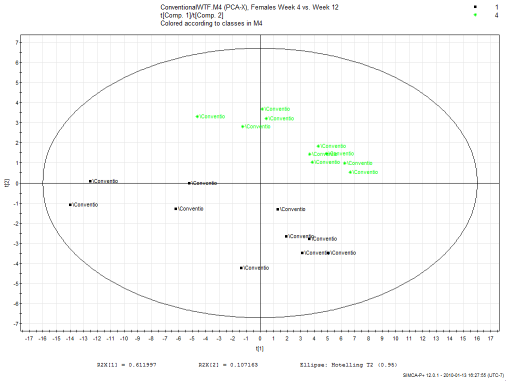

Week 4 vs. Week 16

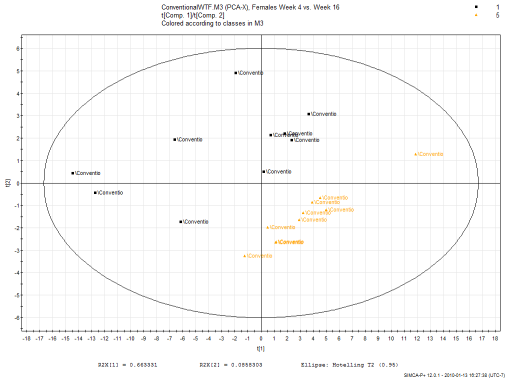

Week 4 vs. Week 20

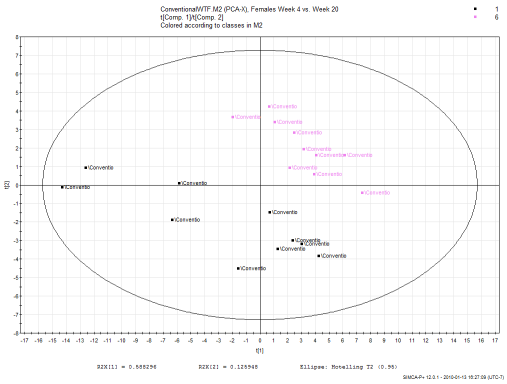

Fig. 22 – PCA plots of urine metabolomics profiles of wild-type female conventional mice referenced to week 4; each group is comprised of the same 10 mice from week 4 and is referenced against the other groups of 10 mice that comprise the other weeks collected.

IL-10 KO population

IL-10 KO population: comparison of male and female at various ages

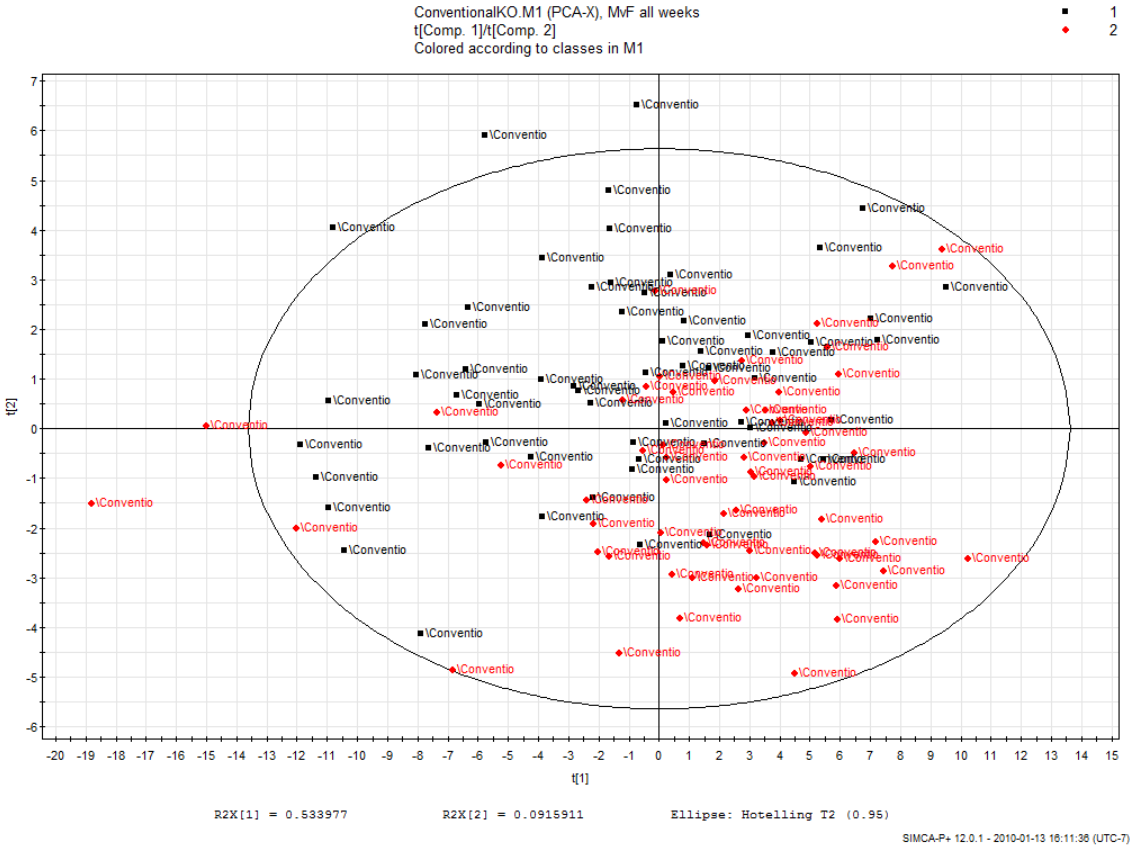

Fig. 23 – PCA plot of the urine metabolomic profiles of all male and female conventional IL-10 KO mice (urine collected from their conventional environments on weeks 4, 6, 8, 12, 16, and 20 of age). Each of the male and female groups are composed of 60 data points (10 points per week). Male mice are shown in red and female mice are shown in black.

Week-by-week comparison

Week 4

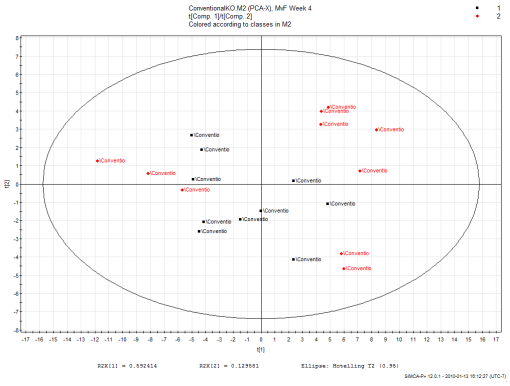

Week 6

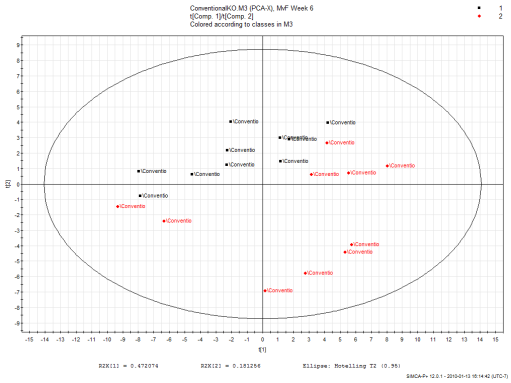

Week 8

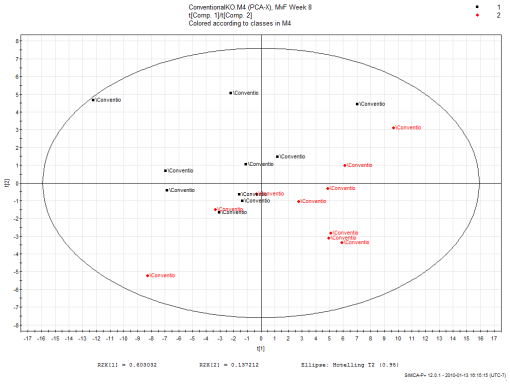

Week 12

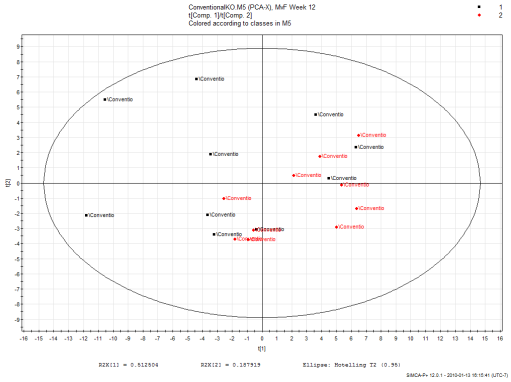

Week 16

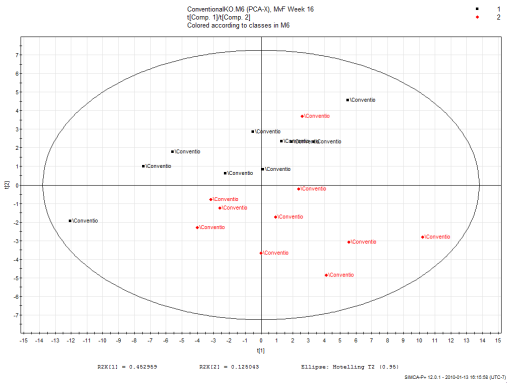

Week 20

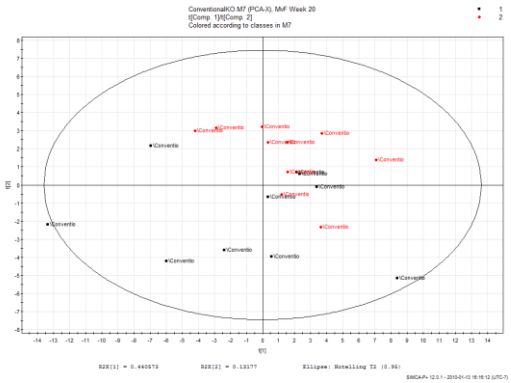

Fig. 24 – PCA plots of the urine metabolomic profiles of the conventional IL-10 KO mice broken up by week of urine collection; males are displayed in red and females are displayed in black. Each week comprises 10 males and 10 females.

IL-10 KO males: comparison of urine metabolomics over all collection weeks

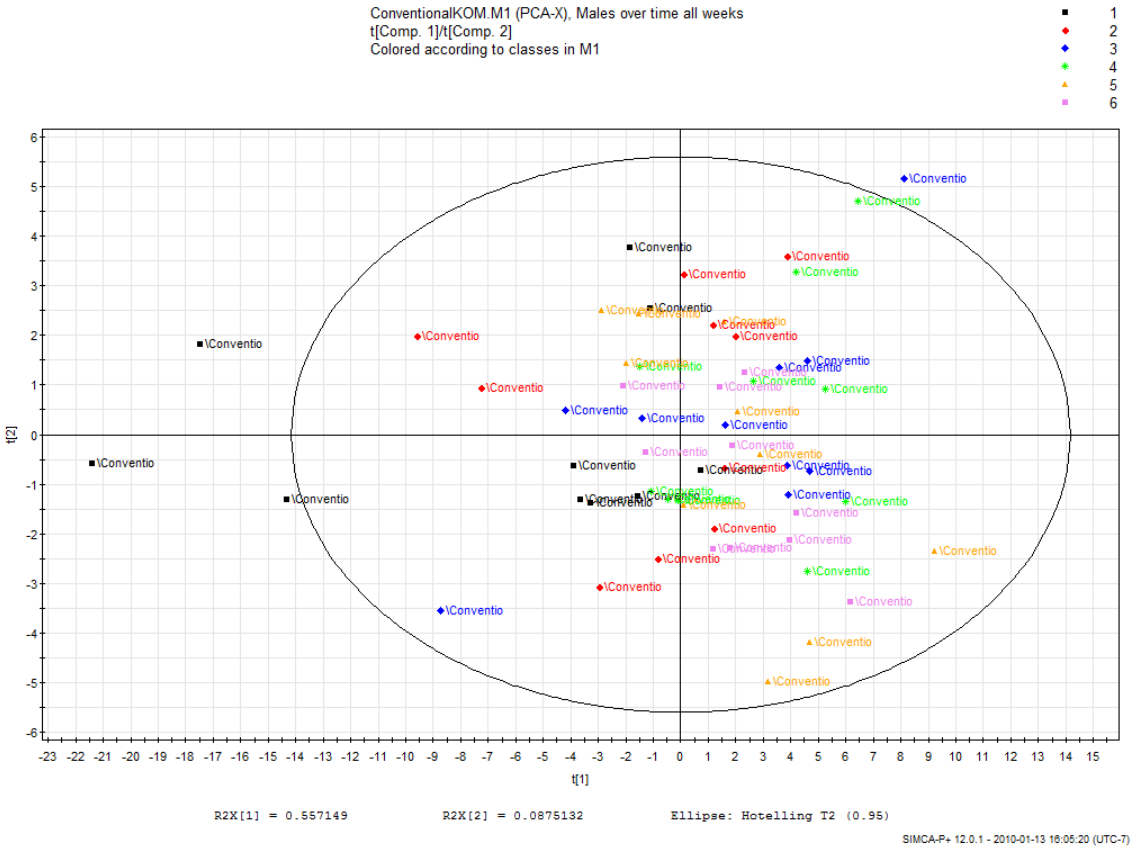

Fig. 25– PCA plot of urine metabolomic profiles of all IL-10 KO male conventional mice over all collection time-points. Each week is constructed from 10 points and is displayed in a different color: week 4 (black), week 6 (red), week 8 (blue), week 12 (green), week 16 (yellow), week 20 (purple). This plot shows the progression of the urine metabolomic profile of male wild-type mice as they grow in a conventional environment.

Reference to week 4 comparison

Week 4 vs. Week 6

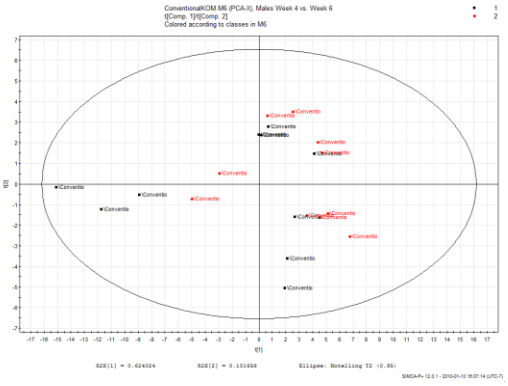

Week 4 vs. Week 8

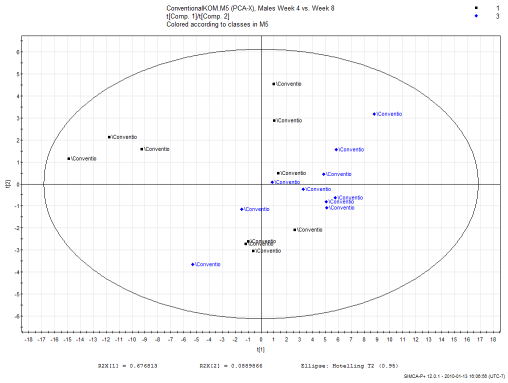

Week 4 vs. Week 12

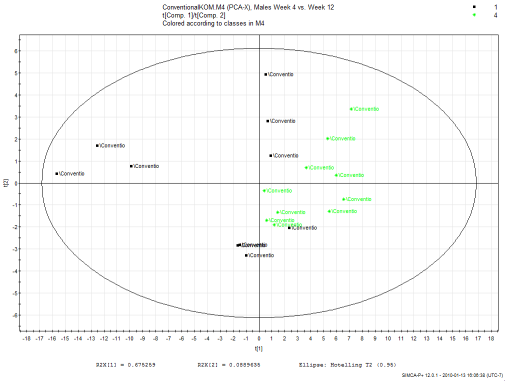

Week 4 vs. Week 16

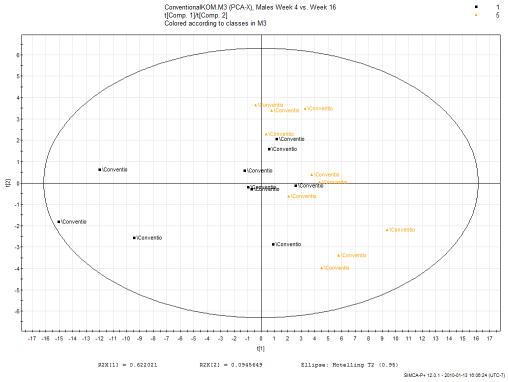

Week 4 vs. Week 20

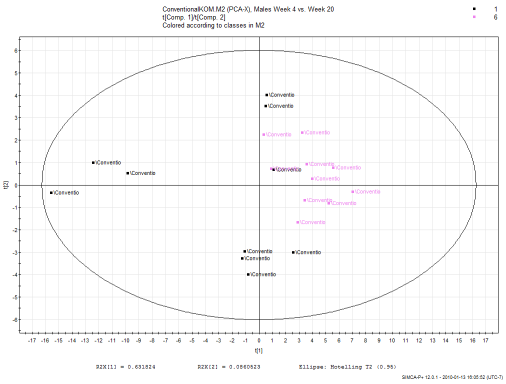

Fig. 26 – PCA plots of urine metabolomic profiles of IL-10 KO male conventional mice referenced to week 4; each group is composed of the same 10 mice from week 4 and is referenced against the other groups of 10 mice that comprise the other weeks collected.

IL-10 KO females: comparison of urine metabolomics over all collection weeks

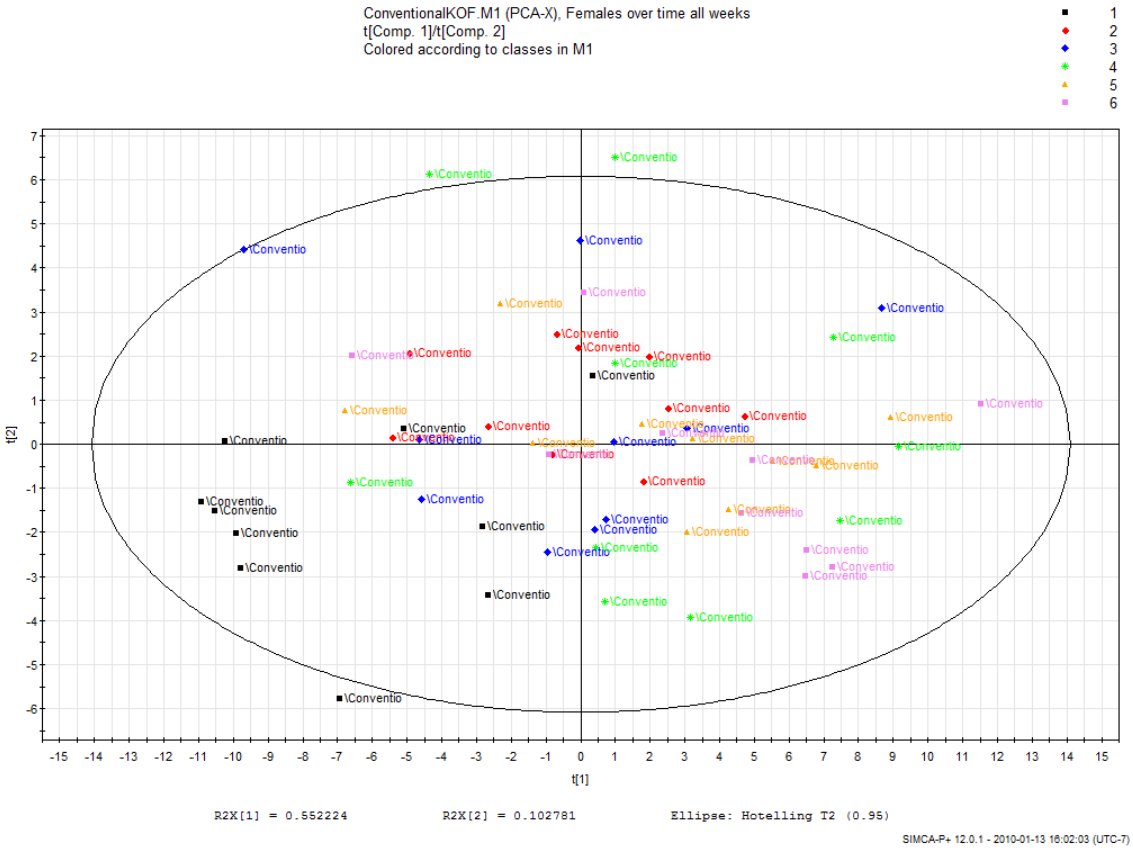

Fig. 27– PCA plot of urine metabolomic profiles of all IL-10 KO female conventional mice over all collection time-points. Each week is constructed from 10 points and is displayed in a different color: week 4 (black), week 6 (red), week 8 (blue), week 12 (green), week 16 (yellow), week 20 (purple). This plot shows the progression of the urine metabolomic profile of female wild-type mice as they grow in a conventional environment.

Reference to week 4 comparison

Week 4 vs. Week 6

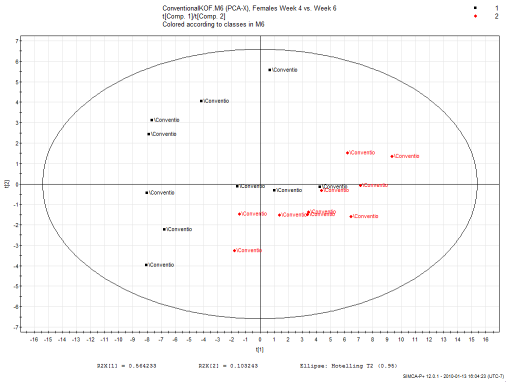

Week 4 vs. Week 8

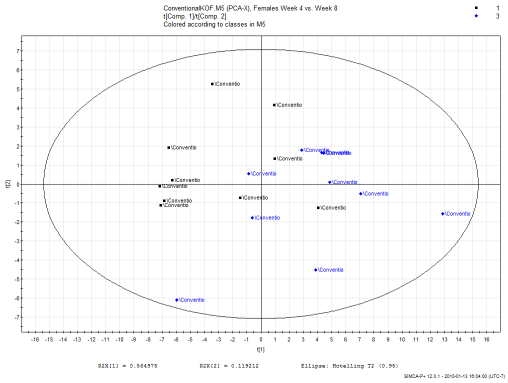

Week 4 vs. Week 12

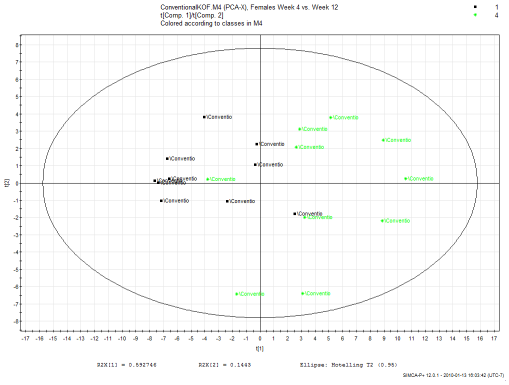

Week 4 vs. Week 16

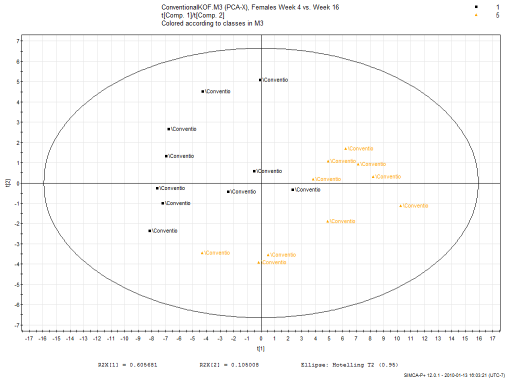

Week 4 vs. Week 20

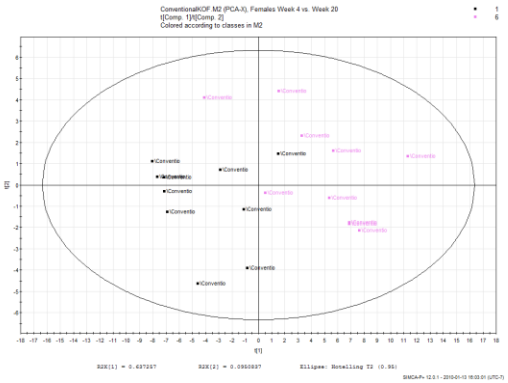

Fig. 28 – PCA plots of urine metabolomic profiles of IL-10 KO female conventional mice referenced to week 4; each group is composed of the same 10 mice from week 4 and is referenced against the other groups of 10 mice that comprise the other weeks collected.

Wild-type vs. IL-10 KO: comparison of conventional WT vs. IL-10 KO mice

Male population

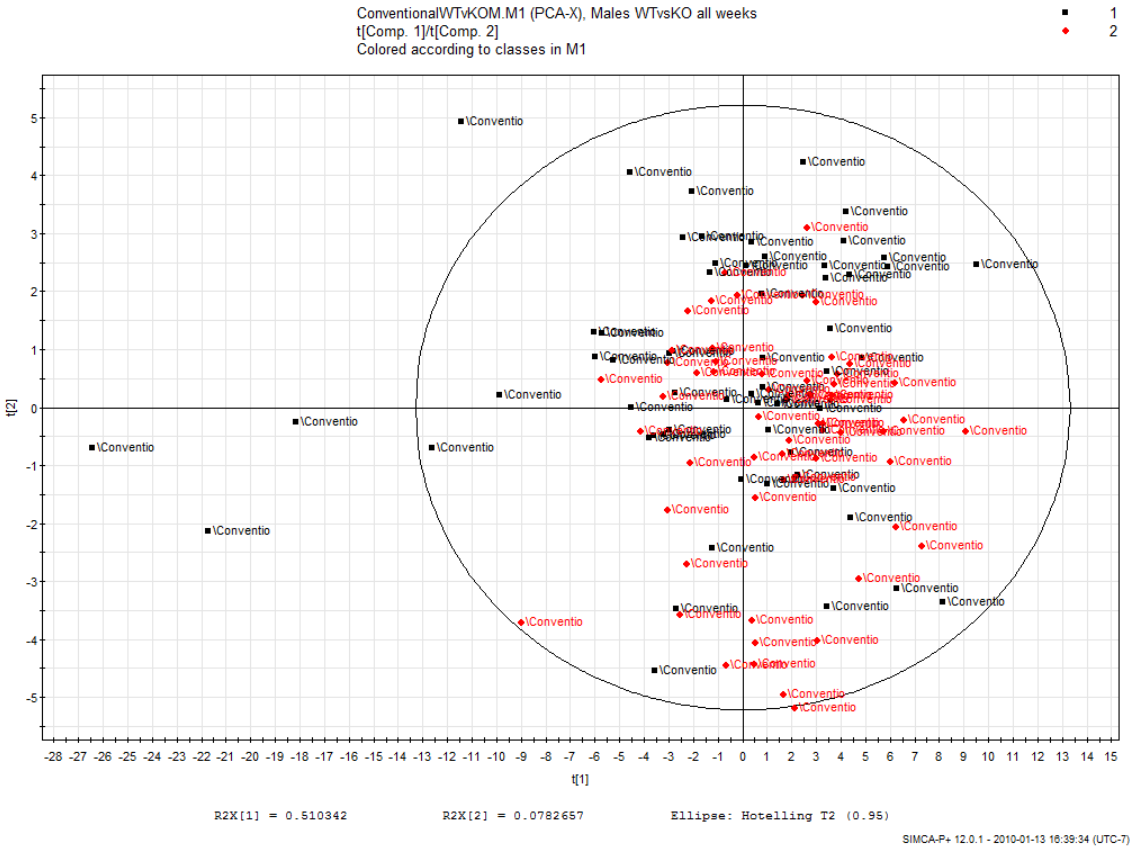

Fig 29 - PCA plot of the urine metabolomic profiles of all male wild-type and IL-10 KO conventional mice collected in their conventional environments on weeks 4, 6, 8, 12, 16 and 20 of age. Both the wild-type and IL-10 KO groups are comprised of 60 data points (10 points per week). Wild-type mice are shown in red and IL-10 KO mice are shown in black.

Week-by-week comparison

Week 4 Week 6

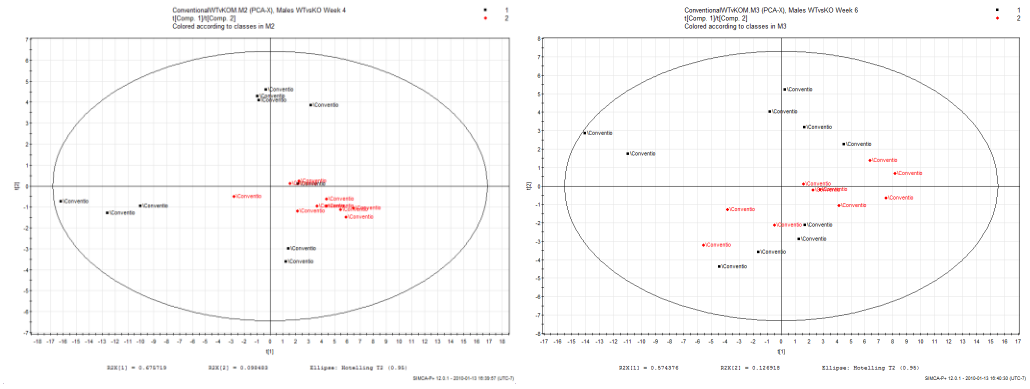

Week 8 Week 12

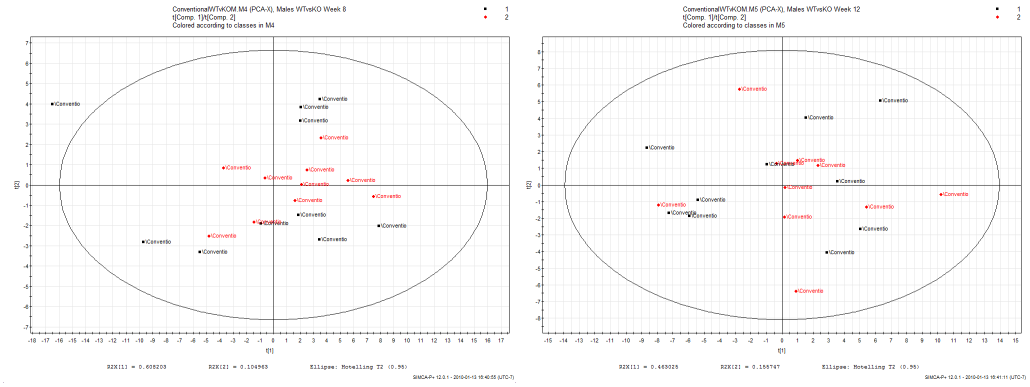

Week 16 Week 20

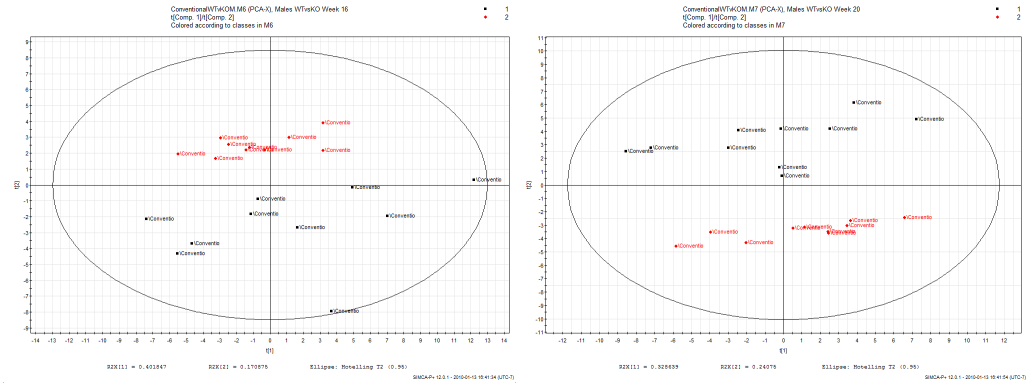

Fig. 30 – PCA plots of the urine metabolomic profiles of the conventional male wild-type and IL-10 KO mice broken up by weeks of urine collection; wild-type are displayed in red and IL-10 KO are displayed in black. Each week is composed of 10 wild-type and 10 IL-10 KO.

Female population

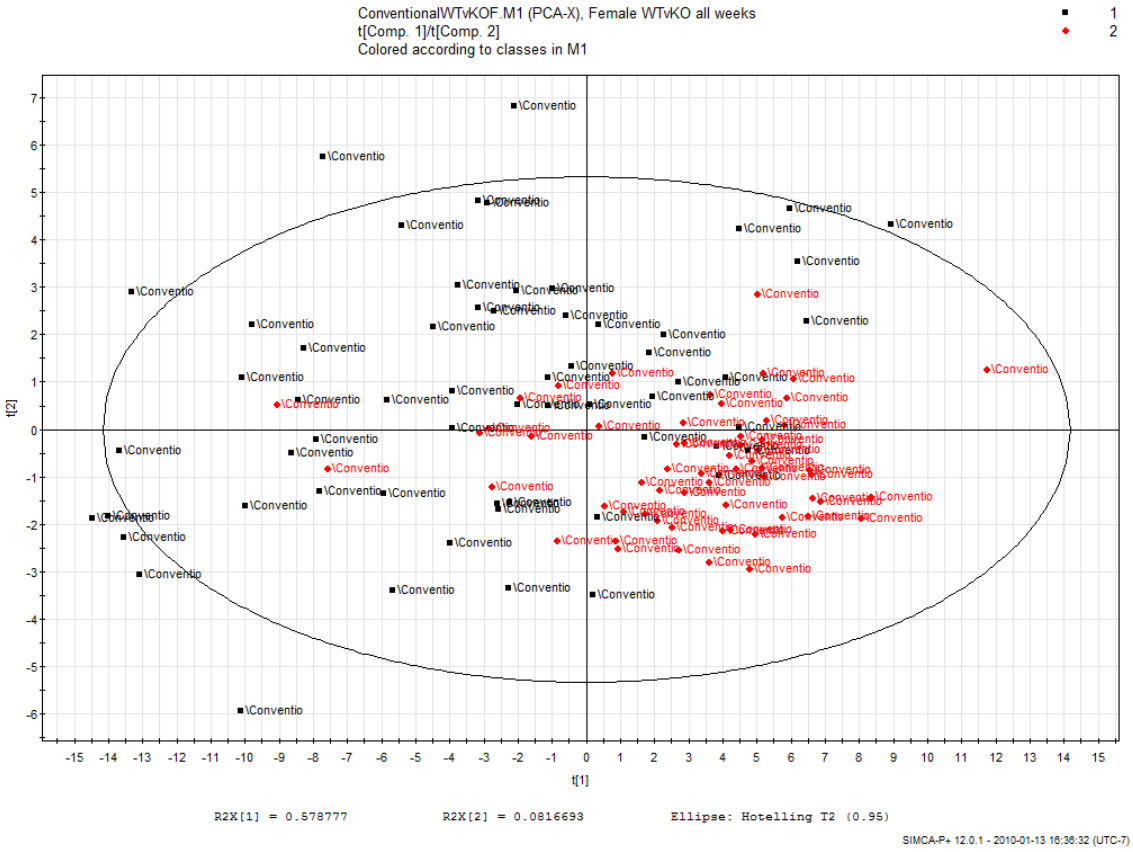

Fig 31 - PCA plot of the urine metabolomic profiles of all female wild-type and IL-10 KO conventional mice (urine collected in their conventional environments on weeks 4, 6, 8, 12, 16, and 20 of age). Each of the wild-type and IL-10 KO groups comprises 60 data points (10 points per week). Wild-type mice are shown in red and IL-10 KO mice are shown in black.

Week-by-week comparison

Week 4

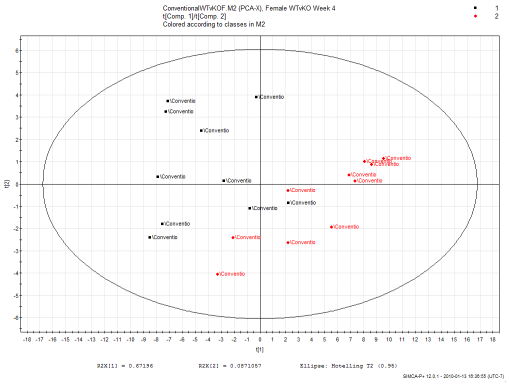

Week 6

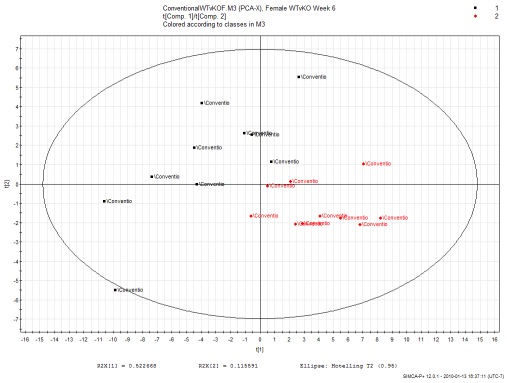

Week 8

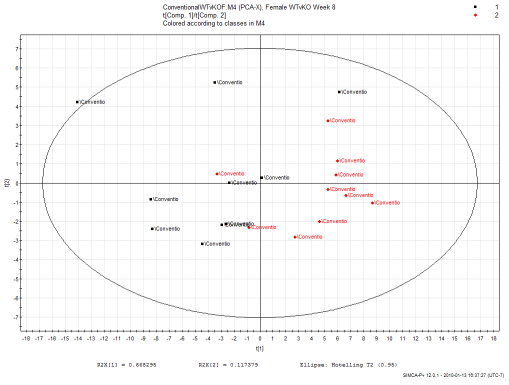

Week 12

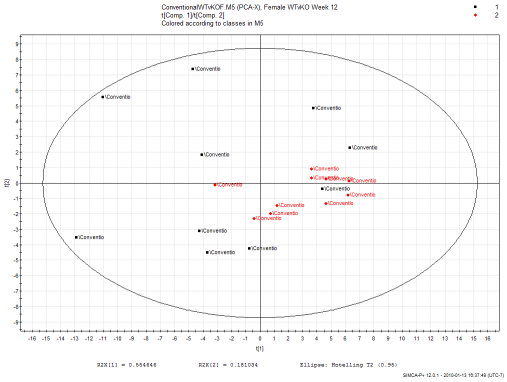

Week 16

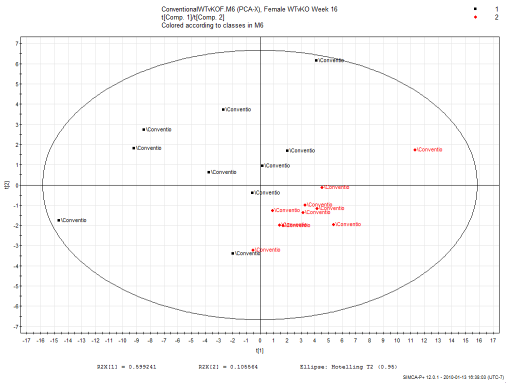

Week 20

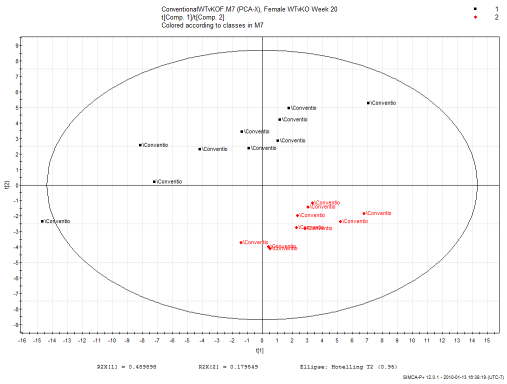

Fig. 32 – PCA plots of the urine metabolomic profiles of the conventional female wild-type and IL-10 KO mice broken up by week of urine collection,;wild-type are displayed in red

and IL-10 KO are displayed in black. Each week is composed of 10 wild-type and 10 IL-10 KO.

Fecal Colonization

Wild-type population

Male: comparison of axenic mice and mice colonized with fecal bacteria

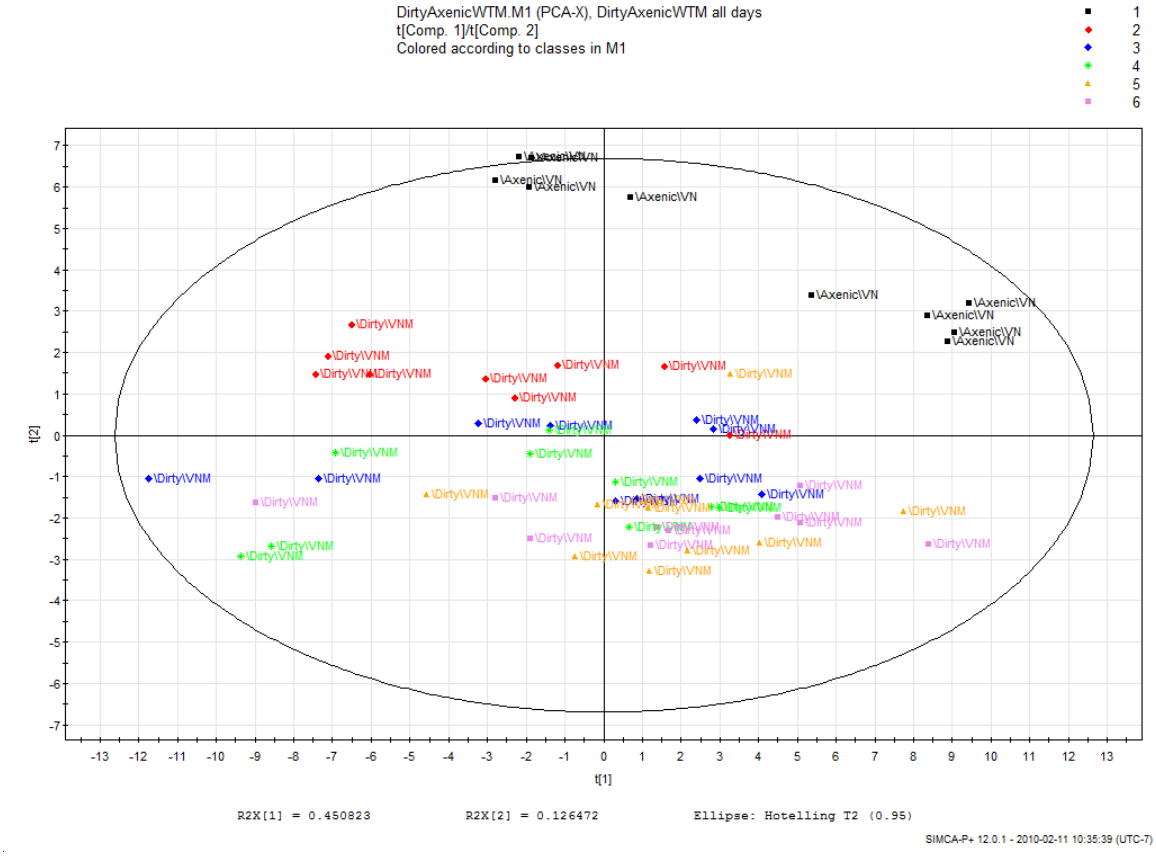

Fig 33 – PCA of week-20 male wild-type axenic mice along with fecal bacteria-colonized mice on days 1-4 and 7 post-colonization. Axenic mice are displayed in black, day 1 in red, day 2 in blue, day 3 in green, day 4 in yellow, and day 7 in pink.

Reference to 20-week axenic

Axenic vs. Day 1

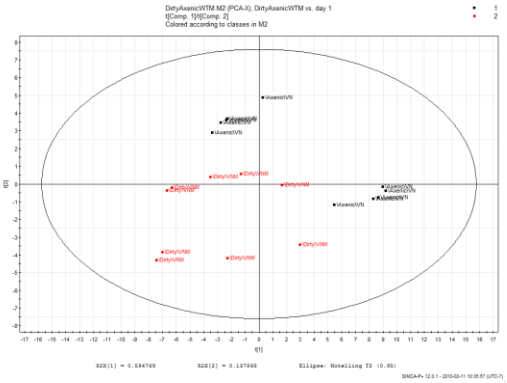

Axenic vs. Day 2

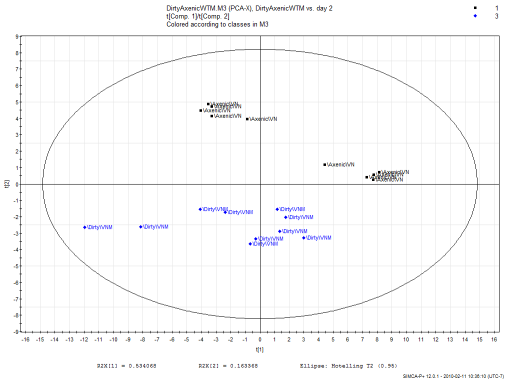

Axenic vs. Day 3

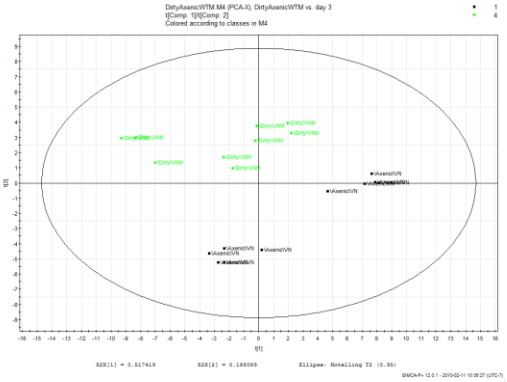

Axenic vs. Day 4

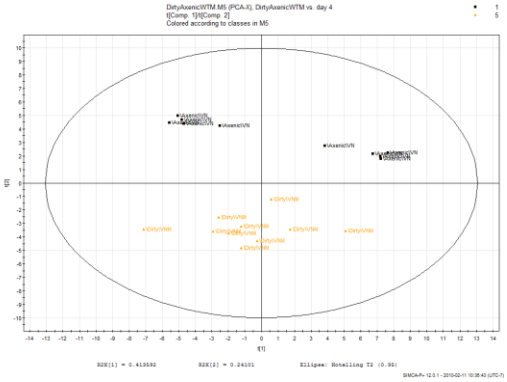

Axenic vs. Day 7

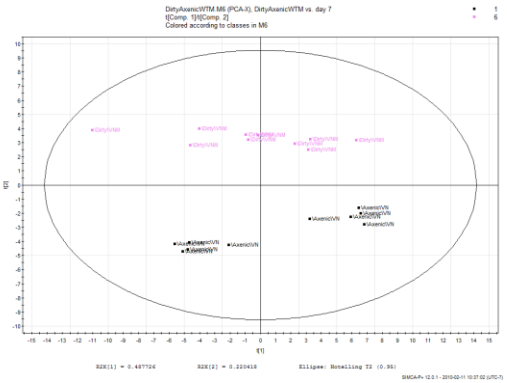

Fig 34 – Day-by-day analysis of male wild-type mice that were colonized with fecal bacteria referenced to 20-week axenic mice; each plot is constructed using 10 axenic

mice and 10 mice that had their urine collected during the indicated day after colonization.

Female: comparison of axenic mice and mice colonized with fecal bacteria

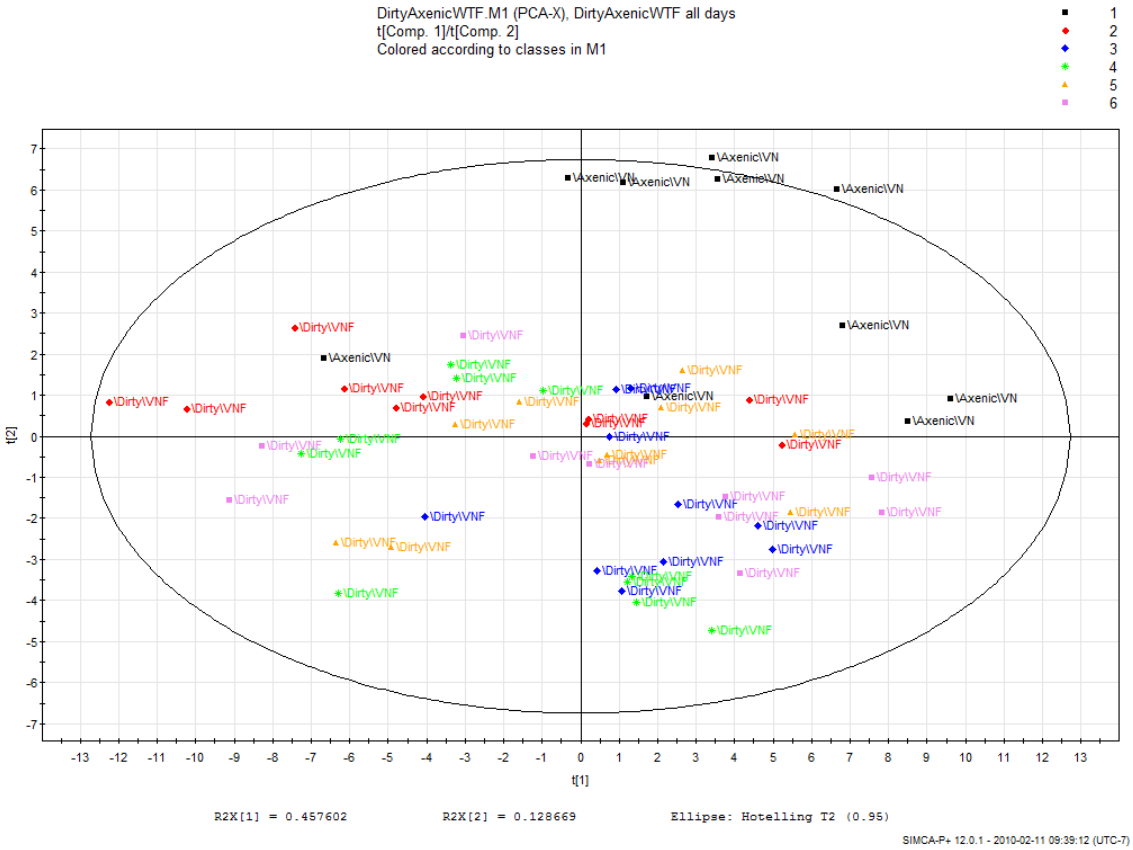

Fig 35 – PCA of week 20 female wild-type axenic mice along with fecal bacteria-colonized mice on days 1-4 and 7 post-colonization. Axenic mice are displayed in black, day 1 in red, day 2 in blue, day 3 in green, day 4 in yellow, and day 7 in pink.

Reference to 20-week axenic

Axenic vs. Day 1

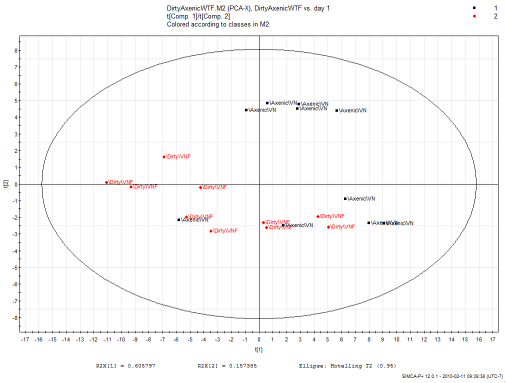

Axenic vs. Day 2

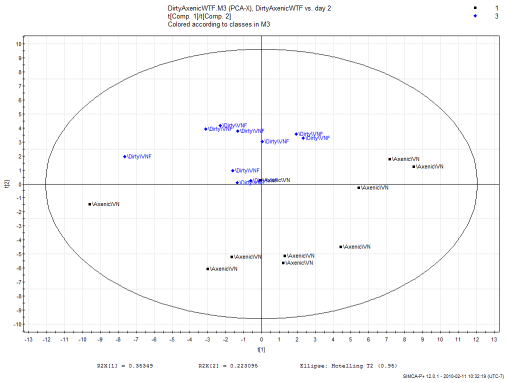

Axenic vs. Day 3

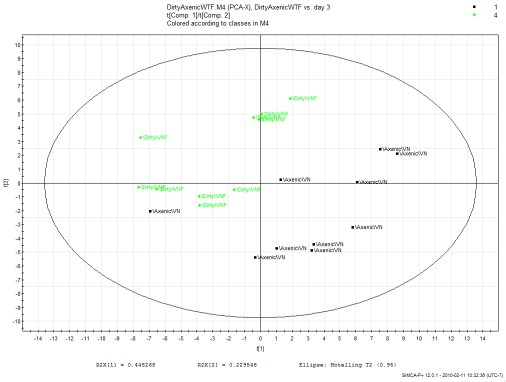

Axenic vs. Day 4

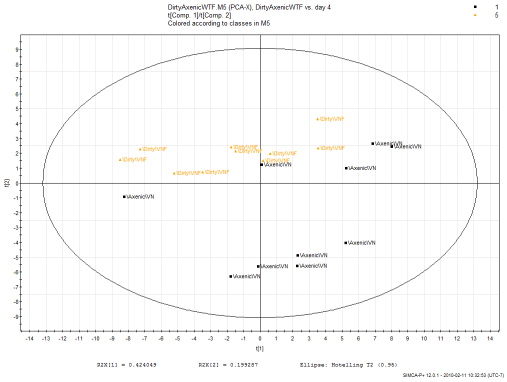

Axenic vs. Day 7

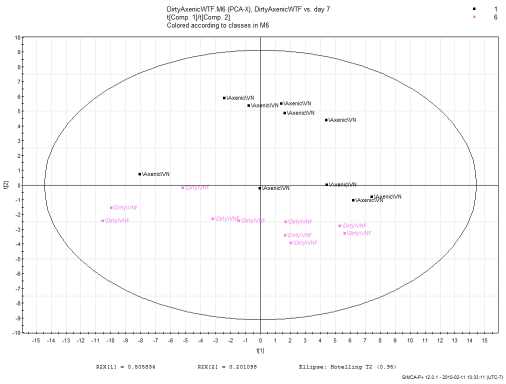

Fig 36 – Day by day analysis of female wild-type mice colonized with fecal bacteria referenced to 20-week axenic mice; each plot is constructed from 10 axenic mice and 10 mice that had their urine collected during the indicated day after colonization.

IL-10 KO population

Male: comparison of axenic mice and mice colonized with fecal bacteria

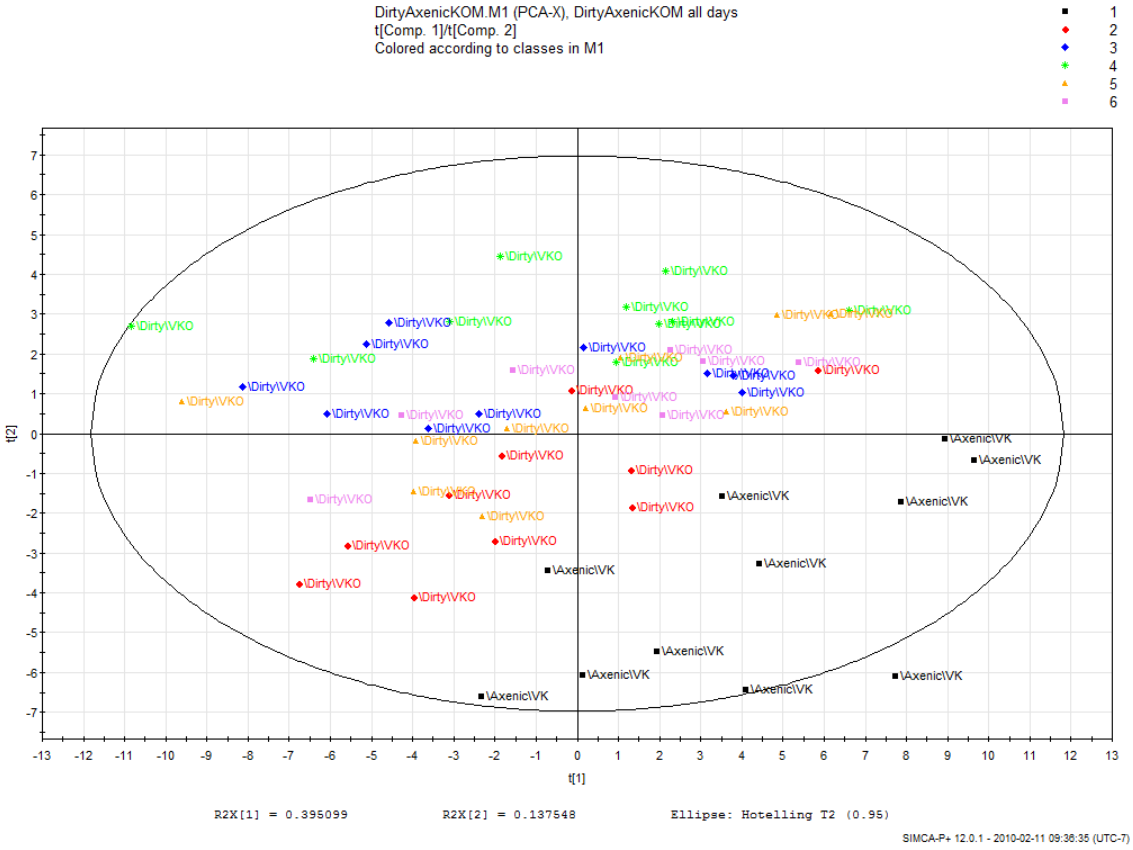

Fig 37 – PCA of week 20 male IL-10 KO axenic mice along with fecal bacteria-colonized mice on days 1-4 and 7 post-colonization. Axenic mice are displayed in black, day 1 in red, day 2 in blue, day 3 in green, day 4 in yellow, and day 7 in pink.

Reference to 20-week axenic

Axenic vs. Day 1

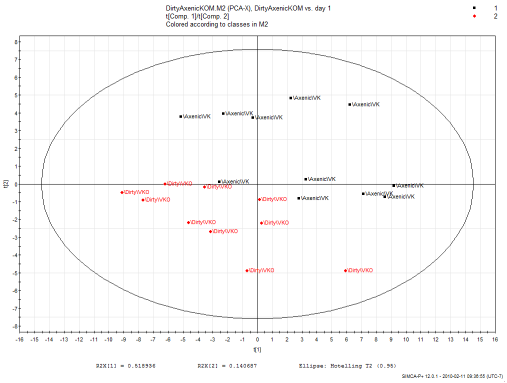

Axenic vs. Day 2

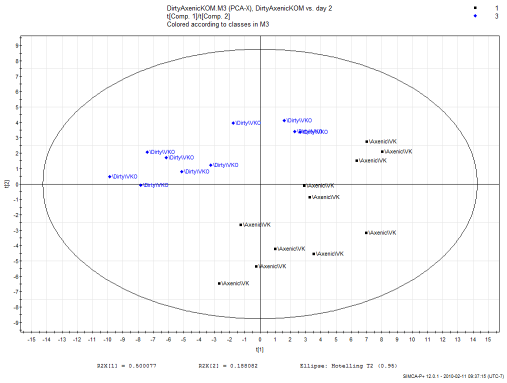

Axenic vs. Day 3

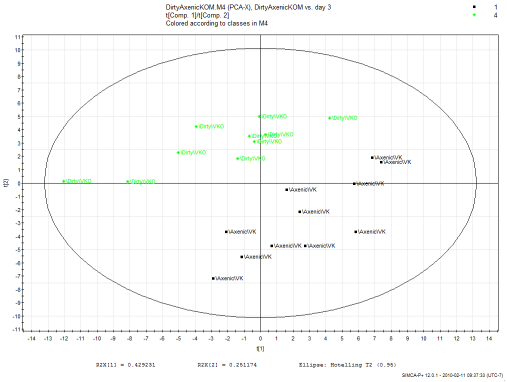

Axenic vs. Day 4

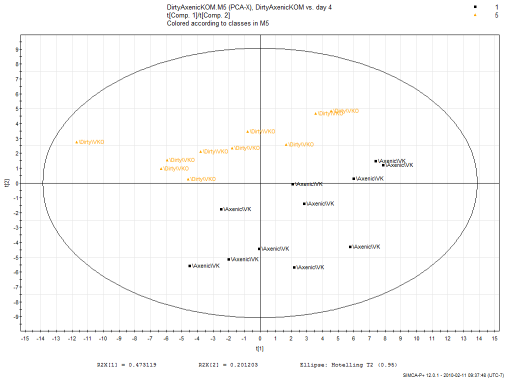

Axenic vs. Day 7

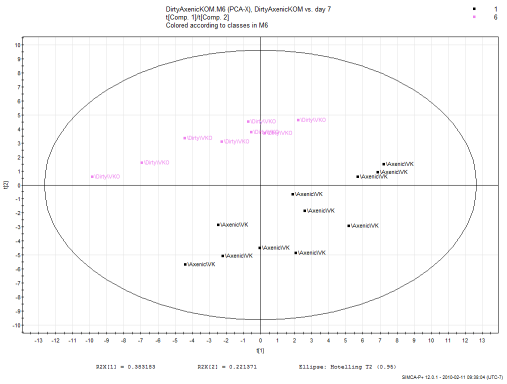

Fig 38 – Day-by-day analysis of male IL-10 KO mice that were colonized with fecal bacteria referenced to 20-week axenic mice; each plot is constructed using 10 axenic

mice and 10 mice that had their urine collected during the indicated day after colonization.

Female: comparison of axenic mice and mice colonized with fecal bacteria

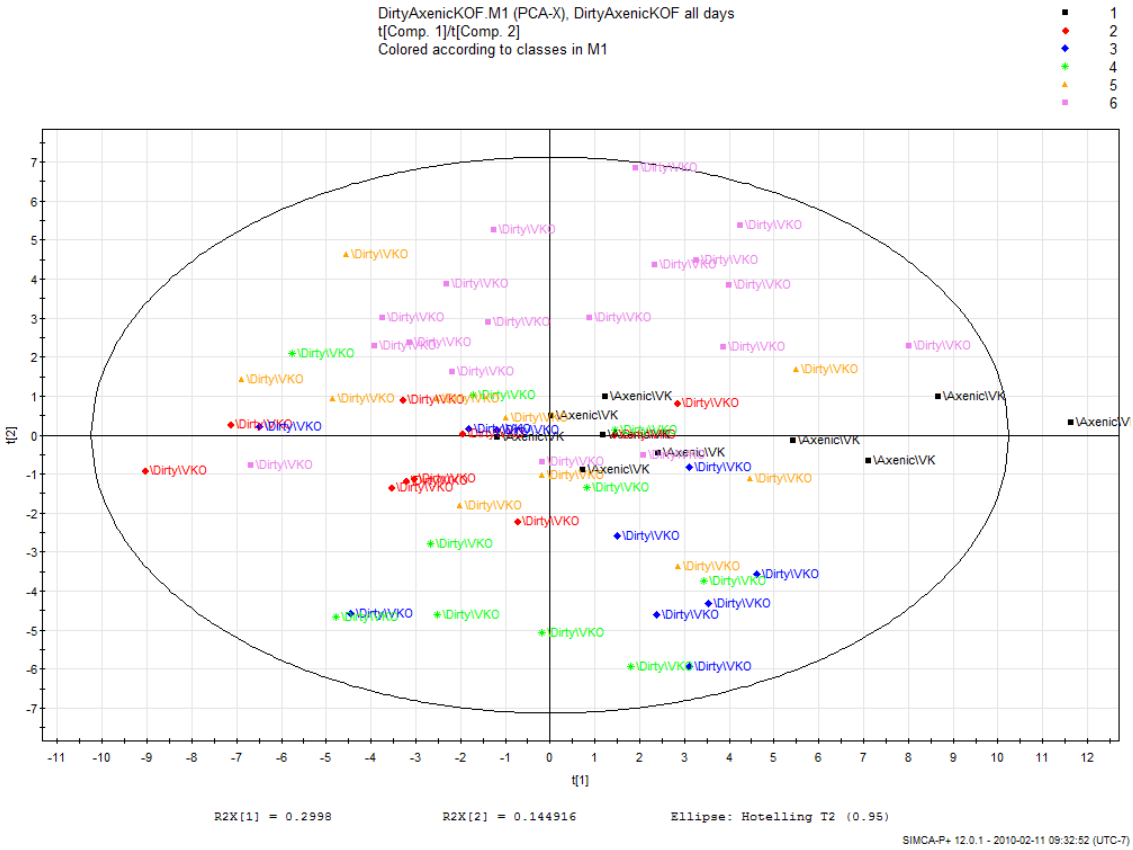

Fig 39 – PCA of week-20 female IL-10 KO axenic mice along with fecal bacteria-colonized mice on days 1-4 and 7 post-colonization. Axenic mice are displayed in black, day 1 in red, day 2 in blue, day 3 in green, day 4 in yellow, and day 7 in pink.

Reference to 20week axenic

Axenic vs. Day 1

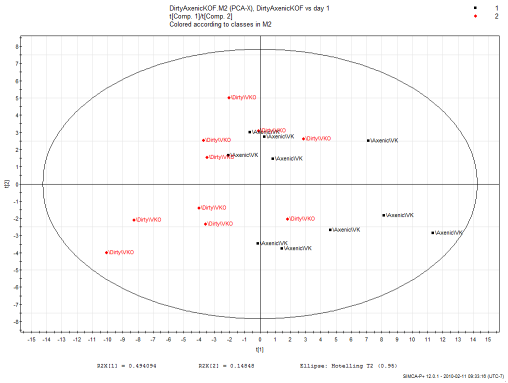

Axenic vs. Day 2

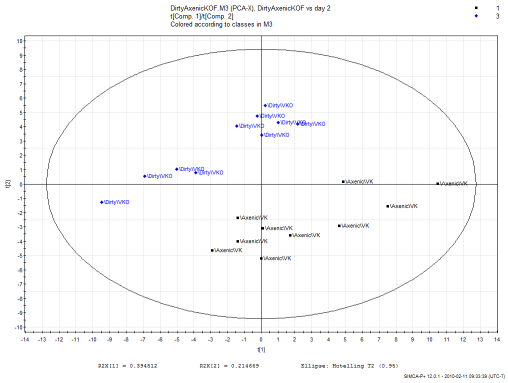

Axenic vs. Day 3

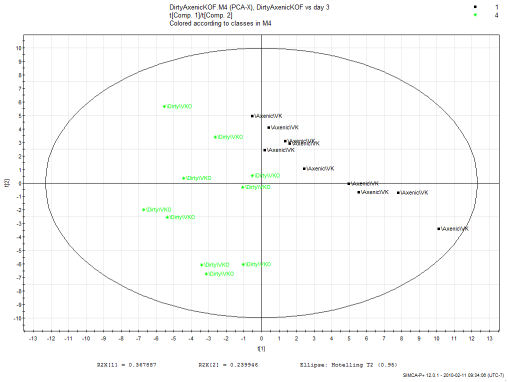

Axenic vs. Day 4

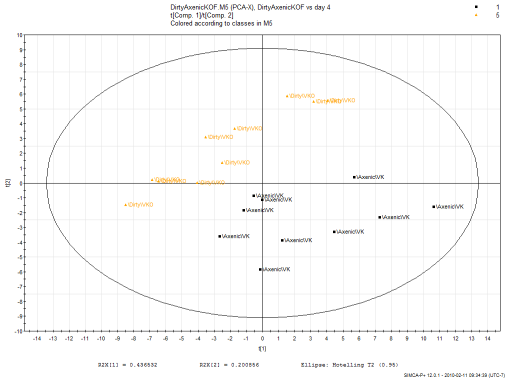

Axenic vs. Day 7

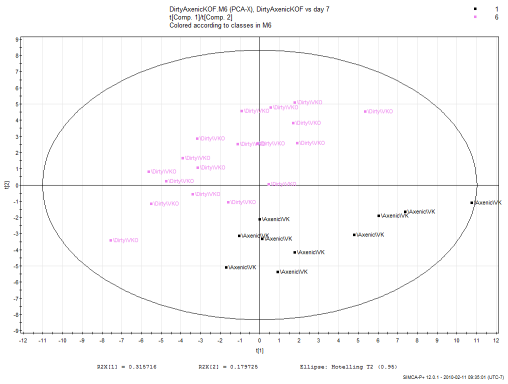

Fig 40 – Day-by-day analysis of female IL-10 KO mice colonized with fecal bacteria in reference to 20-week axenic mice; each plot is constructed using 10 axenic mice and 10 mice that had their urine collected during the indicated day after colonization.

Wild-type vs. IL-10 KO

Males – metabolic trajectory of colonized mice

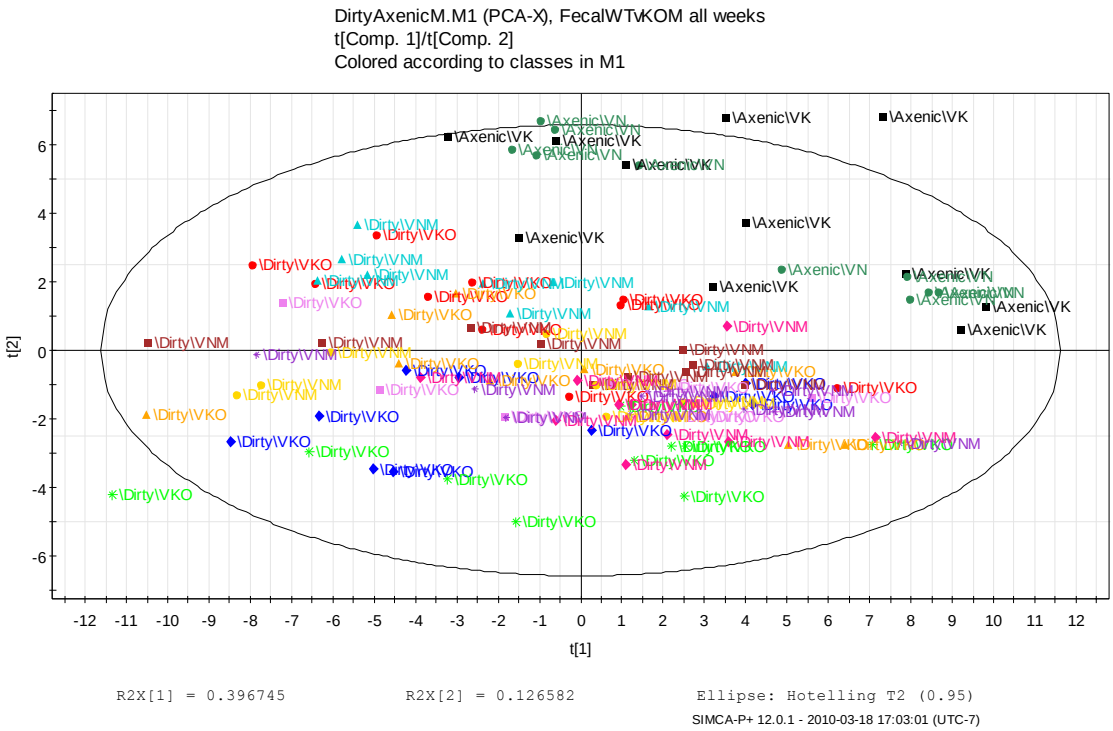

Fig 41 – PCA plot of the axenic 20-week samples from male wild-type and IL-10 KO mice along with all the samples collected after fecal colonization of both wild-type and IL-10 KO mice. Axenic mice cluster together in the upper right of the plot (wild-type dark green, IL-10 KO black). All the post-colonization dates cluster closer to the lower right-hand side of the plot.

Females – metabolic trajectory of colonized mice

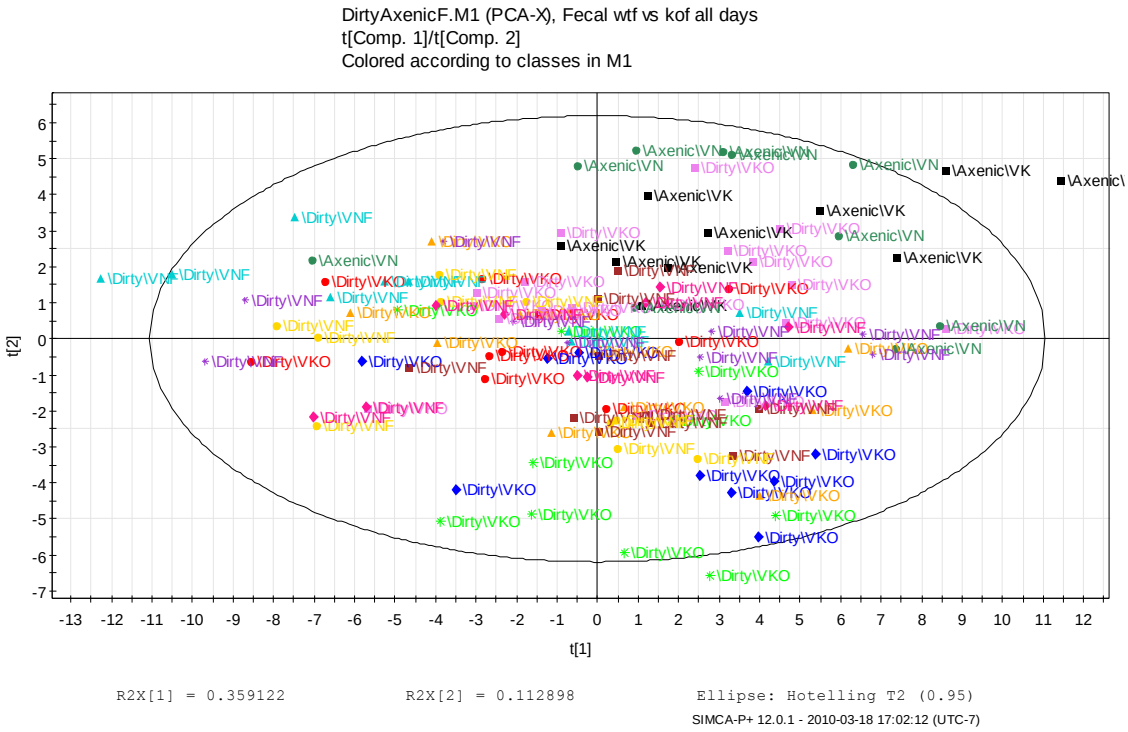

Fig 42 – PCA plot of the axenic 20-week samples from female wild-type and IL-10 KO mice along with all the samples collected after fecal colonization of both wild-type and IL-10 KO mice. Axenic mice cluster together in the upper right of the plot (wild-type dark green, IL-10 KO black). All the post-colonization dates cluster together closer to the lower right-hand side of the plot.

20 week conventional vs. day 7

Male population

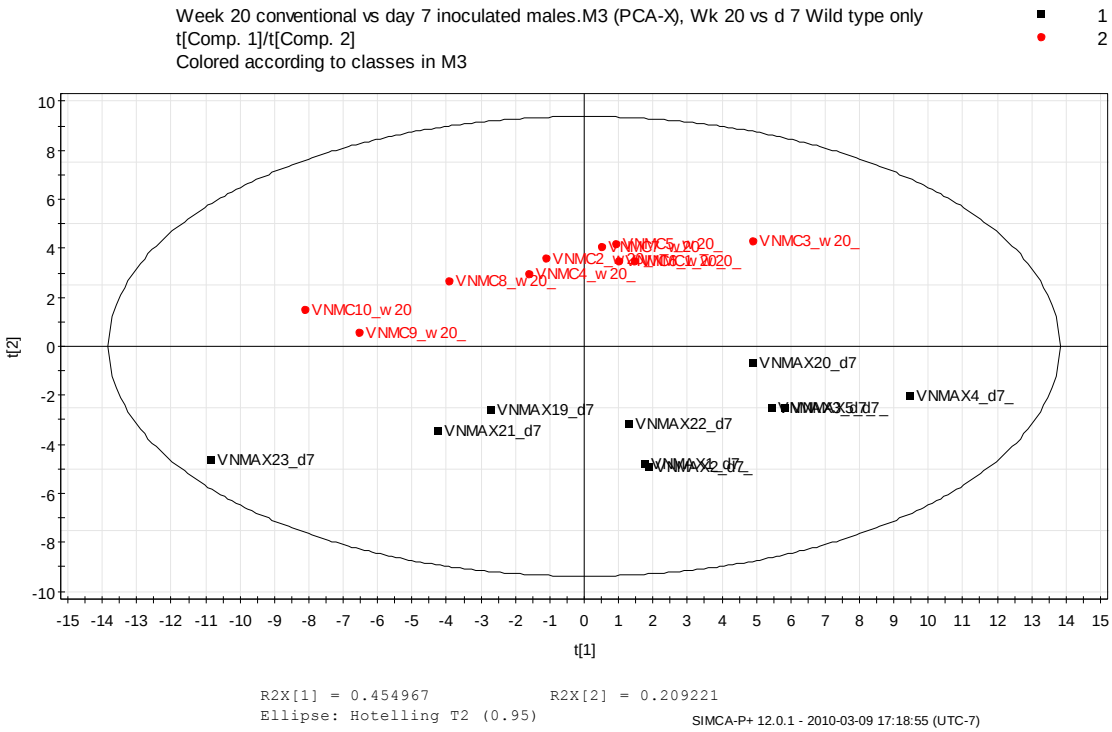

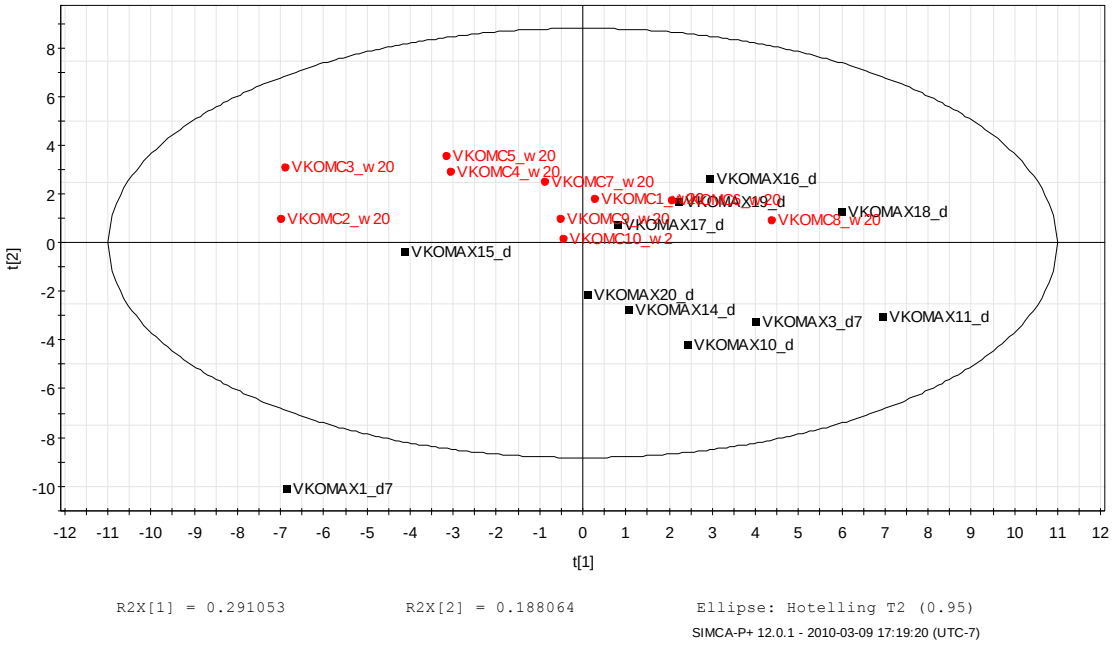

Fig 43 – PCA plots comparing male mice that have been conventionally raised vs. male mice that had been colonized with fecal bacteria at day 7 post-colonization; the colonized mice are displayed in black and the conventionally raised mice are displayed in red. The top graph is the comparison for wild-type mice and the bottom graph is the comparison for the IL-10 KO mice.

Female population

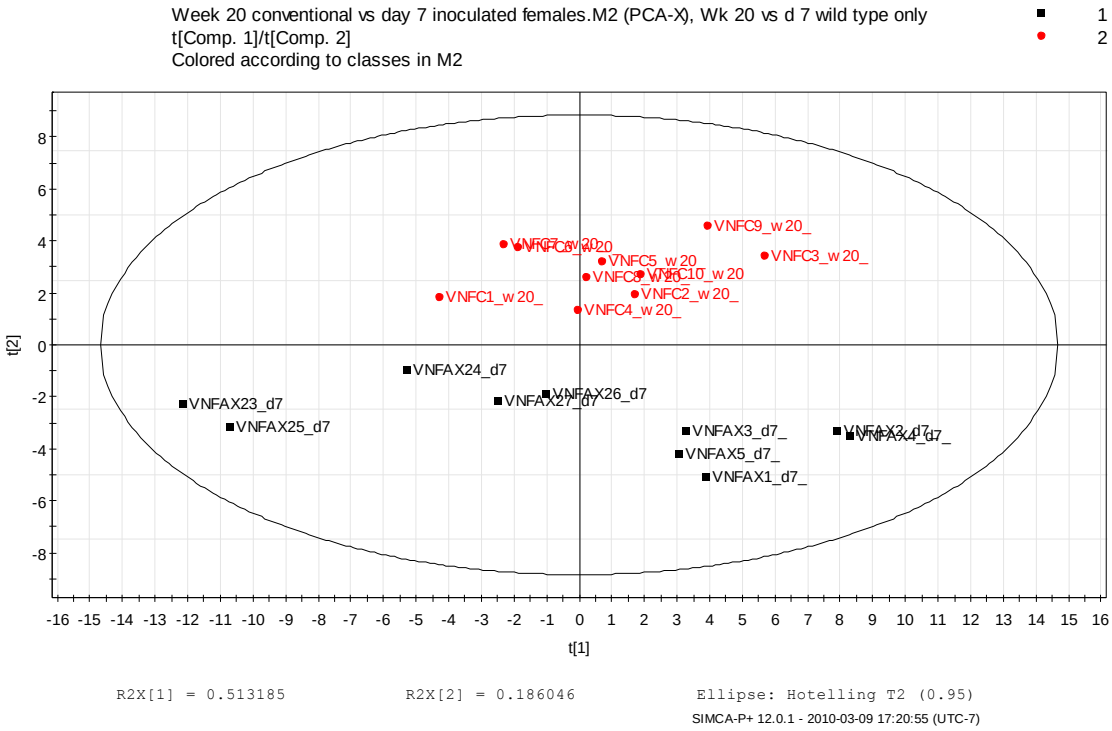

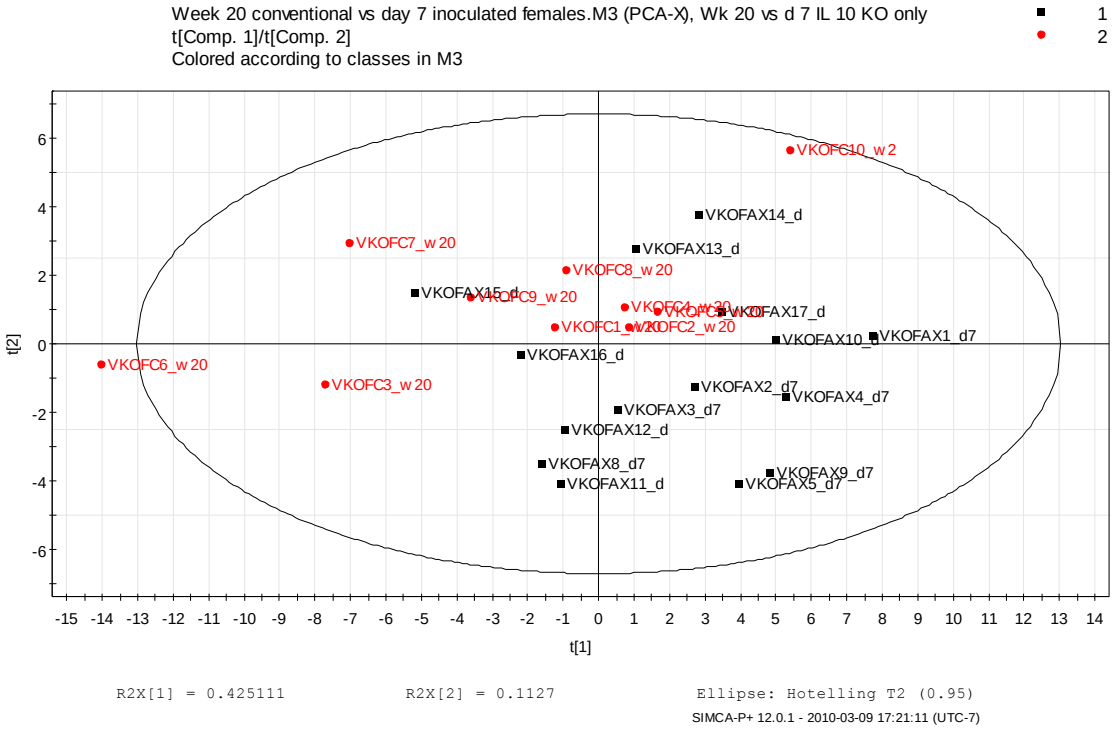

Fig 44 – PCA plots comparing female mice that have been conventionally raised vs. female mice that had been colonized with fecal bacteria at day 7 post-colonization; the colonized mice are displayed in black and the conventionally raised mice are displayed in red. The top graph is the comparison for wild-type mice and the bottom graph is the comparison for the IL-10 KO mice.

Axenic vs. Conventional

Wild-type population

Male – comparison of urine metabolomics over time

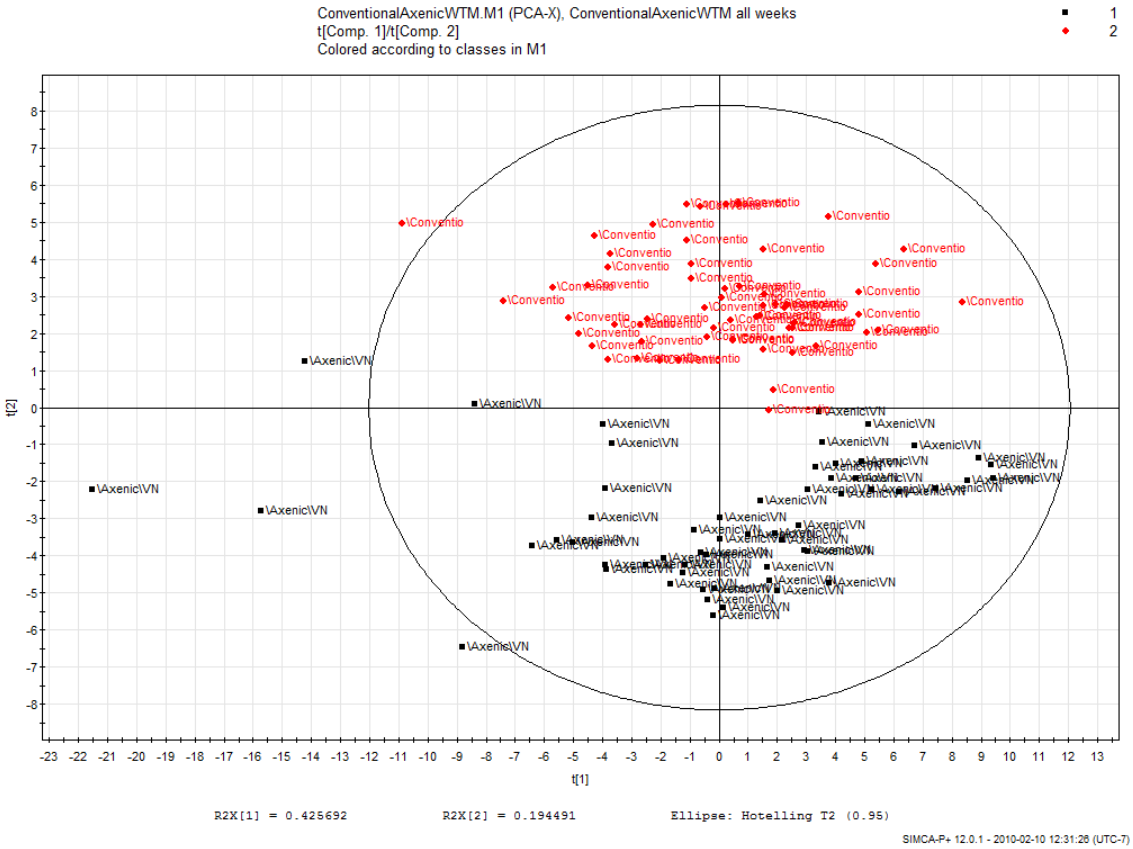

Fig 45 – PCA plot of axenic wild-type males over all time points vs. conventional wild-type males at all time-points; axenic mice are displayed in black and conventional mice are displayed in red. Urine was collected at weeks 4, 6, 8, 12, 16, and 20 either from the germ-free bubble or a conventional environment. 10 samples were collected at each tim-point.

Week-by-week comparison

Week 4

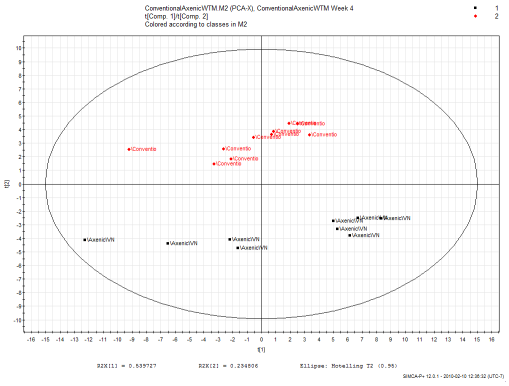

Week 6

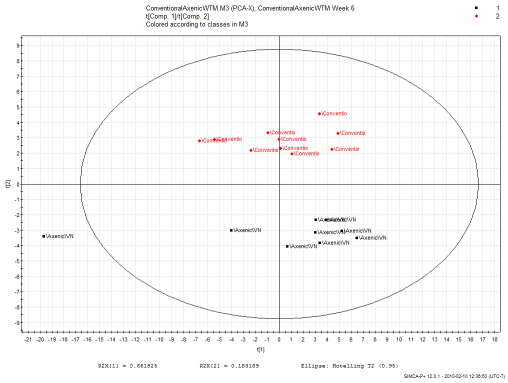

Week 8

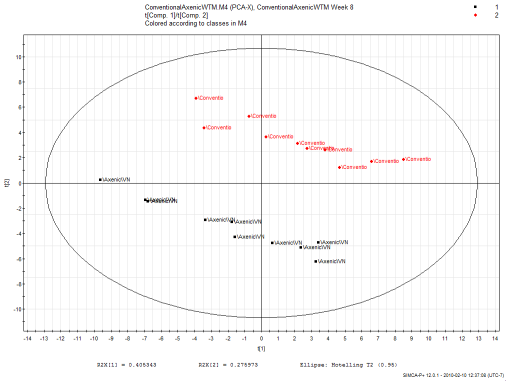

Week 12

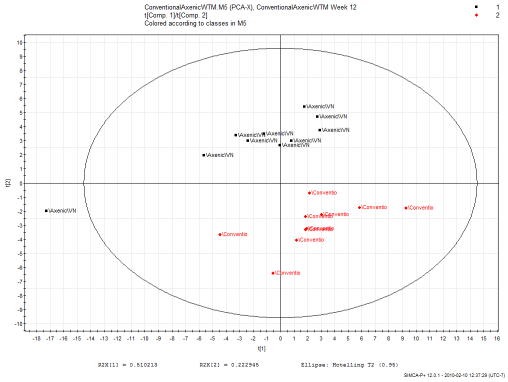

Week 16

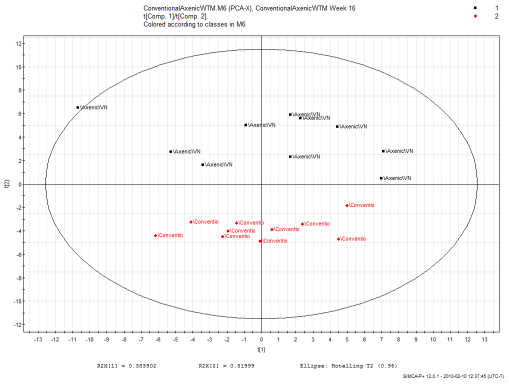

Week 20

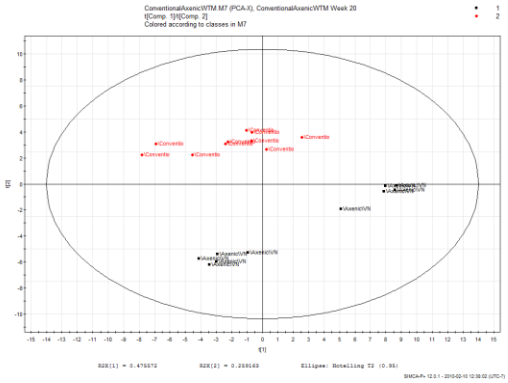

Fig. 46 – PCA plots of the urine metabolomic profiles of the axenic male wild-type and conventional male wild-type mice broken up by week of urine collection; conventional are

displayed in red and axenic are displayed in black. Each week comprises 10 axenic mice and 10 conventional mice.

Female – comparison of urine metabolomics over time

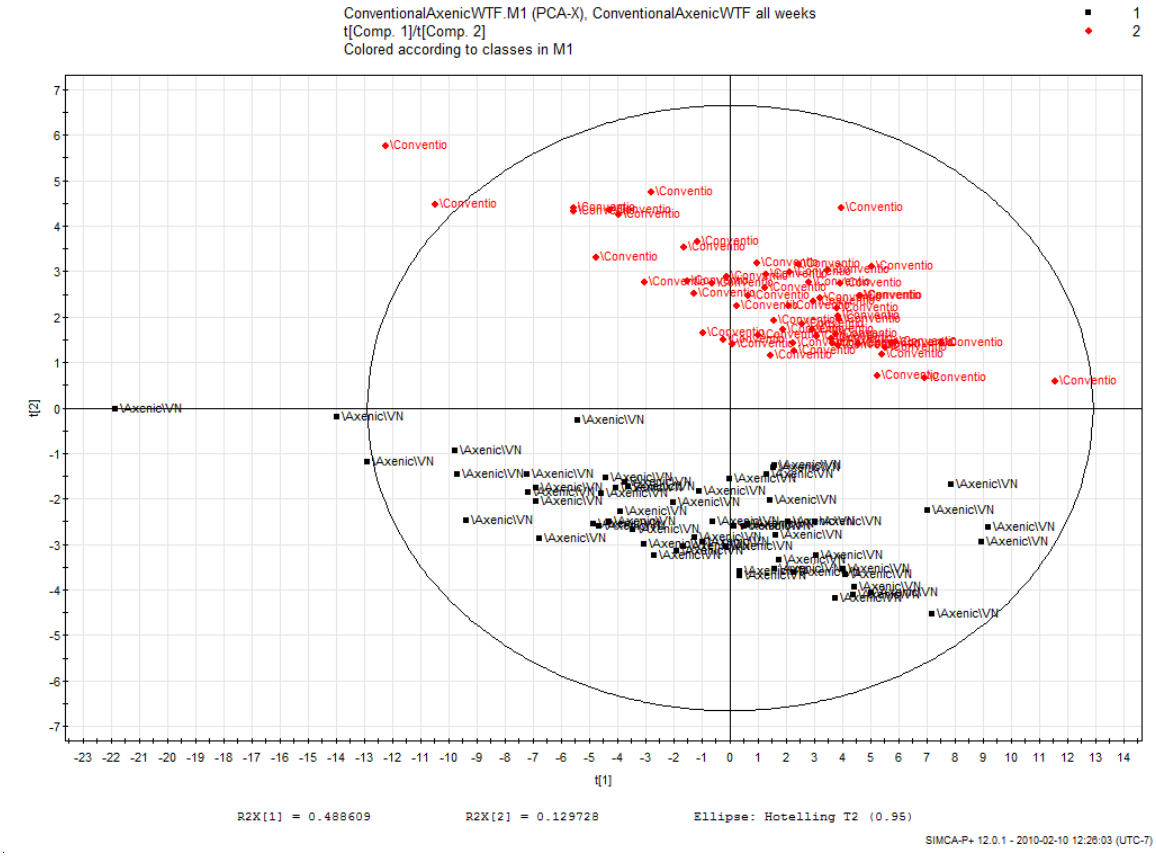

Fig 47 – PCA plot of axenic wild-type females over all time-points vs. conventional wild-type females at all time-points; axenic mice are displayed in black and conventional mice are displayed in red. Urine was collected at weeks 4, 6, 8, 12, 16, and 20, either from the germ-free bubble or a conventional environment. 10 samples were collected at each time point.

Week-by-week comparison

Week 4

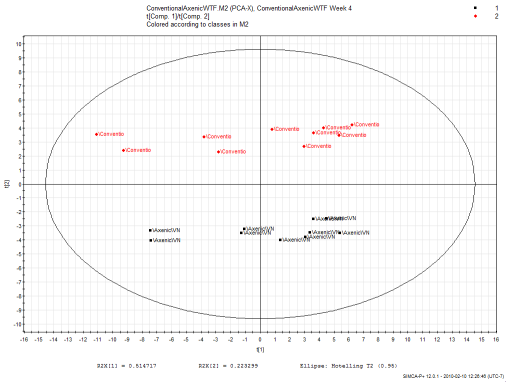

Week 6

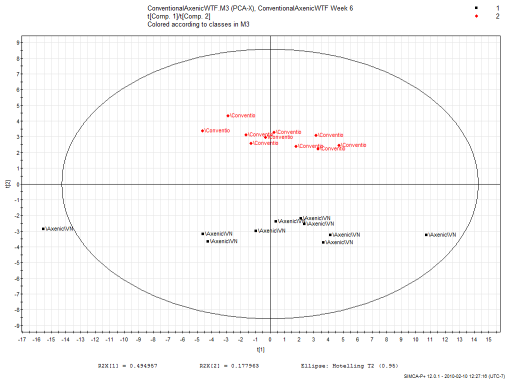

Week 8

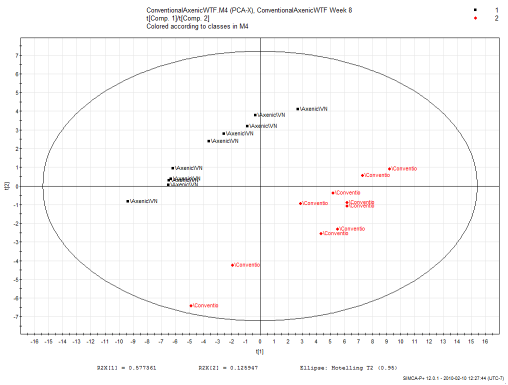

Week 12

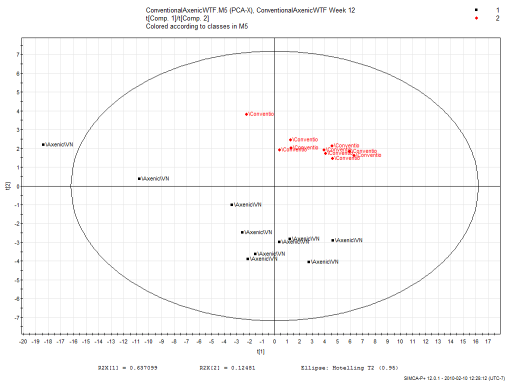

Week 16

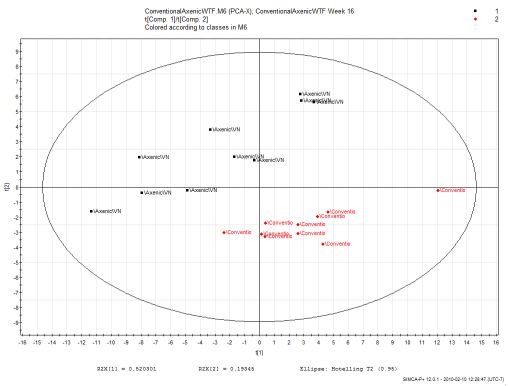

Week 20

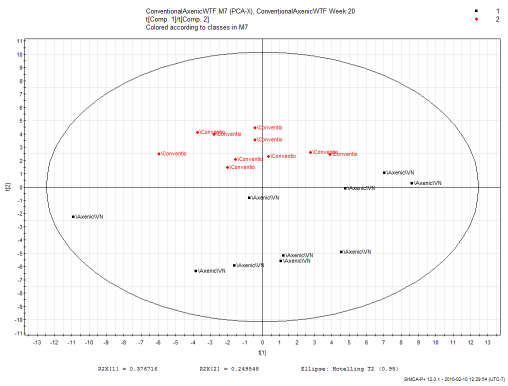

Fig. 48 – PCA plots of the urine metabolomic profiles of the axenic female wild-type and conventional female wild-type mice broken up by week of urine collection; conventional

are displayed in red and axenic are displayed in black. Each week comprises 10 axenic mice and 10 conventional mice.

IL-10 KO

Male – comparison of urine metabolomics over time

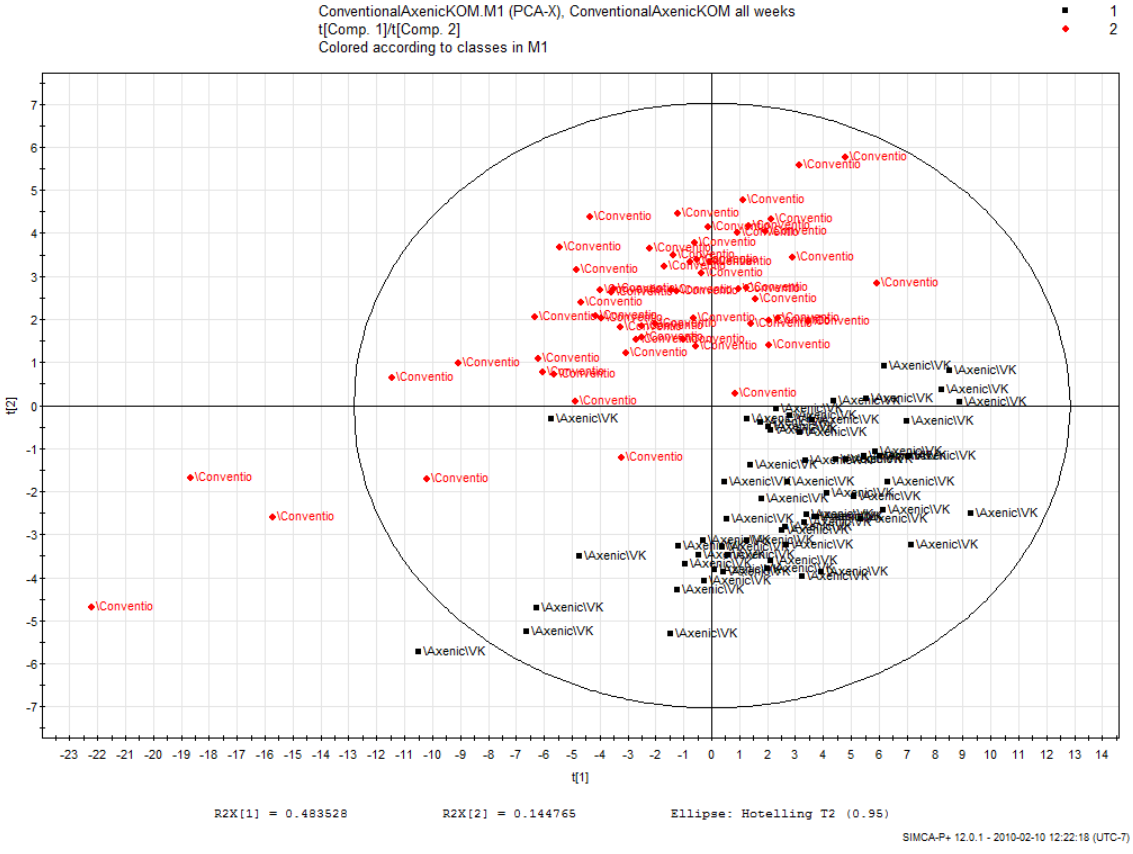

Fig 49 – PCA plot of axenic IL-10 KO males over all time-points vs. conventional IL-10 KO males at all time–points; axenic mice are displayed in black and conventional mice are displayed in red. Urine was collected at weeks 4, 6, 8, 12, 16, and 20 either from the germ-free bubble or a conventional environment. 10 samples were collected at each time point.

Week-by-week comparison

Week 4

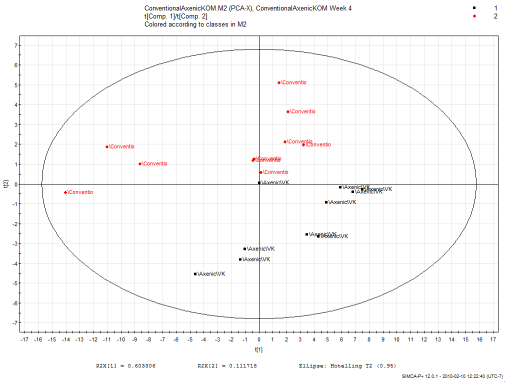

Week 6

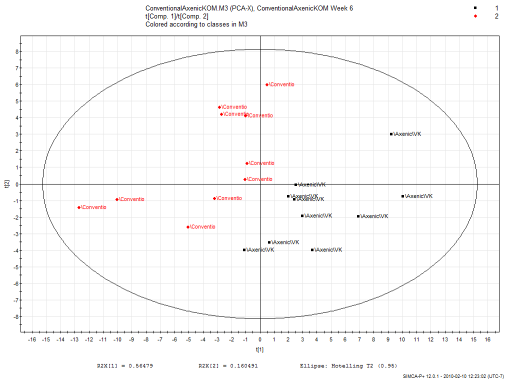

Week 8

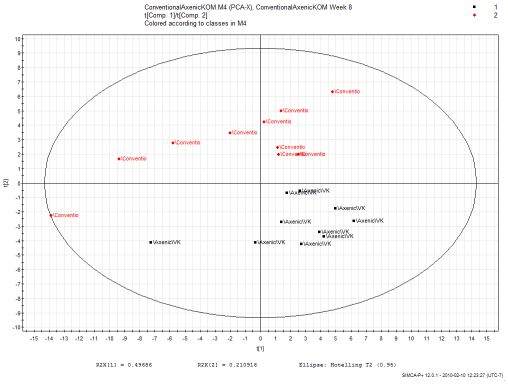

Week 12

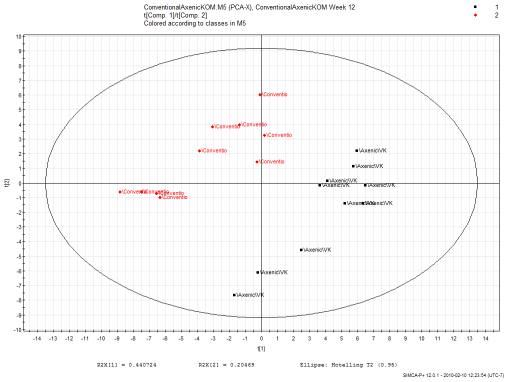

Week 16

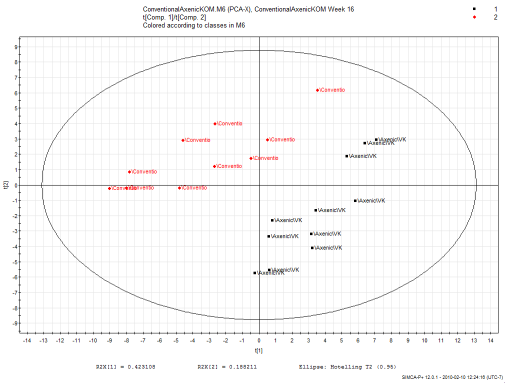

Week 20

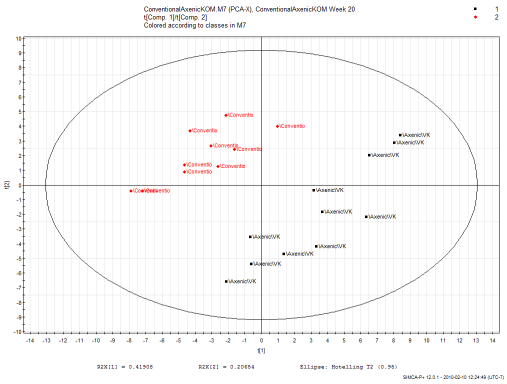

Fig. 50 – PCA plots of the urine metabolomic profiles of the axenic male IL-10 KO and conventional male IL-10 KO mice broken up by week of urine collection; conventional are

displayed in red and axenic are displayed in black. Each week comprises 10 axenic mice and 10 conventional mice.

Female – comparison of urine metabolomics over time

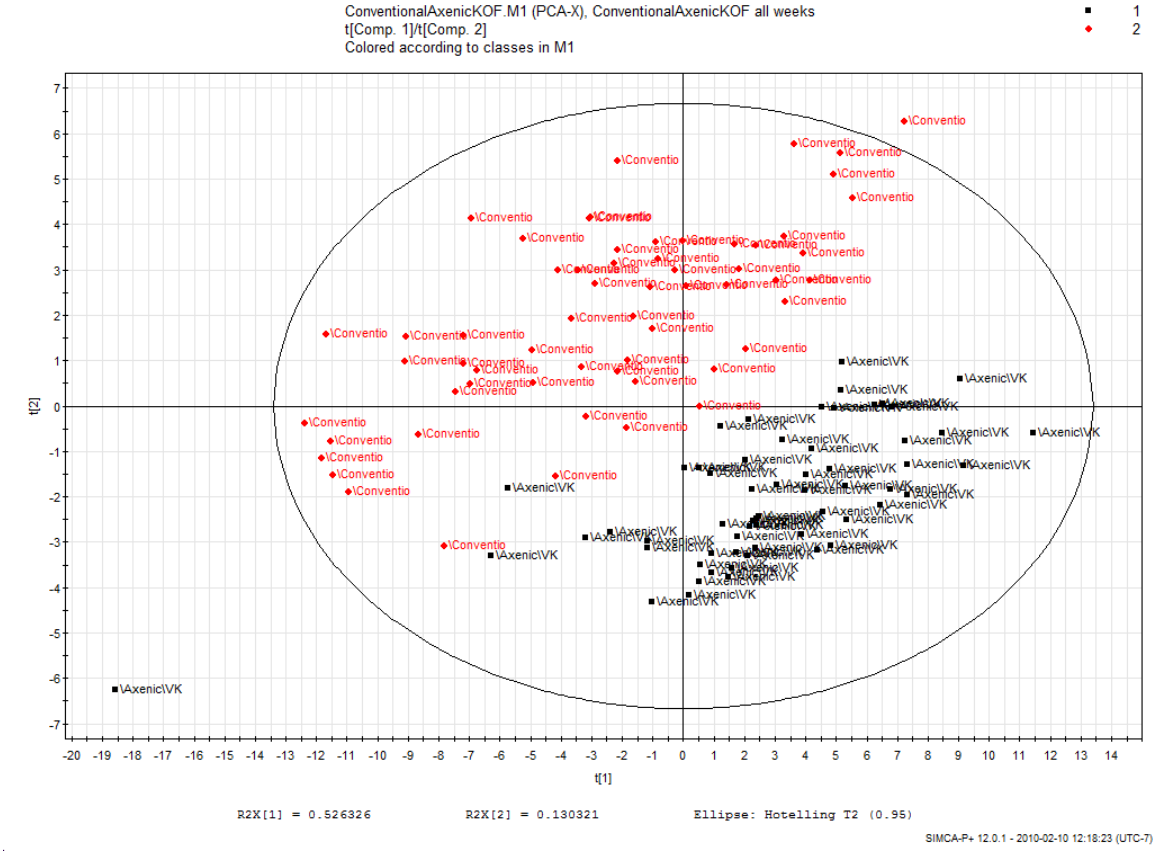

Fig 51 – PCA plot of axenic IL-10 KO females over all time points vs. conventional IL-10 KO females at all time points; axenic mice are displayed in black and conventional mice are displayed in red. Urine was collected at weeks 4, 6, 8, 12, 16, and 20, either from the germ-free bubble or a conventional environment. 10 samples were collected at each time point.

Week-by-week comparison

Week 4

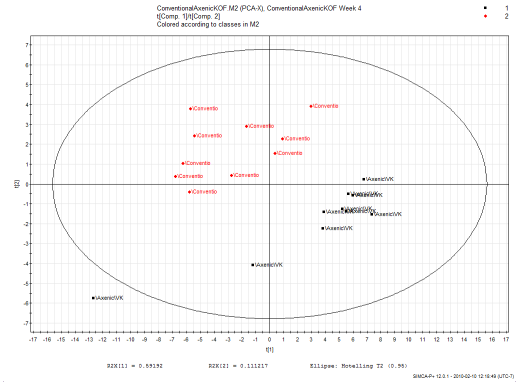

Week 6

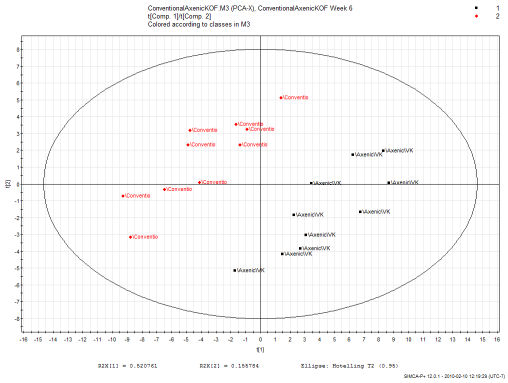

Week 8

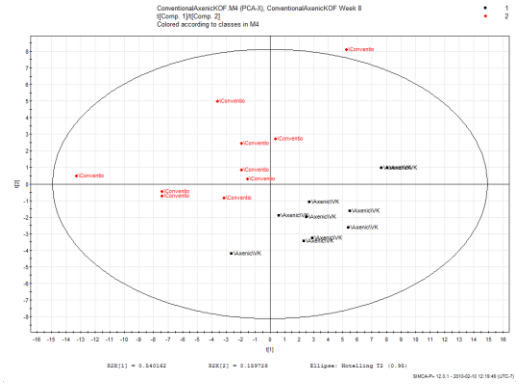

Week 12

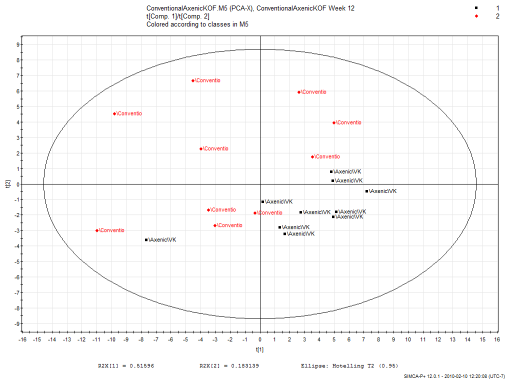

Week 16

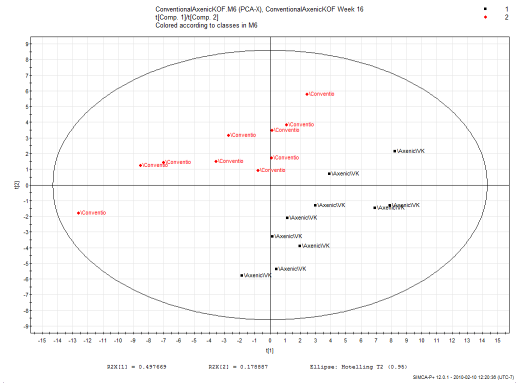

Week 20

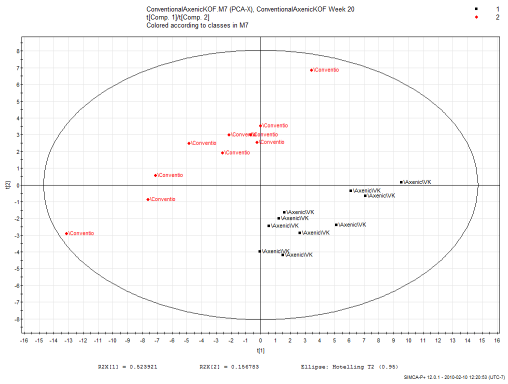

Fig. 52 – PCA plots of the urine metabolomic profiles of the axenic female IL-10 KO and conventional female IL-10 KO mice broken up by week of urine collection; conventional are displayed in red and axenic are displayed in black. Each week comprises 10 axenic mice and 10 conventional mice.